Dear Dr. Müller,

Thank you for the additional assessment on our manuscript "*The biophysics, ecology, and biogeochemistry of functionally diverse, vertically- and horizontally-heterogeneous ecosystems: the Ecosystem Demography Model, version 2.2 — Part 1: Model description*" (gmd-2019-45), and for accepting our manuscript for publication.

We carefully checked the equations one more time (as suggested by Dr. Ian Baker), and identified a few typographical errors. We also found and fixed minor typographical and grammar errors in the text and in two figures (Fig. 4 and Fig. S1), rewrote a few sentences to improve clarity, and changed the font size of some figures to improve legibility. None of these changes affected any of the results, interpretation of the results, or conclusions.

Below we enclose the annotated manuscript and annotated supporting information for reference. In the annotated text, blue text was added, and crossed text was removed.

Sincerely,
Marcos Longo

The biophysics, ecology, and biogeochemistry of functionally diverse, vertically- and horizontally-heterogeneous ecosystems: the Ecosystem Demography Model, version 2.2 — Part 1: Model description

Marcos Longo[1,2,3], Ryan G. Knox[4,5], David M. Medvigy[6], Naomi M. Levine[7], Michael C. Dietze[8], Yeonjoo Kim[9], Abigail L. S. Swann[10], Ke Zhang[11], Christine R. Rollinson[12], Rafael L. Bras[13], Steven C. Wofsy[1], and Paul R. Moorcroft[1]

[1]Harvard University, Cambridge, MA, United States
[2]Embrapa Agricultural Informatics, Campinas, SP, Brazil
[3]Jet Propulsion Laboratory, California Institute of Technology, Pasadena, CA, United States
[4]Massachusetts Institute of Technology, Cambridge, MA, United States
[5]Lawrence Berkeley National Laboratory, Berkeley, CA, United States
[6]University of Notre Dame, Notre Dame, IN, United States
[7]University of Southern California, Los Angeles, CA, United States
[8]Boston University, Boston, MA, United States
[9]Department of Civil and Environmental Engineering, Yonsei University, Seoul 03722, Republic of Korea
[10]University of Washington, Seattle, WA, United States
[11]Hohai University, Nanjing, Jiangsu, China
[12]The Morton Arboretum, Lisle, IL, United States
[13]Georgia Institute of Technology, Atlanta, GA, United States

Correspondence: M. Longo
(mlongo@post.harvard.edu)

Abstract. Earth System Models (ESMs) have been developed to represent the role of terrestrial ecosystems on the energy, water, and carbon cycles. However, many ESMs still lack representation of within-ecosystem heterogeneity and diversity. In this manuscript, we present the Ecosystem Demography Model version 2.2 (ED-2.2). In ED-2.2, the biophysical and physiological ~~cycles~~processes account for the horizontal and vertical heterogeneity of the ecosystem: the energy, water, and carbon cycles are solved separately for ~~each group of individual trees of similar size and functional group (cohorts) living in a micro-environment with similar disturbance history (patches).~~for a series of vegetation cohorts (groups of individual plants of similar size and plant functional type) distributed across a series of spatially-implicit patches (representing collections of micro-environments that have a similar disturbance history). We define the equations that describe the energy, water, and carbon cycles in terms of total energy, water, and carbon, which simplifies the ~~ordinary~~ differential equations and guarantees excellent conservation of these quantities in long-term simulation ($< 0.1\%$ error over 50 years). We also show examples of ED-2.2 simulation results at single sites and across tropical South America. These results demonstrate the model's ability to characterize the variability of ecosystem structure, composition and functioning both at stand~~-~~ and ~~continental scales~~continental scales. ~~In addition, a~~A detailed model evaluation was ~~carried out~~conducted and is presented in a companion

paper (Longo et al., 2019). Finally, we highlight some of the ongoing model developments ~~in ED 2.2~~ ~~that aim at reducing~~ ~~the uncertainties identified in this study~~ designed to improve the model's accuracy and performance and ~~the inclusion of~~ to include processes hitherto not represented in the model.

1 Introduction

The dynamics of the terrestrial biosphere play an integral role in the earth's carbon, water and energy cycles (Betts and Silva Dias, 2010; Santanello Jr et al., 2018; Le Quéré et al., 2018), and consequently, how the earth's climate system is expected to change over the coming decades due to the increasing levels of atmospheric carbon dioxide arising from anthropogenic activities (IPCC, 2014; Le Quéré et al., 2018). Models for the dynamics of the terrestrial biosphere and its bi-directional interaction with the atmosphere have evolved considerably over the past decades (Levis, 2010; Fisher et al., 2014, 2018). As described by Sellers et al. (1997), the first generation of land surface models (LSMs) ~~were~~ was limited to provide boundary conditions to atmospheric models~~, and~~; they only solved a simplified energy and water budget, and accounted for the effects of surface on frictional effects on near-surface winds (e.g. Manabe et al., 1965; Somerville et al., 1974). These models, however, did not account for the active role of vegetation. The second generation of LSMs considered the active role of vegetation and represented the spectral properties of the canopy, the changes in roughness of vegetated surfaces, and the biophysical controls on evaporation and transpiration (Sellers et al., 1997); examples of these models include NCAR/BATS (Dickinson et al., 1986) and SiB (Sellers et al., 1986). The increasing recognition of the role of vegetation in mediating the exchanges of carbon, water and energy between the land and the atmosphere led to the third generation of LSMs, which incorporated explicit representations of plant photosynthesis, and resulting dynamics of terrestrial carbon uptake, turnover and release within terrestrial ecosystems (Sellers et al., 1997); examples of such models included LSM (Bonan, 1995) and SiB2 (Sellers et al., 1996). While the fluxes of carbon, water and energy predicted by these models would change in response to changes in their climate forcing, the biophysical and biogeochemical properties of the ecosystem within each climatological grid cell was prescribed, and thus did not change over time.

Subsequently, building upon previous work (Prentice et al., 1992; Neilson, 1995; Haxeltine and Prentice, 1996), Foley et al. (1996) adopted an approach to calculate the productivity of a series of plant functional types (PFTs), based on a leaf-level model of photosynthesis. The abundance of each PFT within each grid cell was dynamic, with the abundance changes being determined by the relative productivity of the PFTs. This allowed the fast-timescale exchanges of carbon, water, and energy within the plant canopy to be explictly linked with the long-term dynamics of the ecosystem. This approach followed the concept of dynamic global vegetation model (DGVM), originally coined by Prentice et al. (1989) to describe this kind of terrestrial biosphere model in which changes in climate could drive changes in ecosystem composition, structure and functioning~~, and which~~. DGVMs, when run coupled to atmospheric models, would then feedback onto climate. The subsequent generation of terrestrial biosphere-based DGVMs (i.e. DGVMs incorporating couple carbon, water, and energy fluxes) such as LPJ (Sitch et al., 2003), CLM-DGVM (Levis et al., 2004) and TRIFFID/JULES (Hughes et al., 2004; Clark

et al., 2011; Mangeon et al., 2016) have included additional mechanisms such as disturbance through fires and multiple types of mortality.

Analyses have shown that most terrestrial biosphere models are capable of reproducing the current distribution of global biomes (e.g. Sitch et al., 2003; Blyth et al., 2011) and their carbon stocks and fluxes (Piao et al., 2013). However, they diverge markedly in their predictions of how terrestrial ecosystems will respond to future climate change (Friedlingstein et al., 2014). In fully-coupled Earth System Model simulations, some of these differing predictions arise from divergent predictions about the direction and magnitude of regional climate change. However, off-line analyses, in which the models are forced with prescribed climatological forcing, have shown that there is also substantial disagreement between the models about how terrestrial ecosystems will respond to any shift in climate (e.g. Sitch et al., 2008; Zhang et al., 2015). In addition, the transitions between biome types, for example, the transition that occurs between closed-canopy tropical forests and grass- and shrub-dominated savannahs in South America, are generally far more abrupt in typical DGVM results than in observations (Good et al., 2011; Levine et al., 2016).

One important limitation of most DGVMs is that they ~~cannot~~do not represent within-ecosystem diversity and heterogeneity. The representation of plant functional diversity within terrestrial biosphere models is normally coarse, with broadly-defined PFTs defined from a combination of morphological and leaf physiological attributes (Purves and Pacala, 2008). In addition, there is limited variation in the resource conditions (light, water, and nutrient levels) experienced by individual plants within the climatological grid cells of traditional DGVMs. Some models, such as CLM (Oleson et al., 2013), have ~~vertical above-ground heterogeneity in the form of~~have options to represent a multi-layer plant canopy ~~that allows for sun and shade leaves~~(e.g. a two canopy layers allowing for sun and shade leaves), and/or differences in rooting depth between PFTs; however, resource conditions are assumed to be horizontally homogeneous, meaning that there is no horizontal spatial variation in resource conditions experienced by ~~individuals~~individual plants. The lack of significant variability in resource conditions limits the range of environmental niches within the climatological grid cells of terrestrial biosphere, and makes the coexistence between PFTs difficult. Consequently, models ~~would~~ often predict ecosystems comprised of single homogeneous vegetation types (Moorcroft, 2003, 2006).

Field- and laboratory-based studies conducted over the past thirty years indicate that plant functional diversity significantly affects ecosystem functioning (Loreau and Hector, 2001; Tilman et al., 2014, and references therein), and variations in trait expression are strongly driven by disturbances and local heterogeneity of abiotic factors such as soil characteristics (Bruelheide et al., 2018; Both et al., 2019). In many cases, biodiversity increases ecosystem productivity and ecosystem stability (e.g., Tilman and Downing, 1994; Naeem and Li, 1997; Cardinale et al., 2007; García-Palacios et al., 2018), and biodiversity has also been shown to contribute to enhanced ecosystem functionality in highly stressed environments (e.g. Jucker and Coomes, 2012). Other studies have also established correlations between tropical forest diversity and carbon storage and primary productivity (Cavanaugh et al., 2014; Poorter et al., 2015; Liang et al., 2016; Huang et al., 2018).

In addition to the absence of within-ecosystem diversity in conventional terrestrial biosphere models, plants of each PFT are also assumed to be homogeneous in size while, in contrast, most terrestrial ecosystems, particularly forests and woodlands, exhibit marked size-structure of individuals within plant canopies (Hutchings, 1997). This size-related hetero-

geneity is important because plant size strongly affects the amount of light, water, and nutrients individual plants within the canopy can access, which, in turn, affects their performance, dynamics and responses to climatological stress. It also allows ~~representing~~representation of the dynamics of pervasive human-driven degradation of forest ecosystems (Lewis et al., 2015; Haddad et al., 2015), which affects ~~carbon stocks, structure and composition of forests that~~carbon stocks and forest structure and composition, which cannot be easily represented in highly aggregated models (Longo and Keller, 2019).

An alternative approach to simulating the dynamics of terrestrial ecosystems has been individual based vegetation models (Friend et al., 1997; Bugmann, 2001; Sato et al., 2007; Fischer et al., 2016; Maréchaux and Chave, 2017). Also known as forest gap models, due to the importance of canopy gaps for the dynamics of closed canopy forests, these models simulate the birth, growth, and death of individual plants, thereby incorporating diversity and heterogeneity of the plant canopy mechanistically. In forest gap models, the ecosystem properties such as total carbon stocks, and net ecosystem productivity are emergent properties resulting from competition of limiting resources and the differential ability of plants to survive and be productive under a variety of micro-environments (e.g. gaps or the understory of a densely populated patch of old-growth forest).

This approach has two main advantages. First, gap models represent the dynamic changes in the ecosystem structure caused by disturbances such as tree fall, selective logging, and fires. These disturbances create new micro-environments that are significantly different from old-growth vegetation areas, and allow plants with different life strategies (for example, shade-intolerants) to co-exist in the landscape. Second, because individual trees are represented in the model, the results can be directly compared with field measurements. Gap models have various degrees of complexity, with some models being able to represent the interactions between climate variability and gross primary productivity (Friend et al., 1997; Sato et al., 2007), as well as the impact of climate change in the ecosystem carbon balance (Fischer et al., 2016, and references therein). However, because the birth and death of individuals within a plant canopy are stochastic processes, multiple realizations of given model formulation are required to determine the long-term, large-scale dynamics of these models, which limits their applicability over large regions or global scales, and has precluded their use in Earth System Modeling studies.

The need to represent heterogeneity in vegetation structure and composition in terrestrial biosphere models, without the computational burden ~~required to simulate~~of simulating every tree at regional and global scales, led to the development of cohort-based models ~~(Fisher et al., 2018)~~(Hurtt et al., 1998; Moorcroft et al., 2001; Fisher et al., 2018). In the cohort-based approach, individual trees are grouped according to their size (e.g. height or diameter at breast height); functional groups, which can be defined along trait axes (e.g. Reich et al., 1997; Wright et al., 2004; Fortunel et al., 2012), and microenvironment conditions (e.g. whether plants are living in a gap, recently burned fragment, or in a patch of old-growth forest). Over the past two decades, ~~many~~several cohort-based models have emerged, including the Ecosystem Demography Model (ED, Moorcroft et al., 2001; Hurtt et al., 2002; Albani et al., 2006; Medvigy et al., 2009); the Lund-Potsdam-Jena General Ecosystem Simulator (LPJ-GUESS, Smith et al., 2001; Ahlström et al., 2012; Lindeskog et al., 2013); ~~and~~ the Land Model version 3 with Perfect Plasticity Approximation (LM3-PPA, Weng et al., 2015)~~,~~; and the Functionally-Assembled Terrestrial Ecosystem Simulator (FATES, Fisher et al., 2015; Huang et al., 2019). ~~Because~~Similar to gap models, these models ~~also~~ represent functional diversity and heterogeneity of micro-environments, and consequently the ecosystem's structure, diver-

sity and functioning ~~also~~ emerge from the interactions between plants with different life strategies under different resource availability, albeit at a lesser extent than individual-based models (Fisher et al., 2018).

The Ecosystem Demography Model (ED Moorcroft et al., 2001) is a cohort-based model. Through this approach, it addresses the need to incorporate heterogeneity into models of the long-term, large scale response of terrestrial ecosystems to changes in climate and other environmental forcings within a deterministic modeling framework. The size and age-structured partial differential equations that describe the plant community are derived from individual-level properties, but are properly scaled to account for the spatially-localized nature of interactions within plant canopies. The model was later extended by Hurtt et al. (2002) and Albani et al. (2006) to incorporate multiple forms of disturbance including land-clearing, land-abandonment, and forest harvesting. An important difference between ED and most DGVMs is that in ED, PFTs are defined not simply based on their biogeographic ranges, but also represent diversity in plant life-history strategies within any given ecosystem. These different PFTs represent a suite of physiological, morphological, and life-history traits that mechanistically represent the ways different kinds of plants utilize resources (Fisher et al., 2010).

The original ED model formulation was an off-line ecosystem model describing the coupled carbon and water fluxes of a heterogeneous tropical forest ecosystem (Moorcroft et al., 2001). Subsequently, Medvigy et al. (2009) applied a similar approach to develop the Ecosystem Demography model version 2 (ED-2) that describes coupled carbon, water and energy fluxes of the land surface. Since then, the ED-2 model has been continuously developed to improve several aspects of the model (see Supplement S1 for further information): (1) the conservation and thermodynamic representation of energy, water, and carbon cycles of the ecosystems; (2) the representation of several components of the energy, water, and carbon cycles, including the canopy radiative transfer, aerodynamic conductances and eddy fluxes, and leaf physiology (photosynthesis); (3) the structure of the code, including efficient data storage, code parallelization, and version control and code availability. ED-2 has been used in many studies including offline simulations (e.g. Medvigy et al., 2009; Antonarakis et al., 2011; Kim et al., 2012; Zhang et al., 2015; Castanho et al., 2016; Levine et al., 2016), ~~or~~and simulations running interactively with a regional atmospheric model (e.g. Knox et al., 2015; Swann et al., 2015).

In this paper, we describe in detail the biophysical, physiological, ecological and biogeochemical formulation of the most recent version of the ED-2 model (ED-2.2), focusing in particular on the model's formulation of the fast time-scale dynamics of the heterogeneous plant canopy that occur at sub-daily timescales. While many parameterizations and sub-models in ED-2.2 are based on approaches that are also used in other DVGMs, their implementation in ED-2.2 has some critical differences from other ecosystem models and also previous versions of ED: (1) In ED-2.2, the fundamental budget equations use energy and total mass as the main prognostic variables; because we use equations that directly track the time changes of the properties we seek to conserve, we can assess the model conservation of such properties with fewer assumptions. (2) In ED-2.2, all thermodynamic properties are scalable with mass, and the model is constructed such that when individual biomass changes, due to growth and turnover, the thermodynamic properties are also updated to reflect changes in heat and water holding capacity. (3) The water and energy budget equations for vegetation are solved at the individual cohort level and the corresponding equations for environments shared by plants such as soils and canopy air space are solved for each micro-environment in the landscape, and thus ecosystem-scale fluxes are ~~emerging~~emergent properties of the plant

community. This approach allows the model to represent both the horizontal and vertical heterogeneity of environments of the plant communities. It also links the individual's ability to access resources such as light and water and accumulate carbon under a variety of micro-environments, which ultimately drives the long-term dynamics of growth, reproduction, and survivorship.

2 Model overview

2.1 The representation of ecosystem heterogeneity in ED-2.2

In ED-2.2 the terrestrial ecosystem within a given region of interest is represented through a hierarchy of structures to capture the physical and biological heterogeneity in the ecosystem's properties (Fig. 1).

Physical Heterogeneity: The domain of interest (*grid*) is geographically divided into *polygons*. Within each polygon, the time-varying meteorological forcing above the plant canopy is assumed to be spatially uniform. For example, a single polygon may be used to simulate the dynamics of an ecosystem in the neighborhood of an eddy flux tower, or alternatively, a polygon may represent the lower boundary condition within one horizontal grid-cell in an atmospheric model. Each polygon is sub-divided into one or more *sites* that are designed to represent landscape-scale variation in other abiotic properties, such as soil texture, soil depth, elevation, slope, aspect, and topographic moisture index. Each site is defined as a fractional area within the polygon and represents all regions within the polygon that share similar time-invariant physical (abiotic) properties. Both polygons and sites are defined at the beginning of the simulation and are fixed in time, and no geographic information exists below the level of the polygon.

Biotic Heterogeneity: Within each site, horizontal, disturbance-related heterogeneity in the ecosystem at any given time t is characterized through a series of *patches* that are defined by the time elapsed since last disturbance (i.e. *age*, a) and the type of disturbance that generated them. Like sites, patches are not physically contiguous: each patch represents the collection of canopy gap-sized ($\sim 10\,\mathrm{m}$) areas within the site that have a similar disturbance history, defined in terms of the type of disturbance experienced (represented by subscript q, $q \in 1, 2, \ldots, N_Q$; list of indices available at Tab. 1) and time since the disturbance event occurred. The disturbance types accounted for in ED-2.2, and the possible transitions between different disturbance types, are shown in Fig. S1. The collection of gaps within each given site belonging to a polygon follows a probability distribution function α, which can be also thought of as the relative area within a site, that satisfies:

$$\sum_{q=1}^{N_Q} \left[\int_0^\infty \alpha_q(a,t)\,\mathrm{d}a \right] = 1. \tag{1}$$

Similarly, the plant community population is characterized by the number of plants per unit area (hereafter number density, n), and is further classified according to their plant functional type (PFT), represented by subscript f ($f \in 1, 2, \ldots, N_F$; Tab. 1) and the type of gap (q). The number density distribution depends on the individuals' biomass characteristics (size, $\mathbf{C}$), the age since last disturbance (a) and the time (t), and is expressed as $n_{fq}(\mathbf{C}, a, t)$. Size is defined as a vector $\mathbf{C} =$
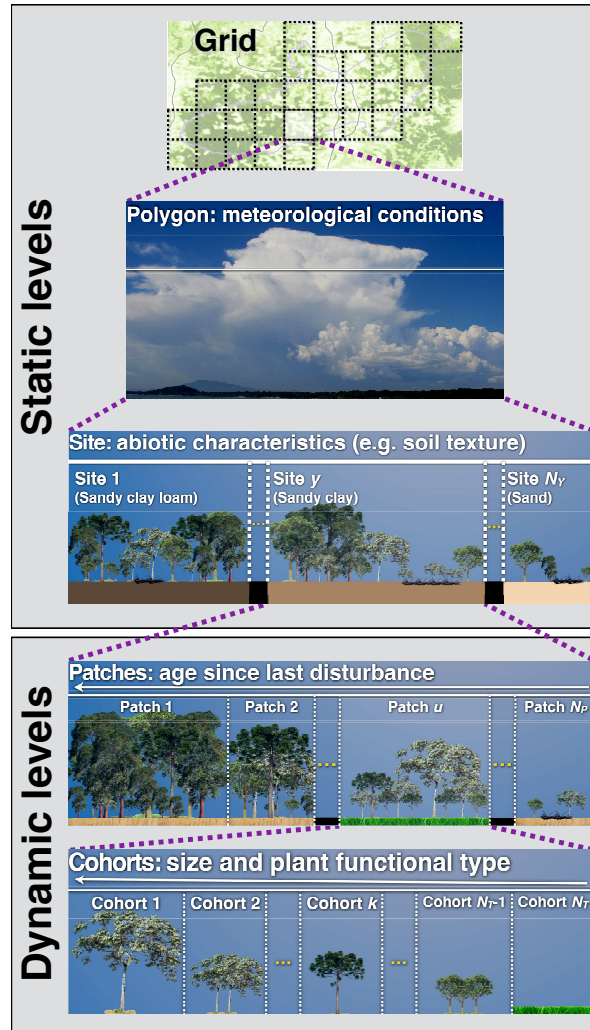
Figure 1. Schematic representation of the multiple hierarchical levels in ED-2.2, organized by increasing level of detail from top to bottom. Static levels (grid, polygons, and sites) are assigned during the model initialization and remain constant throughout the simulation. Dynamic levels (patches and cohorts) may change during the simulation according to the dynamics of the ecosystem.

$n_{fq}^{-1}\,(C_{\mathrm{l}}; C_{\mathrm{r}}; C_{\sigma}; C_{\mathrm{h}}; C_{\mathrm{n}})$ (units: $\mathrm{kg_C\ plant^{-1}}$) corresponding to biomass of leaves, fine roots, sapwood, heartwood, and non-structural storage (starch and sugars), respectively.

Following Moorcroft et al. (2001), Albani et al. (2006), and Medvigy and Moorcroft (2012), the ~~fundamental~~ partial differential equations that describe the dynamics of ~~demographic~~plant density and probability distribution of patches within each site in the size-and-age structured model are defined as (dependencies omitted in the equations for clarity):

$$\underbrace{\frac{\partial n_{fq}}{\partial t}}_{\text{Change rate}} = \underbrace{-\frac{\partial n_{fq}}{\partial a}}_{\text{Aging}} \underbrace{-\boldsymbol{\nabla}_{\mathbf{C}} \cdot (\mathbf{g}_f\, n_{fq})}_{\text{Growth}} \underbrace{-m_f\, n_{fq}}_{\text{Mortality}}, \tag{2}$$

Table 1. List of subscripts associated with ED-2.2 hierarchical levels. N_T is the total number of cohorts, N_G is the total number of soil (ground) layers, N_S is the total number of temporary surface water/snowpack layers, and N_C is the total number of canopy air space layers, currently only used to obtain properties related to canopy conductance. The complete list of subscripts is available at Table S1.

Subscript	Description
X_c	Canopy air space (single layer)
X_{c_j}	Canopy air space, layer j ($j \in \{1, 2, \ldots, N_C\}$)
X_{e_j}	Necromass pools: e_1, metabolic litter (fast); e_2, structural debris (intermediate); e_3, humified/dissolved (slow)
X_f	Plant functional type
X_{g_j}	Soil (ground), layer j ($j \in \{1, 2, \ldots, N_G\}$)
X_q	Disturbance type
X_{s_j}	Temporary surface water/snowpack, layer j ($j \in \{1, 2, \ldots, N_S\}$)
X_{t_k}	Cohort k ($k \in \{1, 2, \ldots, N_T\}$)
X_u	Patch u ($u \in \{1, 2, \ldots, N_P\}$)
X_{y_k}	Property y of cohort k ($k \in \{1, 2, \ldots, N_T\}$). Possible values of y: branch wood (b), structural tissue (heartwood) (h), leaves (l), non-structural carbon storage (starch, sugars) (n), roots (r), total living tissues (α), branch boundary layer (β), carbon balance (Δ), leaf boundary layer (λ), reproductive tissues (ϱ), sapwood (σ)

$$\underbrace{\frac{\partial \alpha_q}{\partial t}}_{\text{Change rate}} = \underbrace{\frac{\partial \alpha_q}{\partial a}}_{\text{Aging}} - \underbrace{\sum_{q'=1}^{N_Q} \left(\lambda_{q'q} \, \alpha_q \right)}_{\text{Disturbance}}, \tag{3}$$

where m_f is mortality rate, which may depend on the PFT, size, and the individual carbon balance; $\mathbf{g}_f$ is the vector of the net growth rates for each carbon pool, which also may depend on the PFT, size, and carbon balance; $\nabla_{\mathbf{C}} \cdot$ ~~is the divergent~~is the divergence operator for the size vector; and $\lambda_{q'q}$ is the transition matrix from gaps generated by previous disturbance q' affected by new disturbance of type q, which may depend on environmental conditions. Boundary conditions are shown in Supplement S2.

Equation (2) and Eq. (3) cannot be solved analytically except for the most trivial cases; therefore the age distribution is discretized into patches (subscript u, $u \in 1, 2, \ldots, N_P$; Tab. 1) of similar age and same disturbance type, and the population size structure living in any given patch u is discretized into cohorts (subscript k, $k \in 1, 2, \ldots, N_T$; Tab. 1) of similar size and same PFT (Fig. 1). Unlike polygons and sites, patches and cohorts are dynamic levels: changes in distribution (fractional area) of patches are driven by aging and disturbance rates, whereas changes in the distribution of cohorts in each patch are driven by growth, mortality, and recruitment (Fig. S2).

The environment perceived by each plant (e.g. incident light, temperature, vapor pressure deficit) varies across large scales as a consequence of changes in climate (macro-environment), but also varies at small scales (within the landscape; micro-environment) because of the horizontal and vertical position of each individual relative to other individuals in the plant community (e.g. Bazzaz, 1979) and the position of the local community in landscapes with complex terrains. Both macro- and micro-environmental conditions drive the net primary productivity of each individual, and ultimately determine growth,

Table 2. Time steps associated with processes resolved by ED-2.2. The thermodynamic sub-step is dynamic and it depends on the error evaluation of the integrator, but it cannot be longer than the biophysics step, which is defined by the user. Other steps are fixed as of ED-2.2. Processes marked with ⋆ are presented in the main paper. Other processes are ~~briefly~~ described in Supplements S3 and S4.

Time Step	Time scale	Processes
Thermodynamics ($\Delta t_{\mathrm{Thermo}}$)	$1\,\mathrm{s}$ - Δt_{Bio}	⋆ Energy and water fluxes ⋆ Eddy fluxes (including CO_2 flux) ⋆ Most thermodynamic state functions
Biophysics (Δt_{Bio})	$2 - 15\,\mathrm{min}$	⋆ Meteorological and CO_2 Forcing ⋆ Radiation model ⋆ Photosynthesis model ⋆ Respiration fluxes (autotrophic and heterotrophic) ⋆ Evaluation of energy, water, and CO_2 budgets
Phenology (Δt_{Phen})	$1\,\mathrm{day}$	Maintenance of active tissues Update of the storage pool Leaf phenology Plant carbon balance Integration of mortality rate due to cold Soil litter pools
Cohort dynamics (Δt_{CD})	$1\,\mathrm{month}$	Growth of structural tissues Mortality rate Reproduction – Cohort creation Integration of fire disturbance rate Cohort fusion, fission, and extinction
Patch dynamics (Δt_{PD})	$1\,\mathrm{yr}$	Annual disturbance rates and patch creation Patch fusion and termination

mortality, and recruitment rates for each individual. Likewise, they can also affect the disturbance rates: for example, during
205 drought conditions (macro-environment) open canopy patches (micro-environment) may experience faster ground desiccation
and consequently increase local fire risk. To account for the variability in micro-environments within the landscape and within
local plant communities, in ED-2.2 the energy, water, and carbon dioxide cycles are solved separately for each patch, and
within each patch, fluxes and storage associated with individual plants are solved for each cohort.

The ED-2.2 model represents processes that have inherently different time scales, therefore the model also has a
210 hierarchy of time steps, in order to attain maximum computational efficiency (Table 2). Processes associated with the short-
term dynamics are presented in this manuscript. A summary of the phenological processes and those associated with longer
term dynamics is presented in ~~Supplement S3~~Supplements S3 and S4 (see also Moorcroft et al., 2001; Albani et al., 2006;
Medvigy et al., 2009).

2.2 Software requirements and model architecture

215 *Software requirements*. The ED-2.2 source code is mainly written in Fortran 90, with a few file management routines written in C. Most input and output files use the Hierarchical Data Format 5 (HDF5) format and libraries (The HDF Group, 2016). In addition, the Message Passing Interface (MPI) is highly recommended for regional simulations and is required for simulations coupled with the *Brazilian Improvements on Regional Atmospheric Modeling System* (BRAMS) atmospheric model (Knox et al., 2015; Swann et al., 2015; Freitas et al., 2017). The source code can be also compiled with Shared Memory

220 Processing (SMP) libraries, which enable parallel processing of thermodynamics and biophysics steps at the patch level, and thus allowing shorter simulation time.

Code design and parallel structure. ED-2.2 has been designed to be run in three different configurations; (1) As a stand-alone land-surface model over a small list of specified locations (sites)~~, or;~~ (2) as a stand-alone land-surface model distributed over a regional grid~~, or;~~ (3) as coupled with ~~the BRAMS atmospheric model as~~an atmospheric model distributed

225 over a regional grid (e.g. ED-BRAMS, Knox et al., 2015; Swann et al., 2015). For regional stand-alone grids, the model partitions the grid into spatially contiguous tiles of polygons, which access the initial and boundary conditions and are integrated independently of each other, but write the results to a unified output file using collective input/output functions from HDF5. In the case of simulations dynamically coupled with ~~the BRAMS model~~an atmospheric model such as BRAMS, polygons are defined to match each atmospheric grid cell.

230 *Memory allocation*. The code uses dynamic allocation of variables and extensive use of pointers to efficiently reduce the amount of data transferred between routines. To reduce the output file size, polygon-, site-, patch-, and cohort-level variables are always written as long vectors, and auxiliary index vectors are used to map variables from higher hierarchical levels to lower hierarchical levels (for example, to which patch a cohort-level variable belongs).

2.3 Model inputs

235 Every ED-2.2 simulation requires an initial state for forest structure and composition (initial state), a description of soil characteristics (edaphic conditions), and a time-varying list of meteorological drivers (atmospheric conditions).

Initial state. To initialize a plant community from inventory data, one must have either the diameter at breast height of every individual or the stem density of different diameter size classes, along with plant functional type identification and location; in addition necromass from the litter layer, woody debris and soil organic carbon are needed. Alternatively, initial

240 conditions can be obtained from airborne LiDAR measurements (Antonarakis et al., 2011, 2014) or a prescribed near bare ground condition may be used for long-term spin up simulations. Previous simulations can be used as initial conditions as well.

Edaphic conditions. The user must also provide soil characteristics such as total soil depth, total number of soil layers, the thickness of each layer, as well as soil texture, color and the bottom soil boundary condition (bedrock, reduced

245 drainage, free drainage, or permanent water table). This flexibility allows the user to easily adjust the soil characteristics according to their regions of interest. Soil texture can be read from standard data sets (e.g. Tempel et al., 1996; Hengl et al.,

Table 3. Atmospheric boundary conditions driving the ED-2.2 model. Variable names and ~~subscript~~subscripts follow a standard notation throughout the manuscript (Tables S1 and S2). Flux variables between two thermodynamic systems are defined by a dot and two indices separated by a comma, and they are positive when the net flux goes from the thermodynamic system represented by the first index to the one represented by the second index.

Variable	Description	Units
u_x	Zonal wind speed	$\mathrm{m\,s^{-1}}$
u_y	Meridional wind speed	$\mathrm{m\,s^{-1}}$
p_a	Free air pressure	Pa
T_a	Free air temperature	K
w_a	Free air specific humidity	$\mathrm{kg_W\,kg^{-1}}$
c_a	Free air CO_2 mixing ratio	$\mathrm{\mu mol_C\,mol^{-1}}$
z_a	Height of the reference point above canopy	m
$\dot{W}_{\infty,a}$	Precipitation mass rate	$\mathrm{kg_W\,m^{-2}\,s^{-1}}$
$\dot{Q}^{\Downarrow}_{\mathrm{TIR}(\infty,a)}$	Downward thermal infrared irradiance	$\mathrm{W\,m^{-2}}$
$\dot{Q}^{\odot}_{\mathrm{PAR}(\infty,a)}$	Downward photosynthetically active irradiance, direct	$\mathrm{W\,m^{-2}}$
$\dot{Q}^{\Downarrow}_{\mathrm{PAR}(\infty,a)}$	Downward photosynthetically active irradiance, diffuse	$\mathrm{W\,m^{-2}}$
$\dot{Q}^{\odot}_{\mathrm{NIR}(\infty,a)}$	Downward near infrared irradiance, direct	$\mathrm{W\,m^{-2}}$
$\dot{Q}^{\Downarrow}_{\mathrm{NIR}(\infty,a)}$	Downward near infrared irradiance, diffuse	$\mathrm{W\,m^{-2}}$

2017) or provided directly by the user. Soil layers, soil color and bottom boundary condition must be provided directly by the user as of ED-2.2. In addition, simulations with multiple sites per polygon also need to provide the fractional areas of each site and the mean soil texture class, soil depth, slope, aspect, elevation, and topographic moisture index of each site.

Atmospheric conditions. Meteorological conditions needed to drive ED-2.2 include temperature, specific humidity, CO_2 molar fraction, pressure of the air above the canopy, precipitation rate, incoming solar (shortwave) irradiance (radiation flux) and incoming thermal (longwave) irradiance (Table 3), at a reference height that is at least a few meters above the canopy. Sub-daily measurements (0.5-6 hours) are highly recommended so the model can properly simulate the diurnal cycle and interdiurnal variability. Meteorological drivers can be either at a single location (e.g. eddy covariance towers), or gridded meteorological drivers such as reanalysis (e.g. Dee et al., 2011; Gelaro et al., 2017) or bias-corrected products based on reanalysis (e.g. Sheffield et al., 2006; Weedon et al., 2014). Whenever available, CO_2 must be provided at comparable temporal and spatial resolution as other meteorological drivers; otherwise, it is possible to provide spatially homogeneous, time-variant CO_2, or constant CO_2, although this may increase uncertainties in the model predictions (e.g. Wang et al., 2007). Alternatively, the meteorological forcing (including CO_2) may be provided directly by BRAMS (Knox et al., 2015; Swann et al., 2015).

Plant functional types. The user must specify which plant functional types (PFTs) are allowed to occur in any given simulation. ED-2.2 has a list of default PFTs, with parameters described in Tables S5-S6. Alternatively, the user can modify the parameters of existing PFTs or define new PFTs through an extensible markup language (XML) file, which is read during the model initialization.

3   Overview of enthalpy, water, and carbon dioxide cycles

Here we present the fundamental equations that describe the biogeophysical and biogeochemical cycles. Because the envi-
ronmental conditions are a function of the local plant community and resources are shared by the individuals, these cycles
must be described at the patch level, and the response of the plant community can be aggregated to the polygon level once the
cycles are resolved for each patch. In ED-2.2, patches do not exchange enthalpy, water, and carbon dioxide with other patches;
270   thus patches are treated as independent systems. Throughout this section, we will only refer to the patch- and cohort-levels,
and indices associated with patches, sites and polygons will be omitted for clarity.

3.1   Definition of the thermodynamic state

Each patch is defined by a *thermodynamic envelope* (Fig. 2), comprised of multiple thermodynamic systems: each soil layer
(total number of layers N_G), each temporary surface water or snow layer (total number of layers N_S), leaves and branchwood
275   portion of each cohort (total number of cohorts N_T), and the canopy air space. For simplicity, roots are assumed to be in
thermal equilibrium with the soil layers and have negligible heat capacity compared to the soil layers. Although patches
do not exchange heat and mass with other patches, they are allowed to exchange heat and mass with the free air (i.e. the
atmosphere above and outside of the air-space control-volume we deem as within canopy) and lose water and associated
energy through surface and sub-surface runoff. We also assume that intensive variables such as pressure and temperature are
280   uniform within each thermodynamic system. Note that free air is not considered a thermodynamic system in ED-2 because
the thermodynamic state is determined directly from the boundary conditions, and thus external to the model.

The fundamental equations that describe the system thermodynamics are the first law of thermodynamics in terms
of enthalpy H ($\mathrm{J\,m^{-2}}$), and the mass continuity for incompressible fluids for total water mass W ($\mathrm{kg_W\,m^{-2}}$):

$$\underbrace{\frac{\mathrm{d}H}{\mathrm{d}t}}_{\text{Change in enthalpy}} = \underbrace{\dot{Q}}_{\text{Net heat flux}} + \underbrace{\dot{H}}_{\text{Enthalpy flux due to mass flux}} + \underbrace{\mathcal{V}\frac{\mathrm{d}p}{\mathrm{d}t}}_{\text{Pressure change}} , \qquad (4)$$

$$\underbrace{\frac{\mathrm{d}W}{\mathrm{d}t}}_{\text{Change in water mass}} = \underbrace{\dot{W}}_{\text{Net water mass flux}} , \qquad (5)$$

where $\mathcal{V}$ is the volume of the thermodynamic system and p is the ambient pressure. The components on the right-hand side
of Eq. (4) and Eq. (5) depend on the thermodynamic system, and will be presented in detail in the following sections. Net
heat fluxes ($\dot{Q}$) represent changes in enthalpy that are not associated with mass exchange (radiative and sensible heat fluxes),
whereas the remaining enthalpy fluxes ($\dot{H}$) correspond to changes in heat capacity due to addition or removal of mass from
290   each thermodynamic system.

The merit of solving the changes in enthalpy over internal energy is that changes in enthalpy are equivalent to the
net energy flux when pressure is constant (Eq. 4). Pressure is commonly included in atmospheric measurements, making it
easy to track changes in enthalpy not related to energy fluxes. In reality, the only thermodynamic system where the distinction

12

Table 4. List of state variables solved in ED-2.2. Unless otherwise noted, the reference equation is the ordinary differential equation that defines the rate of change of the thermodynamic state. The list of fluxes that describe the thermodynamic state is presented in Table 5. For a complete list of subscripts and variables used in this manuscript, refer to Tables S1-S2.

State variable	Description	Units	~~Budget~~Reference equation
c_c	CO_2 mixing ratio — canopy air space	$\mu mol_C \, mol^{-1}$	(23)
h_c	Specific enthalpy — canopy air space	$J \, kg^{-1}$	(18)
$\mathcal{H}_{g_j}$	Volumetric enthalpy — soil layer j	$J \, m^{-3}$	(4)[a]
H_{s_j}	Enthalpy — temporary surface water layer j	$J \, m^{-2}$	(4)
H_{t_k}	Enthalpy — cohort k	$J \, m^{-2}$	(4)
p_c	Atmospheric pressure — canopy air space	Pa	(S81)[b]
w_c	Specific humidity — canopy air space	$kg_W \, kg^{-1}$	(19)
W_{s_j}	Water mass — ~~TSW~~temporary surface water layer j	$kg_W \, m^{-2}$	(5)
W_{t_k}	Intercepted/dew/frost water mass — cohort k	$kg_W \, m^{-2}$	(5)
z_c	Depth (specific volume) — canopy air space	m	(17)[c]
ϑ_{g_j}	Volumetric soil moisture — soil layer j	$m_W^3 \, m^{-3}$	(5)[a]

[a] Budget fluxes are in units of area, and the state variable is updated following the conversion described in Section 3.2.1.
[b] Canopy air space pressure is not solved using ordinary differential equations, but based on the atmospheric pressure from the meteorological forcing.
[c] Canopy air space depth is determined from vegetation characteristics, not from an ordinary differential equation.

between internal energy and enthalpy matters is the canopy air space. Work associated with thermal expansion of solids and liquids is several orders of magnitude smaller than heat (Dufour and van Mieghem, 1975), and changes in pressure contribute significantly less to enthalpy because the specific volume of solids and liquids are comparatively small. Likewise, enthalpy fluxes that do not involve gas phase (e.g. canopy dripping and runoff) are nearly indistinguishable from internal energy flux, whereas differences between enthalpy and internal energy fluxes are significant when gas phase is involved (e.g. transpiration and eddy flux). For simplicity, from this point on we will use the term *enthalpy* whenever internal energy is indistinguishable from enthalpy. The complete list of state variables in ED-2.2 is shown in Table 4.

Variations in enthalpy are more important than their actual values, but they must be consistently defined relative to a pre-determined and known thermodynamic state, at which we define enthalpy to be zero. For any material other than water, enthalpy is defined as zero when the material temperature is $0 \, K$; for water, enthalpy is defined as zero when water is at $0 \, K$ and completely frozen. The general definitions of enthalpy and internal energy states used in all thermodynamic systems in ED-2.2 are described in Supplement S5. In ED-2.2, enthalpy is used as the prognostic variable because these are directly and linearly related to the governing ordinary differential equation (Eq. 4). Temperature is diagnostically obtained based on the heat capacity of each thermodynamic system, and the heat capacities of different thermodynamic systems are defined in Supplement S6.

3.2   Heat ($\dot{Q}$), water ($\dot{W}$), and enthalpy ($\dot{H}$) fluxes

The enthalpy and water cycles for each patch in ED-2.2 are summarized in Fig. 2, and these cycles are solved every thermodynamic sub-step (Δt_{Thermo}), using a fourth-order Runge-Kutta integrator with dynamic time steps to maintain the error within prescribed tolerance. For all fluxes and variables, we follow the subscript notation described in Table S1, and denote
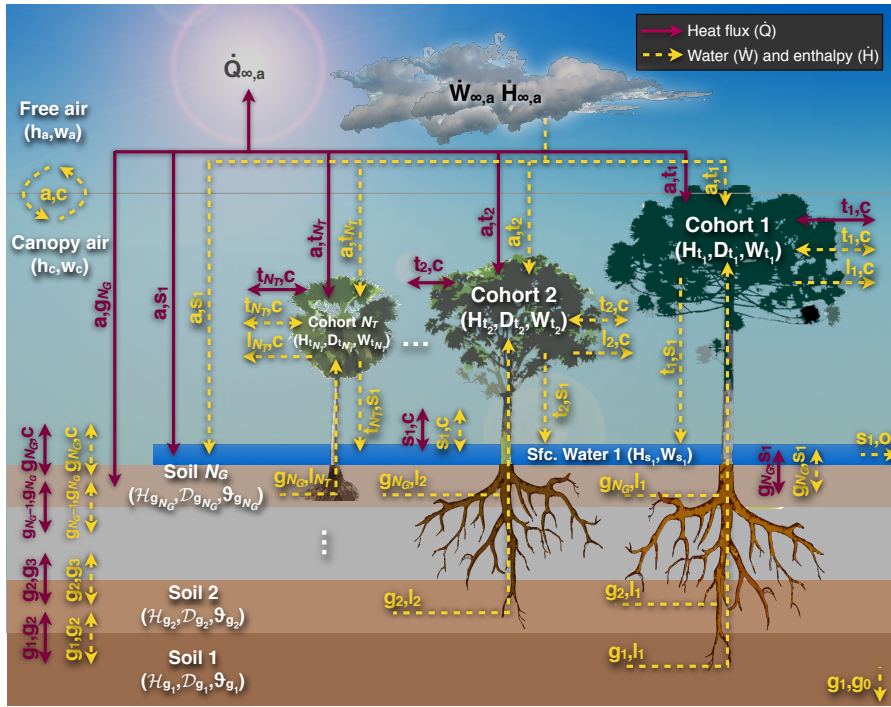
Figure 2. Schematic of the fluxes that are solved in ED-2.2 for a single patch (thermodynamic envelope). In this example, the patch has N_T cohorts, N_G soil layers and $N_S = 1$ temporary surface water. Both N_G and the maximum N_S are specified by the user; N_T is dynamically defined by ED-2.2.. Letters near the arrows are the subscripts associated with fluxes, although the ~~flux variable has~~flux variables have been omitted here for clarity. Solid red arrows represent heat flux with no exchange of mass, and dashed yellow arrows represent exchange of mass and associated enthalpy. Arrows that point to a single direction represent fluxes that can only go in one (non-negative) direction, and arrows pointing to both directions represent fluxes that can be positive, negative, or zero.

flux variables with a dot and two indices separated by a comma, denoting the systems impacted by the flux. For any variable X with that has flux between a system m and a system n, we assume that $\dot{X}_{m,n} > 0$ when the net flux goes from system m to system n, and that $\dot{X}_{m,n} = -\dot{X}_{n,m}$. Arrows in Fig. 2 indicate the directions allowed in ED-2.2. The list of fluxes solved in ED-2.2 is provided in Table 5, and a complete list of variables is provided in Table S2. In addition, the values of global constants and global parameters are listed in Tables S3 and S4, respectively, and the default parameters specific for each tropical plant functional type are presented in Tables S5-S6~~, similar parameters for temperate plant functional types are found in Medvigy et al. (2009)~~.

Comment: No longer needed as we added Table S6.

3.2.1 Soil

In ED-2.2, the soil characteristics (number of soil layers, thickness of each soil layer and total soil depth, soil texture, soil color) are defined by the user, and assumed constant throughout the simulation. Within each patch, each soil layer (comprised by soil matrix and soil water in each layer) is considered a separate thermodynamic system, with the main size dimension being the layer thickness Δz_{g_j}, with $j = 1$ being the deepest soil layer, and $j = N_G$ being the topmost soil layer. Typically,

Table 5. List of energy, water, and carbon dioxide fluxes that define the thermodynamic state in ED-2.2, along with sections and ~~equation~~equations that define them. Fluxes are denoted by a dotted letter, and two subscripts separated with a comma: $\dot{X}_{m,n}$. Positive fluxes go from thermodynamic system m to thermodynamic system n; negative fluxes go in the opposite direction. Acronyms in the description column: canopy air space (CAS); temporary surface water (TSW). The complete list of subscripts and variables used in this manuscript is available in Tables S1-S2, and the list of state variables is shown in Table 4.

Variable	Description	Section	Equation	Units
$\dot{C}_{a,c}$	CO_2 flux from turbulent mixing	4.4	55	
$\dot{C}_{e_j,c}$	Heterotrophic respiration flux (soil carbon pool e_j)	4.8	102	
$\dot{C}_{l_k,c}$	Net leaf (cohort k)–CAS CO_2 flux[a]	4.6	93	$\mathrm{mol_C\,m^{-2}\,s^{-1}}$
$\dot{C}_{n_k,c}$	Storage turnover (cohort k) respiration flux	4.7	100	
$\dot{C}_{r_k,c}$	Fine-root (cohort k) metabolic respiration flux	4.7	99	
$\dot{C}_{\Delta_k,c}$	Growth and maintenance (cohort k) respiration flux	4.7	101	
$\dot{Q}_{a,g_{NG}}$	Net absorbed irradiance (topmost soil layer)	4.3.2	52	
$\dot{Q}_{a,s_j}$	Net absorbed irradiance (TSW layer j)	4.3.2	51	
$\dot{Q}_{a,t_k}$	Net absorbed irradiance (cohort k)	4.3.1	49	
$\dot{Q}_{g_{NG},c}$	Ground–CAS net sensible heat flux	4.5.2	68	$\mathrm{W\,m^{-2}}$
$\dot{Q}_{g_{j-1},g_j}$	Net sensible heat flux between two soil layers	4.1	26	
$\dot{Q}_{s_{NS},c}$	TSW–CAS net sensible heat flux	4.5.2	66	
$\dot{Q}_{s_{j-1},s_j}$	Net sensible heat flux between two TSW layers	4.1	27	
$\dot{Q}_{t_k,c}$	Cohort k–CAS net sensible heat flux	4.5.1	60	
$\dot{H}_{a,c}$	Enthalpy flux from turbulent mixing at the top of CAS.	4.4	54	
$\dot{H}_{a,s_{NS}}$	Enthalpy flux to the top TSW layer associated with throughfall precipitation	4.2	42	
$\dot{H}_{a,t_k}$	Enthaply flux associated with rainfall interception by cohort k	4.2	41	
$\dot{H}_{g_{NG},c}$	Enthalpy flux associated with ground–CAS evaporation[b]	4.5.3	75	
$\dot{H}_{g_{j-1},g_j}$	Enthalpy flux associated with water percolation between two soil layers	4.1	35	
$\dot{H}_{g_j,l_k}$	Enthalpy flux associated with soil water extraction from soil layer j by cohort k	4.6	97	$\mathrm{W\,m^{-2}}$
$\dot{H}_{g_1,g_0}$	Enthalpy flux associated with sub-surface runoff from the bottom soil layer	4.1	29	
$\dot{H}_{l_k,c}$	Enthalpy flux associated with transpiration by cohort k	4.6	98	
$\dot{H}_{s_{NS},c}$	Enthalpy flux associated with TSW–CAS evaporation[b]	4.5.3	75	
$\dot{H}_{s_{NS},o}$	Enthalpy flux associated with surface runoff from the top TSW layer	4.1	34	
$\dot{H}_{s_{j-1},s_j}$	Enthalpy flux associated with water percolation between two TSW layers	4.1	35	
$\dot{H}_{t_k,c}$	Enthalpy flux associated with evaporation[b] of intercepted water (cohort k)	4.5.3	75	
$\dot{H}_{t_k,s_{NS}}$	Enthalpy flux associated with canopy dripping from cohort k to the top TSW layer	4.2	44	
$\dot{W}_{a,c}$	Water flux from turbulent mixing at the top of CAS.	4.4	53	
$\dot{W}_{a,s_{NS}}$	Precipitation throughfall flux to the top TSW layer	4.2	37	
$\dot{W}_{a,t_k}$	Water flux from rainfall interception (cohort k)	4.2	36	
$\dot{W}_{g_{NG},c}$	Ground–CAS evaporation[b] flux	4.5.2	69	
$\dot{W}_{g_{j-1},g_j}$	Water percolation flux between two soil layers	4.1	28	
$\dot{W}_{g_j,l_k}$	Water flux associated with soil water extraction by plants	4.6	96	$\mathrm{kg_W\,m^{-2}\,s^{-1}}$
$\dot{W}_{g_1,g_0}$	Water flux associated with sub-surface runoff from the bottom soil layer	4.1	33	
$\dot{W}_{l_k,c}$	Transpiration flux (cohort k)	4.6	94	
$\dot{W}_{s_{j-1},s_j}$	Water percolation flux between two TSW layers	4.1	30–31	
$\dot{W}_{s_{NS},o}$	Surface runoff water flux from the top TSW layer	4.1	34	
$\dot{W}_{s_{NS},c}$	TSW–CAS evaporation[b] flux	4.5.2	67	
$\dot{W}_{t_k,c}$	Evaporation[b] flux from intercepted water (cohort k)	4.5.1	61	
$\dot{W}_{t_k,s_{NS}}$	Canopy dripping flux from cohort k to the top TSW layer	4.2	43	

[a] Net flux between leaf respiration (positive) and gross primary productivity (negative).
[b] When negative, this flux corresponds to dew or frost formation.

325 the top layer thickness is set to $\Delta z_{g_{N_G}} = 0.02\,\mathrm{m}$, which is a compromise between computational efficiency and ability to represent the stronger gradients near the surface, and layers with increasing thickness (Δz_{g_j}) are added for the entire rooting zone.

The thermodynamic state is defined in terms of the soil volume: the bulk specific enthalpy $\mathcal{H}_{g_j}$ ($\mathrm{J\,m^{-3}}$) and volumetric soil water content ϑ_{g_j} ($\mathrm{m_W^3\,m^{-3}}$), which can be related to Eq. (4)-(5) by defining $H_{g_j} = \mathcal{H}_{g_j}\Delta z_{g_j}$ and $W_{g_j} = \rho_\ell \cdot \vartheta_{g_j} \cdot \Delta z_{g_j}$, where ρ_ℓ is the density of liquid water (Table S3). Soil net fluxes for any layer j are defined as:

$$\underbrace{\dot{Q}_{g_j}}_{\substack{\text{Net heat flux}}} = \underbrace{\dot{Q}_{g_{j-1},g_j} - \dot{Q}_{g_j,g_{j+1}}}_{\substack{\text{Net sensible heat flux} \\ \text{between consecutive layers} \\ (4.1)}} + \underbrace{\delta_{g_j g_{N_G}}\dot{Q}_{a,g_{N_G}}}_{\substack{\text{Absorbed irradiance} \\ (4.3.2)}} - \underbrace{\delta_{g_j g_{N_G}}\dot{Q}_{g_{N_G},c}}_{\substack{\text{Ground--CAS sensible heat} \\ (4.5.2 \text{ and } 4.5.3)}} \quad , \tag{6}$$

$$\underbrace{\dot{H}_{g_j}}_{\substack{\text{Net enthalpy flux} \\ \text{due to water flux}}} = \underbrace{\dot{H}_{g_{j-1},g_j} - \dot{H}_{g_j,g_{j+1}}}_{\substack{\text{Water percolation} \\ \text{between consecutive layers} \\ (4.1)}} - \underbrace{\delta_{g_j g_{N_G}}\dot{H}_{g_{N_G},c}}_{\substack{\text{Gnd. Evaporation} \\ (4.5.2 \text{ and } 4.5.3)}} - \underbrace{\sum_{k=1}^{N_T}\dot{H}_{g_j,l_k}}_{\substack{\text{Water uptake} \\ \text{by cohorts} \\ (4.6)}}, \tag{7}$$

$$\underbrace{\dot{W}_{g_j}}_{\substack{\text{Net water flux}}} = \underbrace{\dot{W}_{g_{j-1},g_j} - \dot{W}_{g_j,g_{j+1}}}_{\substack{\text{Water percolation} \\ \text{between consecutive layers} \\ (4.1)}} - \underbrace{\delta_{g_j g_{N_G}}\dot{W}_{g_{N_G},c}}_{\substack{\text{Gnd. Evaporation} \\ (4.5.2 \text{ and } 4.5.3)}} - \underbrace{\sum_{k=1}^{N_T}\dot{W}_{g_j,l_k}}_{\substack{\text{water uptake} \\ \text{by cohorts} \\ (4.6)}}, \tag{8}$$

where $\delta_{g_j g_{j'}}$ is the Kronecker delta for comparing two soil layers g_j and $g_{j'}$ (1 if $g_j = g_{j'}$; 0 otherwise), CAS is the canopy air space, and subscript o denotes the loss through runoff. References in parentheses underneath the terms correspond to the sections in which each term is presented in detail. In the equations above, we assume $\dot{Q}_{g_0,g_1}$ to be zero (bottom boundary condition in thermal equilibrium), and ($\dot{H}_{g_1,g_0} = -\dot{H}_{g_0,g_1}$; $\dot{W}_{g_1,g_0} = -\dot{W}_{g_0,g_1}$) to be sub-surface runoff fluxes (see section 4.1). In addition, ($\dot{Q}_{g_{N_G},g_{N_G+1}}$; $\dot{H}_{g_{N_G},g_{N_G+1}}$; $\dot{W}_{g_{N_G},g_{N_G+1}}$) are equivalent to ($\dot{Q}_{g_{N_G},s_1}$; $\dot{H}_{g_{N_G},s_1}$; $\dot{W}_{g_{N_G},s_1}$), which are the fluxes between the topmost soil layer and the bottommost temporary surface water layer (see also section 3.2.2).

3.2.2 Temporary surface water (TSW)

Temporary surface water (TSW) exists whenever water falls to the ground, or dew or frost develops on the ground. The layer will be maintained only when the amount of water that reaches the ground exceeds the water holding capacity of the top soil layer (a function of the soil porosity), or when precipitation falls as snow. The maximum number of temporary surface water layers $N_S^{\max}$ is defined by the user, but the actual number of layers N_S and the thickness of each layer depends on the total mass and the water phase, following Walko et al. (2000). When the layer is in liquid phase, only one layer ($N_S = 1$) is maintained. If a snowpack develops, the temporary surface water can be divided into several layers (subscript j, with $j = 1$ being the deepest soil layer, and $j = N_S$ being the topmost TSW layer). Net TSW fluxes are defined as:

$$\underbrace{\dot{Q}_{s_j}}_{\substack{\text{Net heat flux}}} = \underbrace{\dot{Q}_{s_{j-1},s_j} - \dot{Q}_{s_j,s_{j+1}}}_{\substack{\text{Net sensible heat flux}\\ \text{between consecutive layers}\\ (4.1)}} + \underbrace{\dot{Q}_{a,s_j}}_{\substack{\text{Absorbed irradiance}\\ (4.3.2)}} - \underbrace{\delta_{s_j s_{N_S}} \dot{Q}_{s_{N_S},c}}_{\substack{\text{Ground–CAS sensible heat}\\ (4.5.2 \text{ and } 4.5.3)}} , \tag{9}$$

$$\underbrace{\dot{H}_{s_j}}_{\substack{\text{Net enthalpy flux}\\ \text{due to water flux}}} = \underbrace{\dot{H}_{s_{j-1},s_j} - \dot{H}_{s_j,s_{j+1}}}_{\substack{\text{Water percolation}\\ \text{between consecutive layers}\\ (4.1)}} + \underbrace{\delta_{s_j s_{N_S}} \dot{H}_{a,s_{N_S}}}_{\substack{\text{Throughfall}\\ \text{precipitation}\\ (4.2)}} + \underbrace{\delta_{s_j s_{N_S}} \left(\sum_{k=1}^{N_T} \dot{H}_{t_k,s_{N_S}} \right)}_{\substack{\text{Canopy dripping}\\ \text{from cohorts}\\ (4.2)}} - \underbrace{\delta_{s_j s_{N_S}} \dot{H}_{s_{N_S},o}}_{\substack{\text{Surface runoff}\\ (4.1)}} - \underbrace{\delta_{s_j s_{N_S}} \dot{H}_{s_{N_S},c}}_{\substack{\text{Surface water}\\ \text{evaporation}\\ (4.5.2 \text{ and } 4.5.3)}}, \tag{10}$$

$$\underbrace{\dot{W}_{s_j}}_{\substack{\text{Water flux}}} = \underbrace{\dot{W}_{s_{j-1},s_j} - \dot{W}_{s_j,s_{j+1}}}_{\substack{\text{Water percolation}\\ \text{between consecutive layers}\\ (4.1)}} + \underbrace{\delta_{s_j s_{N_S}} \dot{W}_{a,s_{N_S}}}_{\substack{\text{Throughfall}\\ \text{precipitation}\\ (4.2)}} + \underbrace{\delta_{s_j s_{N_S}} \left(\sum_{k=1}^{N_T} \dot{W}_{t_k,s_{N_S}} \right)}_{\substack{\text{Canopy dripping}\\ \text{from cohorts}\\ (4.2)}} - \underbrace{\delta_{s_j s_{N_S}} \dot{W}_{s_{N_S},o}}_{\substack{\text{Surface runoff}\\ (4.1)}} - \underbrace{\delta_{s_j s_{N_S}} \dot{W}_{s_{N_S},c}}_{\substack{\text{Surface water}\\ \text{evaporation}\\ (4.5.2 \text{ and } 4.5.3)}}, \tag{11}$$

where $\delta_{s_j s_{j'}}$ is the Kronecker delta for comparing two TSW layers s_j and $s_{j'}$ (1 if $s_j = s_{j'}$; 0 otherwise), CAS is the canopy air space, and subscript o denotes loss from the thermodynamic envelope through runoff. Terms are described in detail in the sections shown underneath each term. Similarly to the soil fluxes (Section 3.2.1), we assume that $(\dot{Q}_{s_0,s_1}; \dot{H}_{s_0,s_1}; \dot{W}_{s_0,s_1})$ is equivalent to $(\dot{Q}_{g_{N_G},s_1}; \dot{H}_{g_{N_G},s_1}; \dot{W}_{g_{N_G},s_1})$, the fluxes between the topmost soil layer and the bottommost TSW layer. When solving Eq. (9)-(11) for layer s_{N_S}, we assume the terms $\dot{Q}_{s_j,s_{j+1}}$, $\dot{H}_{s_j,s_{j+1}}$ and $\dot{W}_{s_j,s_{j+1}}$ to be all zero, as layer $N_S + 1$ does not exist.

In the case of liquid TSW, the layer thickness of the single layer is defined as $\Delta z_{s_1} = \rho_\ell^{-1} W_{s_1}$, where ρ_ℓ is the density of liquid water (Table S3). In the case of snowpack development, the snow density and the layer thickness of the TSW are solved as described in Supplement S7. The thickness of each layer of snow (Δz_{s_j}) is defined using the same algorithm as LEAF-2 (Walko et al., 2000) and ~~described~~is described in Supplement S7.

3.2.3 Vegetation

In ED-2.2, vegetation is solved as an independent thermodynamic system only if the cohort is sufficiently large. The minimum size is an adjustable parameter and the typical minimum heat capacity solved by ED-2.2 is on the order of $10 \, \mathrm{J \, m^{-2} \, K^{-1}}$ and total area index of $0.005 \, \mathrm{m^2_{leaf+wood} \, m^{-2}}$. Cohorts smaller than this are excluded from all energy and water cycle calculations and assumed to be in thermal equilibrium with canopy air space. The net fluxes of heat, enthalpy and water for each cohort k that can be resolved are:

$$\underbrace{\dot{Q}_{t_k}}_{\substack{\text{Net heat flux}}} = \underbrace{\dot{Q}_{a,t_k}}_{\substack{\text{Cohort's net}\\ \text{absorbed irradiance}\\ (4.3.1)}} - \underbrace{\dot{Q}_{t_k,c}}_{\substack{\text{Cohort–CAS}\\ \text{sensible heat}\\ (4.5.1)}} , \tag{12}$$

$$\underbrace{\dot{H}_{t_k}}_{\substack{\text{Net enthalpy flux} \\ \text{due to water flux}}} = \underbrace{\dot{H}_{a,t_k}}_{\substack{\text{Rainfall} \\ \text{interception} \\ \text{(4.2)}}} - \underbrace{\dot{H}_{t_k,s_{N_S}}}_{\substack{\text{Canopy dripping} \\ \text{(4.2)}}} + \underbrace{\left(\sum_{j=1}^{N_G} \dot{H}_{g_j,l_k} \right)}_{\substack{\text{Ground water} \\ \text{uptake (transpiration)} \\ \text{(4.6)}}} - \underbrace{\dot{H}_{l_k,c}}_{\substack{\text{Transpiration} \\ \text{(4.6)}}} - \underbrace{\dot{H}_{t_k,c}}_{\substack{\text{Evaporation of} \\ \text{intercepted water} \\ \text{(4.5.3)}}} , \tag{13}$$

$$\underbrace{\dot{W}_{t_k}}_{\substack{\text{Water flux}}} = \underbrace{\dot{W}_{a,t_k}}_{\substack{\text{Rainfall} \\ \text{interception} \\ \text{(4.2)}}} - \underbrace{\dot{W}_{t_k,s_{N_S}}}_{\substack{\text{Canopy dripping} \\ \text{(4.2)}}} + \underbrace{\left(\sum_{j=1}^{N_G} \dot{W}_{g_j,l_k} \right)}_{\substack{\text{Ground water} \\ \text{uptake (transpiration)} \\ \text{(4.6)}}} - \underbrace{\dot{W}_{l_k,c}}_{\substack{\text{Transpiration} \\ \text{(4.6)}}} - \underbrace{\dot{W}_{t_k,c}}_{\substack{\text{Evaporation of} \\ \text{intercepted water} \\ \text{(4.5.3)}}} . \tag{14}$$

Each term is described in detail in the sections shown underneath each term on the right-hand side of Eq. (12)-(14).

3.2.4 Canopy air space (CAS)

The canopy air space is a gas, therefore extensive properties akin to the other thermodynamic systems are not intuitive because total mass and total volume cannot be directly compared to observations. Therefore, all prognostic and diagnostic variables are solved in the intensive form. Total enthalpy H_c and total water mass W_c of the canopy air space can be written in terms of air density ρ_c and the equivalent depth of the canopy air space $\overline{z}_c$ as:

$$H_c = \rho_c \overline{z}_c h_c, \tag{15}$$

$$W_c = \rho_c \overline{z}_c w_c, \tag{16}$$

$$\overline{z}_c = \max \left(5.0, \frac{\sum_{k=1}^{N_{T(\text{canopy})}} n_{t_k} \, \text{BA}_{t_k} \, z_{t_k}}{\sum_{k=1}^{N_{T(\text{canopy})}} n_{t_k} \, \text{BA}_{t_k}} \right), \tag{17}$$

where BA_{t_k} (cm^2) and z_{t_k} (m) are the basal area and the height of cohort k, respectively; and $N_{T(\text{canopy})}$ is the number of cohorts that are in the canopy, and we assume that cohorts are ordered from tallest to shortest. In case the canopy is open, $N_{T(\text{canopy})}$ is the total number of cohorts, and a minimum value of 5m is imposed when vegetation is absent or too short, to prevent numerical instabilities. Because the equivalent canopy depth depends only on the cohort size, $\overline{z}_c$ is updated at the cohort dynamics step (Δt_{CD}, Table 2). If we substitute Eq. (15) and Eq. (16) into Eq. (4) and Eq. (5), respectively, and assume that changes in density over short time steps are much smaller than changes in enthalpy or humidity, and then we obtain the following equations for the canopy air space budget:

$$\frac{\text{d}h_c}{\text{d}t} = \frac{1}{\rho_c \overline{z}_c} \left(\dot{Q}_c + \dot{H}_c + \overline{z}_c \frac{\text{d}p_c}{\text{d}t} \right), \tag{18}$$

$$\frac{\text{d}w_c}{\text{d}t} = \frac{1}{\rho_c \overline{z}_c} \dot{W}_c, \tag{19}$$

18

where

$$
\underbrace{\dot{Q}_c}_{\text{Net heat flux}} = \underbrace{\left(\sum_{k=1}^{N_T} \dot{Q}_{t_k,c}\right)}_{\substack{\text{Cohort–CAS} \\ \text{sensible heat (4.5.1 and 4.5.3)}}} + \underbrace{\dot{Q}_{s_{N_S},c}}_{\substack{\text{Surface water–CAS} \\ \text{sensible heat (4.5.2 and 4.5.3)}}} + \underbrace{\dot{Q}_{g_{N_G},c}}_{\substack{\text{Ground–CAS} \\ \text{sensible heat (4.5.2 and 4.5.3)}}} , \tag{20}
$$

$$
\underbrace{\dot{H}_c}_{\text{Net enthalpy flux}} = \underbrace{\dot{H}_{a,c}}_{\substack{\text{Enthalpy flux from} \\ \text{Turbulent mixing (4.4)}}} + \underbrace{\left(\sum_{k=1}^{N_T} \dot{H}_{t_k,c}\right)}_{\substack{\text{Evaporation of} \\ \text{intercepted water} \\ \text{(4.5.1 and 4.5.3)}}} + \underbrace{\left(\sum_{k=1}^{N_T} \dot{H}_{l_k,c}\right)}_{\substack{\text{Transpiration} \\ \text{(4.6)}}} + \underbrace{\dot{H}_{s_{N_S},c}}_{\substack{\text{Surface water} \\ \text{evaporation} \\ \text{(4.5.2 and 4.5.3)}}} + \underbrace{\dot{H}_{g_{N_G},c}}_{\substack{\text{Ground evaporation} \\ \text{(4.5.2 and 4.5.3)}}} , \tag{21}
$$

$$
\underbrace{\dot{W}_c}_{\text{Water flux}} = \underbrace{\dot{W}_{a,c}}_{\substack{\text{Water flux from} \\ \text{Turbulent mixing (4.4)}}} + \underbrace{\left(\sum_{k=1}^{N_T} \dot{W}_{t_k,c}\right)}_{\substack{\text{Evaporation of} \\ \text{intercepted water} \\ \text{(4.5.1 and 4.5.3)}}} + \underbrace{\left(\sum_{k=1}^{N_T} \dot{W}_{l_k,c}\right)}_{\substack{\text{Transpiration} \\ \text{(4.6)}}} + \underbrace{\dot{W}_{s_{N_S},c}}_{\substack{\text{Surface water} \\ \text{evaporation} \\ \text{(4.5.2 and 4.5.3)}}} + \underbrace{\dot{W}_{g_{N_G},c}}_{\substack{\text{Ground evaporation} \\ \text{(4.5.2 and 4.5.3)}}} . \tag{22}
$$

Unlike in the other thermodynamic systems (soil, temporary surface water, and vegetation), the net enthalpy flux of the canopy air space is not exclusively due to associated water flux: the eddy flux between the free air and the canopy air space ($\dot{H}_{a,c}$) includes both water transport and flux associated with mixing of air with different temperatures, and thus enthalpy, between canopy air space and free air.

In addition, we must also track the canopy-air-space pressure p_c. In ED-2.2, CAS pressure is not solved through a differential equation: instead p_c is updated whenever the meteorological forcing is updated, using the ideal gas law and hydrostatic equilibrium following the method described in Supplement S8. The rate of change of canopy air pressure is then applied in Eq. (18). Likewise, CAS density (ρ_c) is updated at the end of each thermodynamic step to ensure that the CAS conforms to the ideal gas law.

3.3 Carbon dioxide cycle

In ED-2.2, the carbon dioxide cycle is a subset of the full carbon cycle, which is shown in Fig. 3. The canopy air space is the only thermodynamic system with CO_2 storage that is solved by ED-2.2; nonetheless, we assume that the contribution of CO_2 to density and heat capacity of the canopy air space is negligible, hence only the molar CO_2 mixing ratio c_c ($\mathrm{mol_C\ mol^{-1}}$) is traced.

The change in CO_2 storage in the canopy air space is determined by the following differential equation:

$$
\frac{\mathrm{d}c_c}{\mathrm{d}t} = \frac{\mathcal{M}_d}{\mathcal{M}_C} \frac{1}{\rho_c \bar{z}_c} \dot{C}_c, \tag{23}
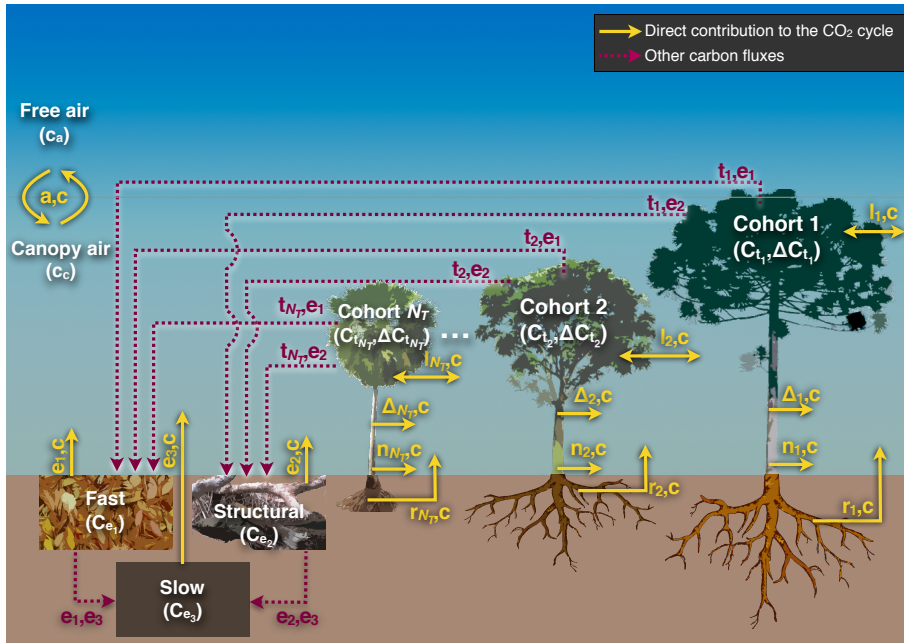$$

Figure 3. Schematic of the patch-level carbon cycle solved in ED-2.2 for a patch containing ~~two~~N_T cohorts. Like Figure 2, letters near the arrows are the subscripts associated with fluxes. Fluxes shown in solid yellow lines are part of the CO_2 cycle discussed in this manuscript, and dashed red lines lines are part of the carbon cycle but do not directly affect the CO_2 flux; these fluxes are summarized in Supplements S3 and S4.

$$\underbrace{\dot{C}_c}_{\substack{\text{Net carbon flux}}} = \underbrace{\dot{C}_{a,c}}_{\substack{\text{Carbon flux from}\\\text{Turbulent mixing}\\(4.4)}} + \underbrace{\sum_{k=1}^{N_T}\dot{C}_{l_k,c}}_{\substack{\text{Net Leaf–CAS flux}\\(\text{Respiration-GPP})\\(4.6)}} + \underbrace{\sum_{k=1}^{N_T}\dot{C}_{r_k,c}}_{\substack{\text{Fine-root}\\\text{Respiration}\\(4.7)}} + \underbrace{\sum_{k=1}^{N_T}\dot{C}_{n_k,c}}_{\substack{\text{Storage turnover}\\\text{Respiration}\\(4.7)}} + \underbrace{\sum_{k=1}^{N_T}\dot{C}_{\Delta_k,c}}_{\substack{\text{Growth and maintenance}\\\text{Respiration}\\(4.7)}} + \underbrace{\sum_{j=1}^{3}\dot{C}_{e_j,c}}_{\substack{\text{Heterotrophic}\\\text{Respiration}\\(4.8)}}, \tag{24}$$

where $\mathcal{M}_d$ and $\mathcal{M}_C$ are the molar masses of dry air and carbon, respectively, used to convert mass to molar fraction (1 $\text{mol}_\text{C} = 1$ mol_{CO_2}). The terms on the right-hand side of Eq. (24) are described in detail in the sections displayed underneath each term. The net leaf–CAS flux ($\dot{C}_{l_k,c}$) for any cohort k is positive when leaf respiration exceeds photosynthetic assimilation. The heterotrophic respiration is based on a simplified implementation of the CENTURY model (Bolker et al., 1998) that combines the decomposition rates from three soil carbon pools, defined by their characteristic life time: fast (metabolic litter and microbial; e_1), intermediate (structural debris; e_2), and slow (humified and passive soil carbon; e_3). Note that the soil carbon pools are not directly related to the soil layers used to describe the thermodynamic state (Section 3.2.1).

In addition to canopy air space, we also define a virtual cohort pool of carbon corresponding to the accumulated carbon balance (C_{Δ_k}). The accumulated carbon balance links short-term carbon cycle components such as photosynthesis and respiration with long-term dynamics that depend on carbon balance such as such as carbon allocation to growth and

20

reproduction, and mortality (Long-term dynamics described in Supplement S3). The accumulated carbon balance is defined by the following equation:

$$\underbrace{\frac{\mathrm{d}C_{\Delta_k}}{\mathrm{d}t}}_{\substack{\text{Change in} \\ \text{carbon balance}}} = -\underbrace{\dot{C}_{l_k,c}}_{\substack{\text{Net Leaf–CAS flux} \\ \text{(Respiration-GPP)} \\ \text{(4.6)}}} - \underbrace{\dot{C}_{r_k,c}}_{\substack{\text{Fine-root} \\ \text{Respiration} \\ \text{(4.7)}}} - \underbrace{\dot{C}_{n_k,c}}_{\substack{\text{Storage turnover} \\ \text{Respiration} \\ \text{(4.7)}}} - \underbrace{\dot{C}_{\Delta_k,c}}_{\substack{\text{Growth and maintenance} \\ \text{Respiration} \\ \text{(4.7)}}} - \underbrace{\dot{C}_{t_k,e_1}}_{\substack{\text{Turnover of} \\ \text{non-lignified litter} \\ \text{(S4)}}} - \underbrace{\dot{C}_{t_k,e_2}}_{\substack{\text{Turnover of} \\ \text{lignified litter} \\ \text{(S4)}}}, \tag{25}$$

where $\dot{C}_{t_k,e_1}$ and $\dot{C}_{t_k,e_2}$ are the individual carbon losses caused by leaf shedding and turnover of living tissues that become part of the litter ($\dot{C}_{t_k,e_1}$) and structural debris ($\dot{C}_{t_k,e_2}$). The transfer of carbon from plants to the soil carbon pools and between the soil carbon pools do not directly impact the carbon dioxide budget, but contribute to the long-term ecosystem carbon stock distribution and carbon balance. These components have been discussed in previous ED and ED2 publications (Moorcroft et al., 2001; Albani et al., 2006; Medvigy, 2006; Medvigy et al., 2009) and are summarized in Supplement S4.

4 Sub-models and parameterizations of terms of the general equations

4.1 Hydrology sub-model and ground energy exchange

The ground model encompasses heat, enthalpy, and water fluxes between adjacent layers of soil and temporary surface water, as well as losses of water and enthalpy due to surface runoff and drainage. Fluxes between adjacent layers are positive when they are upwards, and runoff and drainage fluxes are positive or zero.

Sensible heat flux between two adjacent soil or temporary surface water layers $j-1$ and j ~~are~~is determined ~~based on~~from thermal conductivity Υ_Q and temperature gradient (Bonan, 2008), with an additional term for temporary surface water to scale the flux when the temporary surface water covers only a fraction f_{TSW} of the ground:

$$\dot{Q}_{g_{j-1},g_j} = -\langle \Upsilon_Q \rangle_{g_{j-1},g_j} \left(\frac{\partial T_g}{\partial z} \right)_{g_{j-1},g_j}, \tag{26}$$

$$\dot{Q}_{s_{j-1},s_j} = -f_{\text{TSW}} \langle \Upsilon_Q \rangle_{s_{j-1},s_j} \left(\frac{\partial T_s}{\partial z} \right)_{s_{j-1},s_j}, \tag{27}$$

where the operator $\langle \, \rangle$ is the log-linear interpolation from the mid-point height of layers $j-1$ and j to the height at the interface. The bottom boundary condition of Eq. (26) is $\left(\frac{\partial T}{\partial z} \right)_{g_0,g_1} \equiv 0$. The interface between the top soil layer and the first temporary surface water ($\dot{Q}_{g_{N_G},s_1}$) is found by applying Eq. (27) with $\left(T_{s_0}; \Upsilon_{Q_{s_0}}; \Delta z_{s_0} \right) = \left(T_{g_{N_G}}; \Upsilon_{Q_{g_{N_G}}}; \Delta z_{g_{N_G}} \right)$. Soil thermal conductivity depends on soil moisture and texture properties, and the parameterization is described in Supplement S9. Both the fraction of ground covered by the temporary surface water and the thermal conductivity of the temporary surface water are described in Supplement S10.

Ground water exchange between layers occurs only if water is in liquid phase. The water flux between soil layers g_{j-1} and $g_j, j \in \{2, 3, \ldots, N_G\}$ is determined from Darcy's law (Bonan, 2008):

$$\dot{W}_{g_{j-1},g_j} = -\rho_\ell \left\langle \Upsilon_\Psi \right\rangle_{g_{j-1},g_j} \left[\frac{\partial \Psi}{\partial z} + \frac{\mathrm{d}z_g}{\mathrm{d}z} \right]_{g_{j-1},g_j}, \tag{28}$$

where Ψ is the soil matric potential and Υ_Ψ is the hydraulic conductivity, both defined after Brooks and Corey (1964), with an additional correction term applied to hydraulic conductivity to reduce conductivity in case the soil is partially or completely frozen (Supplement S9). The bottom boundary condition for soil matric potential gradient is $\left(\frac{\partial \Psi}{\partial z} \right)_{g_0,g_1} \equiv 0$.

The term $\frac{\mathrm{d}z_g}{\mathrm{d}z}$ in Eq. (28) is the flux due to gravity, and it is 1 for all layers except the bottom boundary condition, which depends on the sub-surface drainage. Sub-surface drainage at the bottom boundary depends on the type of drainage, and is determined using a slight modification of Eq. (28). Let $\eth$ be an angle-like parameter that controls the drainage beneath the ~~lowest level~~deepest soil layer. Because we assume zero gradient in soil matric potential between the ~~lowest level~~deepest soil layer and the boundary condition, the sub-surface drainage flux ($\dot{W}_{g_1,g_0}$) becomes:

$$\dot{W}_{g_1,g_0} = -\dot{W}_{g_0,g_1} = \rho_\ell \, \Upsilon_{\Psi_{g_1}} \sin \eth. \tag{29}$$

Special cases of Eq. (29) are the zero-flow conditions ($\eth = 0$) and free drainage ($\eth = \frac{\pi}{2}$).

For the temporary surface water, water flux between layers through percolation is calculated similarly to LEAF-2 (Walko et al., 2000). Liquid water in excess of 10% is in principle free to percolate to the layer below, although the maximum percolation of the first surface water layer is limited by the amount of pore space available at the top ground layer:

$$\dot{W}_{s_1,g_{N_G}} = -\dot{W}_{g_{N_G},s_1} = \frac{1}{\Delta t_{\mathrm{Thermo}}} \max \left[0, W_{s_1} \left(\frac{\ell_{s_1} - 0.1}{0.9} \right), \rho_\ell \left(\vartheta_{\mathrm{Po}} - \vartheta_{g_{N_G}} \right) \Delta z_{g_{N_G}} \right], \tag{30}$$

$$\dot{W}_{s_j,s_{j-1}} = -\dot{W}_{s_{j-1},s_j} = \frac{1}{\Delta t_{\mathrm{Thermo}}} \max \left(0, W_{s_j} \frac{\ell_{s_j} - 0.1}{0.9} \right) \quad , \text{ for } j > 1. \tag{31}$$

Surface runoff of liquid water is simulated using a simple extinction function, applied only at the topmost temporary surface water layer:

$$\dot{W}_{s_{N_S},o} = \ell_{s_{N_S}} W_{s_{N_S}} \exp \left(-\frac{\Delta t_{\mathrm{Thermo}}}{t_{\mathrm{Runoff}}} \right), \tag{32}$$

where t_{Runoff} is a user-defined e-folding decay time, usually on the order of a few minutes to a few hours (Table S4).

In addition to the water fluxes due to sub-surface drainage, surface runoff and the transport of water between layers, we must account for the associated enthalpy fluxes. Enthalpy fluxes due to sub-surface drainage and surface runoff are defined based on the water flux and the temperature of the layers where water is lost, by applying the definition of enthalpy

22

(Supplement S5):

$$\dot{H}_{g_1,g_0} = \dot{W}_{g_1,g_0}\, q_\ell \left(T_{g_1} - T_{\ell 0}\right), \tag{33}$$

$$\dot{H}_{s_{N_S},o} = \dot{W}_{s_{N_S},o}\, q_\ell \left(T_{s_{N_S}} - T_{\ell 0}\right), \tag{34}$$

where q_ℓ is the specific heat of liquid water (Table S3), and $T_{\ell 0}$ is defined in Eq. (S53). The enthalpy flux between two adjacent layers is solved similarly, but it must account for the sign of the flux in order to determine the water temperature of the donor layer:

$$\dot{H}_{x_{j-1},x_j} = \begin{cases} \dot{W}_{x_{j-1},x_j}\, q_\ell \left(T_{x_j} - T_{\ell 0}\right) & , \text{if } \dot{W}_{x_{j-1},x_j} < 0 \\ \dot{W}_{x_{j-1},x_j}\, q_\ell \left(T_{x_{j-1}} - T_{\ell 0}\right) & , \text{if } \dot{W}_{x_{j-1},x_j} \geq 0 \end{cases}, \tag{35}$$

where the subscript x_j represents either soil (g_j) or temporary surface water (s_j).

4.2 Precipitation and vegetation dripping

In ED-2.2, precipitating water from rain and snow increases the water storage of the thermodynamic systems, as rainfall can be intercepted by the canopy, or reach the ground. This influx of water also affects the enthalpy storage due to the enthalpy associated with precipitation, although no heat exchange is directly associated with precipitation.

To determine the partitioning of total incoming precipitation ($\dot{W}_{\infty,a}$) into interception by each cohort ($\dot{W}_{a,t_k}$) and direct interception by the ground (throughfall, $\dot{W}_{a,s_{N_S}}$), we use the fraction of open canopy ($\mathcal{O}$) and the total plant area index of each cohort (Φ_{t_k}):

$$\dot{W}_{a,t_k} = (1 - \mathcal{O})\, \dot{W}_{\infty,a} \frac{\Phi_{t_k}}{\sum_{k'=1}^{N_T} \Phi_{t_{k'}}}, \tag{36}$$

$$\dot{W}_{a,s_{N_S}} = \mathcal{O}\, \dot{W}_{\infty,a}, \tag{37}$$

$$\mathcal{O} = \prod_{k=1}^{N_T} (1 - X_{t_k}), \tag{38}$$

where $\Phi_{t_k} = \Lambda_{t_k} + \Omega_{t_k}$ is the total plant area index, Λ_{t_k} and Ω_{t_k} being the leaf and wood area indices, both defined from PFT-dependent allometric relations (Supplement S18); X_{t_k} is the crown area index of each cohort, also defined in Supplement S18. Throughfall precipitation is always placed on the topmost temporary surface water layer. In case no temporary surface water layer exists, a new layer is created, although it may be extinct in case all water is able to percolate down to the top soil layer.

Precipitation is a mass flux, but it also has an associated enthalpy flux ($\dot{H}_{\infty,a}$) that must be partitioned and incorporated to the cohorts and temporary surface water. Similar to the water exchange between soil layers, the enthalpy flux associated with rainfall uses the definition of enthalpy (Supplement S5). Because precipitation temperature is seldom available in meteorological drivers (towers or gridded meteorological forcing data sets), we assume that precipitation temperature

23

is closely associated with the free-air temperature (T_a), and we use T_a to determine whether the precipitation falls as rain, snow, or a mix of both. Importantly, the use of free-air temperature partly accounts for the thermal difference between precipitation temperature and the temperature of intercepted surfaces. Rain is only allowed when T_a is above the water triple point ($T_3 = 273.16\,\mathrm{K}$); in this case, the rain temperature is always assumed to be at T_a. Pure snow occurs when the free-air temperature is below T_3, and likewise snow temperature is assumed to be T_a. When free air temperature is only slightly above T_3, a mix of rain and snow occurs, with the rain temperature assumed to be T_a and snow temperature assumed to be T_3:

$$\dot{H}_{\infty,a} = \dot{W}_{\infty,a} \left[(1 - \ell_a)\, q_i \min\left(T_3, T_a\right) + \ell_a\, q_\ell\left(T_a - T_{\ell 0}\right) \right], \tag{39}$$

where $(q_i; q_\ell)$ are the specific heats of ice and liquid, respectively, and $T_{\ell 0}$ is temperature at which supercooled water would have enthalpy equal to zero (Eq. S53). The fraction of precipitation that falls as rain ℓ_a is based on the Jin et al. (1999) parameterization, slightly modified to make the function continuous:

$$\ell_a = \begin{cases} 1.0 & , \text{if } T_a > 275.66\,\mathrm{K} \\ 0.4 + 1.2\left(T_a - T_3 - 2.0\right) & , \text{if } 275.16\,\mathrm{K} < T_a \leq 275.66\,\mathrm{K} \\ 0.2\left(T_a - T_3\right) & , \text{if } T_3 < T_a \leq 275.16\,\mathrm{K} \\ 0.0 & , \text{if } T_a \leq T_3 \end{cases}. \tag{40}$$

The enthalpy flux associated with precipitation is then partitioned into canopy interception ($\dot{H}_{a,t_k}$) and throughfall ($\dot{H}_{a,s_{N_S}}$) using the same scaling factor as in Eq. (37) and Eq. (36):

$$\dot{H}_{a,t_k} = (1 - \mathcal{O})\,\dot{H}_{\infty,a}\, \frac{\Phi_{t_k}}{\sum_{k'=1}^{N_T} \Phi_{t_{k'}}}, \tag{41}$$

$$\dot{H}_{a,s_{N_S}} = \mathcal{O}\,\dot{H}_{\infty,a}. \tag{42}$$

Leaves and branches can accumulate only a finite amount of water on their surfaces, proportional to their total area. When incoming precipitation rates are too high (or more rarely when dew or frost formation is excessive), any water amount that exceeds the holding capacity is lost to the ground as canopy dripping. Similarly to incoming precipitation, the excess water lost through dripping also has an associated enthalpy that must be taken into account, although dripping has no associated heat flux. The canopy dripping fluxes of water ($\dot{W}_{t_k,s_{N_S}}$) and the associated enthalpy ($\dot{H}_{t_k,s_{N_S}}$) are defined such that the leaves and branches lose the excess water within one time step:

$$\dot{W}_{t_k,s_{N_S}} = -\frac{1}{\Delta t_{\mathrm{Thermo}}} \max\left(0, W_{t_k} - \hat{w}_{\max}\,\Phi_{t_k}\right), \tag{43}$$

$$\dot{H}_{t_k,s_{N_S}} = \dot{W}_{t_k,s_{N_S}} \left[(1 - \ell_{t_k})\, q_i T_{t_k} + \ell_{t_k}\left(T_{t_k} - T_{\ell 0}\right) \right], \tag{44}$$

where ℓ_{t_k} is the liquid fraction of surface water on top of cohort k and $\hat{w}_{\max}$ is the cohort holding capacity, which is an adjustable parameter (Table S4) but typically is of the order of $0.05 - 0.40\,\mathrm{kg_W\,m^{-2}_{Leaf+Wood}}$ (Wohlfahrt et al., 2006).

4.3 Radiation model

The radiation budget is solved using a multi-layer version of the two-stream model (Sellers, 1985; Liou, 2002; Medvigy, 2006) applied to three broad spectral bands: photosynthetically active radiation (PAR, wave lengths between 0.4 and 0.7 μm), near infrared radiation (NIR, wave lengths between 0.7 and 3.0 μm) and thermal infrared radiation (TIR, wave lengths between 3.0 and 15 μm).

4.3.1 Canopy radiation profile

For each spectral band m, the canopy radiation scheme assumes that each cohort corresponds to one layer of vegetation within the canopy, and within each layer the optical and thermal properties are assumed constant. For all bands, the top boundary condition for each band is provided by the meteorological forcing (Table 3). In the cases of PAR ($m = 1$) and NIR ($m = 2$), the downward irradiance is comprised of a beam (direct) and isotropic (diffuse) components, whereas TIR irradiance ($m = 3$) is assumed to be all diffuse. Direct irradiance that is intercepted by the cohorts can be either back-scattered or forward-scattered as diffuse radiation, and direct radiation reflected by the ground is assumed to be entirely diffuse.

Following Sellers (1985), the extinction of downward direct irradiance and the two-stream model for hemispheric diffuse irradiance for each of the spectral bands ($m = 1, 2, 3$) is given by:

$$\underbrace{\mu_k^{\odot} \frac{\mathrm{d}\dot{Q}_{mk}^{\odot}}{\mathrm{d}\tilde{\Phi}}}_{\substack{\text{Downward direct} \\ \text{profile}}} = \underbrace{-\dot{Q}_{mk}^{\odot}}_{\text{Interception}}, \tag{45}$$

$$\underbrace{\overline{\mu}_k \frac{\mathrm{d}\dot{Q}_{mk}^{\Downarrow}}{\mathrm{d}\tilde{\Phi}}}_{\substack{\text{Downward diffuse} \\ \text{profile}}} = \underbrace{-\dot{Q}_{mk}^{\Downarrow}}_{\text{Interception}} + \underbrace{(1-\beta_{mk})\,\varsigma_{mk}\,\dot{Q}_{mk}^{\Downarrow}}_{\substack{\text{Forward scattering} \\ \text{(downward diffuse)}}} + \underbrace{\beta_{ik}\,\varsigma_{mk}\,\dot{Q}_{mk}^{\Uparrow}}_{\substack{\text{Backscattering} \\ \text{(upward diffuse)}}} + \underbrace{\frac{\overline{\mu}_k}{\mu_k^{\odot}}\,\varsigma_{mk}\left(1-\beta_{mk}^{\odot}\right)\dot{Q}_{mk}^{\odot}}_{\substack{\text{Forward scattering} \\ \text{(downward direct)}}} + \underbrace{(1-\varsigma_{mk})\,\dot{Q}_{mk}^{\blacklozenge}}_{\text{Emission}}, \tag{46}$$

$$\underbrace{-\overline{\mu}_k \frac{\mathrm{d}\dot{Q}_{mk}^{\Uparrow}}{\mathrm{d}\tilde{\Phi}}}_{\substack{\text{Upward diffuse} \\ \text{profile}}} = -\underbrace{\dot{Q}_{mk}^{\Uparrow}}_{\text{Interception}} + \underbrace{(1-\beta_{mk})\,\varsigma_{mk}\,\dot{Q}_{mk}^{\Uparrow}}_{\substack{\text{Forward scattering} \\ \text{(upward diffuse)}}} + \underbrace{\beta_{mk}\,\varsigma_{mk}\,\dot{Q}_{mk}^{\Downarrow}}_{\substack{\text{Backscattering} \\ \text{(downward diffuse)}}} + \underbrace{\frac{\overline{\mu}_k}{\mu_k^{\odot}}\,\varsigma_{mk}\,\beta_{mk}^{\odot}\,\dot{Q}_{mk}^{\odot}}_{\substack{\text{Backscattering} \\ \text{(downward direct)}}} + \underbrace{(1-\varsigma_{mk})\,\dot{Q}_{mk}^{\blacklozenge}}_{\text{Emission}}, \tag{47}$$

where index $k \in \{1, 2, \dots, N_T\}$ corresponds to each cohort k or its lower interface (Fig. 4); interface $N_T + 1$ is immediately above the tallest cohort; $\dot{Q}_{mk}^{\odot}$ is the downward direct irradiance incident at interface k; ($\dot{Q}_{mk}^{\Downarrow}$ and $\dot{Q}_{mk}^{\Uparrow}$) are the downward and upward (hemispheric) diffuse irradiances incident at interface k; ς_{mk} is the scattering coefficient, and thus $(1-\varsigma_{mk})$ is the absorptivity; $\beta_{mk}^{\odot}$ and β_{mk} are the backscattered fraction of scattered direct and diffuse irradiances, respectively; $\tilde{\Phi}$ is the effective cumulative plant area index, assumed zero at the top of each layer, and increasing downwards ($\tilde{\Phi}_k$ is the total for
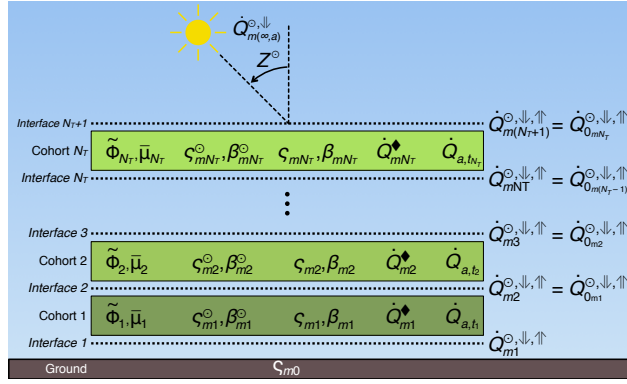
Figure 4. Schematic of the radiation module for a patch with N_T cohorts, showing the grid arrangement of the irradiance profiles relative to the cohort positions. Index k corresponds to each cohort of the interface beneath each cohort, m corresponds to each spectral band; $\left(\dot{Q}^{\odot}_{m(\infty,a)}, \dot{Q}^{\Downarrow}_{m(\infty,a)}\right)$ are the incoming direct and diffuse irradiance (Table 3); $Z^{\odot}$ is the Sun's zenith angle; $\left(\dot{Q}^{\odot}_{mk}, \dot{Q}^{\Downarrow}_{mk}, \dot{Q}^{\Uparrow}_{mk}\right)$ are the downward direct, downward diffuse, and upward diffuse irradiances (Eq. 45-47); $\tilde{\Phi}_k$ is the effective plant area index (Eq. S100); $(\varsigma_{mk}; \beta_{mk})$ are the scattering coefficients and the backscattering fraction for diffuse irradiance (Eq. S101,S102); $(\varsigma^{\odot}_{mk}; \beta^{\odot}_{mk})$ are the scattering coefficients and the backscattering fraction for direct irradiance (Eq. ~~S104,S105~~ S104-S105); $\dot{Q}^{\blacklozenge}_{mk}$ is the black-body irradiance (Eq. 48); and $\dot{Q}^{\odot}_{a,t_k}$ is the net absorbed irradiance (Eq. 49).

layer k); $\mu^{\odot}_k$ and $\overline{\mu}_k$ are the inverse of the optical depth per unit of effective plant area index for direct and diffuse radiation, respectively; and $\dot{Q}^{\blacklozenge}_{mk}$ is the irradiance emitted by a black body at the same temperature as the cohort (T_{t_k}).

545   Equations (45)-(47) simplify for each spectral band. First, ~~$\dot{Q}^{\odot}_{m=3\,k} = 0$~~ $\dot{Q}^{\odot}_{mk} \equiv 0$ for the TIR ($m = 3$) band, because we assume that all incoming TIR irradiance is diffuse. Likewise, the black-body emission $\dot{Q}^{\blacklozenge}_{mk} = \dot{Q}^{\blacklozenge}_{1k} = 0$ for the PAR ($m = 1$) and NIR ($m = 2$) bands, because thermal emission is negligible at these wave lengths. The black-body emission for the TIR band is defined as

$$\dot{Q}^{\blacklozenge}_{m=3\,k} = \sigma_{\text{SB}} T^4_{t_k}, \tag{48}$$

550   where σ_{SB} is the Stefan-Boltzmann constant (Table S3). Note that for emission of TIR radiation (45-47), we assume that emissivity is the same as absorptivity (Kirchhoff's law; Liou, 2002), hence the ~~$1 - \varsigma$~~ $(1 - \varsigma)$ term.

The effective plant area index $\tilde{\Phi}_k$ is the total area (leaves and branches) that is corrected to account for that leaves are not uniformly distributed in the layer. It is defined as $\tilde{\Phi}_k = \Omega_k + f_{\text{Clump}_k} \Lambda_k$, where f_{Clump_k} is the PFT-dependent clumping index (Chen and Black, 1992, default values in Tables S5-S6), Λ_{t_k} is the leaf area index and Ω_{t_k} is the wood area index. $\tilde{\Phi}$ is
555   assumed zero at the top of each layer, increasing downwards.

The optical properties of the leaf layers — optical depth and scattering parameters for direct and diffuse radiation for each of the three spectral bands — are assumed constant within each layer. These properties are determined from PFT-dependent characteristics such as mean orientation factor, spectral band-dependent reflectivity, transmissivity, and emissivity

Comment: Figure 4 was updated. Two subscripts were missing.

(Supplement S11). Because the properties are constant within each layer, it is possible to analytically solve the full profile of
both direct and diffuse radiation, using the solver described in Supplement S12.

Once the profiles of $\dot{Q}_{mk}^{\odot}$, $\dot{Q}_{mk}^{\Downarrow}$ and $\dot{Q}_{mk}^{\Uparrow}$ are determined, we obtain the irradiance that is absorbed by each cohort $\dot{Q}_{a,t_k}$:

$$\dot{Q}_{a,t_k} = \sum_{m=1}^{3} \left[\left(\dot{Q}_{m(k+1)}^{\odot} - \dot{Q}_{mk}^{\odot} \right) + \left(\dot{Q}_{m(k+1)}^{\Downarrow} - \dot{Q}_{mk}^{\Downarrow} \right) + \left(\dot{Q}_{mk}^{\Uparrow} - \dot{Q}_{m(k+1)}^{\Uparrow} \right) \right]. \tag{49}$$

This term is then used in the enthalpy budget of each cohort (Eq. 4 and Eq. 12).

4.3.2 Ground radiation

The ground radiation sub-model determines the irradiance emitted by the ground surface, and the profile of irradiance through the temporary surface water layers and top soil layer. Note that the ground radiation and the canopy radiation model are interdependent: the incoming radiation at the top ground layer is determined from the canopy radiation model, and the ground scattering coefficient (ς_{m0}, see Supplement S11) is needed for the canopy-radiation bottom boundary condition (Supplement S12). However, since the scattering coefficient does not depend on the total incoming radiation, the irradiance profile can be solved for a standardized amount of incoming radiation, and once the downward radiation at the bottom of the canopy has been calculated, the absorbed irradiance for each layer can be scaled appropriately.

Black-body emission from the ground ($\dot{Q}_{m0}^{\blacklozenge}$) is calculated as an area-weighted average of the emissivities of exposed soil and temporary surface water:

$$\dot{Q}_{m0}^{\blacklozenge} = \begin{cases} 0 & , \text{if } m \in (1,2) \\ \dfrac{(1 - f_{\text{TSW}})\,(1 - \varsigma_{3g})\left(\sigma_{\text{SB}} T_{g_{N_G}}^4\right) + f_{\text{TSW}}\,(1 - \varsigma_{3s})\left(\sigma_{\text{SB}} T_{s_{N_S}}^4\right)}{(1 - f_{\text{TSW}})\,(1 - \varsigma_{3g}) + f_{\text{TSW}}\,(1 - \varsigma_{3s})} & , \text{if } m = 3 \end{cases}. \tag{50}$$

where $(1 - \varsigma_{3g})$ and $(1 - \varsigma_{3s})$, are, respectively, the thermal-infrared emissivities of the top soil layer and the temporary surface water (Table S4), and f_{TSW} is the fraction of ground covered by temporary surface water. In ED-2.2, the soil and snow scattering coefficients for the TIR band are assumed constant (Table S4), following Walko et al. (2000).

Once the irradiance profile for the canopy is determined from Eq. (45)-(47), the irradiance absorbed by each temporary surface water layer ($j \in \{1, 2, \ldots, N_S\}$) is calculated by integrating the transmissivity profile for each layer, starting from the top layer:

$$\dot{Q}_{a,s_j} = \begin{cases} \sum_{m=1}^{2} \left\{ f_{\text{TSW}} \left(\dot{Q}_{m1}^{\Downarrow} + \dot{Q}_{m1}^{\odot} \right) \left[1 - \exp\left(-\frac{\Delta \overline{z}_{s_{N_S}}}{\overline{\mu}_s} \right) \right] \right\} + f_{\text{TSW}}\,(1 - \varsigma_{3s}) \left(\dot{Q}_{m=3\,k=1}^{\Downarrow} - \sigma_{\text{SB}} T_{s_{N_S}}^4 \right) & , \text{if } j = N_S \\ \sum_{m=1}^{2} \left\{ f_{\text{TSW}} \left(\dot{Q}_{m1}^{\Downarrow} + \dot{Q}_{m1}^{\odot} \right) \left[\exp\left(-\frac{\sum_{j'=j+1}^{N_S} \Delta \overline{z}_{s_j}}{\overline{\mu}_s} \right) - \exp\left(-\frac{\sum_{j'=j}^{N_S} \Delta \overline{z}_{s_{j'}}}{\overline{\mu}_s} \right) \right] \right\} & , \text{otherwise} \end{cases}, \tag{51}$$

where $\bar{\mu}_s$ is the inverse of the optical depth of temporary surface water.

The irradiance absorbed by the ground is a combination of irradiance of exposed soil and irradiance that is trans-
585 mitted through all temporary surface water layers, and the net absorption of longwave radiation:

$$\dot{Q}_{a,g_{N_G}} = \sum_{m=1}^{2} \left\{ \left[1 - f_{\text{TSW}} + f_{\text{TSW}} \exp\left(-\frac{\sum_{j'=1}^{N_S} \Delta \bar{z}_{s_{j'}}}{\bar{\mu}_s} \right) \right] \left(\dot{Q}_{m1}^{\Downarrow} + \dot{Q}_{m1}^{\odot} \right) \right\}$$
$$+ (1 - f_{\text{TSW}})(1 - \varsigma_{3g}) \left(\dot{Q}_{m=3\,k=1}^{\Downarrow} - \sigma_{\text{SB}} T_{g_{N_G}}^4 \right). \tag{52}$$

4.4 Surface Layer Model

The surface layer model determines the fluxes of enthalpy, water, and carbon dioxide between the canopy air space and the free air above. It is based on the Monin-Obukhov similarity theory (Monin and Obukhov, 1954; Foken, 2006), which has
590 been widely used by biosphere-atmosphere models representing a variety of biomes (e.g. Walko et al., 2000; Best et al., 2011; Oleson et al., 2013), although this is often an extrapolation of the theory that was not originally developed for heterogeneous vegetation, or tall vegetation (Foken, 2006).

In order to obtain the fluxes, we assume that the eddy diffusivity of buoyancy is the same as the diffusivity of enthalpy, water vapor, and CO_2. This assumption allows us to define a single canopy conductance G_c for the three variables,
595 following the algorithm described in ~~Supplement S14.1~~Supplements S13 and S14.1. We then obtain the following equations for fluxes between canopy air space and the free atmosphere:

$$\dot{W}_{a,c} = \rho_c G_c (w_a - w_c), \tag{53}$$
$$\dot{H}_{a,c} = \rho_c G_c \left(\tilde{h}_a - h_c \right), \tag{54}$$
$$\dot{C}_{a,c} = \frac{\mathcal{M}_C}{\mathcal{M}_d} \rho_c G_c (c_a - c_c), \tag{55}$$

600 where $\tilde{h}_a$ is the equivalent enthalpy of air at reference height z_a when the air is adiabatically moved to the top of the canopy air space, using the definition of potential temperature:

$$\tilde{h}_a = h\left(\tilde{T}_a, w_a \right) \qquad \text{, from Eq.(S50)}, \tag{56}$$
$$\tilde{T}_a = \theta_a \left(\frac{p_c}{p_0} \right)^{\frac{\mathcal{R}}{\mathcal{M}_d\, q_{pd}}}, \tag{57}$$

where p_0 is the reference pressure, $\mathcal{R}$ is the universal gas constant, q_{pd} is the specific heat of dry air at constant pressure, and
605 $\mathcal{M}_d$ is the molar mass of dry air (Table S3).

Sensible heat flux between the free atmosphere and canopy air space ($\dot{Q}_{a,c}$) can be derived from the definition of enthalpy and enthalpy flux (Eq. S50 and Eq. 54), although it is not directly applied to the energy balance in the canopy air

space ($\dot{H}_{a,c}$ is used instead).

$$\dot{H}_{a,c} = \rho_c G_c \left[(1 - w_a) q_{pd} \tilde{T}_a + w_a q_{pv} \left(\tilde{T}_a - T_{v0} \right) - (1 - w_c) q_{pd} T_c \!\!/\!\!/ - w_c q_{pv} (T_c - T_{v0}) \right]$$

$$= \underbrace{\rho_c G_c \left(q_{p_a} \tilde{T}_a - q_{p_c} T_c \right)}_{\dot{Q}_{a,c}} - \rho_c G_c (w_a - w_c) q_{pv} T_{v0}, \tag{58}$$

$$\dot{Q}_{a,c} = \dot{H}_{a,c} + \dot{W}_{a,c} q_{pv} T_{v0}. \tag{59}$$

4.5 Heat and water exchange between surfaces and canopy air space

4.5.1 Leaves and branches

Fluxes of sensible heat ($\dot{Q}_{t_k,c}$) and water vapor ($\dot{W}_{t_k,c}$) between the leaf surface and wood surface and the canopy air space follow the same principle of conductance and gradient that define the eddy fluxes between the free atmosphere and canopy air space (Eq. 53;54). Throughout this section, we use subscripts λ_k and β_k to denote leaf and wood boundary layers of cohort k, respectively; the different subscripts are needed to differentiate fluxes coming from the leaves' intercellular space (e.g. transpiration, see also Section 4.6). Let $G_{Q\lambda_k}$ ($\mathrm{m\,s^{-1}}$) and $G_{W\lambda_k}$ ($\mathrm{m\,s^{-1}}$) be the conductances of heat and water between the leaf boundary layer of cohort k and the canopy air space, and $G_{Q\beta_k}$ and $G_{W\beta_k}$ be the wood boundary layer counterparts. The surface sensible heat and surface water vapor fluxes are:

$$\dot{Q}_{t_k,c} = \dot{Q}_{\lambda_k,c} + \dot{Q}_{\beta_k,c} = 2\Lambda_k \dot{q}_{\lambda_k,c} + \pi \Omega_k \dot{q}_{\beta_k,c}, \tag{60}$$

$$\dot{W}_{t_k,c} = \dot{W}_{\lambda_k,c} + \dot{W}_{\beta_k,c} = \Lambda_k \dot{w}_{\lambda_k,c} + \Omega_k \dot{w}_{\beta_k,c}, \tag{61}$$

$$\dot{q}_{\lambda_k,c} = G_{Q\lambda_k} \rho_c q_{p_c} \left(T_{l_k}^{\mathrm{Sfc}} - T_c \right), \tag{62}$$

$$\dot{q}_{\beta_k,c} = G_{Q\beta_k} \rho_c q_{p_c} \left(T_{b_k}^{\mathrm{Sfc}} - T_c \right), \tag{63}$$

$$\dot{w}_{\lambda_k,c} = G_{W\lambda_k} \rho_c \left(w_{l_k}^{\mathrm{Sfc}} - w_c \right), \tag{64}$$

$$\dot{w}_{\beta_k,c} = G_{W\beta_k} \rho_c \left(w_{b_k}^{\mathrm{Sfc}} - w_c \right), \tag{65}$$

where $(\dot{q}_{\lambda_k,c}; \dot{q}_{\beta_k,c}; \dot{w}_{\lambda_k,c}; \dot{w}_{\beta_k,c})$ are the leaf-surface and branch-surface heat and water fluxes by unit of leaf and branch area, respectively; the factors 2 and π in Eq. (60) means that sensible heat is exchanged on both sides of the leaves, and on the longitudinal area of the branches, which are assumed cylindrical. Intercepted water and dew and frost formation is allowed only on one side of the leaves, and an area equivalent to a one-sided flat plate for branches, and therefore only the leaf and wood area indices are used in Eq. (61). Canopy air space temperature, specific humidity, density, and specific heat, leaf temperature, and wood temperature are determined diagnostically. We also assume that surface temperature of leaves and branches to be the same as their internal temperatures (i.e. $T_{l_k}^{\mathrm{Sfc}} \equiv T_{l_k}$ and $T_{b_k}^{\mathrm{Sfc}} \equiv T_{b_k}$). Specific humidity at the leaf surface $w_{l_k}^{\mathrm{Sfc}} = w_{\mathrm{Sat}}(T_{l_k}^{\mathrm{Sfc}}, p_c)$ and branch surface $w_{\beta_k}^{\mathrm{Sfc}} = w_{\mathrm{Sat}}\left(T_{b_k}^{\mathrm{Sfc}}, p_c\right)$ are assumed to be the saturation specific humidity w_{Sat} (Supplement S15).

Heat conductance for leaves and branches are based on the convective heat transfer, as described in Supplement S14.2. Further description of the theory can be found in Monteith and Unsworth (2008, Section 10.1).

4.5.2 Temporary surface water and soil

Sensible heat and water fluxes between the temporary surface water and soil and the canopy air space are calculated similarly to leaves and branches. Surface conductance G_{Sfc} is assumed to be the same for both heat and water, and also the same for soil and temporary surface water:

$$\dot{Q}_{s_{N_S},c} = f_{\text{TSW}}\, G_{\text{Sfc}}\, \rho_c\, q_{p_c} \left(T_{s_{N_S}} - T_c \right), \tag{66}$$

$$\dot{W}_{s_{N_S},c} = f_{\text{TSW}}\, G_{\text{Sfc}}\, \rho_c \left(w_{s_{N_S}} - w_c \right), \tag{67}$$

$$\dot{Q}_{g_{N_G},c} = (1 - f_{\text{TSW}})\, G_{\text{Sfc}}\, \rho_c\, q_{p_c} \left(T_{g_{N_G}} - T_c \right), \tag{68}$$

$$\dot{W}_{g_{N_G},c} = (1 - f_{\text{TSW}})\, G_{\text{Sfc}}\, \rho_c\,\cancel{q_{p_c}} \left(w_{g_{N_G}} - w_c \right), \tag{69}$$

Specific humidity for temporary surface water is computed exactly as leaves and branches, $w_{s_{N_S}} = w_{\text{Sat}}\left(T_{s_{N_S}}, p_c \right)$ (Supplement S15). For soils the specific humidity also accounts for the soil moisture and the sign of the flux, using a method similar to Avissar and Mahrer (1988):

$$w_{g_{N_G}} = \begin{cases} s_g \exp\left(\dfrac{\mathcal{M}_w\, g\, \Psi_{g_{N_G}}}{\mathcal{R}\, T_{g_{N_G}}} \right) w_{\text{Sat}}\left(T_{g_{N_G}}, p_c \right) + (1 - s_g)\, w_c & , \text{if } w_{\text{Sat}}\left(T_{g_{N_G}}, p_c \right) > w_c \\ w_{\text{Sat}}\left(T_{g_{N_G}}, p_c \right) & , \text{if } w_{\text{Sat}}\left(T_{g_{N_G}}, p_c \right) \leq w_c \end{cases}, \tag{70}$$

$$s_g = \frac{1}{2} \left\{ 1.0 - \cos\left[\pi\, \frac{\min\left(\vartheta_{g_{N_G}}, \vartheta_{\text{Fc}} \right) - \vartheta_{\text{Re}}}{\vartheta_{\text{Fc}} - \vartheta_{\text{Re}}} \right] \right\}, \tag{71}$$

where g is the gravity acceleration, $\mathcal{M}_w$ is the water molar mass, and $\mathcal{R}$ is the universal gas constant (Table S3); $T_{g_{N_G}}$, $\vartheta_{g_{N_G}}$ and $\Psi_{g_{N_G}}$ are the temperature, soil moisture and soil matric potential of the topmost soil layer, respectively; and ϑ_{Fc} and ϑ_{Re} are the soil moisture at field capacity and the residual soil moisture, respectively. The exponential term in Eq. ~~70~~(70) corresponds to the soil pore relative humidity derived from the Kelvin equation (Philip, 1957), and s_g is the soil wetness function, which takes a similar functional form as the relative humidity term from Noilhan and Planton (1989) and the β term from Lee and Pielke (1992). The total resistance between the surface and the canopy air space is a combination of the resistance if the surface was bare, plus the resistance due to the vegetation, as described in Supplement S14.3.

4.5.3 Enthalpy flux due to evaporation and condensation

Dew and frost are formed when water in the canopy air space condenses or freezes on any surface (leaves, branches, or ground); likewise, water that evaporates and ice that sublimates from these surfaces immediately become part of the canopy

air space. In terms of energy transfer, two processes occur, the phase change and the mass exchange, and both must be accounted for the enthalpy flux. Phase change depends on the specific latent heat of vaporization ($l_{\ell v}$) and sublimation (l_{iv}), which are linear functions of temperature, based on Eq. (S48) and Eq. (S49):

$$l_{\ell v}(T) = l_{\ell v3} + (q_{pv} - q_\ell)(T - T_3),$$ (72)

$$l_{iv}(T) = l_{iv3} + (q_{pv} - q_i)(T - T_3),$$ (73)

where $l_{\ell v3}$ and l_{iv3} are the specific latent heats of vaporization and sublimation at the water triple point (T_3), q_{pv} is the specific heat of water vapor at constant pressure, and q_i and q_ℓ are the specific heats of ice and liquid water, respectively (Table S3). The temperature for phase change must be the surface temperature because this is where the phase change occurs. In the most generic case, if a surface x at temperature T_x with a liquid water fraction ℓ_x, the total enthalpy flux between the surface and canopy air space $\dot{H}_{x,c}$ associated with the water flux $W_{x,c}$ is:

$$\dot{H}_{x,c} = \dot{W}_{x,c} \left\{ \underbrace{[(1-\ell_x)\, q_i\, T_x + \ell_x\, q_\ell\, (T_x - T_{\ell 0})]}_{\text{Enthalpy flux due to mass exchange}} + \underbrace{[(1-\ell_x)\, l_{iv}(T_x) + \ell_x\, \cancel{l/\{/(\mathbb{T}/l)}\, l_{\ell v}(T_x)]}_{\text{Enthalpy flux due to phase change}} \right\}.$$ (74)

By using the definitions from Eq. (S54), Eq. (74) can be further simplified to:

$$\dot{H}_{x,c} = \dot{W}_{x,c}\,[q_{pv}\,(T_x - T_{v0})] = \dot{W}_{x,c}\,\underbrace{h\,(T_x, w_x = 1)}_{\text{Eq. (S50)}},$$ (75)

which is consistent with the exchange of pure water vapor and enthalpy between the thermodynamic systems. Eq. (75) is used to determine $\dot{H}_{g_{N_G},c}$, $\dot{H}_{s_{N_S},c}$, and $\dot{H}_{t_k,c}$, $k \in \{1, 2, \ldots, N_T\}$.

4.6 Leaf physiology

In ED-2.2, leaf physiology is modeled following Farquhar et al. (1980) and Collatz et al. (1991) for C_3 plants; ~~and~~ Collatz et al. (1992) for C_4 plants~~;~~; and the Leuning (1995) model for stomatal conductance. This sub-model ultimately determines the net leaf-level CO_2 uptake rate of each cohort k ($\dot{A}_k$, $\text{mol}_C\, \text{m}_{\text{Leaf}}^{-2}\, \text{s}^{-1}$), controlled exclusively by the leaf environment, and the corresponding water loss through transpiration ($\dot{E}_k$, $\text{mol}_W\, \text{m}_{\text{Leaf}}^{-2}\, \text{s}^{-1}$).

The exchange of water and CO_2 between the leaf intercellular space and the canopy air space is mediated by the stomata and the leaf boundary layer, which imposes an additional resistance to fluxes of these substances. For simplicity, we assume that the leaf boundary layer air has low storage capacity, and thus the fluxes of any substance (water or CO_2) entering and exiting the boundary layer must be the same. Fluxes of water and carbon between the leaf intercellular space and the canopy air space must overcome both the stomatal resistance and the boundary layer resistance, whereas sensible heat flux and water flux from leaf surface water must overcome the boundary layer resistance only (Fig. 5). The potential fluxes of
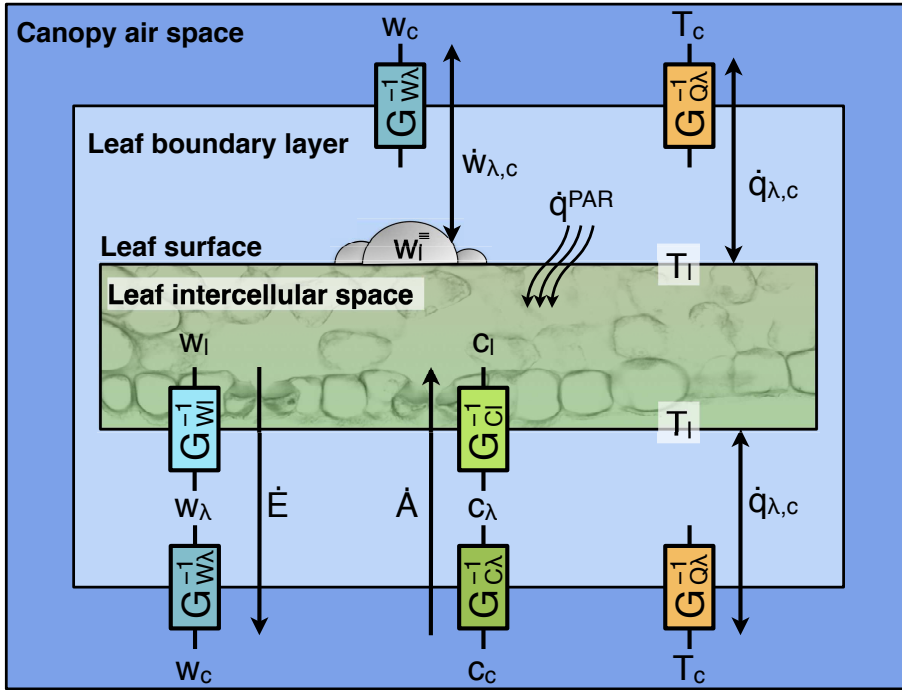
Figure 5. Schematic of fluxes between a leaf and the surrounding canopy air space for a hypostomatous plant during the photo period, as represented in ED-2.2. Conductances are represented by the resistances between the different environments (G^{-1}). Leaf-level sensible heat flux ($\dot{q}_{\lambda_k,c}$; Eq. 60) and leaf-level vapor flux between intercepted water and canopy air space ($\dot{w}_{\lambda_k,c}$; Eq. 61) are also shown for comparison. Cohort index k is omitted from the figure for clarity.

CO_2 and water can be written as:

$$\dot{A}_k = \hat{G}_{C\lambda_k}\left(c_c - c_{\lambda_k}\right) = \hat{G}_{Cl_k}\left(c_{\lambda_k} - c_{l_k}\right) = \frac{\hat{G}_{C\lambda_k}\hat{G}_{Cl_k}}{\hat{G}_{C\lambda_k} + \hat{G}_{Cl_k}}\left(c_c - c_{l_k}\right), \tag{76}$$

$$\dot{E}_k = \hat{G}_{W\lambda_k}\left(w_c - w_{\lambda_k}\right) = \hat{G}_{Wl_k}\left(w_{\lambda_k} - w_{l_k}\right) = \frac{\hat{G}_{W\lambda_k}\hat{G}_{Wl_k}}{\hat{G}_{W\lambda_k} + \hat{G}_{Wl_k}}\left(w_c - w_{l_k}\right), \tag{77}$$

690 $$w_{l_k} = w_{\text{Sat}}\left(T_{t_k}, p_c\right) \qquad \text{(Supplement S15)}, \tag{78}$$

$$\hat{G}_{X\lambda_k} = \frac{\rho_c G_{X\lambda_k}}{\mathcal{M}_d}, \tag{79}$$

$$\hat{G}_{Xl_k} = \frac{\rho_c G_{Xl_k}}{\mathcal{M}_d}, \tag{80}$$

where $G_{X\lambda_k}$ and G_{Xl_k} (units $\mathrm{m\,s}^{-1}$) are the leaf boundary layer and stomatal conductances for element X (either water W or carbon C), respectively; c_{λ_k} and w_{λ_k} are the CO_2 mixing ratio and the specific humidity of the leaf boundary layer, respectively; and c_{l_k} and w_{l_k} are the CO_2 and specific humidity of the leaf intercellular space, respectively. As stated in

695 Eq. (78), we assume the leaf intercellular space to be at water vapor saturation. The leaf boundary-layer conductances are

obtained following the algorithm shown in Supplement S14.2. The net CO_2 assimilation flux and stomatal conductances are described below.

From Farquhar et al. (1980), the net CO_2 assimilation flux is defined as:

$$\dot{A}_k = \underbrace{\dot{V}_{C_k}}_{\text{Carboxylation}} - \underbrace{\frac{1}{2}\dot{V}_{O_k}}_{\substack{\text{Oxygenation} \\ \text{(Photorespiration)}}} - \underbrace{\dot{R}_k}_{\text{Day respiration}} . \tag{81}$$

Oxygenation releases $0.5 \; \text{mol}_{CO_2}$ for every mol_{O_2}, hence the half multiplier, and it is related to carboxylation by means of the CO_2 compensation point Γ_k (Lambers et al., 2008):

$$\dot{V}_{O_k} = \frac{2\Gamma_k}{c_{l_k}}\dot{V}_{C_k}, \tag{82}$$

where c_{l_k} is the CO_2 mixing ratio in the leaf intercellular space. The CO_2 compensation point is determined after Collatz et al. (1991, 1992):

$$\Gamma_k = \begin{cases} \dfrac{o_{\oplus}}{2\,\varpi} & \text{, in case cohort } k \text{ is a } C_3 \text{ plant} \\ 0 & \text{, in case cohort } k \text{ is a } C_4 \text{ plant} \end{cases}, \tag{83}$$

where $o_{\oplus}$ is the reference O_2 mixing ratio (Table S3), and ϖ represents the ratio between the rates of carboxylase to oxygenase and is a function of temperature. The general form of the function describing the metabolic dependence upon temperature for any variable x (including ϖ) is:

$$\mathcal{T}(T,x) = x_{15} \times \mathcal{Q}_{10_x}^{\frac{T-T_{15}}{10}}, \tag{84}$$

where x_{15} is the value of variable x at temperature $T_{15} = 288.15\text{K}$ (15°C), and $\mathcal{Q}_{10_x}$ is the parameter which describes temperature dependence (Table S4).

Because C_4 plants have a mechanism to concentrate CO_2 near the CO_2-fixing enzyme Rubisco (Ribulose-1,5-Biphosphate Carboxylase Oxygenase), photorespiration is nearly nonexistent in C_4 plants (Lambers et al., 2008), hence the assumption that Γ_k is zero. For C_4 plants, the carboxylation rate under Ribulose-1,5-Biphosphate (RuBP) saturated conditions becomes the maximum capacity of Rubisco to perform the carboxylase function ($\dot{V}_{C_k} = \dot{V}_{C_k}^{\text{max}}$). For C_3, this rate is unattainable even under RuBP-saturated conditions because carboxylation and oxygenation are mutually inhibitive reactions (Lambers et al., 2008). Therefore, the maximum attainable carboxylation ($\dot{V}_{C_k} = \dot{V}_{C_k}^{\text{RuBP}}$) is expressed by a modified

Michaelis-Menten kinetics equation:

$$
\dot{V}_{C_k}^{\mathrm{RuBP}} =
\begin{cases}
\dot{V}_{C_k}^{\max} \dfrac{c_{l_k}}{c_{l_k} + \mathcal{K}_{\mathrm{ME}_k}} & \text{, if cohort } k \text{ is a C}_3 \text{ plant} \\[2mm]
\dot{V}_{C_k}^{\max} & \text{, if cohort } k \text{ is a C}_4 \text{ plant}
\end{cases}
, \tag{85}
$$

where $\mathcal{K}_{\mathrm{ME}_k} = \mathcal{K}_{C_k}\left(1 + o_\oplus/\mathcal{K}_{O_k}\right)$ is the effective Michaelis constant, and $\mathcal{K}_{C_k}$ and $\mathcal{K}_{O_k}$ are the Michaelis constants for carboxylation and oxygenation, respectively. Both $\mathcal{K}_{C_k}$ and $\mathcal{K}_{O_k}$ are dependent on temperature, following Eq. (84) (default parameters in Table S4), whereas $\dot{V}_{C_k}^{\max}$ follows a modified temperature-dependent function to account for the fast decline of both productivity and respiration at low and high temperatures (Sellers et al., 1996; Moorcroft et al., 2001):

$$
\mathcal{T}'(T,x) = \frac{\mathcal{T}(T,x)}{\left\{1 + \exp\left[-f_{\mathrm{Cold}}\left(T - T_{\mathrm{Cold}}\right)\right]\right\}\left\{1 + \exp\left[+f_{\mathrm{Hot}}\left(T - T_{\mathrm{Hot}}\right)\right]\right\}}, \tag{86}
$$

where f_{Cold}, f_{Hot}, T_{Cold} and T_{Hot} are PFT-dependent, phenomenological parameters to reduce the function value at low and high temperatures (Tables S5-S6).

The original expression for the initial slope of the carboxylation rate under near-zero CO_2 ($\dot{V}_{C_k}^{\mathrm{InSl}}$) for C$_4$ plants by Collatz et al. (1992) has been modified later (e.g. Foley et al., 1996) to explicitly include $\dot{V}_{C_k}^{\max}$; this is the same expression used in ED-2.2:

$$
\dot{V}_{C_k}^{\mathrm{InSl}} = k_{\mathrm{PEP}}\,\dot{V}_{C_k}^{\max}\,c_{l_k}, \tag{87}
$$

where k_{PEP} represents the initial slope of the response curve to increasing CO_2; the default value in ED-2.2 (Table S4) is the same value used by Collatz et al. (1992).

From the total photosynthetically active irradiance absorbed by the cohort $\dot{Q}_{\mathrm{PAR}:a,t_k}$ (Eq. 49), we define the photon flux that is absorbed by the leaf ($\dot{q}_k^{\mathrm{PAR}}, \mathrm{mol\,m}_{\mathrm{Leaf}}^{-2}\,\mathrm{s}^{-1}$):

$$
\dot{q}_k^{\mathrm{PAR}} = \frac{1}{\mathrm{Ein}}\frac{f_{\mathrm{Clump}_k}}{\tilde{\Phi}_k}\,\dot{Q}_{\mathrm{PAR}:a,t_k}, \tag{88}
$$

where Ein is the average photon-specific energy in the PAR band ($0.4 - 0.7\,\mu\mathrm{m}$; Table S3). Even though a high fraction $\epsilon_k^\star$ of the absorbed irradiance is used to transport electrons needed by the light reactions of photosynthesis (Lambers et al., 2008), only a fraction of the irradiance absorbed by the leaf is absorbed by the chlorophyll; in addition, the number electrons needed by each carboxylation and oxygenation reaction poses an additional restriction to the total carboxylation rate. The product of these three factors is combined into a single scaling factor for total absorbed PAR, the quantum yield (ϵ_k), which is a

PFT-dependent property in ED-2.2 (Tables S5-S6). The maximum carboxylation rate under light limitation $\dot{V}_{C_k}^{\mathrm{PAR}}$ is:

$$
\dot{V}_{C_k}^{\mathrm{PAR}} = \epsilon_k \dot{q}_k^{\mathrm{PAR}} \frac{1}{1 + \dfrac{\dot{V}_{O_k}}{\dot{V}_{C_k}}} = \begin{cases} \epsilon_k \dot{q}_k^{\mathrm{PAR}} \dfrac{c_{l_k}}{c_{l_k} + 2\Gamma_k} & \text{, if cohort } k \text{ is a C}_3 \text{ plant} \\[2ex] \epsilon_k \dot{q}_k^{\mathrm{PAR}} & \text{, if cohort } k \text{ is a C}_4 \text{ plant} \end{cases} \quad .
\tag{89}
$$

Carboxylation may also be limited by the export rate of starch and sucrose that is synthesized by triose phosphate, especially
745 when ~~CO$_2$ concentration is high combined with high irradiance~~CO$_2$ concentration and irradiance are simultaneously high, at low temperatures, or O$_2$ concentration is low (von Caemmerer, 2000; Lombardozzi et al., 2018). This limitation was not included in ED-2.2.

Day respiration comprises all leaf respiration terms that are not dependent on photosynthesis, and it is mostly due to mitochondrial respiration; it is currently represented as a function of the maximum carboxylation rate, following Foley et al.
750 (1996):

$$
\dot{R}_k = f_R \dot{V}_{C_k}^{\mathrm{max}},
\tag{90}
$$

where f_R is a PFT-dependent parameter (Tables S5-S6).

Stomatal conductance is controlled by plants and is a result of a trade-off between the amount of carbon that leaves can uptake and the amount of water that plants may lose. Leuning (1995) proposed a semi-empirical stomatal conductance
755 expression for water based on these trade-offs:

$$
\hat{G}_{Wl_k} = \begin{cases} \hat{G}_{Wl_k}^{\varnothing} + \dfrac{M_k \dot{A}_k}{(c_{\lambda_k} - \Gamma_k)\left(1 + \dfrac{w_{l_k} - w_{\lambda_k}}{\Delta w_k}\right)} & \text{, if } \dot{A}_k > 0 \\[3ex] \hat{G}_{Wl_k}^{\varnothing} & \text{, if } \dot{A}_k \leq 0 \end{cases} \quad ,
\tag{91}
$$

where $\hat{G}_{Wl_k}^{\varnothing}$ is the residual conductance when stomata are closed, M_k is the slope of the stomatal conductance function, and Δw_k is an empirical coefficient controlling conductance under severe leaf-level water deficit; all of them are PFT-dependent parameters (Tables S5-S6). From Cowan and Troughton (1971), stomatal conductance of CO$_2$ is estimated by the ratio f_{Gl}
760 between the diffusivities of water and CO$_2$ in the air (Table S4):

$$
\hat{G}_{Wl_k} = f_{Gl} \hat{G}_{Cl_k}.
\tag{92}
$$

Variables w_{l_k}, $\dot{V}_{C_k}^{\mathrm{max}}$, $\dot{R}_k$, ϖ_k, $\mathcal{K}_{O_k}$, $\mathcal{K}_{C_k}$, Γ_k, and $\mathcal{K}_{\mathrm{ME}_k}$ are functions of leaf temperature and canopy air space pressure, and thus can be determined directly. In constrast, nine variables are unknown for each limitation case as well as for

the case when the stomata are closed: $\dot{E}_k$, $\dot{A}_k$, $\dot{V}_{C_k}$, $\dot{V}_{O_k}$, c_{l_k}, c_{λ_k}, w_{λ_k}, $\hat{G}_{Wl_k}$, and $\hat{G}_{Cl_k}$. The remaining unknown variables are determined numerically, following the algorithm described in Supplement S16.

The stomatal conductance model by Leuning (1995) (Eq. 91) is regulated by leaf vapor pressure deficit, however, Eq. (76) and Eq. (77) do not account for soil moisture limitation on photosynthesis. To represent this additional effect, we define a soil-moisture dependent scaling factor (f_{Wl_k}, Supplement S17) to reduce productivity and transpiration as soil available water decreases. Because stomatal conductance cannot be zero, the scaling factor f_{Wl_k} interpolates between the fully closed case $(\dot{A}_k^\varnothing; \dot{E}_k^\varnothing)$ and the solution without soil moisture limitation $(\dot{A}_k; \dot{E}_k)$, yielding to the actual fluxes of CO_2 ($\dot{C}_{l_k,c}$, $kg_C\,m^{-2}\,s^{-1}$) and water ($\dot{W}_{l_k,c}$, $kg_W\,m^{-2}\,s^{-1}$):

$$\dot{C}_{l_k,c} = -\not{p}_k \mathcal{M}_C \Lambda_k \left[(1 - f_{Wl_k})\, \dot{A}_k^\varnothing + f_{Wl_k}\, \dot{A}_k \right], \tag{93}$$

$$\dot{W}_{l_k,c} = \not{p}_k \mathcal{M}_w \Lambda_k \left[(1 - f_{Wl_k})\, \dot{E}_k^\varnothing + f_{Wl_k}\, \dot{E}_k \right], \tag{94}$$

where $\not{p}_k$ is 1 if the PFT is hypostomatous or 2 if the PFT is amphistomatous or needleleaf (Tables S5-S6). Alternatively, Xu et al. (2016) implemented a process-based plant hydraulics scheme that solves the soil-stem-leaf water flow in ED-2.2; details of this implementation are available in the referred paper.

For simplicity, we assume that the water content in the leaf intercellular space and the plant vascular system are constant, therefore the amount of water lost by the intercellular space through transpiration always matches the amount of water absorbed by roots. Plants may extract water from all layers to which they have access, and the amount of water extracted from each layer is proportional to the available water in the layer relative to the total available water ($W_{g_j}^\star$):

$$\sum_{j=j_{0k}}^{N_G} \dot{W}_{g_j,l_k} = \dot{W}_{l_k,c}, \tag{95}$$

$$\dot{W}_{g_j,l_k} = \dot{W}_{l_k,c} \frac{W_{g_j}^\star - W_{g_{j+1}}^\star}{W_{g_{j0}}^\star}, \tag{96}$$

where $W_{g_j}^\star$ is defined following Supplement S17 and $W_{g(N_G+1)}^\star \equiv 0$. The net water flux in the leaf intercellular space due to transpiration is assumed to be zero, however the associated net energy flux cannot be zero. Water enters the leaf intercellular space as liquid water at the soil temperature, reaches thermal equilibrium with leaves, and is lost to the canopy air space as water vapor at the leaf temperature. Therefore, the enthalpy flux between the soil layers and the cohort is calculated similarly to Eq. (35), whereas the enthalpy flux between the leaf intercellular space and the canopy air space is solved similarly to Eq. (75):

$$\dot{H}_{g_j,l_k} = \dot{W}_{g_j,l_k}\, q_\ell \left(T_{g_j} - T_{\ell 0} \right), \tag{97}$$

$$\dot{H}_{l_k,c} = \dot{W}_{l_k,c}\, q_{pv} \left(T_{t_k} - T_{v0} \right). \tag{98}$$

36

4.7 Non-leaf autotrophic respiration

Respiration from fine roots is defined using a phenomenological function of temperature that has the same functional form as leaf respiration (Moorcroft et al., 2001). Because roots are allowed in multiple layers, and in ED-2.2 roots have a uniform distribution of mass throughout the profile, the total respiration ($\dot{C}_{r_k,c}$: $\mathrm{kg_C\,m^{-2}\,s^{-1}}$) is the integral of the contribution from each soil layer, weighted by the layer thickness:

$$\dot{C}_{r_k,c} = C_{r_k} \frac{\sum_{j=j_{0k}}^{N_G} \left[\mathcal{T}' \left(T_{g_j}, r_{r_k} \right) \Delta z_{g_j} \right]}{\sum_{j=j_{0k}}^{N_G} \Delta z_{g_j}}, \tag{99}$$

where r_{r_k} ($\mathrm{s^{-1}}$) is the PFT-dependent factor that describes the relative metabolic activity of fine roots at the reference temperature $\color{blue}{(15°C}(15°C)$ (Tables S5-S6), and $\mathcal{T}'$ is the same temperature-dependent function from Eq. (86); default parameters are listed in Tables S5-S6.

Total storage respiration is a combination of two terms: a phenomenological term that represents the long-term turnover rate of the accumulated storage pool (individual-based $\dot{R}_{n_k}$ or flux-based $\dot{C}_{n_k,c}$), assumed constant (Medvigy et al., 2009), and a term related to the losses associated with the assimilated carbon for growth and maintenance of the living tissues (individual-based $\dot{R}_{\Delta_k}$ or flux-based $\dot{C}_{\Delta_k,c}$, Amthor, 1984). The latter is a ~~strong~~ function of the plant metabolic rate, which has strong daily variability hence is a function of the daily carbon balance:

$$\dot{C}_{n_k,c} = \tau_{n_k} C_{n_k}, \tag{100}$$

$$\dot{C}_{\Delta_k,c} = \tau_{\Delta_k} C_{\Delta_k}, \tag{101}$$

where $(\tau_{n_k}, \tau_{\Delta_k})$ are the PFT-dependent decay rates associated with storage turnover and consumption for growth, respectively (Tables S5-S6); and C_{Δ_k} ($\mathrm{kg_C\,m^{-2}}$) is the total accumulated carbon from the previous day as defined in Eq. (25). The transport from non-structural storage and the accumulated carbon for maintenance, growth and, storage is summarized in Supplement S3.

4.8 Heterotrophic respiration

Heterotrophic respiration comes from the decomposition of carbon in the three soil/litter carbon pools. For each carbon pool $e_j; j \in (1,2,3)$, we determine the maximum carbon loss based on the characteristic decay rate, which corresponds to the typical half-life for ~~metabolic litter (e_1),~~ metabolic and microbial litter (fast, e_1), ~~structural litter (e_2),~~ structural litter (intermediate, e_2), and ~~slow soil organic matter (e_3)~~ humified and passive soil carbon (slow, e_3), determined from Bolker et al. (1998):

$$\dot{C}_{e_j,c} = C_{e_j} f_{he_j} B_{e_j} \mathcal{E}_T \left(\overline{T}_{g20} \right) \mathcal{E}_{\vartheta'} \left(\overline{\vartheta}'_{20} \right), \tag{102}$$

where $f_{h\mathbf{e}}$ is the fraction of decay that is lost through respiration (Table S4), and by definition f_{he_3} must be always one (slow soil carbon can only be lost through heterotrophic respiration); $\cancel{B_{\mathbf{e}}}B_{e_j}$ are the decay rates at optimal conditions of soil carbon e_j, based on Bolker et al. (1998) (Table S4); $\overline{T}_{g_{20}}$ and $\overline{\vartheta}'_{20}$ are the average temperature and relative soil moisture of the top $0.2\,\mathrm{m}$ of soil; the relative soil moisture for each layer is defined as:

$$\vartheta'_{g_j} = \frac{\vartheta_{g_j} - \vartheta_{\mathrm{Re}}}{\vartheta_{\mathrm{Po}} - \vartheta_{\mathrm{Re}}};\tag{103}$$

and $\mathcal{E}_T(\overline{T}_{g_{20}})$ and $\mathcal{E}_{\vartheta'}(\overline{\vartheta}'_{20})$ are functions that reduces the decomposition rate due to temperature or soil moisture under ~~extreme~~non-optimal conditions:

$$\mathcal{E}_T(\overline{T}_{g_{20}}) = \frac{1}{\left\{1 + \exp\left[-\hat{f}_{\mathrm{Cold}}\left(\overline{T}_{g_{20}} - T_{g_{\mathrm{Cold}}}\right)\right]\right\}\left\{1 + \exp\left[\cancel{H} + \hat{f}_{\mathrm{Hot}}\left(\overline{T}_{g_{20}} - T_{g_{\mathrm{Hot}}}\right)\right]\right\}},\tag{104}$$

$$\mathcal{E}_{\vartheta'}(\overline{\vartheta}'_{20}) = \frac{1}{\left\{1 + \exp\left[-\hat{f}_{\mathrm{Dry}}\left(\overline{\vartheta}'_{20} - \vartheta'_{\mathrm{Dry}}\right)\right]\right\}\left\{1 + \exp\left[+\hat{f}_{\mathrm{Wet}}\left(\overline{\vartheta}'_{20} - \vartheta'_{\mathrm{Wet}}\right)\right]\right\}},\tag{105}$$

where $(\hat{f}_{\mathrm{Cold}};T_{g_{\mathrm{Cold}}})$, $(\hat{f}_{\mathrm{Hot}};T_{g_{\mathrm{Hot}}})$, $(\hat{f}_{\mathrm{Dry}};\vartheta'_{\mathrm{Dry}})$ and $(\hat{f}_{\mathrm{Wet}};\vartheta'_{\mathrm{Wet}})$ are phenomenological parameters to decrease decomposition rates at low and high temperatures, and dry and saturated soils, respectively (Table S4). The decay fraction from fast and structural soil carbon that is not lost through heterotrophic respiration is transported to the slow soil carbon (Supplement S4).

5 Results

5.1 Conservation of energy, water, and carbon dioxide

The ED-2.2 simulations show a high degree of conservation of the total energy, water, and carbon (Fig. 6). In the example simulation for one patch at Paracou, French Guiana (GYF), a tropical forest site, the accumulated deviation from perfect closure (residual) of the energy budget over 50 years (2,629,800 time steps) was 0.1% of the total enthalpy storage — sum of enthalpy stored at the canopy air space, cohorts, temporary surface water and soil layers (Fig. 6a) and 0.002% of the accumulated losses through eddy flux, the largest cumulative flux of enthalpy. Results for the water budget were even better, with maximum accumulated residuals of 0.04% of the total water stored in the ED-2.2 thermodynamic systems, or 0.0006% of the total water input by precipitation (Fig. 6b), and the accumulated residual of carbon was 0.008% of the total carbon storage or 0.017% the total accumulated loss through eddy flux. The average absolute residual errors by time step, relative to the total storage, ranged from $3.6 \cdot 10^{-11}$ (carbon) to $3.8 \cdot 10^{-10}$ (energy), and thus orders of magnitude less than the truncation error of single-precision numbers ($1.2 \cdot 10^{-7}$) and the model tolerance for each time step ($1.2 \cdot 10^{-5}$).

The conservation of energy and water of ED-2.2 also represents a substantial improvement from previous versions of the model. We carried out additional decadal-long simulations with ED-2.2 and two former versions of the model (ED-2.0.12 and ED-2.1) and the most similar configuration possible among versions, and found that cumulative residual of enthalpy
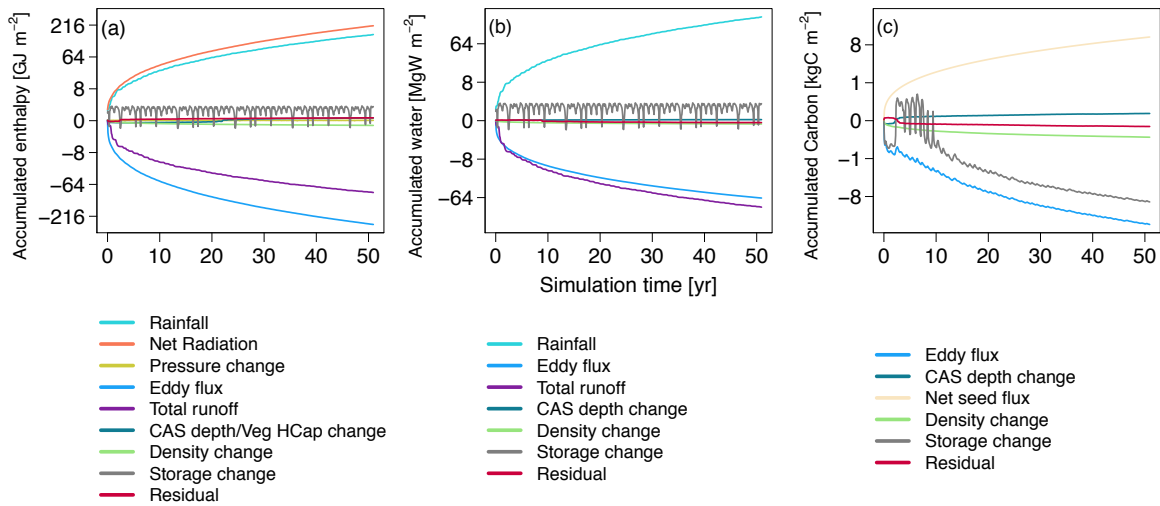
Figure 6. Example of (a) enthalpy, (b) water, and (c) carbon conservation assessment in ED-2.2, for a single-patch simulation at GYF for 50 years. Terms are presented as the cumulative contribution to the change storage. Total storage is the combination of canopy air space, cohorts, temporary surface water and soil layers in the case enthalpy and water, and canopy air space, cohorts, seed bank, and soil carbon pools in the case of carbon. Positive (negative) values mean accumulation (loss) by the combined storage pool over the time. Pressure change accounts for changes in enthalpy when pressure from the meteorological forcing is updated, and density change accounts for changes in mass to ensure the ideal gas law. Canopy air space (CAS) change and vegetation heat capacity (Veg Hcap) change reflect the addition/subtraction of carbon, water, and enthalpy due to the vegetation dynamics modifying the canopy air space depth and the total heat capacity of the vegetation due to biomass accumulation or loss. Storage change is the net gain or loss of total storage, and residual corresponds to the deviation from the perfect closure. Note that we present the y axis in cube root scale to improve visualization of the smallest terms.

845 relative to eddy flux loss decreased from 15.2% (ED-2.0.12) or 5.7% (ED-2.1) to $6.1 \cdot 10^{-5}\%$ (ED-2.2) (Fig. S3a-c). Similarly, the cumulative violation of perfect water budget closure, relative to total precipitation input, decreased from 3.4% (ED-2.0.12) or 1.1% (ED-2.1) to $1.2 \cdot 10^{-4}\%$ (ED-2.2) (Fig. S3d-f).

5.2 Simulated ecosystem heterogeneity

Because ED-2.2 accounts for the vertical distribution of the plant community and the local heterogeneity of ecosystems, it is
850 possible to describe the structural variability of ecosystems using continuous metrics. To illustrate this, we show the results of a ~~5 century~~6-century simulation (~~1500 − 2002~~$1400 − 2002$) carried out for tropical South America, starting from near-bare ground conditions and driven by the Princeton Global Meteorological Forcing (Sheffield et al., 2006, ; $1969 − 2008$), and with active fires (Supplement S3.4). For the last 100 years, we also prescribed land use changes derived from Hurtt et al. (2006) and Soares-Filho et al. (2006). The distribution of basal area binned by diameter at breast height (DBH) classes show high
855 variability across the domain, and even within biome boundaries (Fig. 7). For example, larger trees (DBH $\geq 50\,\mathrm{cm}$) are nearly absent outside the Amazon biome, with the exception of more humid regions such as the Atlantic Forest along the Brazilian coast, western Colombia, and Panama (Fig. 7d,e). In contrast, in seasonally dry areas as the Brazilian cerrado, intermediate-sized trees ($10 \leq \mathrm{DBH} < 50\,\mathrm{cm}$) contribute the most to the basal area (e.g. areas near site BSB, Fig. 7b,c). Even within the
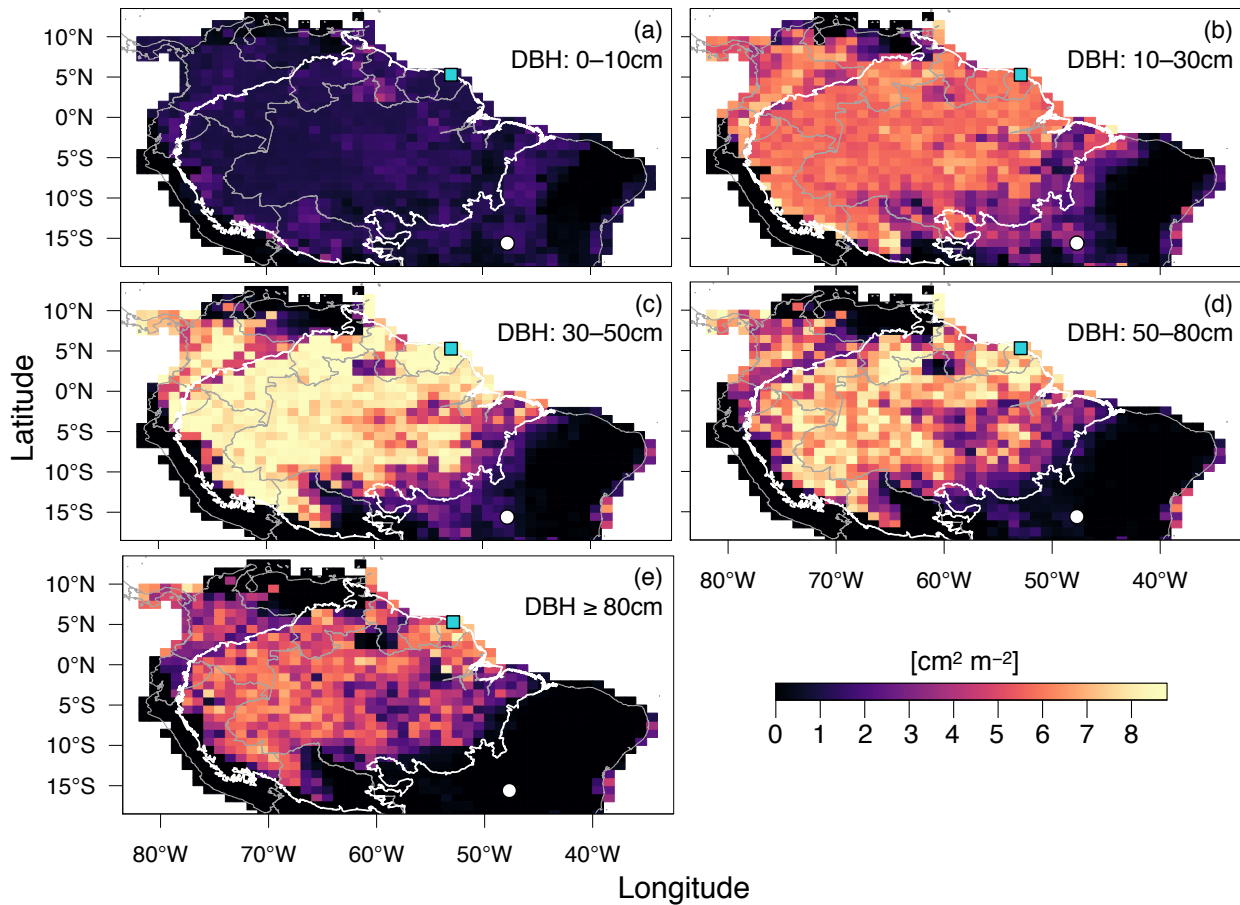
Figure 7. Simulated distribution of size-dependent basal area across tropical South America, aggregated for the following diameter at breast height (DBH) bins: (a) $0-10$ cm; (b) $10-30$ cm; (c) $30-50$ cm; (d) $50-80$ cm; (e) ≥ 80 cm. Maps were obtained from the final state of a ~~500-year~~6-century simulation (~~1500–2000~~1400–2002), initialized with near-bare ground conditions, active fires, and with prescribed land use changes between 1900 and ~~2000~~2002. Points indicate the location of the example sites (Fig. 8): (□) Paracou (GYF), a tropical forest site; (○) Brasília (BSB), a woody savanna site. White contour is the domain of the Amazon biome, and grey contours are the political borders.

Amazon ecoregion, basal area shows variability in the contribution of trees with different sizes, including the areas outside

860   the arc of deforestation along the southern and eastern edges of the biome (Fig. 7). Similarly, the abundance of different

plant functional groups shows great variability across the region, with dominance of grasses and early-successional tropical

trees in deforested regions and in drier areas in the Brazilian Cerrado, whereas late-succesional tropical trees dominating the

tropical forests, albeit with lower dominance in parts of Central Amazonia (Fig. S4).

        The variability of forest structural and functional composition observed in regional simulations emerge from both

865   the competition among cohorts in the local microenvironment and the environmental controls on the disturbance regime. In

Fig. 8 we present the impact of different disturbance regimes modulating the predicted ecosystem structure and composition for two sites: Paracou (GYF), a tropical forest region in French Guiana, and Brasília (BSB), a woody savanna site in Central Brazil. Both sites were simulated for 500 years using a 40-year meteorological forcing developed from local meteorological observations, following the methodology described in Longo et al. (2018); we allowed fires to occur but for simplicity we did not prescribe land use change. After 500 years of simulation, the structure at the two sites are completely different, with large, late-successional trees dominating the canopy at GYF (Fig. 8a) and open areas with shorter, mostly early-successional trees dominating the landscape at BSB (Fig. 8b). For GYF, the structural and functional composition is achieved only after 200 years of simulation, whereas in BSB a dynamic steady state caused by the strong fire regime is achieved in about 100 years (Fig. S5). At both sites, early sucessional trees dominate the canopy at recently disturbed areas (Fig. 8c,d) with late-successional (GYF) or mid-successional trees (BSB) increasing in size only at the older patches (> 30 years, Fig. 8c,d), and the variation of basal area as a function of age since last disturbance show great similarity at both sites (Fig. 8e). However, the disturbance regimes are markedly different: at GYF, fires never occurred and disturbance was driven exclusively by tree fall (prescribed at $1.11\%, \mathrm{yr}^{-1}$), whereas fires substantially increase the disturbance rates at BSB (average fire return interval of 19.3 years). Consequently, old-growth patches (older than 100 years) are nonexistent at BSB and abundant at GYF (Fig. S5Fig. 8f). In addition, the high disturbance regime at BSB meant that large trees and late-sucessional trees (slow growers) failed to establish, but succeeded and maintained a stable population at GYF (Fig. S5).

The impacts of simulating structurally and functionally diverse ecosystems are also observed in the fluxes of energy, water, carbon, and momentum. For example, in Fig. 9 we show the monthly average fluxes from the last 40 years of simulation at GYF, along with the interannual variability of the fluxes aggregated to the polygon-level (hereafter *polygon variability*, error bars) and the interannual variability of the fluxes accounting for the patch probability (hereafter *patch variability*, colors in the background). The polygon-level variability can be thought as the variability attributable exclusively to climate variability, whereas the patch variability also incorporates the impact of the structural heterogeneity in the variability. Most highly aggregated ("big-leaf") models characterize the polygon-level variability, but not the patch variability. However, in all cases, the patch variability far exceeded the polygon variability, indicating that structural variability is as important as the interannual variability in complex ecosystems. In the case of sensible heat, polygon variable was between 39 and 64% of the patch variability (Fig. 9a). The polygon-to-patch variability ratio was similar for both friction velocity ($19 - 39\%$) and water fluxes ($17 - 44\%$) (Fig. 9b,c). In the case of gross primary productivity, the relevance of patch variability was even higher, with polygon-to-patch variability ratio ranging from 3.7% during the dry season to 17% during the wet season (Fig. 9d). Importantly, the broader range of fluxes across patches in the site can be entirely attributed to structural and functional diversity, because all patches were driven by the same meteorological forcing.
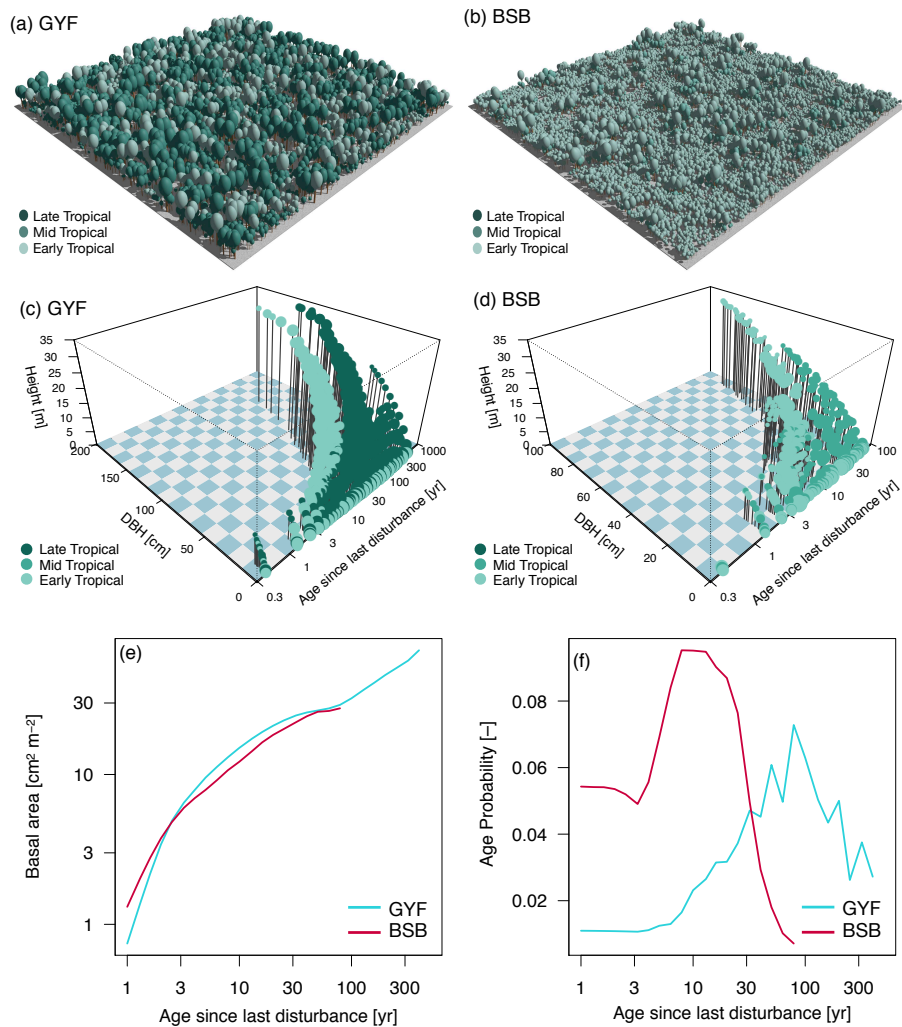
41

Figure 8. Example of size, age, and functional structure simulated by ED-2.2, after 500 years of simulation using local meteorological forcing and active fires. (a-b) Individual realization of simulated stands for sites (a) Paracou (GYF, tropical forest); (b) Brasília (BSB, woody savanna) using POV Ray. The number of individuals shown is proportional to the simulated stem density, the distribution in local communities is proportional to the patch area, the crown size and stem height are proportional to the cohort size, and the crown color indicates the functional group. (c-d) Distribution of cohorts as a function of size (diameter at breast height (DBH) and height), as function of and age since last disturbance (patch age) for sites (c) GYF and (d) BSB. Crown sizes are proportional to the logarithm of the stem density within each patch. (e,f) Patch-specific properties as a function of age since last disturbance (patch age) for sites GYF and BSB after 500 years of simulation: (e) basal area and (f) probability density function of age (patch area). See Fig. 7 for the location of both example sites.
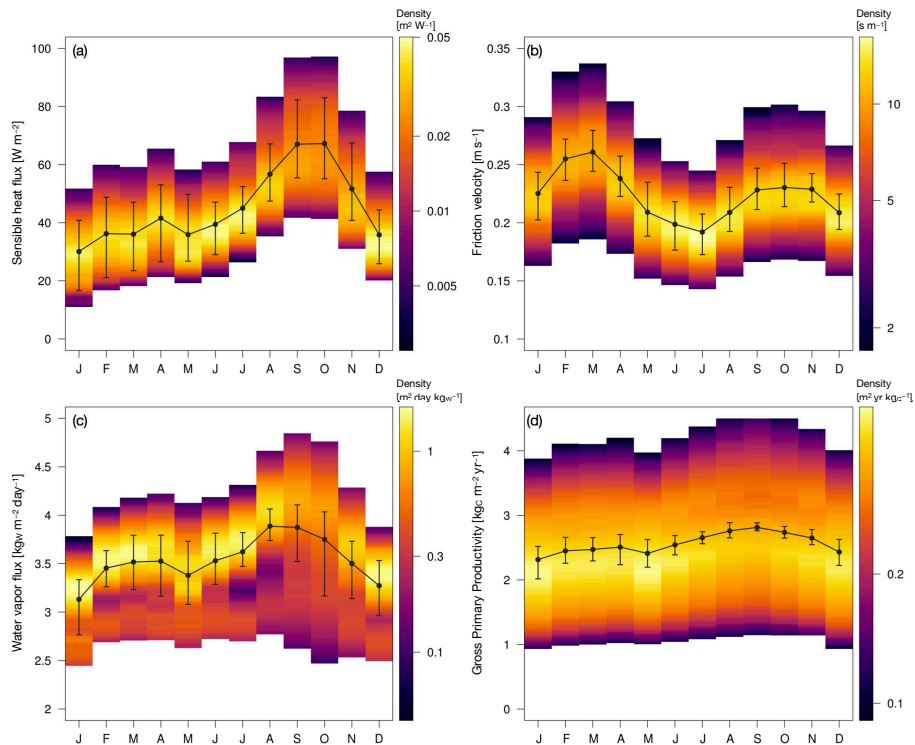
Figure 9. Monthly averages and variability of fluxes attributable to meteorological conditions and plant community heterogeneity combined with interannual variability. Results are shown for GYF, a tropical forest site for (a) sensible heat flux; (b) friction velocity (momentum flux); (c) water vapor flux; and (d) gross primary productivity. The variability was calculated for the last 40 years of a 500-year simulation starting from near-bare ground. Points correspond to the 40-year monthly averages for the entire polygon, line bars correspond to the $2.5 - 97.5\%$ quantile of monthly averages aggregated at the polygon level (polygon interannual variability), and background colors represent the 40-year probability density function of monthly means for each simulated patch, and scaled by the area of each patch (patch interannual variability). Density function colors outside the $2.5 - 97.5\%$ quantile interval are not shown. Note that the density function scale is logarithmic. See Fig. 7 for the location of the example site.

6   Discussion

6.1   Conservation of biophysical and biogeochemical properties

As demonstrated in Section 5.1, it is possible to represent the long-term, large-scale dynamics of heterogeneous and functionally diverse plant canopy while still accurately conserving the fluxes of carbon, water and energy fluxes that occur the ecosystem. ED-2.2 exhibits excellent conservation of energy, water, and carbon dioxide even in multi-decadal scales. After 50 years of simulation, the accumulated residuals from perfect closure never exceeded 0.1% of the total energy, water, and carbon stored in the pools resolved by the model (Fig. 6), which is significantly less than the error accepted in each time step (1%).

The model's excellent conservation of these three key properties is possible because the ordinary differential equations are written directly in terms of the variables that we sought to conserve, thus reducing the effects of non-linearities.

A key feature that facilitates the model's high level of energy conservation is the use of enthalpy as the primary ~~state variables~~energy-related state variable within the model. This contrasts with most terrestrial biosphere models, which use temperature as their energy state variable (e.g. Best et al., 2011; Oleson et al., 2013). By using enthalpy, the model can seamlessly incorporate energy storage changes caused by rapid changes in water content and consequently heat capacity. It also reduces errors near phase changes (freezing or melting), when changes in energy may not correspond to changes in temperature. Nonetheless, the residual errors in ED-2.2 are larger than the error of each time steps after integrating the model over multiple decades (Fig. 6), which suggests that the errors may have a systematic component that deserves further investigation. The main contribution to the remaining residual errors in carbon, water, and energy fluxes comes from the linearization of the prognostic equations due to changes in density in the canopy air space (Eq. 18-19;23). The magnitude of these residuals would likely be further reduced by using the bulk enthalpy, water content, and carbon dioxide content in the canopy air space as the state variables instead of the specific enthalpy, specific humidity and CO_2 mixing ratio.

Unlike most existing terrestrial biosphere models (but see SiB2, e.g. Baker et al., 2003; Vidale and Stöckli, 2005), in ED-2.2 we explicitly include the dynamic storage of energy, water, and carbon dioxide in the canopy air space. Canopy air space storage is particularly important in tall, dense tropical forests; accounting for this storage term, as well as the energy storage of vegetation allows a more realistic representation of the fluxes between the ecosystem and the air above (see also Haverd et al., 2007). In addition, the separation of the ecosystem fluxes in the model into eddy fluxes and change in canopy air space storage allows a thorough evaluation of the model's ability to represent both the total exchange and the ventilation of water, energy and carbon in and out of the ecosystem with eddy covariance towers, as shown in the companion paper (Longo et al., 2019).

6.2 Heterogeneity of ecosystems

It has been long advocated that terrestrial biosphere models must incorporate demographic processes and ecosystem heterogeneity to improve their predictive ability in a changing world (Moorcroft, 2006; Purves and Pacala, 2008; Evans, 2012; Fisher et al., 2018). In ED-2.2, we aggregate individuals and forest communities according to similar characteristics (Fig. 1). For example, individuals are only aggregated into cohorts if they are of similar size, same functional group, and live in comparable micro-environments. Likewise, local plant communities are aggregated only if their disturbance history and their vertical structure are similar. The level of aggregation of ED-2.2 still allows mechanistic representation of ecological processes such as how individuals' access to and competition for resources vary depending on their size, adaptation, and presence of other individuals. This approach allows representing a broad range of structure and composition of ecosystems (Fig. 7,S4), as opposed to simplified biome classification. In this manuscript, we presented the functional diversity using only the default tropical plant functional types (PFTs), which describe the functional diversity along a single functional trait axis of broadleaf tropical trees. However, the ED-2.2 framework allows users to easily modify the traits and trade-offs of existing PFTs, or include new functional groups; previous studies using ED-2.2 have leveraged this feature of the code to define PFTs according to the research question both in the tropics (e.g. Xu et al., 2016; Trugman et al., 2018; Feng et al., 2018) and in the extra-tropics (e.g. Raczka et al., 2018; Bogan et al., 2019).

44

Previous analysis by Levine et al. (2016) has shown that the dynamic, fine-scale heterogeneity and functional diversity of the plant canopy in ED-2.2 is essential for capturing macro-scale patterns in tropical forest properties. Specifically, Levine et al. (2016) found that ED-2.1 was able to characterize the smoother observed transition in tropical forest biomass across a dry-season length gradient in the Amazon, whereas a highly aggregated (big-leaf like) version of ED-2.1 predicted abrupt shifts in biomass, which is commonly observed in many dynamic global vegetation models (e.g. Good et al., 2011). Results from two related studies have shown that the incorporation of sub-grid scale heterogeneity and diversity within ED-2 also improves its ability to correctly capture the responses of terrestrial ecosystems to environmental perturbation. First, in an assessment of the ability of four terrestrial biosphere models to capture the impact of rainfall changes on biomass in Amazon forests (Powell et al., 2013), ED-2.1 was the only model that captured the timing and average magnitude of above-ground biomass loss that was observed in two experimental drought treatments while all three big-leaf model formulations predicted minimal impacts of the drought experiment. Second, a recent analysis by Longo et al. (2018) on the impact of recurrent droughts in the Amazon found that drought-induced carbon losses in ED-2.2 arose mostly from the death of canopy trees, a characteristic that is consistent with field and remote sensing observations of drought impacts in the region (Phillips et al., 2010; Yang et al., 2018).

Importantly, since its inception, the ED model accounts for the disturbance-driven horizontal heterogeneity of ecosystems (Moorcroft et al., 2001). As demonstrated in Moorcroft et al. (2001), the continuous development of treefall gaps is fundamental to explaining the long-term trajectory of biomass accumulation in tropical forests; for example, by representing both recently disturbed and old-growth fragments of forests, it is possible to simulate micro-environments where either shade-intolerant plants thrive or slow-growing, shade-tolerant individuals dominate the canopy (Fig. 8a,c). Moreover, ED-2.2 can also represent dynamic and diverse disturbance regimes, which ultimately mediate the regional variation of ecosystem properties. For example, tropical forests and woody savannas may share similarities in local communities with similar age since disturbance (Fig. 8e); however, because fire disturbances frequently affect large areas in the savannas, fragments of old-growth vegetation are nearly absent in these regions (Fig. 8f), which creates an environment dominated mostly by smaller trees (Fig. S5c).

Furthermore, the heterogeneity of ecosystems in ED-2.2 is integrated across all time scales, because we solve the biophysical and biogeochemical cycles for each cohort and each patch separately (Fig. 2-3). While solving the cycles at sub-grid scale adds complexity, it also improves the characterization of heterogeneity of available water and energy for plants of different sizes, even within the same polygon: for example, the light profile and soil water availability are not only determined by meteorological conditions, but also by the number of individuals, their height and their rooting depth, and their traits and trade-offs that determine their ability to extract soil moisture or assimilate carbon. As a result, the variability in ecosystem functioning represented by ED-2.2 is significantly increased relative to the variability that a highly aggregated model based on the average ecosystem structure would be able to capture (Fig. 9).

6.3 Current and Future Developments

In this manuscript, we focused on describing the biophysical and biogeochemical core of the ED-2.2 model, and appraising its ability to represent both short-term (intra-annual and interannual) and long-term (decades to century) processes. However, the ED-2.2 community is continuously developing and improving the model. In this section we summarize some of the recent and ongoing model developments being built on top of the ED-2.2 dynamic core.

Terrestrial biosphere models still show significant uncertainties in representing photosynthesis due to missing processes and inconsistencies in parameter estimations (Rogers et al., 2017). We are currently implementing the carboxylation limitation by the maximum electron transport rate and by the triose phosphate utilization (von Caemmerer, 2000; Lombardozzi et al., 2018), and constrained by observations (Norby et al., 2017)~~, and incorporating nitrogen and phosphorus limitation~~, and nitrogen and phosphorus limitation have been recently incorporated (Medvigy et al., 2019). In addition, the model has also been recently updated to mechanistically represent plant hydraulics, and ~~first~~initial results indicate a significant improvement of ~~the~~ the model's ~~prediction~~predictions of water use efficiency and water stress in tropical forests in Central America (Xu et al., 2016). Also, to better represent the dynamics of soil carbon in ED-2.2, we are implementing and optimizing a more detailed version of the CENTURY decomposition model (Bolker et al., 1998).

To improve the representation of surface and soil water dynamics, the model has been coupled with a hydrological routine model that accounts for lateral flux of water as a function of terrain characteristics and simulates river discharge (Pereira et al., 2017; Arias et al., 2018). Moreover, an integrated approach of hydraulic routing based on TOPMODEL (Walko et al., 2000; Beven and Freer, 2001), which allows exchange of water and internal energy exchange between different sites as a function of topographic characteristics, is being implemented in ED-2.2.

The ED-2.2 model framework is designed to simulate functionally diverse ecosystems, but trait values within each functional group are fixed. To account for the observed plasticity in many leaf traits, a new parameterization of leaf trait variation as function of the light level, based on the parameterization by Lloyd et al. (2010) and (Xu et al., 2017) is being implemented. In addition, the ED-2.2 model has also been recently updated to represent the light competition and parasite-host relationships between lianas and trees (di Porcia e Brugnera et al., 2019), and it is currently being extended to incorporate plant functional types from different biogeographic regions, such as temperate semi-arid shrublands (Pandit et al., 2018), as well as boreal ecosystems, building on previous works using ED-1 (Ise et al., 2008).

Anthropogenic forest degradation is pervasive throughout the tropics (Lewis et al., 2015). To improve the model's ability to represent damage and recovery from degradation, we are implementing a selective logging module that represents the direct impact of felling of marketable ~~individuals~~tree stems, and accounts the damage associated with skid trails, roads and decks, which are modulated by logging intensity and logging techniques (Pereira Jr. et al., 2002; Feldpausch et al., 2005). In addition, the original fire model has been recently improved to account for size- and bark-thickness-dependent survivorship (Trugman et al., 2018), and is being developed to account for natural and anthropogenic drivers of ignition, fire intensity, fire spread and fire duration, building on existing process-based fire models (Thonicke et al., 2010; Le Page et al., 2015).

The complexity and sophistication of ED-2.2 also creates important scientific challenges. For example, the multiple processes for functionally diverse ecosystems represented by the model also requires a large number of parameters, with some of them being highly uncertain given the scarcity of data. To explore the effect of parameter uncertainty on model results and leverage the growing number of observations, the ED-2.2 model has been fully integrated with the Predictive Ecosystem Analyzer (LeBauer et al., 2013; Dietze et al., 2014), a hierarchical-Bayesian-based framework that constrains model parameters based on available data and quantifies the uncertainties on model predictions due to parameter uncertainty.

Importantly, the need to incorporate terrestrial ecosystem heterogeneity in Earth System Models has been long advocated (e.g. Moorcroft, 2006; Purves et al., 2008; Evans, 2012), but only recently global models have been incorporating ecological mechanisms that allow representing functionally diverse and heterogeneous biomes at global scale without relying on artificial climate envelopes. ~~One example is~~Two examples are the Geophysical Fluid Dynamics Laboratory (GFDL) Land Model version 3 with Perfect Plasticity Approximation (Weng et al., 2015, LM3-PPA;) and the Functionally Assembled Terrestrial Ecosystem Simulation (FATES; Fisher et al., 2015), which incorporated the patch and cohort structure of ED-2.2 into the Community Land Model (CLM; Oleson et al., 2013) framework.

7   Conclusions

ED-2.2 represents a significant advance in how to integrate a variety of processes ranging across multiple time scales in heterogeneous landscapes: it retains all the detailed representation of the long-term dynamics of functionally diverse, spatially heterogeneous landscapes and long-term dynamics from the original ED ecosystem model (Moorcroft et al., 2001; Hurtt et al., 2002; Albani et al., 2006), but also solves for the associated energy, water, and CO_2 fluxes of plants living in horizontally and vertically stratified micro-environments within the plant canopy, which was initially implemented by Medvigy et al. (2009) (ED-2) by adapting the big-leaf land surface model LEAF-3 (Walko et al., 2000) to the cohort-based structure of ED-2.

The results presented in the model description demonstrated that ED-2.2 has a high degree of conservation of carbon, energy, and water, even over multi-decadal scales (Fig. 6). Importantly, the current formulation of the model allows ~~us to represent~~representation of functional and structural diversity both at local and regional scales (Fig. 7-8;S4-S5), and the effect of the heterogeneity on energy, water, carbon, and momentum fluxes (Fig. 9). In the companion paper, we use data from eddy covariance towers, forest inventory, bottom-up estimates of carbon cycles and remote sensing products to assess the strengths and limitations of the current model implementation (Longo et al., 2019).

This manuscript focused on the ~~milestone~~major updates ~~into~~ the energy, water, and carbon cycle within the ED-2.2 framework; ~~however,t~~the model continues to be actively developed. Some of the further developments include: implementing more mechanisms that influence photosynthesis and water cycle, such as plant hydraulics~~, nutrient cycling,~~; additional nutrient cycles; expanding the representation of plant functional diversity, including trait plasticity and lianas~~, as well as~~; and expanding the types of natural and anthropogenic disturbances. ED-2.2 is a collaborative, open-source model that is readily available from its repository, and the scientific community is encouraged to use the model and contribute with new model developments.

47

References

1060   Ahlström, A., Schurgers, G., Arneth, A., and Smith, B.: Robustness and uncertainty in terrestrial ecosystem carbon response to CMIP5 climate change projections, Environ. Res. Lett., 7, 044 008, https://doi.org/10.1088/1748-9326/7/4/044008, 2012.

Albani, M., Medvigy, D., Hurtt, G. C., and Moorcroft, P. R.: The contributions of land-use change, CO_2 fertilization, and climate variability to the eastern US carbon sink, Glob. Change Biol., 12, 2370–2390, https://doi.org/10.1111/j.1365-2486.2006.01254.x, 2006.

Amthor, J. S.: The role of maintenance respiration in plant growth, Plant Cell Environ., 7, 561–569, https://doi.org/10.1111/1365-
1065   3040.ep11591833, 1984.

Antonarakis, A. S., Saatchi, S. S., Chazdon, R. L., and Moorcroft, P. R.: Using Lidar and Radar measurements to constrain predictions of forest ecosystem structure and function, Ecol. Appl., 21, 1120–1137, https://doi.org/10.1890/10-0274.1, 2011.

Antonarakis, A. S., Munger, J. W., and Moorcroft, P. R.: Imaging spectroscopy- and lidar-derived estimates of canopy composition and structure to improve predictions of forest carbon fluxes and ecosystem dynamics, Geophys. Res. Lett., 41, 2535–2542,
1070   https://doi.org/10.1002/2013GL058373, 2014.

Arias, M. E., Lee, E., Farinosi, F., Pereira, F. F., and Moorcroft, P. R.: Decoupling the effects of deforestation and climate variability in the Tapajós river basin in the Brazilian Amazon, Hydrol. Process., 32, 1648–1663, https://doi.org/10.1002/hyp.11517, 2018.

Avissar, R. and Mahrer, Y.: Mapping frost-sensitive areas with a three-dimensional local-scale numerical model. Part I. Physical and numerical aspects, J. Appl. Meteor., 27, 400–413, https://doi.org/10.1175/1520-0450(1988)027<0400:MFSAWA>2.0.CO;2, 1988.

1075   Baker, I., Denning, A. S., Hanan, N., Prihodko, L., Uliasz, M., Vidale, P.-L., Davis, K., and Bakwin, P.: Simulated and observed fluxes of sensible and latent heat and CO_2 at the WLEF-TV tower using SiB2.5, Glob. Change Biol., 9, 1262–1277, https://doi.org/10.1046/j.1365-2486.2003.00671.x, 2003.

Bazzaz, F. A.: The physiological ecology of plant succession, Annu. Rev. Ecol. Syst., 10, 351–371, https://doi.org/10.1146/annurev.es.10.110179.002031, 1979.

1080   Best, M. J., Pryor, M., Clark, D. B., Rooney, G. G., Essery, R. L. H., Ménard, C. B., Edwards, J. M., Hendry, M. A., Porson, A., Gedney, N., Mercado, L. M., Sitch, S., Blyth, E., Boucher, O., Cox, P. M., Grimmond, C. S. B., and Harding, R. J.: The Joint UK Land Environment Simulator (JULES), model description – Part 1: Energy and water fluxes, Geosci. Model Dev., 4, 677–699, https://doi.org/10.5194/gmd-4-677-2011, 2011.

Betts, A. K. and Silva Dias, M. A. F.: Progress in understanding land-surface-atmosphere coupling from LBA research, J. Adv. Model.
1085   Earth Syst., 2, https://doi.org/10.3894/JAMES.2010.2.6, http://dx.doi.org/10.3894/JAMES.2010.2.6, 2010.

Beven, K. and Freer, J.: A dynamic TOPMODEL, Hydrol. Process., 15, 1993–2011, https://doi.org/10.1002/hyp.252, 2001.

Blyth, E., Clark, D. B., Ellis, R., Huntingford, C., Los, S., Pryor, M., Best, M., and Sitch, S.: A comprehensive set of benchmark tests for a land surface model of simultaneous fluxes of water and carbon at both the global and seasonal scale, Geosci. Model Dev., 4, 255–269, https://doi.org/10.5194/gmd-4-255-2011, 2011.

1090   Bogan, S. A., Antonarakis, A. S., and Moorcroft, P. R.: Imaging spectrometry-derived estimates of regional ecosystem composition for the Sierra Nevada, California, Remote Sens. Environ., 228, 14–30, https://doi.org/10.1016/j.rse.2019.03.031, 2019.

Bolker, B. M., Pacala, S. W., and Parton, W. J.: Linear analysis of soil decomposition: insights from the CENTURY model, Ecol. Appl., 8, 425–439, https://doi.org/10.1890/1051-0761(1998)008[0425:LAOSDI]2.0.CO;2, 1998.

Bonan, G. B.: Land-atmosphere CO2 exchange simulated by a land surface process model coupled to an atmospheric general circulation
1095   model, J. Geophys. Res.-Atmos., 100, 2817–2831, https://doi.org/10.1029/94JD02961, 1995.
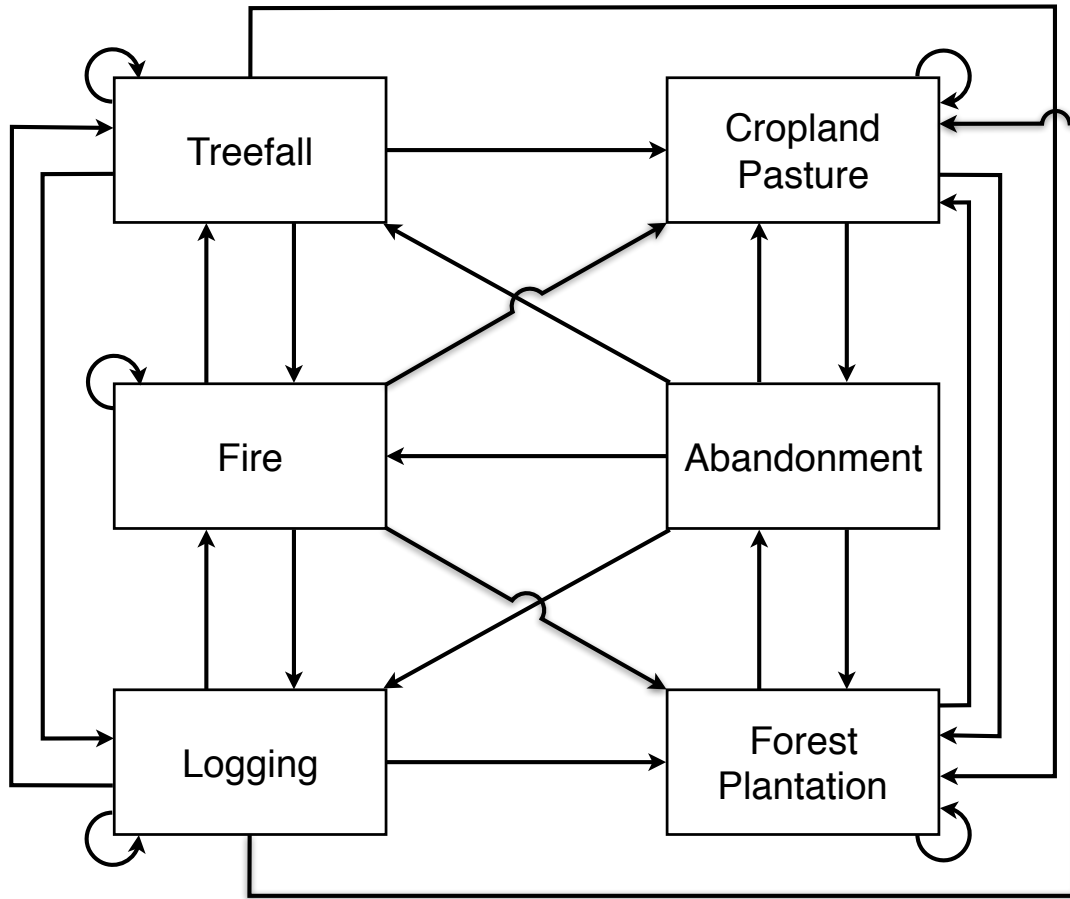
Figure S1: ~~Schematics~~Schematic of disturbance types that generate new patches in ED-2.2. Patches are classified according to the last disturbance type (boxes), and new disturbances that create new patches are indicated by arrows (the arrow head points to the new disturbance type). The absence of arrows between some disturbance patches (e.g. from cropland to tree fall) indicate that such transition is not allowed. Arrows pointing to the same disturbance type indicate generation of new patches without change in the disturbance type. **(Figure was updated: some arrows were missing.)**
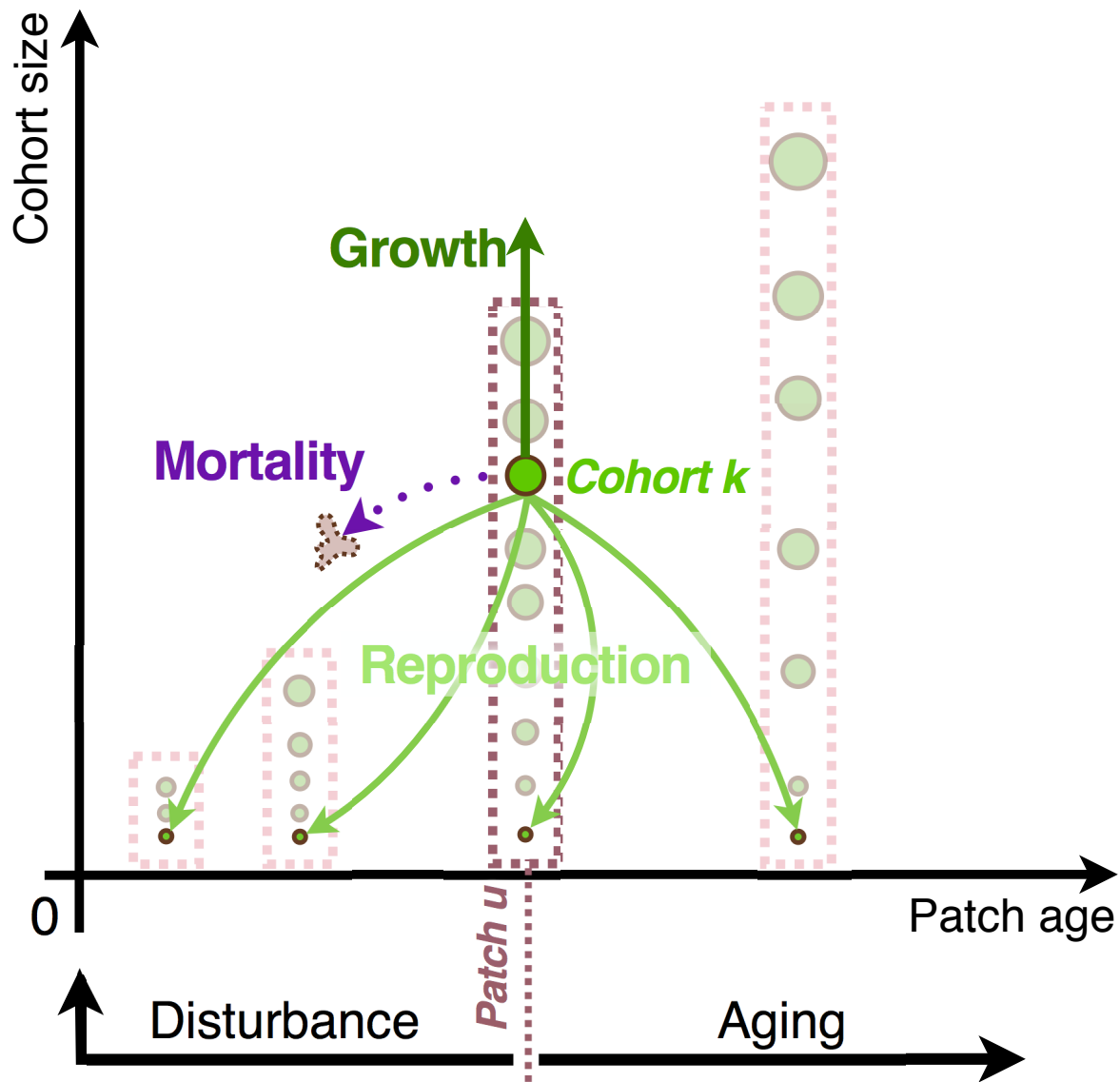
Figure S2: Schematics of ecosystem dynamics in ED-2.2, based on Fig. 5 of Moorcroft et al. (2001). The diagram shows a simplified case in which only of plant functional type and one disturbance type exist. Each dashed box corresponds to one patch, and each circle correspond to one cohort. Changes in the ecosystem structure are represented by arrows: ~~grey~~green and purple arrows are associated with cohort dynamics, and black arrows are associated with patch dynamics. Every cohort time step, cohorts can grow in size, some of the cohort population is lost through mortality, and new cohorts are generated from reproduction. Every patch time step, patch age is increased linearly due to age, and a fraction of each patch is lost through disturbance, which resets patch age.
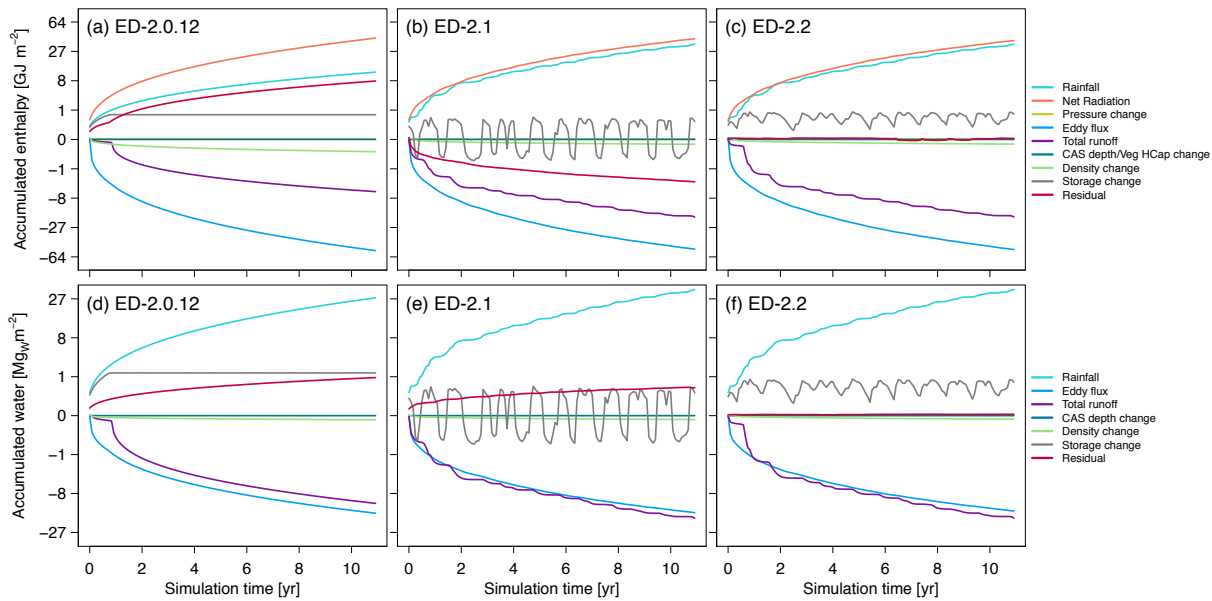
Figure S3: Comparison of budget closure for (a-c) enthalpy and (d-f) water between three different ED-2 versions: (a,d) ED-2.0.12 (`https://github.com/EDmodel/ED2/releases/tag/rev-12`), the first stable version of ED-2.0 (Medvigy et al., 2009) using the current model code structure; (b,e) ED-2.1 (`https://github.com/EDmodel/ED2/releases/tag/rev-64`); (c,f) ED-2.2. Simulations were carried out for a single-patch simulation at GYF for 11 years, without vegetation dynamics (earlier releases did not account for changes in energy and water when vegetation dynamics was active). Terms are presented as the cumulative contribution to the change storage. Total storage is the combination of canopy air space, cohorts, temporary surface water and soil layers. Positive (negative) values mean accumulation (loss) by the combined storage pool over the time. Pressure change accounts for changes in enthalpy when pressure from the meteorological forcing is updated, and density change accounts for changes in mass to ensure the ideal gas law. Canopy air space (CAS) change and vegetation heat capacity (Veg Hcap) change reflect the addition/subtraction of carbon, water, and enthalpy due to the vegetation dynamics modifying the canopy air space depth and the total heat capacity of the vegetation due to biomass accumulation or loss. Storage change is the net gain or loss of total storage, and residual corresponds to the deviation from the perfect closure. Note that we present the y axis in cube root scale to improve visualization of the smaller terms. Details on developments of ED-2.0.12, ED-2.1, and ED-2.2 are described in Supplement S1.
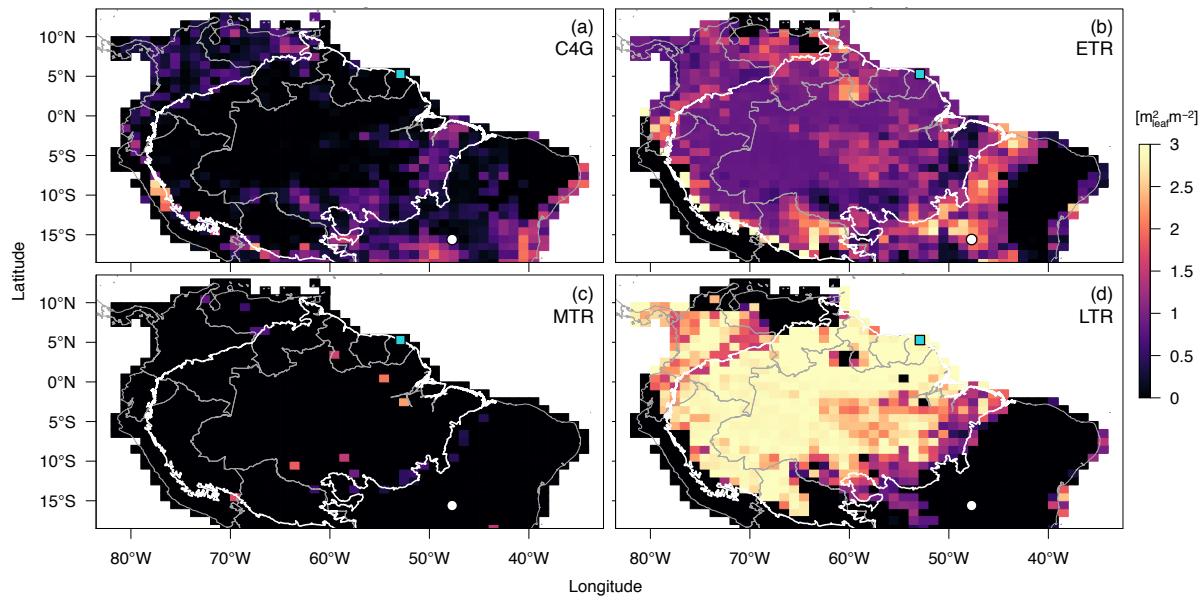
Figure S4: Simulated distribution of PFT-dependent leaf area index across tropical South America: (a) C$_4$ grasses (C4G); (b) Early-successional, tropical trees (ETR); (c) mid-successional, tropical trees (MTR); (d) late-successional, tropical trees (LTR). Maps were obtained from the final state of a ~~500-year~~6-century simulation (~~1500–2000~~1400–2002), initialized with near-bare ground conditions, active fires, and with prescribed land use changes between 1900 and ~~2000~~2002. Points indicate the location of the example sites (Fig. 8): (□) Paracou (GYF), a tropical forest site; (◯) Brasília (BSB), a woody savanna site. White contour is the domain of the Amazon biome, and grey contours are the political borders.
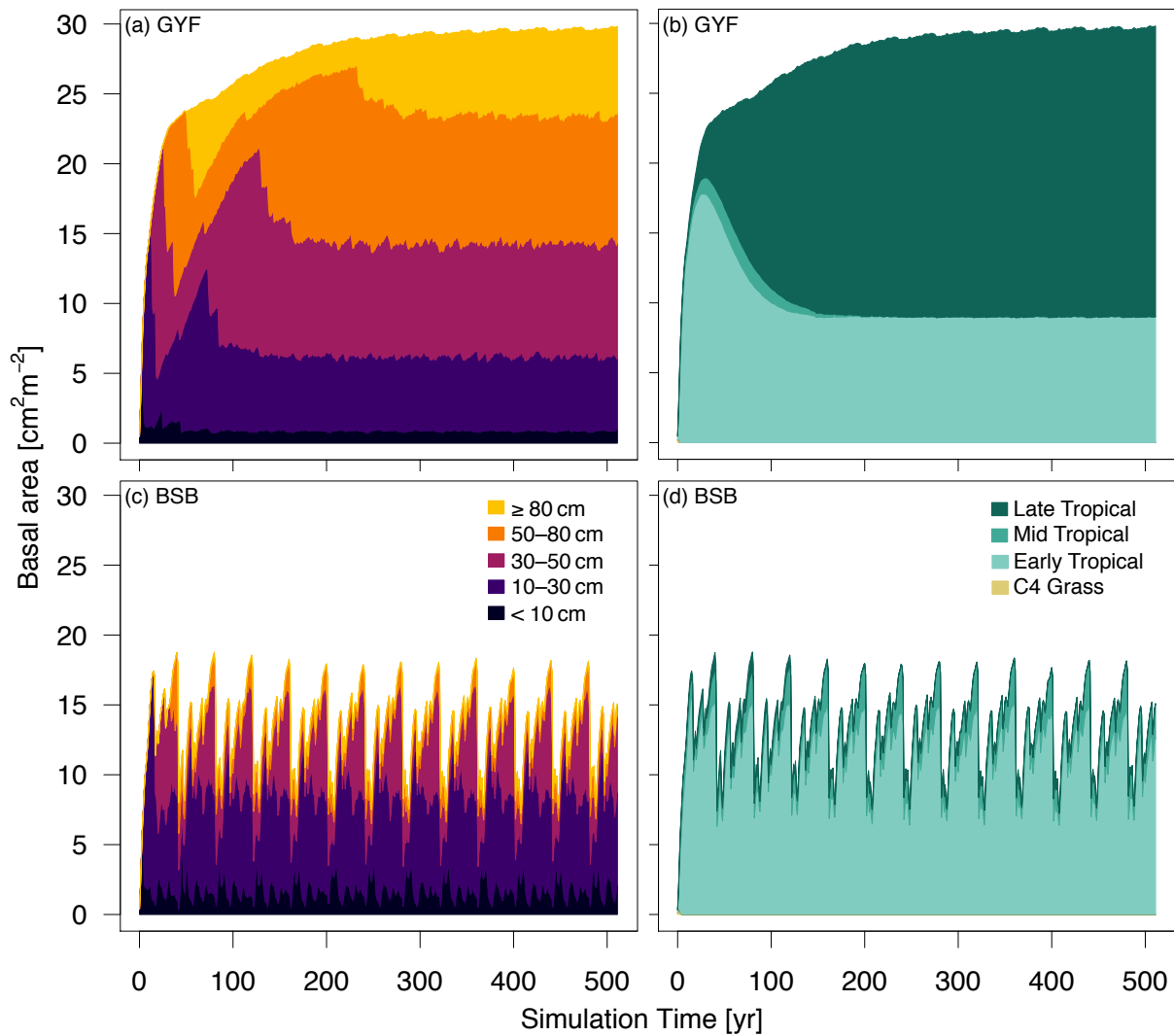
Figure S5: Simulated time series of basal area for near-bare ground simulations for (a,b) Paracou (GYF, tropical forest) and (c,d) Brasília (BSB, woody savanna), using local meteorological forcing and active fires, colored by the relative contribution of (a,c) plants of different sizes and (b,d) plants of different functional groups. See Fig. S4 for the location of both example sites.

Soil classes – ED.2.2
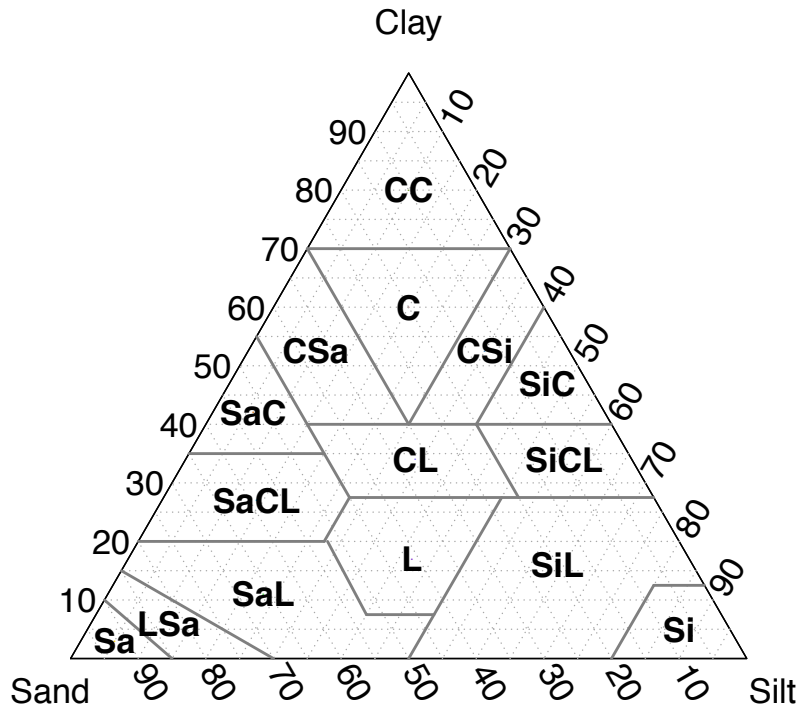
Figure S6: Barycentric diagram of volumetric percentage of soil particle sizes (sand, silt, and clay) along with the canonical soil texture classes in ED-2.2. Classes are: Sa – sand, LSa – loamy sand, SaL – sandy loam, SiL – silty loam, L – loam, SaCL – sandy clay loam, SiCL – silty clay loam, CL – clayey loam, SaC – sandy clay, SiC – silty clay, C – clay, Si – silt, CC – heavy clay, CSa – clayey sand, and CSi – clayey silt.
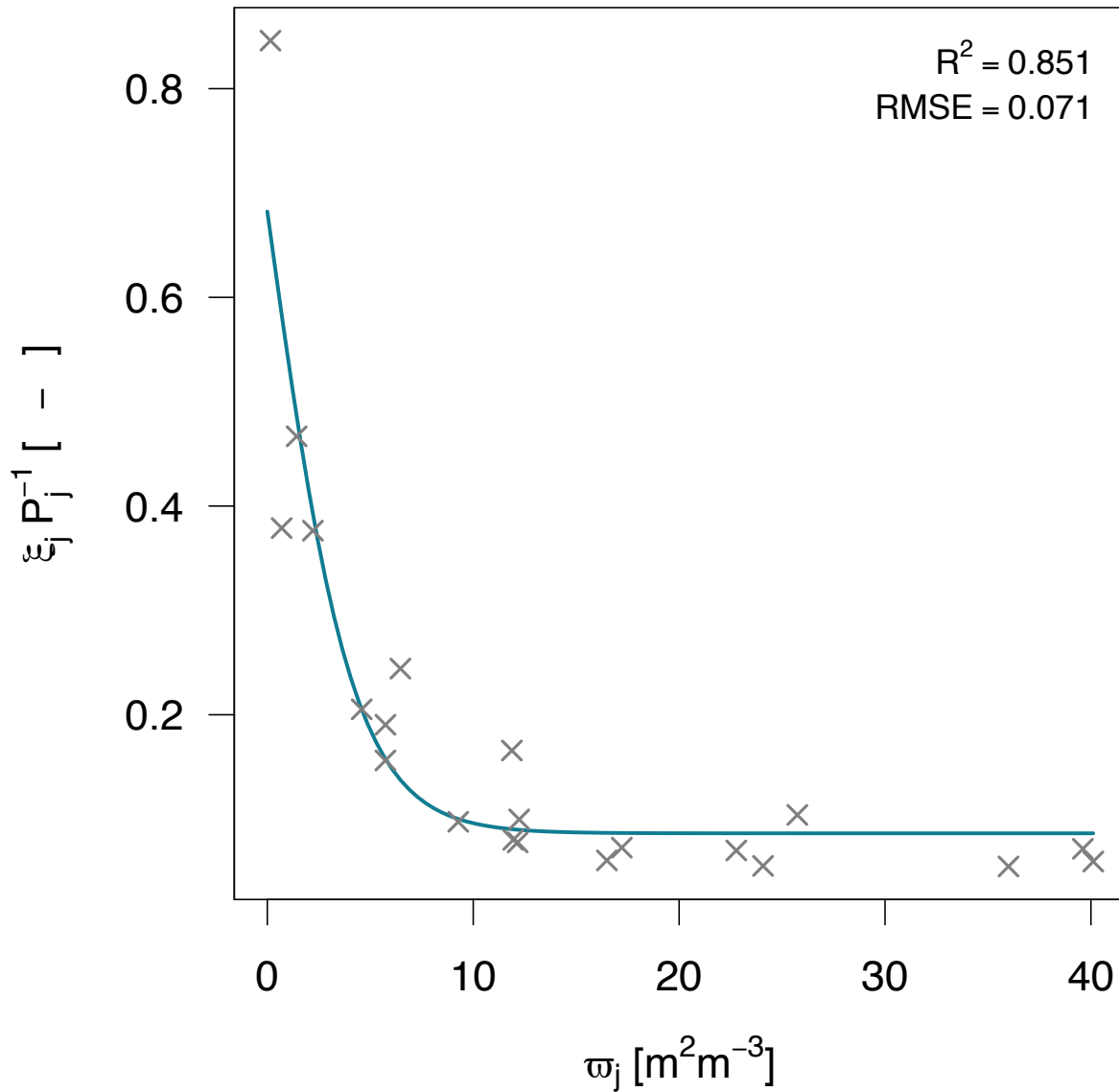
Figure S7: Fitted curve (Eq. S135) relating the effective drag coefficient ($\xi_j / \mathcal{P}_j$, $\xi_j \mathcal{P}_j^{-1}$) with plant area density (ϕ_j). Data points for fitting were extracted from Figure 3a of Wohlfahrt and Cernusca (2002) using a digitizer tool. Adjusted R^2 and the root mean square error (RMSE) are shown in the top right.
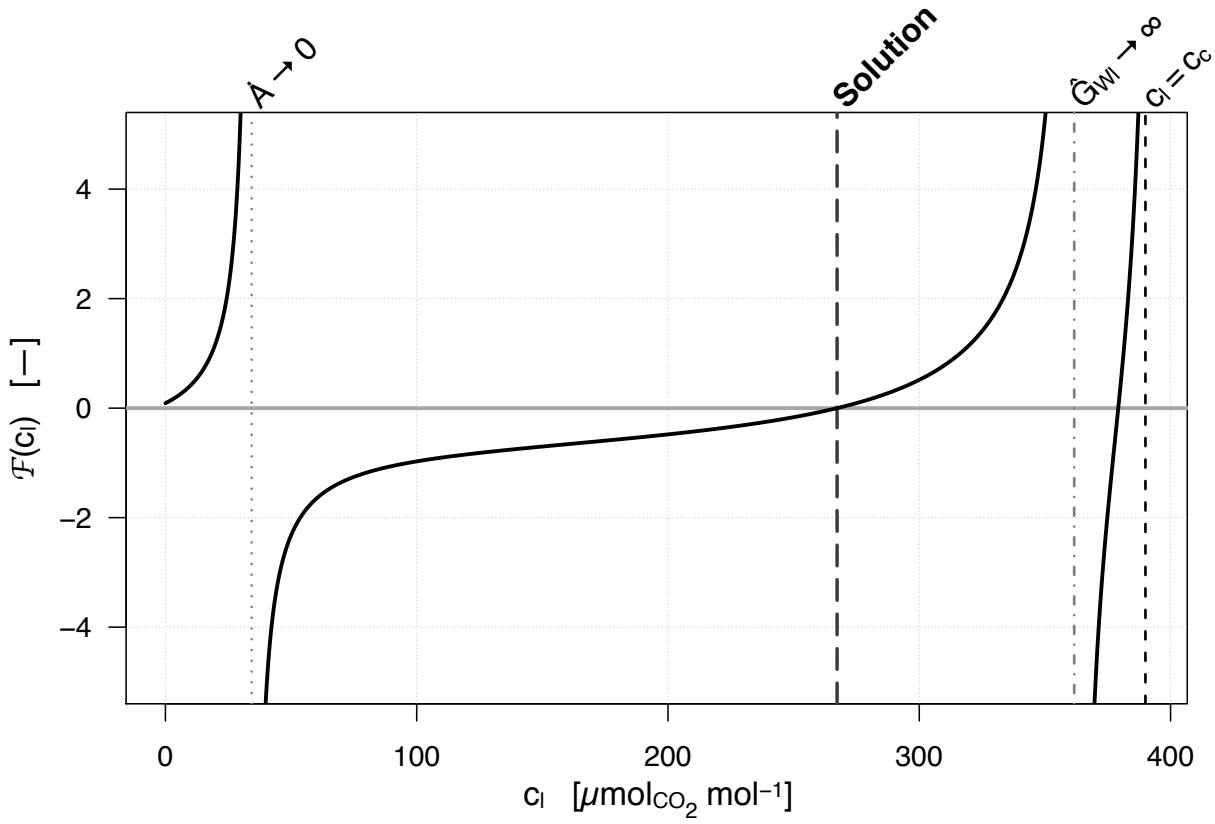
Figure S8: Example for the function $\mathcal{F}(c_{l_k})$ curve for the RuBP-saturated case for a mid-successional, tropical broadleaf tree when $\hat{Q}_{\mathrm{PAR}:a,l_k} = 100\,\mathrm{W\,m}^{-2}$, $T_{t_k} = T_c = 301.15\,\mathrm{K}$, $w_c = 0.017\,\mathrm{kg_W\,kg_{Air}^{-1}}$, $u_{t_k} = 0.25\,\mathrm{m\,s}^{-1}$, and $c_c = 390\,\mu\mathrm{mol_C\,mol_{Air}^{-1}}$. Vertical lines shows the solution and the singularities within the plausible range.
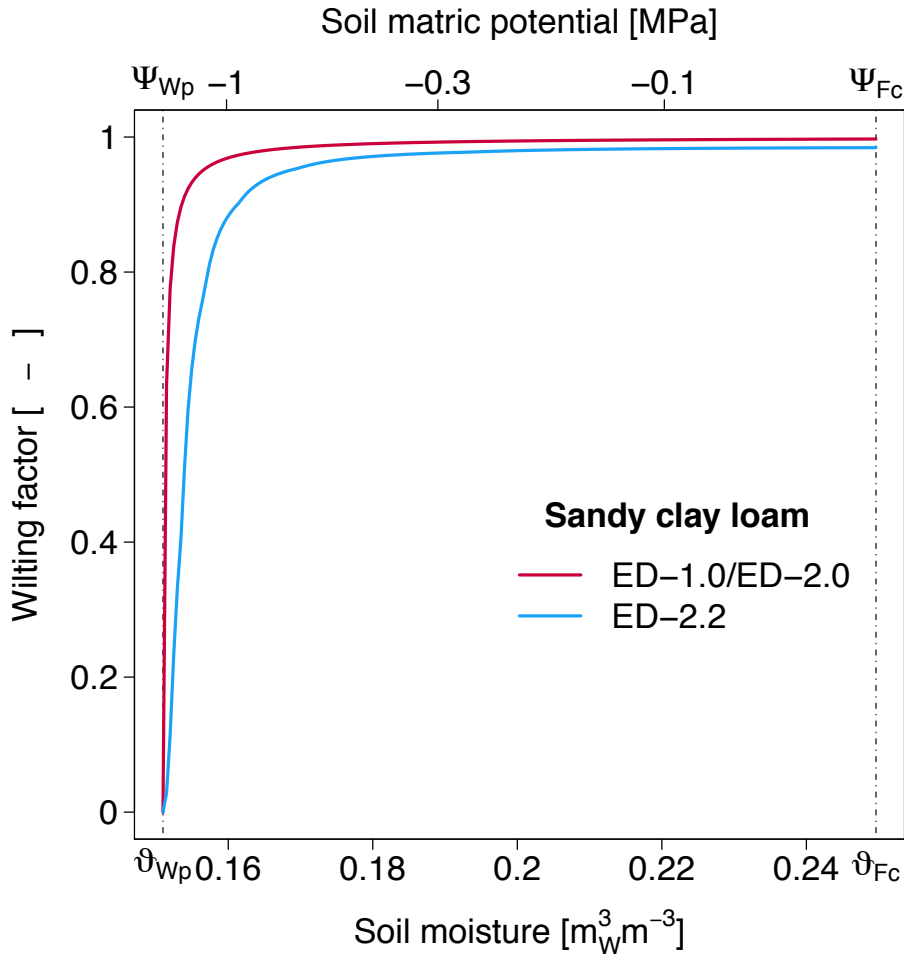
Figure S9: Example of the wilting factor (f_{Wl_k}, Eq. S201) response to soil moisture change for the original implementation in ED (ED-1.0 and ED-2.0, Moorcroft et al., 2001; Medvigy et al., 2009) and the ED-2.2 model approach. Results here are shown for the idealized case with constant soil moisture profile in a 3-m deep, sandy clay loam soil, for a mid-successional tropical cohort with default parameters (Table S5), with diameter at breast height of 30 cm and leaf area index of 1 $m_{Leaf}^2 m^{-2}$, non-limited leaf-level transpiration rate $\dot{E}_k = 9.0$ $kg_W m_{Leaf}^{-2} day^{-1}$. Values are shown for soil moisture columns ranging from wilting point ($\vartheta_{Wp}; \Psi_{Wp}$) to field capacity ($\vartheta_{Fc}; \Psi_{Fc}$).

Table S1: List of subscripts used in the manuscript. Fluxes are denoted by a dotted letter, and two subscripts separated with a comma: $\dot{X}_{m,n}$. This means positive (negative) flux going from thermodynamic system m (n) to thermodynamic system n (m). N_T is the total number of cohorts, N_G is the total number of soil (ground) layers, N_S is the total number of temporary surface water/snowpack layers, and N_C is the total number of canopy air space layers, currently only used to obtain properties related to canopy conductance.

Subscript	Description
X_3	Property at the water's triple point ($T_3 = 273.16$ K)
X_a	Air above canopy, from the meteorological forcing
X_{b_k}	Branch wood of cohort k ($k \in \{1, 2, \ldots, N_T\}$)
$X_\mathbf{C}$	Size vector (leaves, fine roots, sapwood, heartwood, and non-structural storage)
X_C	Carbon component
X_c	Canopy air space (single layer)
X_{c_j}	Canopy air space, layer j ($j \in \{1, 2, \ldots, N_C\}$)
X_d	Non-water component of thermodynamic system
X_{e_j}	Necromass pools: e_1, metabolic litter (fast); e_2, structural debris (intermediate); e_3, humified/dissolved (slow)
X_f	Plant functional type
X_{Fc}	Soil property at field capacity
X_{Fr}	Soil property at critical moisture for fire ignition
X_{g_j}	Soil (ground), layer j ($j \in \{1, 2, \ldots, N_G\}$)
X_{h_k}	Structural (heartwood) of cohort k ($k \in \{1, 2, \ldots, N_T\}$)
X_i	Ice
$X_{i\ell}$	Ice-liquid phase transition
X_{iv}	Ice-vapor phase transition
X_k	Cohort k ($k \in \{1, 2, \ldots, N_T\}$), for variables that are only defined for cohorts
X_ℓ	Liquid water
$X_{\ell v}$	Liquid-vapor phase transition
X_{l_k}	Leaves of cohort k ($k \in \{1, 2, \ldots, N_T\}$)
X_{Ld}	Soil property at critical moisture for leaf shedding (drought-deciduous phenology)
X_m	Spectral band: $m = 1$, PAR; $m = 2$, NIR; $m = 3$, TIR
X_{n_k}	Non-structural carbon storage (starch, sugars) of cohort k
X_o	Surface runoff
X_p	Property at constant pressure
X_{Po}	Soil property at soil porosity (water saturation)
X_q	Disturbance type
X_{r_k}	Roots of cohort k
X_{Re}	Soil property at residual soil moisture
X_{Sat}	Phase equilibrium (saturation)
X_{s_j}	Temporary surface water/snowpack, layer j ($j \in \{1, 2, \ldots, N_S\}$)
X_{t_k}	Cohort k ($k \in \{1, 2, \ldots, N_T\}$)
X_U	Property associated with momentum (forced convection)
X_u	Patch u ($u \in \{1, 2, \ldots, N_P\}$)
X_v	Water vapor
X_w	Water component of thermodynamic system (any phase)

Subscript	Description
X_{Wp}	Soil property at permanent wilting point
X_x	West-East direction
$X_{\mathbf{x}}$	Horizontal direction
X_y	South-north direction
X_z	Vertical direction
X_{α_k}	Total living tissues (leaves, fine roots, sapwood) of cohort k ($k \in \{1,2,\ldots,N_T\}$)
X_{β_k}	Branch boundary layer of cohort k ($k \in \{1,2,\ldots,N_T\}$)
X_{Δ_k}	Carbon balance of cohort k ($k \in \{1,2,\ldots,N_T\}$)Q
X_Θ	Property associated with buoyancy (free convection)
X_κ	Soil textural component: $\kappa = 0$, water; $\kappa = 1$, sand; $\kappa = 2$, silt; $\kappa = 3$, clay
X_{λ_k}	Leaf boundary layer of cohort k ($k \in \{1,2,\ldots,N_T\}$)
X_{ϱ_k}	Reproductive tissues (seeds, fruits, flowers, cones) of cohort k ($k \in \{1,2,\ldots,N_T\}$)
X_{σ_k}	Sapwood of cohort k ($k \in \{1,2,\ldots,N_T\}$)
X_∞	Fluxes that depend on air above layer a, such as radiation and rainfall
$X_\varnothing$	Bare ground equivalent
X_*	Frost
$X_\circledast$	Pure, fresh snow

Table S2: List of variables used in this manuscript. For variables used in various thermodynamic systems, the subscript is omitted (see Table S1 for a comprehensive list of subscripts). Variable dimensions are shown in standard units for reference. Units with subscript are specific to a single substance: kg_W means kilograms of water, and kg_C means kilograms of carbon, and kg_D means kilogram of non-water material.

Variable	Description	Units
A	Site area	—
$\dot{A}$	Net leaf-level CO_2 uptake rate	$mol_C\,m_{Leaf}^{-2}\,s^{-1}$
$\mathcal{A}$	Mean leaf/branch inclination relative to horizontal plane	rad
a	Patch age since last disturbance	s
$æ$	Aging factor for density-independent mortality (temperate PFTs)	yr
B	Soil carbon decay rates under optimal conditions	s^{-1}
$\mathcal{B}_C$	Carbon to oven-dry biomass ratio	$kg_C\,kg_{Bio}^{-1}$
$\mathcal{B}_W$	Water to oven-dry biomass ratio	$kg_W\,kg_{Bio}^{-1}$
b	Slope of the logarithm of the water retention curve	—
BA	Basal area	cm^2
C	Carbon mass (area-based, extensive)	$kg_C\,m^{-2}$
$\mathbf{C}$	Size (carbon mass) vector	$kg_C\,plant^{-1}$
$\mathcal{C}$	Empirical coefficients for determining biomass of individual tissues	—
$C^{\bullet}$	Expected carbon mass given size, PFT, and demographic density	$kg_C\,m^{-2}$
C°	Carbon mass needed to bring tissue to allometry given size and PFT	$kg_C\,m^{-2}$
$\dot{C}$	Carbon flux	$kg_C\,m^{-2}\,s^{-1}$
$\dot{C}^{\star}$	Carbon flux to necromass pools due to mortality	$kg_C\,m^{-2}\,s^{-1}$
CHD	Chilling days	day
c	Carbon mixing ratio (intensive)	$mol_C\,mol^{-1}$
D	"Dry material" mass (area-based, extensive)	$kg_D\,m^{-2}$
$\mathcal{D}$	"Dry material" mass (volume-based, extensive)	$kg_D\,m^{-3}$
d	Specific mass of "dry material" (intensive)	$kg_D\,kg^{-1}$
DBH	Diameter at breast height	cm
$Đ$	Auxiliary variable for solution of canopy radiation transfer	—
$ð$	Sub-surface drainage impediment parameter	—
E	Average projection of leaves and branches onto the horizontal	—
$\dot{E}$	Leaf-level transpiration rate	$mol_C\,m_{Leaf}^{-2}\,s^{-1}$
$\mathcal{E}$	Penalty reduction function for extreme temperatures and soil moistures	—
Ein	Average photon specific energy in the PAR band	$J\,mol^{-1}$
$\hat{e}_l$	Leaf elongation factor given environmental constraints	—
$\mathcal{F}$	Dimensionless function of intercellular carbon dioxide	—
f_{AG}	Fraction of woody biomass that is above ground	—
f_{Clump}	Clumping factor	—
f_{Gl}	Ratio between stomatal conductance of CO_2 and water	—
$f_{G\lambda}$	Ratio between leaf boundary layer conductance of CO_2 and water	—
f_h	Fraction of the decay of soil carbon pools that are respired	—
f_{LD}	Fraction of carbon reabsorption before leaf shedding	—
f_{lw}	Down-regulation factor for photosynthesis due to soil moisture limitation	—
f_R	Ratio between day respiration and maximum carboxylation	—
f_r	Ratio between fine root and leaf biomass on allometry given size and PFT	—

Variable	Description	Units
f_{TSW}	Fraction of ground covered by water or snow	—
$f_{\mathcal{V}}$	Volumetric fraction	—
f_δ	Fraction of reproduction that is randomly dispersed	—
f_σ	Scaling factor between height, sapwood, and leaf biomass on allometry	m^{-1}
G	Conductance (rate form)	$\text{m}\,\text{s}^{-1}$
$\hat{G}$	Conductance (flux form)	$\text{kg}\,\text{m}^{-2}\,\text{s}^{-1}$ or $\text{mol}\,\text{m}^{-2}\,\text{s}^{-1}$
g	Gravity acceleration	$\text{m}\,\text{s}^{-2}$
$\mathbf{g}$	Net growth rate	$\text{kg}_\text{C}\,\text{plant}^{-1}\,\text{s}^{-1}$
GDD	Growing degree-days	$\text{K}\,\text{day}$
Gr	Grashof number	—
$\mathcal{H}$	Bulk specific enthalpy	$\text{J}\,\text{m}^{-3}$
H	Enthalpy (area-based, extensive)	$\text{J}\,\text{m}^{-2}$
$\dot{H}$	Enthalpy flux associated with mass flux	$\text{W}\,\text{m}^{-2}$
h	Specific enthalpy (intensive)	$\text{J}\,\text{kg}^{-1}$
$\tilde{h}$	Specific enthalpy at reference height	$\text{J}\,\text{kg}^{-1}$
$\mathcal{I}$	Fire intensity parameter	s^{-1}
i	Fraction of water in solid phase (ice)	—
K	Eddy diffusivity	$\text{m}^2\,\text{s}^{-1}$
$\mathcal{K}_\text{C}$	Michaelis constant for carboxylation	$\text{mol}_\text{C}\,\text{mol}^{-1}$
$\mathcal{K}_\text{ME}$	Effective Michaelis constant	$\text{mol}_\text{C}\,\text{mol}^{-1}$
$\mathcal{K}_\text{O}$	Michaelis constant for oxygenation	$\text{mol}_{\text{O}_2}\,\text{mol}^{-1}$
k_{PEP}	Slope of CO_2-limited carboxylation rate	$\text{mol}\,\text{mol}_\text{C}^{-1}$
$\mathcal{L}$	Obukhov length scale	m
l	Specific latent heat	$\text{J}\,\text{kg}^{-1}\,\text{K}^{-1}$
$l_{i\ell 3}$	Specific latent heat of fusion at triple point temperature	$\text{J}\,\text{kg}^{-1}\,\text{K}^{-1}$
l_{iv3}	Specific latent heat of sublimation at triple point temperature	$\text{J}\,\text{kg}^{-1}\,\text{K}^{-1}$
ℓ	Fraction of water in liquid phase	—
$\pounds$	Fraction of living tissues that are lignified	—
M	Slope of stomatal conductance function	—
$\mathcal{M}$	Molar mass	$\text{kg}\,\text{mol}^{-1}$
MCWD	Maximum cumulative water deficit	mm
m	Mortality rate	s^{-1}
n	Cohort demographic density	$\text{plant}\,\text{m}^{-2}$
N_C	Number of canopy air space layers	—
N_F	Number of plant functional types	—
N_G	Number of soil layers	—
N_P	Number of patches	—
N_Q	Number of disturbance types	—
N_S	Actual number of temporary surface water layers	—
N_S^{max}	Maximum number of temporary surface water layers	—
N_T	Number of cohorts	—
$N_{T(\text{canopy})}$	Number of canopy cohorts	—
Nu	Nusselt number	—
$\mathcal{O}$	Open canopy fraction	—
o	Oxygen mixing ratio	$\text{mol}_{\text{O}_2}\,\text{mol}^{-1}$

Variable	Description	Units
$\mathcal{P}$	Sheltering factor for momentum	—
p	Atmospheric pressure	Pa
$p_{vi}^{\equiv}$	Saturation pressure: vapor-ice	Pa
$p_{v\ell}^{\equiv}$	Saturation pressure: vapor-liquid	Pa
Pr	Prandtl number	—
$\dot{Q}$	Heat flux (no mass exchange involved)	$\mathrm{W\,m^{-2}}$
$\dot{Q}^{\odot}$	Downward direct irradiance	$\mathrm{W\,m^{-2}}$
$\dot{Q}^{\Downarrow}$	Downward hemispheric diffuse irradiance	$\mathrm{W\,m^{-2}}$
$\dot{Q}^{\Uparrow}$	Upward hemispheric diffuse irradiance	$\mathrm{W\,m^{-2}}$
$\dot{Q}^{\blacklozenge}$	Irradiance emitted by black body	$\mathrm{W\,m^{-2}}$
$\mathcal{Q}_{10}$	Temperature coefficient for temperature-response function	—
$\dot{q}^{\mathrm{PAR}}$	Photon flux absorbed by leaves	$\mathrm{W\,m_{Leaf}^{-2}}$
q	Specific heat (intensive)	$\mathrm{J\,kg^{-1}}$
$q^{\mathrm{(OD)}}$	Specific heat of oven-dry tissue (intensive)	$\mathrm{J\,kg^{-1}}$
q_p	Specific heat at constant pressure (intensive)	$\mathrm{J\,kg^{-1}}$
$\dot{R}$	Leaf-level dark respiration rate	$\mathrm{mol_C\,m_{Leaf}^{-2}\,s^{-1}}$
$\mathcal{R}$	Gas constant for typical air	$\mathrm{J\,mol^{-1}\,K^{-1}}$
r	Decay rate associated with root respiration	$\mathrm{s^{-1}}$
Re	Reynolds number	—
Ri_B	Bulk Richardson number	—
S	Elements of the flux matrix for solving the canopy radiation transfer model	—
$\mathbf{S}$	Flux matrix for solving the canopy radiation transfer model	—
$\mathcal{S}$	Above-canopy velocity variance to momentum flux ratio	—
SLA	Specific leaf area	$\mathrm{m_{Leaf}^2\,kg_C^{-1}}$
s_g	Soil wetness function for ground evaporation	—
s_l	Soil wetness function for drought-deciduous phenology	—
β	Joint eddy mixing length scale (shear- and wake-driven turbulence)	—
TSW	Temporary surface water	—
T	Temperature	K
T_3	Temperature of water triple point	K
$T_{\ell 0}$	Zero-energy temperature of supercooled liquid water	K
T_{Phen}	Temperature threshold for cold-deciduous leaf phenology	K
T_{v0}	Zero-energy temperature of supercooled water vapor	K
$T_{\mathcal{V}}$	Virtual temperature	K
$\mathcal{T}$	Temperature coefficient function ($\mathcal{Q}_{10}$ function)	—
$\mathcal{T}'$	Penalty reduction function for extreme temperatures	—
$\mathfrak{T}_{\mathrm{GS}}$	Extended growing season (for cold-deciduous leaf phenology)	—
$\mathfrak{T}_{\mathrm{SS}}$	Extended senescing season (for cold-deciduous leaf phenology)	—
t	Time	s
t_{Runoff}	Runoff decay time	s
$t_{\odot}$	Daytime duration	min
TKE	(Specific) Turbulent kinetic energy	$\mathrm{m^2\,s^{-2}}$
P	Auxiliary variable for solution of canopy radiation transfer	—
p	Number of leaf sides with stomata	—
$\dot{U}$	Momentum flux	$\mathrm{kg\,m^{-1}\,s^{-2}}$
$u_{\mathbf{x}}$	Horizontal wind speed	$\mathrm{m\,s^{-1}}$

Variable	Description	Units
u_z	Vertical wind velocity	$\mathrm{m\,s^{-1}}$
$u^\star$	Friction velocity	$\mathrm{m\,s^{-1}}$
$\dot{V}_C$	Leaf-level carboxylation rates	$\mathrm{mol_C\,m_{Leaf}^{-2}\,s^{-1}}$
$\dot{V}_C^{\mathrm{RuBP}}$	RuBP-saturated carboxylation rates	$\mathrm{mol_C\,m_{Leaf}^{-2}\,s^{-1}}$
$\dot{V}_C^{\mathrm{CO_2}}$	CO_2-limited carboxylation rate	$\mathrm{mol_C\,m_{Leaf}^{-2}\,s^{-1}}$
$\dot{V}_C^{\mathrm{PAR}}$	Light-limited carboxylation rate	$\mathrm{mol_C\,m_{Leaf}^{-2}\,s^{-1}}$
$\dot{V}_O$	Leaf-level oxygenation (photorespiration) rate	$\mathrm{mol_{O_2}\,m_{Leaf}^{-2}\,s^{-1}}$
$\mathcal{V}$	Volume	$\mathrm{m^3}$
v	Fraction of water in gas phase (water vapor)	—
W	Water mass (area-based, extensive)	$\mathrm{kg_W\,m^{-2}}$
$\dot{W}$	Water flux	$\mathrm{kg_W\,m^{-2}\,s^{-1}}$
$\mathcal{W}$	Water mass (volume-based, extensive)	$\mathrm{kg_W\,m^{-3}}$
w	Specific humidity (intensive)	$\mathrm{kg_W\,kg^{-1}}$
$w^{\equiv}$	Saturation specific humidity (intensive)	$\mathrm{kg_W\,kg^{-1}}$
$\hat{w}_{\max}$	Cohort water holding capacity of rainfall interception, dew and frost	$\mathrm{kg_W\,m_{Leaf+Wood}^{-2}}$
X	Crown area index	$\mathrm{m_{Crown}^2\,m^{-2}}$
$x^\star$	Characteristic dimension for boundary-layer generating obstacle	m
Y	Auxiliary functions, used only in the sections where they are described	—
$\mathcal{Y}$	Boolean variable controlling fire ignition	—
y	Auxiliary constants, used only in the sections where they are described	—
Z	Zenith distance	rad
$\mathcal{Z}$	Empirical coefficients to determine height	—
z	Height ($z > 0$) or depth ($z < 0$)	m
$z^\star$	Height above displacement height	m
z^-	Height of crown base	m
z_0	Roughness length	m
z_d	Displacement height	m
α	Probability distribution of gap ages	—
β	Backscattering coefficient, diffuse irradiance	—
$\beta^\odot$	Backscattering coefficient, direct irradiance	—
Γ	CO_2 compensation point	$\mathrm{mol_C\,mol^{-1}}$
γ	Growth rate	$\mathrm{s^{-1}}$
Δt	Time step	s
Δw	Stomatal conductance control on severe leaf-level water vapor deficit	$\mathrm{kg_W\,kg^{-1}}$
Δz	Layer thickness	m
δ_{ij}	Kronecker delta (1 if $i = j$, 0 otherwise)	—
ϵ	Quantum yield	—
ε	Thermal dilatation coefficient	$\mathrm{K^{-1}}$
$\mathcal{F}$	Coefficients for generic function of CO_2 uptake rate (Table S9)	—
ζ	Dimensionless Obukhov length	—
ζ_0	Dimensionless roughness length	—
η	Thermal diffusivity of air	$\mathrm{m^2\,s^{-1}}$
θ	Potential temperature	K
$\theta_\mathcal{V}$	Virtual potential temperature	K
$\theta_\mathcal{V}^\star$	Characteristic scale: Virtual potential temperature	K
ϑ	Volumetric soil moisture	$\mathrm{m_W^3\,m^{-3}}$

Variable	Description	Units
ι_U	Turbulence intensity	—
κ	von Kármán constant	—
$\varkappa$	Auxiliary variable for solution of canopy radiation transfer	—
Λ	Leaf area index	$m_{Leaf}^2\,m^{-2}$
λ	Disturbance rate	s^{-1}
μ	Inverse of optical depth per unit of plant area index	$m_{Plant}^2\,m^{-2}$
$\mu^{\odot}$	Same as above, specific for direct radiation	$m_{Plant}^2\,m^{-2}$
$\overline{\mu}$	Same as above, specific for diffuse radiation	$m_{Plant}^2\,m^{-2}$
ν	Kinematic viscosity	$m^2\,s^{-1}$
Ξ	Cumulative cohort drag area per unit ground area	$m_{Plant}^2\,m^{-2}$
ξ	Drag coefficient	—
ϖ	Oxygenase:Carboxylase ratio	$mol_{O_2}\,molC^{-1}$
ρ	Density	$kg\,m^{-3}$
ϱ	Recruitment rate	s^{-1}
$\hat{\sigma}$	Survivorship fraction following disturbance	—
σ_{SB}	Stefan-Boltzmann constant	$W\,m^{-2}\,K^{-4}$
σ_u	Standard deviation of wind speed	$m\,s^{-1}$
ς	Scattering coefficient, diffuse irradiance	—
$\varsigma^{\odot}$	Scattering coefficient, direct irradiance	—
ς_R	Reflectance coefficient	—
ς_T	Transmittance coefficient	—
τ	Turnover rate (active tissues or non-structural carbon)	s^{-1}
Υ_Q	Thermal conductivity	$W\,m^{-1}\,K^{-1}$
Υ_Ψ	Hydraulic conductivity	$m\,s^{-1}$
Φ	Total plant area index	$m_{Plant}^2\,m^{-2}$
$\tilde{\Phi}$	Clump-corrected, effective total plant area index	$m_{Plant}^2\,m^{-2}$
ϕ	Plant area density	$m_{Plant}^2\,m^{-3}$
φ_U	Dimensionless stability function of momentum (eddy flux)	—
φ_Θ	Dimensionless stability function of heat (eddy flux)	—
χ	Mean orientation factor	—
Ψ	Soil matric potential	m
ψ_U	Dimensionless flux profile function of momentum (eddy flux)	—
ψ_Θ	Dimensionless flux profile function of heat (eddy flux)	—
Ω	Branch wood area index	$m_{Wood}^2\,m^{-2}$
ω	Leaf shedding rate	s^{-1}

Table S3: List of universal (physical) constants used in ED-2.2. For parameters that can be constrained and optimized, refer to Tables S4 (global) and S5-S6 (PFT-dependent).

Symbol	Value	Description
Ein	$2.17 \cdot 10^{-5}$ J mol^{-1}	Average photon specific energy in the PAR band
g	9.807 m s^{-2}	Gravity acceleration
$\mathcal{M}_C$	$1.201 \cdot 10^{-2}$ kg mol^{-1}	Molar mass of carbon
$\mathcal{M}_d$	$2.897 \cdot 10^{-2}$ kg mol^{-1}	Molar mass of dry air
$\mathcal{M}_w$	$1.802 \cdot 10^{-2}$ kg mol^{-1}	Molar mass of water
$l_{i\ell 3}$	$3.34 \cdot 10^{5}$ J kg^{-1}	Specific latent heat of melting at the water triple point
l_{iv3}	$l_{i\ell 3} + l_{\ell v3}$	Specific latent heat of sublimation at the water triple point
$l_{\ell v3}$	$2.50 \cdot 10^{6}$ J kg^{-1}	Specific latent heat of vaporization at the water triple point
$o_{\oplus}$	0.209 mol$_{O_2}$ mol^{-1}	Reference oxygen mixing ratio
p_0	10^5 Pa	Reference pressure for potential temperature
q_i	2093 J kg^{-1} K^{-1}	Specific heat of ice
q_ℓ	4186 J kg^{-1} K^{-1}	Specific heat of liquid water
q_{pd}	1005 J kg^{-1} K^{-1}	Specific heat of dry air at constant pressure
q_{pv}	1859 J kg^{-1} K^{-1}	Specific heat of water vapor at constant pressure
$\mathcal{R}$	8.315 J mol^{-1} K^{-1}	Ideal gas constant
T_0	273.15 K	Zero degrees Celsius
T_3	273.16 K	Water triple point
κ	0.40	von Kármán constant
$\rho_{\divideontimes}$	200 kg m^{-3}	Density of frost
ρ_ℓ	1000 kg m^{-3}	Density of liquid water
$\rho_{\circledast}$	100 kg m^{-3}	Reference density of fresh snow
σ_{SB}	$5.67 \cdot 10^{-8}$ W m^{-2} K^{-4}	Stefan-Boltzmann constant
Υ_{Q_ℓ}	0.57 W m^{-1} K^{-1}	Thermal conductivity of liquid water

Table S4: List of default values for global parameters used in ED-2.2. Soil carbon parameters $x_{\mathbf{e}}$ are shown as vectors $(x_{e_1}; x_{e_2}; x_{e_3})$ corresponding to the fast, intermediate, and slow pools, respectively. Optical parameters are shown as vectors $(x_{\mathrm{PAR}}; x_{\mathrm{NIR}}; x_{\mathrm{TIR}})$ corresponding to the photosynthetically active (PAR), near infrared and thermal infrared bands, respectively. For default PFT-specific parameters, refer to Tables S5–S6; physical constants are listed in Table S3.

Symbol	Value	Description
$B_{\mathbf{e}}$	$(11.0; 4.5; 0.2)\ \mathrm{yr}^{-1}$	Optimal decay rates of soil carbon pools
$\mathcal{B}_C$	$0.5\ \mathrm{kg_C\,kg_{Bio}^{-1}}$	Carbon:oven-dry-biomass ratio
$\hat{f}_{\mathrm{Cold}}$	0.24	Decay parameter for decomposition at cold temperatures
$\hat{f}_{\mathrm{Dry}}$	0.60	Decay parameter for decomposition at dry conditions
$\hat{f}_{\mathrm{Hot}}$	12.0	Decay parameter for decomposition at hot temperatures
$\hat{f}_{\mathrm{Wet}}$	36.0	Decay parameter for decomposition at wet conditions
f_{Gl}	1.6	Water:CO_2 diffusivity ratio
$f_{G\lambda}$	1.4	Water:CO_2 leaf-boundary-layer conductance ratio
$f_{h\mathbf{e}}$	$(1.0; 0.3; 1.0)$	Fraction of decay due to heterotrophic respiration
f_{LD}	0.5	Fraction of carbon retained by plants when shedding leaves
$\mathcal{I}$	$0.5\ \mathrm{yr}^{-1}$	Fire intensity parameter
$\mathcal{K}_{C_{15}}$	$214.2\ \mu\mathrm{mol_{CO_2}\,mol^{-1}}$	Michaelis constant for carboxylation at $15\,^{\circ}\mathrm{C}$
$\mathcal{K}_{O_{15}}$	$0.2725\ \mathrm{mol_{O_2}\,mol^{-1}}$	Michaelis constant for oxygenation at $15\,^{\circ}\mathrm{C}$
k_{PEP}	$17949\ \mathrm{mol_{Air}\,mol_{CO_2}^{-1}}$	Initial slope for the PEP carboxylase (C_4 photosynthesis)
Pr	0.74	Prandtl number
$\mathcal{Q}_{10}(\mathcal{K}_C)$	2.1	Temperature factor for Michaelis constant (carboxylation)
$\mathcal{Q}_{10}(\mathcal{K}_O)$	1.2	Temperature factor for Michaelis constant (oxygenation)
$\mathcal{Q}_{10}(\varpi)$	0.57	Temperature factor for carboxylase:oxygenase ratio
$T_{g\mathrm{Cold}}$	$291.15\ \mathrm{K}$	Temperature threshold for decomposition at cold temperatures
$T_{g\mathrm{Hot}}$	$318.15\ \mathrm{K}$	Temperature threshold for decomposition at hot temperatures
T_{Phen}	$278.15\ \mathrm{K}$	Temperature threshold for cold-deciduous leaf phenology
t_{Runoff}	$3600\ \mathrm{s}$	E-folding Decay time for surface runoff
$\hat{w}_{\max}$	$0.11\ \mathrm{kg_W\,m^2_{Leaf+Wood}}$	Water holding capacity
$z_{0\varnothing}$	$0.01\ \mathrm{m}$	Roughness length of bare soil
z_{Fr}	$-0.50\ \mathrm{m}$	Soil depth used to evaluate fuel dryness
λ_{TF}	$0.014\ \mathrm{yr}^{-1}$	Tree fall disturbance rate
$\vartheta'_{\mathrm{Dry}}$	0.48	Relative moisture threshold for decomposition at dry conditions
$\vartheta'_{\mathrm{Wet}}$	0.98	Relative moisture threshold for decomposition at wet conditions
$\overline{\mu}_s$	$0.05\ \mathrm{m}$	Inverse of the optical depth of temporary surface water
ς_{3g}	0.02	Scattering coefficients (thermal infrared) for bare soil
$\varsigma_{R_s}^{\circledast}$	$(0.518; 0.435; 0.030)$	Reflectance coefficients (thermal infrared) for pure snow
ϖ_{15}	4561	Carboxylase:oxygenase ratio at $15\,^{\circ}\mathrm{C}$
$\tilde{\psi}_0$	0.190	Flux profile function of momentum at roughness height

Table S5: List of default parameters that depend on plant functional type (PFT) used in ED-2.2 ~~and described in the text~~ for tropical and subtropical regions, for default ED-2.2 PFTs. The ~~default tropical and subtropical~~ PFTs are C_4 tropical grass (C4G), C_3 tropical grass (C3G); early successional tropical tree (ETR); mid-successional tropical tree (MTR); late-successional tropical tree (LTR); subtropical conifers (ARC); additional PFTs can be specified by the user and provided directly to ED-2.2 through extensible markup language (XML). Spectral-dependent parameters x are provided as vectors (x_{PAR}; x_{NIR}; x_{TIR}), corresponding to the visible (photosynthetically active), nearinfrared, and thermal infrared, respectively. The default parameters for temperate PFTs are shown in Table S6. The values of constants and default global parameters are shown in Table S3.

Symbol	PFT-specific value						Units	Description
	C4G	C3G	ETR	MTR	LTR	ARC		
α	15.15	15.15	16.22	31.58	∞	900.09	yr	Aging factor for density-independent mortality
B_{Wl}	1.85	1.85	1.85	1.85	1.85	1.85	—	Water:oven-dry-biomass ratio for leaves
B_{Wb}	0.70	0.70	0.70	0.70	0.70	0.70	—	Water:oven-dry-biomass ratio for wood
C_{0l}	0.158	0.158	0.418	0.560	0.701	0.410	—	Scaling coefficient for leaf biomass allometry
C_{1l}	0.975	0.975	0.975	0.975	0.975	0.975	—	Exponent coefficient for leaf biomass allometry
C_{0h}	0.0627	0.0627	0.166	0.222	0.282	0.163	—	Scaling coefficient for heartwood biomass allometry (sub-canopy)
C_{1h}	2.432	2.432	2.432	2.432	2.432	2.432	—	Exponent coefficient for heartwood biomass allometry (sub-canopy)
C_{2h}	0.0647	0.0647	0.172	0.230	0.291	0.168	—	Scaling coefficient for heartwood biomass allometry (canopy)
C_{3h}	2.426	2.426	2.426	2.426	2.426	2.426	—	Exponent coefficient for heartwood biomass allometry (canopy)
f_{AG}	0.70	0.70	0.70	0.70	0.70	0.70	—	Fraction of above-ground biomass
f_{Cold}	0.40	0.40	0.40	0.40	0.40	0.40	—	Decay parameter to down-regulate metabolism at cold temperatures
f_{Clump}	1.00	1.00	0.80	0.80	0.80	0.735	—	Clumping index
f_{Hot}	0.40	0.40	0.40	0.40	0.40	0.40	—	Decay parameter to down-regulate metabolism at hot temperatures
f_n	0.00	0.00	0.10	0.10	0.10	0.10	—	Fraction of carbon storage retained in storage pool
f_r	1.00	1.00	1.00	1.00	1.00	1.00	—	Fine-root:leaf biomass ratio
f_R	0.035	0.015	0.015	0.015	0.015	0.015	—	Respiration:carboxylation ratio
f_ϱ	1.0	1.0	0.30	0.30	0.30	0.30	—	Fraction of carbon allocation to reproduction at maturity
f_σ	3900	3900	3900	3900	3900	3900	—	Sapwood:leaf biomass scaling factor
$\hat{G}_{lw}^{\varnothing}$	0.01	0.01	0.01	0.01	0.01	0.001	$\mathrm{mol\,m^{-2}\,s^{-1}}$	Residual conductance (closed stomata)
$\hat{G}_r$	900	900	600	600	600	600	$\mathrm{m^2\,kg_C^{-1}\,yr^{-1}}$	Scaling factor for fine root conductance
ℓ_h	1.0	1.0	1.0	1.0	1.0	0.79	—	Fraction of lignified tissues (sapwood and hardwood)
ℓ_l	0.0	0.0	0.0	0.0	0.0	0.00	—	Fraction of lignified tissues (leaves and fine roots)
M	7.2	9.0	9.0	9.0	9.0	7.2	—	Slope factor for stomatal conductance
m_ϱ	0.95	0.95	0.95	0.95	0.95	0.95	$\mathrm{mo^{-1}}$	Loss rate of reproductive tissues
$Q_{10}(\dot{V}_C)$	2.40	2.40	2.40	2.40	2.40	2.40	—	Temperature dependence factor for carboxylation rate

Table S5: (Continued)

Symbol	PFT-specific value						Units	Description
	C4G	C3G	ETR	MTR	LTR	ARC		
$Q_{10}(r_r)$	2.40	2.40	2.40	2.40	2.40	2.40	—	Temperature dependence factor for fine root respiration
$q_l^{(OD)}$	3218	3218	3218	3218	3218	3218	$J\,kg^{-1}\,K^{-1}$	Specific heat of oven-dry leaf biomass
$q_b^{(OD)}$	1217	1217	1217	1217	1217	1217	$J\,kg^{-1}\,K^{-1}$	Specific heat of oven-dry wood biomass
r_{15}	0.246	0.246	0.246	0.246	0.246	0.246	s^{-1}	Fine-root respiration rate at 15 °C
SLA	22.70	22.70	16.02	11.65	9.66	6.32	$m^2\,kg_C^{-1}$	Specific leaf area
T_{Cold}	288.15	283.15	283.15	283.15	283.15	277.86	K	Cold temperature threshold for metabolic activity
T_F	275.65	275.65	275.65	275.65	275.65	258.15	K	Temperature threshold for plant hardiness to frost
T_{Hot}	318.15	318.15	318.15	318.15	318.15	318.15	K	Hot temperature threshold for metabolic activity
b	1	1	1	1	1	2	—	Number of sides of leaf with stomata
$\dot{V}_{C_{15}}^{max}$	12.5	18.75	18.75	12.5	6.25	15.62	$\mu mol_C\,m^{-2}\,s^{-1}$	Maximum carboxylation rate at 15 °C
$x_\beta^\star$	0.05	0.05	0.05	0.05	0.05	0.05	m	Typical obstacle size for branches and twigs
$x_\lambda^\star$	0.05	0.05	0.10	0.10	0.10	0.05	m	Typical leaf width
Z_0	0	0	0	0	0	0	m	Offset parameter for tree height allometry
Z_1	0.0352	0.0352	0.0352	0.0352	0.0352	0.0352	—	Slope coefficient for leaf biomass allometry
Z_2	0.694	0.694	0.694	0.694	0.694	0.694	—	Exponent coefficient for leaf biomass allometry
Z_∞	61.7	61.7	61.7	61.7	61.7	61.7	m	Asymptote height (relative to Z_0 at $\lim_{DBH\to\infty}$)
$z_{l_{max}}$	1.5	1.5	35.0	35.0	35.0	35.0	m	Maximum attainable height
z_t^{Repro}	1.5	1.5	18.0	18.0	18.0	18.0	m	Plant height at reproductive maturity
Δq_b^{Bond}	63.10	63.10	63.10	63.10	63.10	63.10	$J\,kg^{-1}\,K^{-1}$	Specific heat associated with bonding between wood and water
Δw	0.016	0.016	0.016	0.016	0.016	0.016	$mol_w\,mol^{-1}$	Leaf water deficit down-regulation parameter (stomatal conductance)
ϵ	0.055	0.080	0.080	0.080	0.080	0.08	—	Quantum yield
ρ_t	—	—	0.53	0.71	0.90	0.52	$g\,cm^{-3}$	Wood density
$\hat{\sigma}^{FR}$	0.0	0.0	0.0	0.0	0.0	0.00	—	Survivorship to fire disturbance
$\hat{\sigma}^{TF}(z_t < 10\,m)$	0.25	0.25	0.10	0.10	0.10	0.10	—	Survivorship of small trees to tree fall disturbance
$\hat{\sigma}^{TF}(z_t \geq 10\,m)$	0.0	0.0	0.0	0.0	0.0	0.0	—	Survivorship of large trees to tree fall disturbance
ς_R^{Leaf}	(0.100;0.400;0.040)		(0.100;0.400;0.050)	(0.100;0.400;0.050)	(0.100;0.400;0.050)	(0.090;0.577;0.030)	—	Leaf reflectance
ς_R^{Wood}	(0.160;0.250;0.040)		(0.110;0.250;0.100)	(0.110;0.250;0.100)	(0.110;0.250;0.100)	(0.110;0.250;0.100)	—	Wood reflectance
ς_T^{Leaf}	(0.050;0.200;0.000)		(0.050;0.200;0.000)	(0.050;0.200;0.000)	(0.050;0.200;0.000)	(0.050;0.248;0.000)	—	Leaf transmittance
ς_T^{Wood}	(0.028;0.248;0.000)		(0.001;0.001;0.000)	(0.001;0.001;0.000)	(0.001;0.001;0.000)	(0.001;0.001;0.000)	—	Wood transmittance
τ_l	2.0	2.0	1.0	0.50	0.33	0.042	yr^{-1}	Leaf turnover rate
τ_n	0.333	0.333	0.167	0.167	0.167	0.167	yr^{-1}	Storage turnover rate
τ_r	2.0	2.0	1.0	0.50	0.33	0.042	yr^{-1}	Fine-root turnover rate
τ_Δ	0.333	0.333	0.333	0.333	0.333	0.450	dy^{-1}	Growth respiration factor
χ	0.00	0.00	0.10	0.10	0.10	0.01	—	Mean orientation factor

Table S6: List of default parameters that depend on plant functional type (PFT) used in ED-2.2 for temperate regions, for default ED-2.2 PFTs. The PFTs are C_3 temperate grass (C3T); mid-latitude ("Northern") pines (NPN); subtropical ("Southern") pines (SPN); late-successional conifers (LCN), early-successional hardwood tree (EHW); mid-succesional hardwood tree (MHW), late-successional tropical tree (LHW); additional PFTs can be specified by the user and provided directly to ED-2.2 through extensible markup language (XML). Spectral-dependent parameters x are provided as vectors (x_{PAR}; x_{NIR}; x_{TIR}), corresponding to the visible (photosynthetically active), nearinfrared, and thermal infrared, respectively. The default parameters for tropical and subtropical PFTs are shown in Table S5. The values of constants and default global parameters are shown in Table S3.

Symbol	PFT-specific value							Units	Description
	C3T	NPN	SPN	LCN	EHW	MHW	LHW		
α	15.15	294.74	232.56	424.30	162.76	262.61	233.64	yr	Aging factor for density-independent mortality
B_{Wl}	2.50	2.50	2.50	2.50	2.50	2.50	2.50	—	Water:oven-dry-biomass ratio for leaves
B_{Wb}	0.7	0.7	0.7	0.7	0.7	0.7	0.7	—	Water:oven-dry-biomass ratio for wood
C_{0l}	0.0800	0.0240	0.0240	0.0454	0.0129	0.0480	0.0170	—	Scaling coefficient for leaf biomass allometry
C_{1l}	1.0000	1.8990	1.8990	1.6829	1.7477	1.4550	1.7310	—	Exponent coefficient for leaf biomass allometry
C_{0h}	1×10^{-5}	0.1470	0.1470	0.1617	0.0265	0.1617	0.2350	—	Scaling coefficient for heartwood biomass allometry (sub-canopy)
C_{1h}	1.0000	2.2380	2.2380	2.1536	2.9595	2.4572	2.2518	—	Exponent coefficient for heartwood biomass allometry (sub-canopy)
C_{2h}	1×10^{-5}	0.1470	0.1470	0.1617	0.0265	0.1617	0.2350	—	Scaling coefficient for heartwood biomass allometry (canopy)
C_{3h}	1.0000	2.2380	2.2380	2.1536	2.9595	2.4572	2.2518	—	Exponent coefficient for heartwood biomass allometry (canopy)
f_{AG}	0.70	0.70	0.70	0.70	0.70	0.70	0.70	—	Fraction of above-ground biomass
f_{Cold}	0.40	0.40	0.40	0.40	0.40	0.40	0.40	—	Decay parameter to down-regulate metabolism at cold temperatures
f_{Clump}	0.840	0.735	0.735	0.735	0.840	0.840	0.840	—	Clumping index
f_{Hot}	0.40	0.40	0.40	0.40	0.40	0.40	0.40	—	Decay parameter to down-regulate metabolism at hot temperatures
f_n	0.00	0.00	0.00	0.00	0.00	0.00	0.00	—	Fraction of carbon storage retained in storage pool
f_r	1.0000	0.3463	0.3463	0.3463	1.1274	1.1274	1.1274	—	Fine-root:leaf biomass ratio
f_R	0.02	0.02	0.02	0.02	0.02	0.02	0.02	—	Respiration:carboxylation ratio
f_ϱ	1.0	1.0	0.30	0.30	0.30	0.30	0.30	—	Fraction of carbon allocation to reproduction at maturity
f_σ	3900	3900	3900	3900	3900	3900	3900	—	Sapwood:leaf biomass scaling factor
$\hat{G}_{lw}^{\varnothing}$	0.020	0.001	0.001	0.001	0.020	0.020	0.020	$molm^{-2}s^{-1}$	Residual conductance (closed stomata)
$\hat{G}_r$	160	150	150	150	150	150	150	$m^2 kg_C^{-1} yr^{-1}$	Scaling factor for fine root conductance
$\pounds_h$	1.00	0.79	0.79	0.79	0.79	0.79	0.79	—	Fraction of lignified tissues (sapwood and hardwood)
$\pounds_l$	0.0	0.0	0.0	0.0	0.0	0.0	0.0	—	Fraction of lignified tissues (leaves and fine roots)
M	8.0	6.4	6.4	6.4	6.4	6.4	6.4	—	Slope factor for stomatal conductance
m_ϱ	0.95	0.95	0.95	0.95	0.95	0.95	0.95	mo^{-1}	Loss rate of reproductive tissues
$Q_{10}(\dot{V}_C)$	2.40	2.40	2.40	2.40	2.40	2.40	2.40	—	Temperature dependence factor for carboxylation rate
$Q_{10}(r_r)$	2.40	2.40	2.40	2.40	2.40	2.40	2.40	—	Temperature dependence factor for fine root respiration
$q_l^{(OD)}$	3218	3218	3218	3218	3218	3218	3218	$Jkg^{-1}K^{-1}$	Specific heat of oven-dry leaf biomass
$q_b^{(OD)}$	1217	1217	1217	1217	1217	1217	1217	$Jkg^{-1}K^{-1}$	Specific heat of oven-dry wood biomass
r_{15}	0.246	0.246	0.246	0.246	0.246	0.246	0.246	s^{-1}	Fine-root respiration rate at 15°C

Table S6: (Continued)

Symbol	PFT-specific value							Units	Description
	C3T	NPN	SPN	LCN	EHW	MHW	LHW		
SLA	22.70	6.0	9.0	10.0	30.0	24.2	60.0	$m^2\,kg_C^{-1}$	Specific leaf area
T_{Cold}	277.86	277.86	277.86	277.86	277.86	277.86	277.86	K	Cold temperature threshold for metabolic activity
T_F	193.15	193.15	263.15	213.15	193.15	253.15	253.15	K	Temperature threshold for plant hardiness to frost
T_{Hot}	318.15	318.15	318.15	318.15	318.15	318.15	318.15	K	Hot temperature threshold for metabolic activity
b	1	2	2	2	1	1	1	—	Number of sides of leaf with stomata
$\hat{V}_{C_{15}}^{max}$	18.30	11.35	11.35	4.54	20.39	17.45	6.98	$\mu mol_C\,m^{-2}\,s^{-1}$	Maximum carboxylation rate at 15°C
$x_\beta^\star$	0.05	0.05	0.05	0.05	0.05	0.05	0.05	m	Typical obstacle size for branches and twigs
$x_\lambda^\star$	0.05	0.05	0.05	0.05	0.05	0.05	0.05	m	Typical leaf width
z_0	0.0	1.3	1.3	1.3	1.3	1.3	1.3	m	Offset parameter for tree height allometry
z_1	0.7500	0.0388	0.0388	0.0444	0.0653	0.0496	0.0540	—	Slope coefficient for leaf biomass allometry
z_2	1	1	1	1	1	1	1	—	Exponent coefficient for leaf biomass allometry
z_∞	0.478	27.140	27.140	22.790	22.680	25.180	23.387	m	Asymptote height (relative to z_0 at $\lim_{DBH\to\infty}$)
$z_{r_{max}}$	0.454	27.113	27.113	22.767	22.657	25.155	23.364	m	Maximum attainable height
z_r^{Repro}	0.45	18.0	18.0	18.0	18.0	18.0	18.0	m	Plant height at reproductive maturity
Δq_b^{Bond}	63.10	63.10	63.10	63.10	63.10	63.10	63.10	$J\,kg^{-1}\,K^{-1}$	Specific heat associated with bonding between wood and water
Δw	0.016	0.016	0.016	0.016	0.016	0.016	0.016	$mol_w\,mol^{-1}$	Leaf water deficit down-regulation parameter (stomatal conductance)
ϵ	0.080	0.080	0.080	0.080	0.080	0.080	0.080	—	Quantum yield
ρ_l	—	—	—	—	—	—	—	$g\,cm^{-3}$	Wood density (currently not used)
$\hat{\sigma}^{FR}$	0.0	0.0	0.0	0.0	0.0	0.0	0.0	—	Survivorship to fire disturbance
$\hat{\sigma}^{TF}(z_r < 10\,m)$	0.25	0.10	0.10	0.10	0.10	0.10	0.10	—	Survivorship of small trees to tree fall disturbance
$\hat{\sigma}^{TF}(z_r \geq 10\,m)$	0.0	0.0	0.0	0.0	0.0	0.0	0.0	—	Survivorship of large trees to tree fall disturbance
ς_R^{Leaf}	(0.110;0.577,0.040)	(0.110;0.577,0.030)			(0.110;0.577,0.050)			—	Leaf reflectance
ς_R^{Wood}	(0.160;0.110,0.040)	(0.110;0.110,0.040)			(0.110;0.250;0.100)			—	Wood reflectance
ς_T^{Leaf}	(0.028;0.248;0.000)	(0.160;0.248;0.000)						—	Leaf transmittance
ς_T^{Wood}		(0.001;0.001;0.000)						—	Wood transmittance
τ_l	2.0	0.333	0.333	0.333	—	—	—	yr^{-1}	Leaf turnover rate (not applicable for hardwoods, which are deciduous)
τ_n	0.000	0.000	0.000	0.000	0.624	0.624	0.624	yr^{-1}	Storage turnover rate
τ_r	2.0	3.927	4.118	3.800	5.773	5.083	5.071	yr^{-1}	Fine-root turnover rate
τ_Δ	0.333	0.450	0.450	0.450	—	—	—	dy^{-1}	Growth respiration factor (not applicable for hardwoods, which are deciduous)
χ	0.00	0.00	0.00	0.00	0.00	0.00	0.00	—	Mean orientation factor

Table S7: List of soil component properties (air, sand, silt, and clay), used to derive most soil-texture dependent properties. Most parameters are based on Monteith and Unsworth (2008); values for silt were unavailable and assumed to be intermediate between sand and clay. The volumetric fractions of the default soil texture types in ED-2.2 are listed in Table S8.

Symbol	Soil components				Units	Description
	Air	Sand	Silt	Clay		
q	1010	800	850	900	$J\,kg^{-1}\,K^{-1}$	Specific heat
ρ	1.200	2660	2655	2650	$kg\,m^{-3}$	Bulk density
Υ_Q	0.025	8.80	5.87	2.92	$W\,m^{-1}\,K^{-1}$	Thermal conductivity

Table S8: List of volumetric fractions of sand, silt, and clay (f_V) for the default soil texture types in ED-2.2 (Fig. S6). Component-specific properties of soils are listed in Table S7.

Class	Description	Volumetric fractions		
		Sand	Silt	Clay
Sa	Sand	0.920	0.050	0.030
LSa	Loamy sand	0.825	0.115	0.060
SaL	Sandy loam	0.660	0.230	0.110
SiL	Silt loam	0.200	0.640	0.160
L	Loam	0.410	0.420	0.170
SaCL	Sandy clay loam	0.590	0.140	0.270
SiCL	Silty clay loam	0.100	0.560	0.340
CL	Clayey loam	0.320	0.340	0.340
SaC	Sandy clay	0.520	0.060	0.420
SiC	Silty clay	0.060	0.470	0.470
C	Clay	0.200	0.200	0.600
Si	Silt	0.075	0.875	0.050
CC	Heavy clay	0.100	0.100	0.800
CSa	Clayey sand	0.375	0.100	0.525
CSi	Clayey silt	0.125	0.350	0.525

Table S9: Coefficients used in Eq. (S191) for each limitation and photosynthetic path. The special case in which the stomata are closed is also shown for reference.

Case	C$_3$ photosynthesis				C$_4$ photosynthesis			
	F^A	F^B	F^C	F^D	F^A	F^B	F^C	F^D
Closed stomata ($\dot{A}_k^{\varnothing}$)	0	0	0	1	0	0	0	1
RuBP-saturated ($\dot{A}_k^{\mathrm{RuBP}}$)	$\dot{V}_{C_k}^{\max}$	$-\dot{V}_{C_k}^{\max}\Gamma_k$	1	$\mathcal{K}_{\mathrm{ME}_k}$	0	$\dot{V}_{C_k}^{\max}$	0	1
CO$_2$-limited ($\dot{A}_k^{\mathrm{InSl}}$)	$\dot{V}_{C_k}^{\max}$	$-\dot{V}_{C_k}^{\max}\Gamma_k$	1	$\mathcal{K}_{\mathrm{ME}_k}$	$k_{\mathrm{PEP}}\dot{V}_{C_k}^{\max}$	0	0	1
Light-limited ($\dot{A}_k^{\mathrm{PAR}}$)	$\epsilon_k\,\dot{q}_k$	$-\epsilon_k\,\dot{q}_k\Gamma_k$	1	$2\Gamma_k$	0	$\epsilon_k\,\dot{q}_k$	0	1

S1 ED-2 developments since ED-2.0 and ED-2.2

In this Supplement, we list the main developments in the Ecosystem Demography Model version 2 (ED-2), with focus on mentioned in this manuscript (Fig. S3). The complete list of implementations, improvements, and code fixes are available on the GitHub website (`https://github.com/EDmodel/ED2`).

S1.1 Version 2.0 (ED-2.0)

This is the version described in Medvigy (2006); Medvigy et al. (2009), and it is the first version of the ED model that implements energy and water cycles at sub-daily scale. The biophysics core was adapted from the LEAF-2 land surface model (Walko et al., 2000), which is part of the Regional Atmospheric Model System (RAMS). The main differences in the ED-2.0 biophysics core include (1) solution of the energy and water cycle for each cohort and patch; (2) use of 4th order Runge-Kutta solver to improve numerical stability. In addition, this version allowed leaf phenology to be prescribed from external data (Supplement S3.1.3). The photosynthesis solver was largely the same as in ED-1.0 (Moorcroft et al., 2001).

S1.2 Version 2.0.12 (ED-2.0.12)

Most developments between ED-2.0 and ED-2.0.12 relate to code organization and structure. ED-2.0 was partly written in C (legacy from ED-1) and partly written in Fortran (legacy from LEAF-2). To simplify the code and ensure data were correctly transferred between subroutines, we rewrote most of the code in Fortran. The only exceptions were a few file handling functions that remained in C because we could not find equivalent functions in Fortran.

In addition, this version uses Hierarchical Data Format 5 (HDF5) format and libraries (The HDF Group, 2016) to generate model outputs. HDF5 allows a more efficient framework to output variables in the dynamic patch and cohort structures. It also introduced an XML model parameter input file, rather than relying solely on hard-coded defaults, which makes it easier to perform model calibration, sensitivity analyses, and ensemble error propagation. Importantly, this was the last version of ED-2 that used temperature as prognostic variable for leaves and canopy air space.

S1.3 Version 2.1 (ED-2.1)

Most ED-2.1 developments aimed at improving the energy cycle representation in ED-2.1. ~~Importantly, leaf~~Leaf enthalpy and canopy air space enthalpy replaced temperature as the prognostic variables (Eq. 4; Sec. 3.2.3-3.2.4). The main advantages of energy-related prognostic equations include: (1) simplification the numeric integration, as total energy changes must be equivalent to net energy flux; (2) improved conservation of energy when water fluxes are large and cause rapid changes in heat capacity of the thermodynamic systems; (3) elimination of singularity at the water's fusion point ($0\,^\circ$C), when enthalpy changes due to freezing or melting, but the temperature remains the same.

To ensure the model was thermodynamically consistent, we also: (1) implemented a mechanistic representation of heat capacity for vegetation (leaves and branches, Supplement S6.2) that is scaled with leaf and branch biomass (e.g. Dufour and van Mieghem, 1975); (2) replaced the original LEAF-2-based surface layer model (that was based on Louis, 1979) with the parameterization by Beljaars and Holtslag (1991), as the latter parameterization improved numerical stability of eddy covariance fluxes under thermally stable conditions; (3) included an option to prescribe silt, clay, and sand fractions to define site-specific soil texture characteristics (Supplement S9) instead of the original ED-2.0 implementation that required soils to be assigned to one of the 12 fixed classes originally defined in LEAF-2 (Walko et al., 2000); (4) implemented the capability of saving the entire ecosystem and thermodynamic state of the model into HDF5 files, which can be used to stop and start simulations and yield the same results of uninterrupted simulations, a desirable feature for simulations with long runtimes.

S1.4 Version 2.2 (ED-2.2)

The ED-2.2 version implemented several improvements and fixed inconsistencies in the representation of the energy, water, and carbon dioxide cycles. First, we redefined enthalpy (S5), to ensure that it would be a true thermodynamic state variable (i.e. path independent, see Dufour and van Mieghem, 1975), by making latent heat of vaporization a linear function of temperature (Eq. 72-73). Moreover, we identified missing components of the energy cycle that precluded the conservation: (1) the transfer of internal energy from soils to leaves before transpiration (Eq. 97); (2) the enthalpy exchange associated with vaporization and condensation also accounts the mass transfer of water between the thermodynamic systems (e.g. Eq. 75; 98). Furthermore, to ensure results from ED-2.2 consistently conserve mass and energy, we implemented detailed conservation verification during the model execution, which now reports any violation of energy, water, and carbon conservation, generates detailed output of the violation, and interrupts the simulation. Finally, to improve computational efficiency of the energy, water, and carbon cy-

cle solvers at sub-daily time steps, we implemented a shared-memory parallelization of the most computationally-intensive subroutines. The parallelization was written to allow users to select any number of cores (depending on core availability), and ~~to account~~it accounts for patch ages in order to balance the load among cores.

In addition, we rewrote the photosynthesis to allow temperature-dependent functions to be expressed as functions of Q_{10}. We retained the original Arrhenius-based functions as legacy options, but the new option increases the options for assimilating data into the model. The current Q_{10}-based parameters fix the low-temperature optimum in tropical plants previously noted by Rogers et al. (2017). Importantly, we rewrote the photosynthesis solver to ensure that it would always converge to a unique solution for net assimilation rate, stomatal conductance, and intercellular carbon dioxide concentration given the environmental conditions (Supplement S16).

The ED-2.2 version also includes improvements in the representation of conductances between different thermodynamic systems. First, the leaf boundary-layer conductance now accounts for differences in leaf and branch characteristics of each cohort, and to account for both free and forced convection under both laminar and turbulent flow (Supplement S14.2). Second, we implemented ground-to-canopy conductance formulations (Sellers et al., 1986; Massman, 1997; Massman and Weil, 1999) that account for the cumulative drag profile of vegetated areas obtained from the cohort structure, as well as the stability of the surface layer (Supplement S14.3).

Finally, in ED-2.2 we replaced the version control to GitHub, which makes the new code developments readily available to the scientific community and encourages users to post issues, code fixes and model improvements and developments to the main code repository in open and collaborative forums.

S2 Boundary conditions for the ecosystem dynamics equations

The boundary conditions for Eq. (2) and (3) are:

$$
\underbrace{n_{fq}\left(\mathbf{C}_{f_0}, a, t\right)}_{\text{Recruit}} = \frac{1}{\mathbf{g}_{f_0} \cdot \mathbf{1}} \left\{ \underbrace{\int_{\mathbf{C}_{f_0}}^{\infty} \left(1 - f_{\delta_f}\right) \varrho_f \, n_{fq} \mathrm{d}\mathbf{C}}_{\text{Local recruitment}} + \underbrace{\sum_{q'=1}^{N_Q} \left[\int_{\mathbf{C}_{f_0}}^{\infty} \int_0^{\infty} f_{\delta_f} \, \varrho_f \, n_{FQ'X'Y} \alpha_{fq'} \, \mathrm{d}a \, \mathrm{d}\mathbf{C} \right]}_{\text{Non-local, random dispersal}} \right\},
$$

(S1)

$$
\underbrace{n_{fq}\left(\mathbf{C}_f, 0, t\right)}_{\text{Population at new gap}} = \underbrace{\sum_{q'=1}^{N_Q} \left[\int_0^{\infty} \hat{\sigma}_{fq'} \, n_{fq'} \, \alpha_{q'} \, \mathrm{d}a \right]}_{\text{Disturbance Survivors}},
$$

(S2)

$$\underbrace{\alpha_q(0,t)}_{\text{Probability of new gap}} = \underbrace{\sum_{q'=1}^{N_Q} \lambda_{q'q} \alpha_{q'} da}_{\text{Disturbance rates}}, \tag{S3}$$

where $\mathbf{C}_{f_0}$ is the size of the smallest individual of PFT f; $\mathbf{g}_{f_0}$ is the growth rate for individuals of PFT f with size $\mathbf{C}_{f_0}$; $\mathbf{1}$ is the unity vector for size; ϱ_f is the recruitment rate, which ~~may depend~~ depends on the PFT, size, and carbon balance; f_{δ_f} is the fraction of recruits of PFT f that are randomly dispersed instead of locally recruited; and $\hat{\sigma}_{fq}$ is size-dependent survivorship probability for a PFT f following a disturbance of type q (for a complete list of subscripts and variable meanings, refer to Tables S1 and S2). Both $\mathbf{g}_f$ and m_f are functions of the plant size and the individual's carbon balance. The individual's carbon balance depends on the environment perceived by each individual; in turn, the environment perceived by each individual is modulated by both the plant community living in the same gap and the general landscape environment. Likewise, the disturbance rates may be affected by the local plant community in the gap and the regional landscape environment.

S3 Long-term carbon dynamics and relation with carbon balance

S3.1 Leaf phenology

The phenological strategy of the plant functional types~ can be evergreen, drought-deciduous, or cold-deciduous. The plant's phenology strategy is defined by two functions: (i) the leaf elongation factor ($\hat{e}_{l_k}$), defined as the ratio between the environmentally-constrained leaf biomass and the potential (maximum) leaf biomass, and the rate of leaf shedding ($\omega_{l_k}(t)$) which can either be prognosed, or prescribed from observations.

S3.1.1 Evergreen plants

For evergreen PFTs, the elongation factor is always 1, the rate of leaf shedding ($\omega_{l_k}(t)$) is zero, and their rate of leaf turnover is governed by the PFT-dependent leaf turnover parameter (τ_{l_k}, see Eq. S12, and Tables S5–S6). The leaf phenology of tropical trees can also be represented by an empirical model that is driven by the seasonality of light availability (see Kim et al., 2012).

S3.1.2 Drought-deciduous tropical phenology

The drought-deciduous phenology assumes that leaf flushing and leaf senescence are controlled by the water availability in the rooting zone. The elongation factor $\hat{e}_{l_k}$ is determined by the following parameterization:

$$
\hat{e}_{l_k} = \begin{cases} 1 & \text{, if } s_{l_k} \geq 1 \\ s_{l_k} & \text{, if } 0.05 \leq s_{l_k} < 1 \text{ ,} \\ 0 & \text{, if } s_{l_k} < 0.05 \end{cases} \tag{S4}
$$

$$
s_{l_k} = \frac{1}{|z_{r_k}|\,\Delta t_{\text{El}}} \int_{t'-\Delta t_{\text{El}}}^{t'} \left(\sum_{j=j(z_{r_k})}^{N_G} \left\{ \frac{\max\left[0, \Psi_{g_j}(t') + \frac{1}{2}\left(z_{g_j} + z_{g_{j+1}}\right) - \Psi_{\text{Wp}}\right]}{\Psi_{\text{Ld}} - \Psi_{\text{Wp}}} \right\} \right) dt, \tag{S5}
$$

where s_{l_k} is a 10-day running average of soil moisture accessed by cohort k (normalized by the difference between the water potential threshold and the wilting point), z_{r_k} is the rooting depth of cohort k (Supplement S18), Δt_{El} is the time scale for changes in phenology (assumed to be 10 days), $j(z_{r_k})$ is the soil layer containing the deepest roots of cohort k, Ψ_{g_j} is the soil matric potential at soil layer j, Ψ_{Ld} is the soil matric potential below which plants start shedding leaves (assumed -1.2 MPa), Ψ_{Wp} is the soil matric potential at the wilting point, and z_{g_j} is the depth of soil layer j ($z_{g_{N_G+1}} \equiv 0$, otherwise z_g is negative). Leaf shedding occurs whenever soil is drier than the threshold defined by Ψ_{Ld} and drought conditions are increasing. Specifically:

$$
\omega_{l_k} = \frac{1}{\Delta t_{\text{Phen}}} \max\left[0, \frac{C_{l_k}}{C_{l_k}^{\bullet}} - f_{\text{El}}\right]. \tag{S6}
$$

S3.1.3 Cold-deciduous phenology

The prognostic cold-deciduous leaf phenology approach is a thermal sum and chilling sum-based model identical to that of Albani et al. (2006), which, in turn, is based on Botta et al. (2000). At each patch, growing degree-days (GDD) are accumulated during the extended growing season ($\mathfrak{T}_{\text{GS}}$, January–August for the Northern Hemisphere, and July–February for the Southern Hemisphere), and the chilling days (CHD) in the extended senescing season ($\mathfrak{T}_{\text{SS}}$, November–June for the Northern Hemisphere, and May–December for the Southern Hemisphere):

$$
\text{GDD}(t) = \begin{cases} 0 & \text{, if } t \notin \mathfrak{T}_{\text{GS}} \\ \sum_{t'=t_{\text{GS}}(0)}^{t} \max\left(0, \overline{T}_c(t') - T_{\text{Phen}}\right) & \text{, otherwise} \end{cases}, \tag{S7}
$$

$$\text{CHD}(t) = \begin{cases} 0 & \text{, if } \overline{T}_c(t) \geq T_{\text{Phen}}, \text{ or } t \notin \mathfrak{T}_{\text{SS}} \\ \text{CHD}(t - \Delta t_{\text{Phen}}) + 1 & \text{, otherwise} \end{cases}, \tag{S8}$$

where $\overline{T}_c$ is the daily average canopy air space temperature, $\Delta t_{\text{Phen}} = 1$ day is the phenology time step (Table 2), $t_{\text{GS}}(0)$ is the beginning of the growing season, and $T_{\text{Phen}} = 278.15$ K ($5\,^{\circ}$C) is the leaf phenology threshold (Albani et al., 2006). The valued elongation factor $\hat{e}_{l_k}$ is then determined by the following series of conditions:

$$\hat{e}_{l_k}(t) = \begin{cases} 0 & \text{, if } \overline{T}_s(t) < 275.15 \text{ K} \\ 0 & \text{, if } \overline{T}_s(t) < 284.30 \text{ K and } t_{\odot} < 655 \text{ min} \\ 1 & \text{, if GDD} \geq -68.0 + 638.0 \exp\left[-0.01\,\text{CHD}(t)\right] \\ \hat{e}_{l_k}(t - \Delta t_{\text{Phen}}) & \text{, otherwise} \end{cases}, \tag{S9}$$

where $t_{\odot}$ is the daytime duration.

If desired, cold-deciduous phenology can be prescribed rather than prognosed, as described in Medvigy et al. (2009) and Viskari et al. (2015). The timing of leaf onset and leaf senescence are empirically determined from either field observations or from remote sensing (e.g. Zhang et al., 2003) by fitting the following curves, which are then used to determine $\hat{e}_{l_k}$ in the model:

$$\hat{e}_{l_k} = \begin{cases} \dfrac{1}{1 + (y_0 t)^{y_1}} & \text{, if } t \in \mathfrak{T}_{\text{GS}} \\ \dfrac{1}{1 + (y_2 t)^{y_3}} & \text{, if } t \in \mathfrak{T}_{\text{SS}} \end{cases}, \tag{S10}$$

where y_0, y_1, y_2, and y_3 are empirical parameters, determined from data prior to running the ED-2.2 model and provided to the model as inputs; t is the time, provided as day of year (i.e. 1 for January 1st, 365 for December 31 in non-leap years, and 366 for December 31 in leap years); $\mathfrak{T}_{\text{GS}}$ is the extended growing season (e.g. January–July for the Northern Hemisphere, July–January for the Southern Hemisphere); and $\mathfrak{T}_{\text{SS}}$ is the senescing season (e.g. August–December for the Northern Hemisphere, February–June for the Southern Hemisphere).

S3.2 Carbon allocation to living tissues and non-structural carbon

The accumulated carbon balance (C_{Δ_k}, Eq. 25) over the phenology time step Δt_{Phen} is used to update the non-structural carbon storage (C_{n_k}) as well as the changes in carbon stocks of living tissues (leaves: C_{l_k}; fine roots C_{r_k} and sapwood C_{σ_k}) due to carbon allocation, turnover losses, and phenology. Changes in living tissues and non-structural carbon are interdependent and described

by the following system of equations (see also Medvigy et al., 2009; Kim et al., 2012):

$$\frac{dC_{n_k}}{dt} = \frac{1}{\Delta t_{\text{Phen}}} \left[\int_{t-\Delta t_{\text{Phen}}}^{t} \frac{dC_{\Delta_k}}{dt} \, dt' \right] + \left(f_{\text{LD}} \, \omega_{l_k} - \gamma_{l_k} \right) C_{l_k} - \gamma_{r_k} C_{r_k} - \gamma_{\sigma_k} C_{\sigma_k} - \tau_{n_k} C_{n_k}, \quad \text{(S11)}$$

$$\frac{dC_{l_k}}{dt} = \left(\gamma_{l_k} - \tau_{l_k} - \omega_{l_k} \right) C_{l_k}, \quad \text{(S12)}$$

$$\frac{dC_{r_k}}{dt} = \left(\gamma_{r_k} - \tau_{r_k} \right) C_{r_k}, \quad \text{(S13)}$$

$$\frac{dC_{\sigma_k}}{dt} = \gamma_{\sigma_k} C_{\sigma_k}, \quad \text{(S14)}$$

where $\hat{e}_{l_k}$ is the elongation factor (Supplement S3.1); f_{LD} is the fraction of carbon retained from active leaf drop as storage, currently assumed to be 0.5; $(\gamma_{l_k}; \gamma_{r_k}; \gamma_{\sigma_k})$ are the growth rates of leaves, fine roots, and sapwood, respectively; $(\tau_{l_k}; \tau_{r_k}; \tau_{n_k})$ are the background turnover rates of leaves, fine roots, and non-structural carbon, and are typically assumed constant (Tables S5–S6; but see Kim et al., 2012); and ω_{l_k} is the phenology-driven leaf shedding rate (Supplement S3.1).

The allocation to living tissues depends on whether the plant carbon balance and environmental conditions are favorable for growing, and it is proportional to the amount of carbon needed by each pool to reach the expected carbon stock given size and environmental constrains (Supplement S18). First, let $\left(C_{l_k}^{\odot}; C_{r_k}^{\odot}; C_{\sigma_k}^{\odot} \right)$ be the biomass increment needed to bring leaves, fine roots, and sapwood, respectively to the expected carbon stock given the plant size and PFT $\left(C_{l_k}^{\bullet}; C_{r_k}^{\bullet}; C_{\sigma_k}^{\bullet} \right)$:

$$C_{l_k}^{\odot} = \max \left[0, \hat{e}_{l_k} C_{l_k}^{\bullet} - C_{l_k} \left(1 - \tau_{l_k} \Delta t_{\text{Phen}} \right) \right], \quad \text{(S15)}$$

$$C_{r_k}^{\odot} = \max \left[0, C_{r_k}^{\bullet} - C_{r_k} \left(1 - \tau_{r_k} \Delta t_{\text{Phen}} \right) \right], \quad \text{(S16)}$$

$$C_{\sigma_k}^{\odot} = \max \left[0, C_{\sigma_k}^{\bullet} - C_{\sigma_k} \right], \quad \text{(S17)}$$

$$C_{\alpha_k}^{\odot} = C_{l_k}^{\odot} + C_{r_k}^{\odot} + C_{\sigma_k}^{\odot}, \quad \text{(S18)}$$

where $C_{\alpha_k}^{\odot}$ is the biomass increment needed to bring all living tissues to expected biomass given size and PFT, and Δt_{Phen} is the phenology time step (Table 2). Growth rates of leaves (γ_{l_k}), fine roots (γ_{r_k}) and sapwood (γ_{σ_k}) are proportional to the amount needed by each tissue to be brought back to the expected biomass given size and PFT, but also constrained by the amount of non-structural carbon (C_{n_k}) available:

$$\gamma_{l_k} = \max \left\{ 0, \frac{1}{\Delta t_{\text{Phen}}} \frac{\hat{e}_{l_k} C_{l_k}^{\odot}}{C_{\alpha_k}^{\odot}} \min \left[\omega_k C_{\alpha_k}^{\odot}, C_{n_k} \left(1 - \tau_{n_k} \right) + C_{\Delta_k} \right] \right\}, \quad \text{(S19)}$$

S32

$$\gamma_{r_k} = \max\left\{0, \frac{1}{\Delta t_{\text{Phen}}} \frac{C_{r_k}^{\odot}}{C_{\alpha_k}^{\odot}} \min\left[\mathcal{O}_{\alpha_k} C_{\alpha_k}^{\odot}, C_{n_k}\left(1 - \tau_{n_k}\right) + C_{\Delta_k}\right]\right\}, \tag{S20}$$

$$\gamma_{\sigma_k} = \max\left\{0, \frac{1}{\Delta t_{\text{Phen}}} \frac{C_{\sigma_k}^{\odot}}{C_{\alpha_k}^{\odot}} \min\left[\mathcal{O}_{\alpha_k} C_{\alpha_k}^{\odot}, C_{n_k}\left(1 - \tau_{n_k}\right) + C_{\Delta_k}\right]\right\}. \tag{S21}$$

When the cohorts are actively shedding leaves due to phenology, $(\gamma_{l_k}; \gamma_{r_k}; \gamma_{\sigma_k})$ are assumed to be zero. In case carbon balance is sufficiently negative to consume the entire non-structural carbon pool, carbon stocks of living tissues will be depleted and mortality rates will increase (Supplement S3.4).

S3.3 Carbon allocation to structural tissues and reproduction

Growth of structural (C_{h_k}) and reproductive (C_{ϱ_k}) tissues are calculated at the cohort dynamics time step (Δt_{CD}, Table 2), after the biomass of living tissues and phenology have been updated:

$$C_{h_k}(t) = C_{h_k}(t - \Delta t_{\text{CD}}) + \gamma_{h_k} C_{n_k}(t) \Delta t_{\text{CD}}, \tag{S22}$$

$$C_{\varrho_k}(t) = \varrho_{t_k} C_{n_k}(t), \tag{S23}$$

$$\gamma_{h_k} = \frac{1}{\Delta t_{\text{CD}}} - \varrho_{t_k} - \gamma_{n_k}, \tag{S24}$$

$$\varrho_{t_k} = \frac{1}{\Delta t_{\text{CD}}} \begin{cases} 0.0 & \text{, if } z_{t_k} < z_{t_k}^{\text{Repro}} \text{ or } \omega_{l_k} > 0 \\ f_\varrho & \text{, otherwise} \end{cases}, \tag{S25}$$

$$\gamma_{n_k} = \frac{1}{\Delta t_{\text{CD}}} \begin{cases} 1.0 & \text{, if } \omega_{l_k} > 0 \\ f_n & \text{, otherwise} \end{cases}, \tag{S26}$$

where z_{t_k} is the cohort height (Supplement S18); $z_{t_k}^{\text{Repro}}$ is the minimum height for reproduction, currently defined as the maximum height for grasses and 18 m for ~~tropical~~ trees (based on Wright et al., 2005); f_ϱ is the fraction of carbon storage allocated for reproduction when trees are above minimum reproductive height, currently defined as 1.0 for grasses and 0.3 for tropical and temperate trees (Moorcroft et al., 2001); f_n is the fraction of carbon storage that is kept as storage, currently assumed to be 0 for grasses and temperate trees, and 0.1 for tropical trees; and ω_{l_k} is the phenology-driven leaf shedding rate (Supplement S3.1). The total reproduction biomass C_{ϱ_k} is transferred either to the patches' seed bank or to the soil carbon pools. The fraction that is transferred to the soil carbon pools is defined in terms of a mortality factor (m_{ϱ_k}), by default equivalent to 95% in a month, which accounts for both the allocation to reproductive accessories (fruits, flowers, or cones), which are eventually lost, and the seedling mortality rate; the remainder $(1 - m_{\varrho_k})$ is transferred to the seed bank. Carbon storage C_{n_k} is updated after carbon allocation

to structural carbon and reproduction.

S3.4 Mortality rates

Following Moorcroft et al. (2001) and Albani et al. (2006), the individual-based mortality rate (m_{t_k}) of any cohort k is the sum of four terms:

$$m_{t_k} = \underbrace{m_{t_k}^{\text{DI}}}_{\substack{\text{Aging} \\ \text{(Density-Independent)}}} + \underbrace{m_{t_k}^{\text{DD}}}_{\substack{\text{Carbon starvation} \\ \text{(Density dependent)}}} + \underbrace{m_{t_k}^{\text{CF}}}_{\substack{\text{Cold/Frost}}} + \underbrace{m_{t_k}^{\text{FR}}}_{\substack{\text{Fire}}}. \tag{S27}$$

As in Moorcroft et al. (2001), density-independent mortality is the component attributable to aging of the cohort, and it depends both on the typical tree fall disturbance rate λ_{TF} (Table S4) and the cohort wood density:

$$m_{t_k}^{\text{DI}} = \lambda_{\text{TF}} + \frac{1}{\text{æ}}, \tag{S28}$$

$$\tag{S29}$$

where æ is a PFT-specific term to account for the excess mortality in addition to the background mortality due to plant life span (Tables S5-S6). For tropical broadleaf trees, æ is parameterized following Moorcroft et al. (2001):

$$\text{æ} = \frac{0.0933 \, \rho_{\text{LTR}}}{\lambda_{\text{TF}} \left(\rho_{\text{LTR}} - \rho_{t_k} \right)}, \tag{S30}$$

where ρ_{t_k} (g cm^{-3}) is the wood density of tropical broadleaf cohort k (Table S5), and ρ_{LTR} is the wood density for late-successional, tropical broadleaf trees (Table S5).

Mortality due to cold or frost is also determined through a phenomenological parameterization that linearly increases mortality when the monthly mean canopy air space temperature $\overline{T}_c$ falls below a temperature threshold (Albani et al., 2006):

$$m_{t_k}^{\text{CF}} = 3.0 \max \left[0, \min \left(1, 1 - \frac{\overline{T}_c - T_{F_k}}{5} \right) \right], \tag{S31}$$

where T_{F_k} is a cold temperature threshold that represents the plant hardiness to cold, currently assumed to be 275.65 K for all tropical plants (Tables S5-S6).

Mortality due to fire in ED-2.2 follows the original implementation by Moorcroft et al.

(2001), and assumes that while fire depends on local scale dryness, once it ignites, it can spread throughout the entire site. Unlike other mortality rates, here we take multiple patches into account (patches are denoted by subscript u). First, let $\lambda_{u,u_0}^{\text{FR}}$ be the disturbance rate associated with fires affecting patch u (and creating patch u_0), defined as in Moorcroft et al. (2001):

$$
\lambda_{u,u_0}^{\text{FR}} = \mathcal{I} \sum_{u=1}^{N_P} \sum_{k=1}^{N_{T_u}} \left\{ \left[C_{ul_k} + f_{\text{AG}_{uk}} \left(C_{u\sigma_k} + C_{uh_k} \right) \right] \mathcal{Y}_u \, \alpha_u \right\},
\tag{S32}
$$

where N_P is the number of patches, N_{T_u} is the number of cohorts in patch u, $\mathcal{Y}_u$ is the binary ignition function, α_u is the relative area of patch u, and $\mathcal{I} = 0.5\ \text{m}^2\,\text{kgC}^{-1}\,\text{yr}^{-1}$ is a phenomenological parameter that controls fire intensity, and $f_{\text{AG}_{uk}}$ is the fraction of the tissue that is above ground (Tables S5-S6).

The ignition switch is defined in terms of the dryness of the environment, following the original formulation by Moorcroft et al. (2001), which uses soil moisture to estimate dryness:

$$
\mathcal{Y}_u =
\begin{cases}
1 & , \text{if } \left(\frac{1}{|z_{\text{Fr}}|} \int_{z_{\text{Fr}}}^{0} \vartheta_g \, dz \right) < \vartheta_{\text{Fr}} \\
0 & , \text{otherwise}
\end{cases}
,
\tag{S33}
$$

where z_{Fr} is the maximum soil depth to consider when assessing dryness and ϑ_{Fr} is the average soil moisture below which ignition occurs. Both z_{Fr} and ϑ_{Fr} are adjustable parameters; default values are $z_{\text{Fr}} = -0.50$ m and $\vartheta_{\text{Fr}} = \vartheta\left(\Psi_{\text{Fr}}\right)$ ($\Psi_{\text{Fr}} = -1.4$ MPa). Once the fire disturbance rate is determined, mortality rate can be determined from the definition of disturbance rate ~~(c.f. Moorcroft et al., 2001)~~(Moorcroft et al., 2001):

$$
m_{ut_k}^{\text{FR}} = \ln \left[\frac{1}{\hat{\sigma}_{ut_k}^{\text{FR}} + \left(1 - \hat{\sigma}_{ut_k}^{\text{FR}}\right) \exp\left(-\lambda_{u,u_0}^{\text{FR}} \Delta t_{\text{PD}}\right)} \right],
\tag{S34}
$$

where $\hat{\sigma}_{ut_k}^{\text{FR}}$ is the survivorship fraction of cohort t_k of patch u following fire disturbance; this value is currently assumed to be zero for all plants in ED-2.2.

Density-dependent mortality rate ($m_{t_k}^{\text{DD}}$) is called so because it describes the limitations of carbon uptake due to competition with other trees to access shared resources such as light and water. Similarly to Moorcroft et al. (2001), the density-dependent mortality rate is parameterized with a logistic function:

$$m_{t_k}^{\text{DD}}(t) = \frac{y_1}{1 + \exp\left[y_2\left(\frac{\overline{C}_{\Delta_k}}{\overline{C}_{\Delta_k}^\bullet} - y_3\right)\right]}, \tag{S35}$$

where $(y_1; y_2; y_3) = (5.0, 20.0, 0.2)$ are the default (but adjustable) parameters for tropical plants; $\overline{C}_{\Delta_k}$ is the average carbon balance of cohort k over a 12-month period ending at time t, and $\overline{C}_{\Delta_k}^\bullet$ is the average carbon balance the cohort would attain if ~~it had no light or water limitation~~neither light nor water were limiting carbon uptake. The current implementation includes only light and moisture, although the idea can be extended to any limiting resource.

S4 Input fluxes for soil carbon pools

Soil carbon is represented by three pools characterized by their typical decay rates: the fast soil carbon (subscript e_1), is comprised by metabolic litter (non-lignified leaf and fine-root litter); the intermediate soil carbon (subscript e_2) represents the decaying structural tissues and lignified materials, and the slow soil carbon (e_3) represents the dissolved soil organic matter. Changes in soil carbon content of the three pools are described by the following ordinary differential equations:

$$\frac{d\dot{C}_{e_1}}{dt} = \dot{C}_{t_k,e_1} + \dot{C}_{t_k,e_1}^\star - \dot{C}_{e_1,c} - \dot{C}_{e_1,e_3}, \tag{S36}$$

$$\frac{d\dot{C}_{e_2}}{dt} = \dot{C}_{t_k,e_2} + \dot{C}_{t_k,e_2}^\star - \dot{C}_{e_2,c} - \dot{C}_{e_2,e_3}, \tag{S37}$$

$$\frac{d\dot{C}_{e_3}}{dt} = \dot{C}_{e_1,e_3} + \dot{C}_{e_2,e_3} - \dot{C}_{e_3,c}, \tag{S38}$$

where $(\dot{C}_{t_k,e_1}; \dot{C}_{t_k,e_2})$ are the influxes from cohorts to fast and structural soil carbon that are due to maintenance and shedding of living tissues; $(\dot{C}_{t_k,e_1}^\star; \dot{C}_{t_k,e_2}^\star)$ are the influxes from cohorts to fast and structural soil carbon that are due to mortality; $(\dot{C}_{e_1,c}; \dot{C}_{e_2,c}; \dot{C}_{e_3,c})$ are the effluxes from all soil carbon pools through heterotrophic respiration; and $(\dot{C}_{e_1,e_3}; \dot{C}_{e_2,e_3})$ are the decay fluxes that are transported from fast and structural carbon pools to the soil organic matter pool.

Heterotrophic respiration terms are discussed in Section 4.8. The transport terms between cohorts and the fast and the structural carbon pools are defined as:

$$\dot{C}_{t_k,e_1} = \left(1 - \pounds_{l_k}\right)\left[(1 - f_{\text{LD}})\,\omega_{l_k}\,C_{l_k} + \tau_{l_k}\,C_{l_k} + \tau_{r_k}\,C_{r_k}\right], \tag{S39}$$

$$\dot{C}_{t_k,e_2} = \pounds_{l_k}\left(f_{\text{LD}}\,\omega_{l_k}\,C_{l_k} + \tau_{l_k}\,C_{l_k} + \tau_{r_k}\,C_{r_k}\right), \tag{S40}$$

$$\dot{C}^{\star}_{t_k,e_1} = m_{t_k} \left[\left(1 - \pounds_{l_k} \right) \left(C_{l_k} + C_{r_k} \right) + \left(1 - \pounds_{h_k} \right) \left(C_{\sigma_k} + C_{h_k} \right) + C_{n_k} \right] + m_{\varrho_k} C_{\varrho_k}, \tag{S41}$$

$$\dot{C}^{\star}_{t_k,e_2} = m_{t_k} \left[\pounds_{l_k} \left(C_{l_k} + C_{r_k} \right) + \pounds_{h_k} \left(C_{\sigma_k} + C_{h_k} \right) \right], \tag{S42}$$

where $(\pounds_{l_k}; \pounds_{h_k})$ are the fraction of soft — leaves and fine roots — and woody — sapwood and hardwood — tissues that are lignified, and $(\tau_{l_k}; \tau_{r_k})$ are the leaf and fine root turnover rates (Tables S5–S6); f_{LD} is the fraction of carbon reabsorbed by cohorts when shedding leaves (Table S4); ω_{l_k} is the phenology-driven leaf shedding rate; m_{t_k} is the mortality rate (Supplement S3.4); and m_{ϱ_k} is the rate of loss associated with reproduction (reproductive accessories and seedling mortality; Supplement S3.3).

The decay rates that are transported from fast and structural pools to dissolved soil carbon pools are also determined from the complementary fraction of decay functions, i.e. the fraction of decay that is not lost through heterotrophic respiration (see Section 4.8):

$$\dot{C}_{e_j,e_3} = \frac{1 - f_{he_j}}{f_{he_j}} \dot{C}_{e_j,c}, \tag{S43}$$

where the subscript e_j corresponds to either the fast (e_1) or the structural (e_2) soil carbon; f_{he_j} is the fraction of decay that is lost through respiration (Table S4); and $\dot{C}_{e_j,c}$ is the heterotrophic respiration flux from these soil carbon pools.

S5 Definition of enthalpy as a state function

Enthalpy is an extensive thermodynamic variable, therefore the total enthalpy of any thermodynamic system consisting of two or more materials is the sum of enthalpies of each material. Likewise, enthalpy must increase linearly with mass, therefore the total enthalpy of any material (H_x) is defined as $H_x = X \cdot h_x$, where X is the mass of this material and h_x is the specific enthalpy of this material.

For any material other than water (hereafter, dry material), h_d is defined as zero when the dry material temperature is 0 K; for water, the zero level is also at 0 K, with the additional condition that water is completely frozen. The specific enthalpy for dry material (h_d), ice (h_i), liquid water (h_ℓ) and water vapor (h_v) are defined as:

$$h_d(T) = \underbrace{q_d \cdot T}_{\text{Heating}} \tag{S44}$$

$$h_i(T) = \underbrace{q_i \cdot T}_{\text{Heating ice}} \tag{S45}$$

$$h_\ell(T) = \underbrace{h_i(T_{i\ell})}_{\text{Ice enthalpy at melting point}} + \underbrace{l_{i\ell}(T_{i\ell})}_{\text{Melting ice}} + \underbrace{q_\ell(T - T_{i\ell})}_{\text{Heating liquid}} \tag{S46}$$

$$h_v(T) = \underbrace{h_\ell(T_{\ell v})}_{\text{Liquid enthalpy at vaporization point}} + \underbrace{l_{\ell v}(T_{\ell v})}_{\text{Vaporization}} + \underbrace{q_{pv}(T - T_{\ell v})}_{\text{Heating vapor}} \tag{S47}$$

where q_d, q_i and q_ℓ are the specific heats for dry material, ice and liquid water, respectively; q_{pv} is the specific heat at constant pressure for water vapor; $T_{i\ell}$ and $T_{\ell v}$ are the temperatures where ice melted and liquid water vaporized; and $l_{i\ell}$ and $l_{\ell v}$ are the latent heat of melting and vaporization, respectively. Equation (S47) is still valid even when ice sublimates, because $l_{iv}(T) = l_{i\ell}(T) + l_{\ell v}(T)$ for any temperature T. By definition (e.g. Dufour and van Mieghem, 1975), the latent heat associated with phase change is the difference in enthalpy between the two phases at the temperature in which the phase change happens, therefore, we can determine the dependency of latent heat on temperature:

$$\left(\frac{\partial l_{\ell v}}{\partial T}\right)_p = \left(\frac{\partial h_v}{\partial T}\right)_p - \left(\frac{\partial h_\ell}{\partial T}\right)_p = q_{pv} - q_\ell, \tag{S48}$$

$$\left(\frac{\partial l_{i\ell}}{\partial T}\right)_p = \left(\frac{\partial h_\ell}{\partial T}\right)_p - \left(\frac{\partial h_i}{\partial T}\right)_p = q_\ell - q_i. \tag{S49}$$

If we further assume that the transition between ice and liquid phases can only occur at the water triple point (T_3), and that the latent heat of fusion $l_{i\ell 3} \equiv l_{i\ell}(T_3)$ and vaporization $l_{\ell v 3} \equiv l_{\ell v}(T_3)$ are known (Table S3), we can combine Eq. (S44)-(S47) to obtain a generic state function for specific enthalpy h:

$$h = \frac{H}{D+W} = d\,q_d\,T + w\left[i\,q_i\,T + \ell\,q_\ell\,(T - T_{\ell 0}) + v\,q_{pv}\,(T - T_{v0})\right], \tag{S50}$$

$$d = \frac{D}{D+W}, \tag{S51}$$

$$w = \frac{W}{D+W}, \tag{S52}$$

$$T_{\ell 0} = T_3 - \frac{q_i\,T_3 + l_{i\ell 3}}{q_\ell}, \tag{S53}$$

$$T_{v0} = T_3 - \frac{q_i\,T_3 + l_{i\ell 3} + l_{\ell v 3}}{q_{pv}}, \tag{S54}$$

where d and w are the specific mass of other materials and water, respectively, and i, ℓ, and v are fraction of ice, liquid water, and vapor, respectively. Importantly, (S50) does not contain any information about the temperature at which the phase changes had occurred, which is necessary because enthalpy must be a state function (i.e. path-independent).

Temperature T and phase fractions $(i; \ell; v)$ of any thermodynamic system are diagnosed from enthalpy. In the case of canopy air space, i, and ℓ are all assumed to be zero, and thus $v = 1$. The canopy air space temperature T_c is obtained by inverting Eq. S50 and using that $d = 1 - w$:

$$T_c = \frac{h_c + w\,q_{pv}\,T_{v0}}{(1-w)\,q_{pd} + w\,q_{pv}}. \tag{S55}$$

For other thermodynamic systems, v is assumed to be zero. To obtain the temperature and the liquid fraction, we eliminate i from Eq. (S50) by using that $i = 1 - \ell$, and define two critical values of specific enthalpy: h_{i3}, the enthalpy when the water is at the triple point temperature (T_3) but entirely frozen, and $h_{\ell 3}$, when water is entirely in liquid phase and still at triple point temperature:

$$h_{i3} = d\,q_d\,T_3 + w\,q_i\,T_3, \tag{S56}$$
$$h_{\ell 3} = h_{i3} + w\,l_{i\ell 3} = d\,q_d\,T_3 + w\,q_\ell\,(T_3 - T_{\ell 0}). \tag{S57}$$

Liquid water and ice can coexist when $T = T_3$, and this only occurs when $h_{i3} < h < h_{\ell 3}$. Therefore, we obtain T and ℓ by comparing the specific enthalpy with h_{i3} and $h_{\ell 3}$:

$$T = \begin{cases} \frac{h}{d\,q_d + w\,q_i} & \text{, if } h < h_{i3} \\ T_3 & \text{, if } h_{i3} \leq h \leq h_{\ell 3}, \\ \frac{h + w\,q_\ell\,T_{\ell 0}}{d\,q_d + w\,q_\ell} & \text{, if } h > h_{\ell 3} \end{cases} \tag{S58}$$

$$\ell = \begin{cases} 0 & \text{, if } h < h_{i3} \\ \frac{h - h_{i3}}{l_{i\ell 3}\,w} & \text{, if } h_{i3} \leq h \leq h_{\ell 3}. \\ 1 & \text{, if } h > h_{\ell 3} \end{cases} \tag{S59}$$

S6 Specific heat capacity of the thermodynamic systems

From Eq. (S50), we must know the mass and specific heats of each material for each thermodynamic system. For water, specific heat depends on the phase: q_i (ice); q_ℓ (liquid); q_{pv} (vapor at constant pressure); values are shown in Table S3. The specific heats of dry materials are defined below.

S6.1 Soil

Soil water of layer j is normally expressed in terms of liquid-equivalent volumetric fraction (ϑ_{g_j}), thus the bulk density of water in the layer is simply $\mathcal{W}_{g_j} = \rho_\ell \vartheta_{g_j}$. Dry soil is a combination of sand, silt, clay, and air filling any pore space not filled by water, and its bulk density $\mathcal{D}_{g_j}$ for each layer is based on Monteith and Unsworth (2008, Section 15.3):

$$\mathcal{D}_{g_j} = \left[\sum_{\kappa=0}^{3} \rho_\kappa \mathcal{V}_{0\kappa} \left(z_{g_j} \right) \right], \tag{S60}$$

$$\mathcal{V}_{0\kappa} \left(z_{g_j} \right) = \begin{cases} \vartheta_{\mathrm{Po}} - \vartheta_{g_j} \approx \frac{\vartheta_{\mathrm{Re}} + \vartheta_{\mathrm{Po}}}{2} & \kappa = 0 \\ f_{\mathcal{V}_\kappa} \left(1 - \vartheta_{\mathrm{Po}} \right) & \kappa \neq 0 \end{cases}, \tag{S61}$$

where κ indices 0, 1, 2, 3 correspond to air, sand, silt, and clay, respectively; ρ_κ (Table S7) and $\mathcal{V}_{0\kappa}$ (Table S8) are the specific gravity and the reference volumetric fraction of each component, and z_{g_j} is the depth of soil layer j. The volumetric soil content depends on the following texture-dependent variables: $f_{\mathcal{V}_\kappa}$, the soil texture-dependent, volumetric fraction of each soil component excluding water and air; ϑ_{Po}, the total porosity or maximum soil moisture and ϑ_{Re} is the residual water content, defined in Supplement S9. In reality, the volumetric fraction of air is not constant and depends on soil moisture; nevertheless, the total air mass is three orders of magnitude less than the solid materials, thus the contribution of varying air in the pore space to changes in specific heat is negligible. To reduce the maximum error associated with this assumption, we use the volumetric fraction corresponding to halfway between the minimum and maximum soil moisture.

Specific heat of dry soil of layer j (q_{dg_j}) is also determined following Monteith and Unsworth (2008), as the weighted average of the specific heats of the four components (Table S7):

$$q_{dg_j} = \frac{\sum_{\kappa=0}^{3} \left(\rho_\kappa \mathcal{V}_{0\kappa} q_\kappa \right)}{\sum_{\kappa=0}^{3} \left(\rho_\kappa \mathcal{V}_{0\kappa} \right)}. \tag{S62}$$

S6.2 Vegetation

In ED-2.2, vegetation biomass of the different tissues is usually expressed in $\mathrm{kg_C\,m^{-2}}$; for the energy budget, however, we must account for the total internal mass ($\mathrm{kg\,m^{-2}}$) because internal energy is also stored in non-carbon material, including the interstitial and intracellular water of

leaves and above ground wood (internal water). Internal water is considered a plant functional trait that remains constant throughout the simulations, although it can be different for different plant functional types. The extensive mass of the vegetation tissue (D_{t_k}) for any cohort k is given by:

$$D_{t_k} = D_{l_k} + D_{b_k}, \tag{S63}$$

$$D_{l_k} = \frac{1}{\mathcal{B}_C} C_{l_k} (1 + \mathcal{B}_{Wl}), \text{ and} \tag{S64}$$

$$D_{b_k} = \frac{1}{\mathcal{B}_C} f_{AG} C_{b_k} (1 + \mathcal{B}_{Wb}), \text{ and} \tag{S65}$$

where $\mathcal{B}_C = 2.0$ is the conversion from carbon to oven dry biomass, following Baccini et al. (2012); n_{t_k} is the demographic density of cohort k (plant m^{-2}); C_{l_k} and C_{b_k} are the carbon biomass of leaves and wood for each cohort (kg$_C$ m^{-2}), respectively; D_{l_k} and D_{b_k} are the extensive internal mass leaves and wood, respectively; f_{AG} is the fraction of woody biomass that is above ground (assumed 0.7 for all tree PFTs); and $\mathcal{B}_{Wl} = 0.7$ (Forest Products Laboratory, 2010) and $\mathcal{B}_{Wb} = 1.85$ (Kursar et al., 2009) are the water to oven-dry mass ratios for leaves and wood.

The vegetation specific heat excluding intercepted water (q_{dt_k}) is based on the Gu et al. (2007) parameterization and determined by the weighted average of leaves and wood specific heats, which in turn are weighted averages of the specific heat of the oven-dry materials and water:

$$q_{dt_k} = \frac{1}{D_{t_k}} \left[D_{l_k} \frac{q_l^{(\text{OD})} + \mathcal{B}_{Wl} q_\ell}{1 + \mathcal{B}_{Wl}} + D_{b_k} \left(\frac{q_b^{(\text{OD})} + \mathcal{B}_{Wb} q_\ell}{1 + \mathcal{B}_{Wb}} + \Delta q_b^{\text{Bond}} \right) \right] \tag{S66}$$

where $q_l^{(\text{OD})}$ and $q_b^{(\text{OD})}$ are the specific heats of oven-dry leaves and wood, respectively. The default values are taken from Forest Products Laboratory (2010) and Jones (2014) and assumed the same for all PFTs (Tables S5-S6); and Δq_b^{Bond} is a term included by Gu et al. (2007) and Forest Products Laboratory (2010) to represent the additional heat capacity associated with the bonding between wood and water (Tables S5-S6). Although $q_b^{(\text{OD})}$ and Δq_b^{Bond} are both functions of temperature in Gu et al. (2007), we further simplified them to constants in ED-2.2, using their original equations at 15 °C (Tables S5-S6). In addition, using q_ℓ as the specific heat for water is equivalent to assuming that internal water does not freeze.

S6.3 Canopy air space

The specific heat at constant pressure of the canopy air space (q_{pc}) is determined similarly to the vegetation and soils, as the weighted average between dry air and water vapor:

$$q_{pc} = (1 - w_c)\, q_{pd} + w_c q_{pv}, \tag{S67}$$

where q_{pd} and q_{pv} are the specific heats of dry air and water vapor at constant pressure (Table S3).

S7 Snowpack depth dynamics

In addition to enthalpy and total water, we must also track the changes in snowpack depth of each layer (Δz_{s_j}) and density (ρ_{s_j}) over time. The ordinary differential equation that governs changes in depth over time is defined as:

$$\frac{\mathrm{d}N z_{//}\left(\Delta z_{s_j}\right)}{\mathrm{d}t} = \begin{cases} \underbrace{\rho_{wa}\,\dot{W}_{a,s_j}}_{\substack{\text{Throughfall}\\\text{precipitation}\\(4.2)}} + \underbrace{\left(\sum_{k=1}^{N_T} \rho_{wt_k}\,\dot{W}_{t_k,s_j}\right)}_{\substack{\text{Canopy dripping}\\\text{from cohorts}\\(4.2)}} - \underbrace{\rho_{ws_j}\,\dot{W}_{s_j,o}}_{\substack{\text{Surface runoff}\\(4.1)}} - \underbrace{\rho_{wx}\dot{W}_{s_j,c}}_{\substack{\text{Surface water}\\\text{evaporation}\\(4.5.2)\text{ and }(4.5.3)}} - \underbrace{\delta_{s_1 s_j}\rho_{ws_j}\,\dot{W}_{s_1,g_{N_G}}}_{\substack{\text{Surface water}\\\text{percolation}\\(4.1)}} & , \text{if } s_j = s_{N_S} \\[2em] 0 & , \text{otherwise} \end{cases} , \tag{S68}$$

$$\rho_{ws_j} = \frac{W_{s_j}}{\Delta z_{s_j}} \tag{S69}$$

$$\rho_{wx} = \begin{cases} \rho_{ws_{N_S}} & , \text{if } \dot{W}_{s_{N_S},c} \geq 0 \\ \rho_{wc} & , \text{if } \dot{W}_{s_{N_S},c} < 0 \end{cases} \tag{S70}$$

where $\delta_{s_j s_{j'}}$ is the Kronecker delta for comparing two TSW layers s_j and $s_{j'}$ (1 if $s_j = s_{j'}$, 0 otherwise), ρ_{wa} is the precipitation density, ρ_{wt_k} is the canopy interception density, ρ_{wc} is the density of condensing water vapor. Precipitation density is defined based on Jin et al. (1999), but slightly modified to make it continuous:

$$\rho_{wa} = \frac{\rho_{ia}\rho_\ell}{\ell_a \rho_{ia} + (1 - \ell_a)\,\rho_\ell}, \tag{S71}$$

$$\rho_{ia} = \begin{cases} 169.16 & , \text{if } T_a > 275.16\ \text{K} \\ 50. + 1.7\,(T_a - 258.16)^{1.5} & , \text{if } 258.16\ \text{K} < T_a \leq 275.66\ \text{K} , \\ 50. & , \text{if } T_a \leq 258.16\ \text{K} \end{cases} \tag{S72}$$

S42

where ρ_ℓ is the density of liquid water (Table S3). For the canopy dripping flux, water density is similar to Eq. (S71), except that we assume the density of frozen water to be the same as frost density (ρ_*, Table S3). A similar assumption is done for water condensing from canopy air space, with the additional assumption that the liquid fraction of condensation is the same as the liquid fraction of the top TSW layer:

$$\rho_{wt_k} = \frac{\rho_* \rho_\ell}{\ell_{t_k} \rho_* + (1 - \ell_{t_k}) \rho_\ell},\tag{S73}$$

$$\rho_{wc} = \frac{\rho_* \rho_\ell}{\ell_{s_{N_S}} \rho_* + \left(1 - \ell_{s_{N_S}}\right) \rho_\ell}.\tag{S74}$$

The maximum allowed number of snow layers is determined by the user, but the actual number of snow layers is dynamically determined, following the same algorithm as Walko et al. (2000). Multiple layers only exist when ice is present, otherwise a single layer ($N_S = 1$) is enforced. When ice is present, the model selects N_S to be the maximum number of layers that satisfies $W_{s_j} \geq 5 \,\mathrm{kg_W\,m^{-2}}$ for all layers $s_j, j \in 1, 2, \ldots, N_S$, to ensure numerical stability. The layer thickness distribution (Δz_{s_j}) for any given N_S is defined as:

$$\Delta z_{s_j} = z_s \frac{2^{\min(j-1, N_S - j)}}{2^{\left\lfloor \frac{N_S + 1}{2} \right\rfloor} + 2^{\left\lfloor \frac{N_S}{2} \right\rfloor} - 2},\tag{S75}$$

$$z_s = \sum_{j=1}^{N_S} \Delta z_{s_j},\tag{S76}$$

where z_s is the total depth of the snow, and $\lfloor x \rfloor$ is the floor function (i.e. the nearest integer value to x that is not greater than x). The layer distribution described by Eq. (S75) ensures that the layers near the ground and near the canopy air space are thinner than the intermediate layers, to improve the representation of exchanges between the snowpack and the canopy air space, soils, and incoming irradiance (Walko et al., 2000).

S8 Canopy-Air-Space Pressure

Canopy-air-space pressure p_c is assumed to remain constant throughout the integration time step (Δt_{Thermo}). At the end of the time step, the air pressure above canopy p_a is updated using the meteorological forcing, at which time p_c and h_c are also updated. To determine p_c, we combine three assumptions:

1. Both canopy air space and the air above are a mix of two perfect gases, dry air and water

vapor (Dufour and van Mieghem, 1975):

$$p = \rho \mathcal{R} \left[\frac{1}{\mathcal{M}_d} (1 - w) + \frac{1}{\mathcal{M}_w} w \right] T = \rho \frac{\mathcal{R}}{\mathcal{M}_d} T_{\mathcal{V}}, \tag{S77}$$

$$T_{\mathcal{V}} = T \left[1 - \left(1 - \frac{\mathcal{M}_d}{\mathcal{M}_w} w \right) \right], \tag{S78}$$

where $\mathcal{R}$ is the universal gas constant, and $\mathcal{M}_d$ and $\mathcal{M}_w$ are the molar masses of dry air and water (Table S3); and $T_{\mathcal{V}}$ is the virtual temperature, which is the temperature that pure dry air would be at if pressure and density were the same as the observed air:

2. p_c instantaneously changes when p_a is updated, and this update does not involve any exchange of mass or energy. This is equivalent to assuming that potential temperature of the canopy air space θ_c and air aloft θ_a do not change when pressure is updated, even if enthalpy and temperature change. Potential temperature, approximated to the potential temperature of dry air, is defined as:

$$\theta = T \left(\frac{p_0}{p} \right)^{\frac{\mathcal{R}}{\mathcal{M}_d q_{pd}}}, \tag{S79}$$

where p_0 is the reference pressure level and q_{pd} is the specific heat of dry air at constant pressure (Table S3).

3. The layer between canopy air space depth $\bar{z}_c$ and reference height of the ~~air aloft~~free air z_a is in hydrostatic equilibrium:

$$\frac{\partial p}{\partial z} = -\rho g, \tag{S80}$$

where g is the gravity acceleration (Table S3).

Combining these three assumptions and defining $\theta_{\mathcal{V}} \equiv \theta(T_{\mathcal{V}})$ yields:

$$p_c = \left[p_a^{\frac{\mathcal{R}}{\mathcal{M}_d q_{pd}}} + \frac{g (z_a - \bar{z}_c)}{q_{pd} \overline{\theta_{\mathcal{V}}}} p_0^{\frac{\mathcal{R}}{\mathcal{M}_d q_{pd}}} \right]^{\frac{\mathcal{M}_d q_{pd}}{\mathcal{R}}}, \tag{S81}$$

where $\overline{\theta_{\mathcal{V}}}$ is the virtual potential temperature averaged between z_a and $\bar{z}_c$. Once pressure is updated at the biophysics time step, temperature and enthalpy are also updated using Eq. (S79)

S44

and Eq. (S50), respectively. Because canopy air pressure is known at all times, canopy air density ρ_c can be determined diagnostically using Eq. (S77).

S9   Soil thermal and hydraulic properties

Most of the soil hydraulic properties in ED-2.2 are derived from LEAF-3 (Walko et al., 2000) and use the soil classification based on the United States Department of Agriculture (e.g. Cosby et al., 1984). Soils in tropical forests often fall under the *Clay* class of the USDA classification, even though their sand, silt, and clay fractions often vary significantly from the average values of this class. To avoid large deviations from observations, we further split the original *Clay* class into four categories, named as *Clayey sand*, *Clayey silt*, *Clay*, and *Heavy Clay*, as shown in Fig. S6; the default fractions of each component for the default soil texture types in ED-2.2 are listed in Table S8. In addition to the standard classes, the model can derive site-specific properties based on the actual clay, silt, and sand fractions, which can be provided directly by the user.

The main hydraulic properties follow the parameterization by Cosby et al. (1984), shown here for reference:

$$\vartheta_{\text{Po}} = 0.0505 - 0.0142\, f_{\mathcal{V}_{\text{Sand}}} - 0.0037\, f_{\mathcal{V}_{\text{Clay}}}, \tag{S82}$$

$$\Psi_{\text{Po}} = -0.01 \cdot 10^{2.17 - 1.58\, f_{\mathcal{V}_{\text{Sand}}} - 0.63\, f_{\mathcal{V}_{\text{Clay}}}}, \tag{S83}$$

$$b = 3.10 - 0.3 \cdot f_{\mathcal{V}_{\text{Sand}}} + 15.7 \cdot f_{\mathcal{V}_{\text{Clay}}}, \tag{S84}$$

$$\Upsilon_{\Psi_{\text{Po}}} = 6.817 \times 10^{-6} \cdot 10^{-0.60 + 1.26\, f_{\mathcal{V}_{\text{Sand}}} - 0.64\, f_{\mathcal{V}_{\text{Clay}}}}, \tag{S85}$$

where $f_{\mathcal{V}_{\text{Sand}}}$ and $f_{\mathcal{V}_{\text{Clay}}}$ are the volumetric fraction of sand and clay, respectively; ϑ_{Po} ($\text{m}^3_{\text{W}}\,\text{m}^{-3}$) is the volumetric soil porosity (maximum soil moisture possible), $\Psi_{\text{Po}}\Upsilon_{\Psi_{\text{Po}}}$ (m) is the soil matric potential at porosity, b is the slope of the logarithmic water retention curve (Clapp and Hornberger, 1978), and $\Upsilon_{\Psi}^{(\text{Po})}$ ($\text{kg}_{\text{W}}\,\text{m}^{-2}\,\text{s}^{-1}$) is the soil hydraulic conductivity at bubbling pressure, assumed to occur when soil moisture $\vartheta = \vartheta_{\text{Po}}$.

The equation that describes soil matric potential as a function of soil moisture is taken from Clapp and Hornberger (1978); soil hydraulic conductivity is defined after Brooks and Corey (1964), with an additional correction term applied to hydraulic conductivity to reduce conductivity in case the soil is partially or completely frozen:

$$\Psi = \Psi_{\text{Po}} \left(\frac{\vartheta_{\text{Po}}}{\vartheta} \right)^b, \tag{S86}$$

$$\Upsilon_\Psi = \left[10^{-7(1-\ell)} \right] \Upsilon_{\Psi_{\text{Po}}} \left(\frac{\vartheta}{\vartheta_{\text{Po}}} \right)^{2b+3}, \tag{S87}$$

where Ψ_{Po} and $\Upsilon_{\Psi_{\text{Po}}}$ are the soil-texture dependent, matric potential and hydraulic conductivity at bubbling pressure, assumed to be the same as porosity (ϑ_{Po}); and ℓ is the fraction of liquid water of soil moisture.

Additional reference points are determined using the above equations combined with Eq. (S86) and (S87). The permanent wilting point ϑ_{Wp} and residual soil moisture ϑ_{Re} are defined as the soil moisture when soil matric potential is equivalent to -1.5 and -3.1 MPa, respectively:

$$\vartheta_{\text{Wp}} = \vartheta_{\text{Po}} \cdot \left(-\frac{g \rho_\ell \Psi_{\text{Po}}}{1.5 \cdot 10^6} \right)^{\frac{1}{b}}, \tag{S88}$$

$$\vartheta_{\text{Re}} = \vartheta_{\text{Po}} \cdot \left(-\frac{g \rho_\ell \Psi_{\text{Po}}}{3.1 \cdot 10^6} \right)^{\frac{1}{b}}, \tag{S89}$$

where g is the gravity acceleration and ρ_ℓ is the density of liquid water (Table S3).

Field capacity (ϑ_{Fc}) is often defined from soil matric potential (e.g. Hodnett and Tomasella, 2002; Saxton and Rawls, 2006). However, this definition is based on field measurements and the definition of ϑ_{Fc} from soil matric potential can substantially across studies, with values ranging from -0.1 kPa to -0.5 kPa (Romano and Santini, 2002). In ED-2.2, we follow Romano and Santini (2002) and define field capacity in terms of hydraulic conductivity, and assume that the drainage flux of water becomes negligible at hydraulic conductivity of 0.1 $\text{kg}_\text{W}\,\text{m}^{-2}\,\text{day}^{-1}$:

$$\vartheta_{\text{Fc}} = \vartheta_{\text{Po}} \cdot \left(\frac{1.16 \cdot 10^{-9}}{\Upsilon_{\Psi_{\text{Po}}}} \right)^{\frac{1}{2b+3}}. \tag{S90}$$

Soil thermal conductivity at soil layer j $(\Upsilon_{Q_{g_j}})$ is a function of the soil texture and soil moisture, and is determined using the *de Vries* weighted average of conductivities of each constituent of the soil (e.g. Parlange et al., 1998):

$$\Upsilon_{Q_{g_j}} = \frac{\sum_{\kappa=0}^{3} \left[\left(\frac{3\Upsilon_{Q_\ell}}{2\Upsilon_{Q_\ell} + \Upsilon_{Q_\kappa}} \right) \mathcal{V}_\kappa \left(z_{g_j} \right) \Upsilon_{Q_\kappa} \right] + \vartheta_{g_j} \Upsilon_{Q_\ell}}{\sum_{\kappa=0}^{3} \left[\left(\frac{3\Upsilon_{Q_\ell}}{2\Upsilon_{Q_\ell} + \Upsilon_{Q_\kappa}} \right) \mathcal{V}_\kappa \left(z_{g_j} \right) \right] + \vartheta_{g_j}}, \tag{S91}$$

$$\mathcal{V}_\kappa \left(z_{g_j} \right) = \begin{cases} \vartheta_{\text{Po}} - \vartheta_{g_j} & \kappa = 0 \\ \mathcal{V}_\kappa^{\text{Dry}} \left(1 - \vartheta_{\text{Po}} \right) & \kappa \neq 0 \end{cases}, \tag{S92}$$

where $\mathcal{V}_\kappa\left(z_{g_j}\right)$ is the volumetric fraction for soil components air, sand, silt, and clay ($\kappa = 0, 1, 2, 3$, respectively) at soil layer j; Υ_{Q_κ} is the thermal conductivity for air, sand, silt, and clay (Table S7), respectively; Υ_{Q_ℓ} is the thermal conductivity of water (Table S3); $\mathcal{V}_\kappa^{\mathrm{Dry}}$ is the dry matter volumetric fraction; and ϑ_{Po} is the soil porosity. In Eq. (S91), the weights are the product between the volumetric fraction and a function that represents both the ratio of the thermal gradient of the soil constituents and the thermal gradient of water and the shape of each soil constituent (Camillo and Schmugge, 1981); in ED-2.2 we assume all particles to be spherical.

S10 Thermal and hydraulic properties of temporary surface water

The fraction of ground covered by the temporary surface water (f_{TSW}) is determined following Niu and Yang (2007), with the same coefficients used in the Community Land Model (NCAR-CLM Oleson et al., 2013):

$$f_{\mathrm{TSW}} = \begin{cases} 0 & \text{if } N_S = 0 \\ \tanh\left[\frac{\Sigma_{j=1}^{N_S} z_{s_j}}{2.5 z_{0\varnothing}} \left(\frac{\overline{\rho}_s}{\rho_\circledast}\right)^{-1.0}\right] & \text{if } N_S > 0 \end{cases}, \tag{S93}$$

$$\overline{\rho}_s = \frac{\Sigma_{j=1}^{N_S} W_{s_j}}{\Sigma_{j=1}^{N_S} z_{s_j}}, \tag{S94}$$

where N_S is the number of temporary surface water layers, z_{s_j} (m) is the vertical position of the temporary surface water layer j; W_{s_j} ($\mathrm{kg\,m^{-2}}$) is the water mass of temporary surface water layer j, $z_{0\varnothing}$ is the bare soil roughness (Table S4); $\rho_\circledast$ is the reference density of fresh snow (Table S3).

The thermal conductivity of each temporary surface water layer ($\Upsilon_{Q_{s_j}}$) is a function of the layer temperature T_{s_j} and the bulk layer density ρ_{ws_j} (Eq. S69), and is found using the same parameterization as LEAF-2 (Walko et al., 2000):

$$\Upsilon_{Q_{s_j}} = y_0 \cdot \left[y_1 + y_2\,\rho_{ws_j} + y_3\left(\rho_{ws_j}\right)^2 + y_4\left(\rho_{ws_j}\right)^3\right] \cdot \exp\left(y_5\,T_{s_j}\right), \tag{S95}$$

where $(y_0; y_1; y_2; y_3; y_4; y_5) = \left(1.093 \times 10^{-3}; 0.03; 3.03 \times 10^{-4}; -1.77 \times 10^{-7}; 2.25 \times 10^{-9}; 0.028\right)$ are empirical constants.

S11 Optical properties of vegetation, soil, and temporary surface water.

The inverse of the optical depth per unit of plant area index (μ) for a radiation beam coming from any given angle of incidence Z is determined from the same parameterization described by Sellers (1985) and Oleson et al. (2013):

$$\mu(Z, \chi_k) = \frac{\cos Z}{E(Z, \chi_k)}, \tag{S96}$$

where $E(Z, \chi_k)$ is the average projection of all leaves and branches onto the horizontal, defined after Goudriaan (1977):

$$E(Z, \chi_k) = Y_{1_k} + Y_{2_k} \cos Z, \tag{S97}$$

$$Y_{1_k} = 0.5 - 0.633 \chi_k - 0.33 \chi_k^2, \tag{S98}$$

$$Y_{2_k} = 0.877 \left(1 - 2 Y_{1_k}\right), \tag{S99}$$

where Z is 0 when the beam is coming from the zenith and π when coming from the nadir (Fig. 4 in the main text); and χ_k is the mean orientation of leaves and branches, a PFT-dependent parameter that ranges from -1 (vertical leaves) to +1 (horizontal leaves), with 0 corresponding to spherically distributed leaves (Tables S5-S6). Equation (S97) is valid only when $-0.4 \le \chi_k \le 0.6$, which is the case for most plants in the wild (Goudriaan, 1977), and also all plant functional types in ED-2.2.

In the case of direct radiation, $\mu_k^{\odot} = \mu(Z^{\odot}, \chi_k)$, where $Z^{\odot}$ is the solar zenith angle, whereas all angles between 0 and $\pi/2$ contribute equally to downward diffuse radiation. In the case of upward radiation, the actual angles are between $\pi/2$ and π; in practice, the contribution of each angle is similar to the downward hemisphere except for the sign, hence the negative sign on the left-hand side of Eq. (47) in the main text. The contribution of all different zenith angles is represented by $\overline{\mu}_k$, which is the average across all possible angles (Sellers, 1985):

$$\overline{\mu}_k = \int_0^{\frac{\pi}{2}} \frac{\cos Z}{E(Z, \chi_k)} \sin Z \, dZ = \frac{1}{Y_{2_k}} \left[1 + \frac{Y_{1_k}}{Y_{2_k}} \ln \left(\frac{Y_{1_k}}{Y_{1_k} + Y_{2_k}} \right) \right]. \tag{S100}$$

The scattering parameters ς_{mk}, β_{mk} and $\beta_{mk}^{\odot}$ for each band m and cohort k are found using the same formulation as the Community Land Model (CLM, Oleson et al., 2013), which is mostly derived from Goudriaan (1977) and Sellers (1985). The scattering coefficient is defined as:

$$\varsigma_{mk} = \varsigma_{R_{mk}} + \varsigma_{T_{mk}}, \tag{S101}$$

where $\varsigma_{R_{mk}}$ and $\varsigma_{T_{mk}}$ are the PFT- and spectral-band-dependent reflectance and transmittance, respectively (Tables S5-S6). The cohort parameters are found by taking the weighted average of the PFT-dependent, leaf ($\varsigma_{R_{mk}}^{\text{Leaf}}$; $\varsigma_{T_{mk}}^{\text{Leaf}}$) and branchwood ($\varsigma_{R_{mk}}^{\text{Wood}}$; $\varsigma_{T_{mk}}^{\text{Wood}}$) properties, using $f_{\text{Clump}_k} \Lambda_k$ and Ω_k as weights, respectively.

Both the bulk diffuse backscattering β_{mk} and forwarding scattering $1 - \beta_{mk}$ contain contributions from reflectance and transmittance because leaves and branches are not perfectly horizontal; therefore the fraction depends on the mean leaf and branch inclination relative to the horizontal plane ($\mathcal{A}_k$), which is related to the leaf orientation by the same approximation used by Oleson et al. (2013):

$$\beta_{mk} = \frac{1}{2\,\varsigma_{mk}} \left[\varsigma_{R_{mk}} + \varsigma_{T_{mk}} + (\varsigma_{R_{mk}} - \varsigma_{T_{mk}}) \cos^2 \mathcal{A}_k \right], \tag{S102}$$

$$\cos \mathcal{A}_k \approx \frac{1 + \chi_k}{2}. \tag{S103}$$

For direct radiation, backscattering $\beta_{mk}^{\odot}$ and single-scattering albedo $\varsigma_{mk}^{\odot}$ are the same as Sellers (1985) and Oleson et al. (2013), and are determined by taking the limit $\varsigma_{mk} \to 0$ of Eq. (46) and (47) in the main text, assuming isotropic scattering of leaves and branches, and the projected area from Eq. (S97):

$$\beta_{mk}^{\odot} = \frac{\overline{\mu}_k + \mu_k^{\odot}}{\overline{\mu}_k} \frac{\varsigma_{mk}^{\odot}}{\varsigma_{mk}}, \tag{S104}$$

$$\begin{aligned}
\frac{\varsigma_{mk}^{\odot}}{\varsigma_{mk}} &= \frac{1}{2} \int_0^{\frac{\pi}{2}} \frac{E(Z^{\odot}, \chi_k) \cos Z}{E(Z^{\odot}, \chi_k) \cos Z + E(Z, \chi_k) \cos Z^{\odot}} \sin Z \, dZ \\
&= \frac{1}{2(1 + Y_{2_k} \mu_k^{\odot})} \left\{ 1 - \frac{Y_{1_k} \mu_k^{\odot}}{1 + Y_{2_k} \mu_k^{\odot}} \ln \left[\frac{1 + (Y_{1_k} + Y_{2_k}) \mu_k^{\odot}}{Y_{1_k} \mu_k^{\odot}} \right] \right\}.
\end{aligned} \tag{S105}$$

The effective ground scattering coefficient ς_{m0} is the weighted average of the exposed soil scattering and the combined backscattering of temporary surface water and soil scattering of irradiance transmitted through the temporary surface water:

$$\varsigma_{m0} = (1 - f_{\text{TSW}}) \varsigma_{R_{mg}} + f_{\text{TSW}} \varsigma_{R_{ms}} (1 + \varsigma_{T_{ms}} \varsigma_{R_{mg}}), \tag{S106}$$

where f_{TSW} is the fraction of ground covered by temporary surface water, $\varsigma_{R_{mg}}$ is the reflectance

of the top soil layer; and $\varsigma_{R_{ms}}$ and $\varsigma_{T_{ms}}$ are the reflectance and transmittance of the temporary surface water, respectively. Soil reflectance is a function of the soil color and volumetric soil moisture at the topmost layer, determined from the same parameterization and soil color classes as in Oleson et al. (2013):

$$\varsigma_{R_{mg}} = \min\left[\varsigma_{R_m}^{\text{Po}} + 0.11 - 0.40\,\vartheta_{g_{N_G}}, \varsigma_{R_m}^{\text{Re}}\right], \tag{S107}$$

where $\varsigma_{R_m}^{\text{Re}}$ and $\varsigma_{R_m}^{\text{Po}}$ are the soil color-dependent reflectance for dry and saturated soils, respectively.

The temporary surface water reflectance $\varsigma_{R_{ms}}$ depends on the liquid fraction, snow grain size and age, impurities, and the direction of incoming radiation, but here we simply assume a linear interpolation of soil reflectance at saturation and pure snow reflectance ($\varsigma_{R_{ms}}^{\circledast}$; Table S4), assumed constant for each band:

$$\varsigma_{R_{ms}} = \varsigma_{R_{ms}}^{\circledast} + \ell_{s_{N_S}}\left(\varsigma_{R_m}^{\text{Po}} - \varsigma_{R_{ms}}^{\circledast}\right). \tag{S108}$$

Following Verseghy (1991) and Walko et al. (2000), the transmissivity of intercepted irradiance for PAR and NIR is solved following Beer's law, with a direction-independent extinction coefficient:

$$\varsigma_{T_{ms}} = \begin{cases} \exp\left(-\dfrac{\sum_{j=1}^{N_S}\Delta\overline{z}_{s_j}}{f_{\text{TSW}}\overline{\mu}_s}\right) & \text{, if } m \in (1,2) \\ 0 & \text{, if } m = 3 \end{cases}, \tag{S109}$$

where $\overline{\mu}_s = 0.05\,\text{m}$ is the inverse of the optical depth per unit of temporary surface water depth, defined here to be the same coefficient used by Verseghy (1991) and Walko et al. (2000), and the additional f_{TSW}^{-1} term accounts for the clumping of the temporary surface water, when the water does not cover all ground. Temporary surface water is assumed to be opaque for the TIR band ($m = 3$), following Walko et al. (2000).

S12 Solving the two-stream linear system of canopy radiation in ED-2.2.

Because we assume that the optical properties are constant within each layer, it is possible to find an analytical solution for the full profile of direct and diffuse radiation. First, let $\dot{Q}_{mk}^{\odot}$, $\dot{Q}_{mk}^{\Downarrow}$, and

$\dot{Q}^{\Uparrow}_{mk}$ be the solution for band m and interface k immediately beneath the cohort (i.e. at $\tilde{\Phi} = \tilde{\Phi}_k$), and $\dot{Q}^{\odot}_{0_{mk}}$, $\dot{Q}^{\Downarrow}_{0_{mk}}$, and $\dot{Q}^{\Uparrow}_{0_{mk}}$ be the solution for band m and interface k immediately above the cohort (i.e. at $\tilde{\Phi} = 0$), as shown in Fig. 4. The direct radiation profile within each layer is simply given by:

$$\dot{Q}^{\odot}_{mk} = \dot{Q}^{\odot}_{0_{mk}} \exp\left(-\frac{\tilde{\Phi}_k}{\mu^{\odot}_k}\right), \tag{S110}$$

$$\dot{Q}^{\odot}_{0_{mk}} = \dot{Q}^{\odot}_{m(k+1)}, \tag{S111}$$

$$\dot{Q}^{\odot}_{m(N_T+1)} = \dot{Q}^{\odot}_{m(\infty,a)}, \tag{S112}$$

where $\dot{Q}^{\odot}_{m(\infty,a)}$ is the above-canopy, incoming direct radiation for band m and serves as the top boundary condition. Because the value at interface $N_T + 1$ is known, it is possible to determine all levels by integrating the layers from top to bottom.

For the diffuse components, an analytic solution can be found by defining two auxiliary variables $\dot{Q}^{+}_{mk} \equiv \dot{Q}^{\Downarrow}_{mk} + \dot{Q}^{\Uparrow}_{mk}$ and $\dot{Q}^{-}_{mk} = \dot{Q}^{\Downarrow}_{mk} - \dot{Q}^{\Uparrow}_{mk}$. By subtracting (adding) Eq. (46) from (to) Eq. (47), and using Eq. (S110)-(S112) we obtain:

$$\frac{d\dot{Q}^{+}_{mk}}{d\tilde{\Phi}} = -\frac{1 - (1 - 2\beta_{mk})\,\varsigma_{mk}}{\overline{\mu}_k}\dot{Q}^{-}_{mk} + \frac{(1 - 2\beta^{\odot}_{mk})\,\varsigma_{mk}}{\mu^{\odot}_{mk}}\dot{Q}^{\odot}_{m(k+1)}, \tag{S113}$$

$$\frac{d\dot{Q}^{-}_{mk}}{d\tilde{\Phi}} = -\frac{1 - \varsigma_{mk}}{\overline{\mu}_k}\dot{Q}^{+}_{mk} + \frac{\varsigma_{mk}}{\mu^{\odot}_k}\dot{Q}^{\odot}_{m(k+1)} + \frac{2(1 - \varsigma_{mk})}{\overline{\mu}_k}\dot{Q}^{\blacklozenge}_{mk}. \tag{S114}$$

By differentiating Eq. (S113) and Eq. (S114) and substituting the first derivatives by Eq. (S114) and Eq. (S113), we obtain two independent, second-order ordinary differential equations:

$$\frac{d^2\dot{Q}^{+}_{mk}}{d\tilde{\Phi}^2} = \varkappa^2_{mk}\dot{Q}^{+}_{mk} + \kappa^{+}_{mk}\exp\left(-\frac{\tilde{\Phi}}{\mu^{\odot}_k}\right) - 2\varkappa^2_{mk}\dot{Q}^{\blacklozenge}_{ik}, \tag{S115}$$

$$\frac{d^2\dot{Q}^{-}_{mk}}{d\tilde{\Phi}^2} = -\varkappa^2_{mk}\dot{Q}^{-}_{mk} + \kappa^{-}_{mk}\exp\left(-\frac{\tilde{\Phi}}{\mu^{\odot}_k}\right), \tag{S116}$$

where

$$\varkappa^2_{mk} = \frac{[1 - (1 - 2\beta_{mk})\,\varsigma_{mk}]\,(1 - \varsigma_{mk})}{\overline{\mu}^2_k}, \tag{S117}$$

$$\kappa^{+}_{mk} = -\left[\frac{1 - (1 - 2\beta_{mk})\,\varsigma_{mk}}{\overline{\mu}_k} + \frac{1 - 2\beta^{\odot}_{mk}}{\mu^{\odot}_k}\right]\frac{\varsigma_{mk}\,\dot{Q}^{\odot}_{m(k+1)}}{\mu^{\odot}_k}, \tag{S118}$$

$$\kappa_{mk}^- = -\left[\frac{(1-\varsigma_{mk})\left(1-2\beta_{mk}^\odot\right)}{\overline{\mu}_k} + \frac{1}{\mu_k^\odot}\right]\frac{\varsigma_{mk}\,\dot{Q}_{m(k+1)}^\odot}{\mu_k^\odot}. \tag{S119}$$

The solution of Eq. (S115)-(S116) is the combination of the homogeneous and the particular solution, and can be determined analytically:

$$\dot{Q}_{mk}^+\left(\tilde{\Phi}\right) = x_{mk}^{+-}\exp\left(-\varkappa_{mk}\tilde{\Phi}\right) + x_{mk}^{++}\exp\left(+\varkappa_{mk}\tilde{\Phi}\right) + \frac{\kappa^+\mu_k^{\odot 2}}{1-\varkappa_{mk}^2\mu_k^{\odot 2}}\exp\left(-\frac{\tilde{\Phi}}{\mu_k^\odot}\right) + 2\dot{Q}_{mk}^\blacklozenge \tag{S120}$$

$$\dot{Q}_{mk}^-\left(\tilde{\Phi}\right) = x_{mk}^{--}\exp\left(-\varkappa_{mk}\tilde{\Phi}\right) + x_{mk}^{-+}\exp\left(+\varkappa_{mk}\tilde{\Phi}\right) + \frac{\kappa^-\mu_k^{\odot 2}}{1-\varkappa_{mk}^2\mu_k^{\odot 2}}\exp\left(-\frac{\tilde{\Phi}}{\mu_k^\odot}\right) \tag{S121}$$

where x_{mk}^{+-}, x_{mk}^{++}, x_{mk}^{--}, and x_{mk}^{-+} are coefficients to be determined. We can reduce the number of coefficients to two by differentiating Eq. (S120)-(S121) and comparing them to Eq. (S113)-(S114), and using the fact that they must be equal for any $\tilde{\Phi}$, $\mu_k^\odot$, $\varkappa_{mk}$, and $\dot{Q}_{mk}^\blacklozenge$. We call these parameters $x_{m(2k-1)}$ and $x_{m(2k)}$, $k \in \{1,2,\ldots,N_T\}$. By further recalling the definition of $\dot{Q}_{mk}^+$ and $\dot{Q}_{mk}^-$, we obtain the profile of downward and upward diffuse irradiances:

$$\dot{Q}_{mk}^\Downarrow\left(\tilde{\Phi}\right) = x_{m(2k-1)}\mathcal{D}_{mk}^+\exp\left(-\varkappa_{mk}\tilde{\Phi}\right) + x_{m(2k)}\mathcal{D}_{mk}^-\exp\left(+\varkappa_{mk}\tilde{\Phi}\right) + \mathcal{P}_{mk}^+\exp\left(-\frac{\tilde{\Phi}}{\mu_k^\odot}\right) + \dot{Q}_{mk}^\blacklozenge, \tag{S122}$$

$$\dot{Q}_{mk}^\Uparrow\left(\tilde{\Phi}\right) = x_{m(2k-1)}\mathcal{D}_{mk}^-\exp\left(-\varkappa_{mk}\tilde{\Phi}\right) + x_{m(2k)}\mathcal{D}_{mk}^+\exp\left(+\varkappa_{mk}\tilde{\Phi}\right) + \mathcal{P}_{mk}^-\exp\left(-\frac{\tilde{\Phi}}{\mu_k^\odot}\right) + \dot{Q}_{mk}^\blacklozenge, \tag{S123}$$

where

$$\mathcal{D}_{mk}^\pm = \frac{1}{2}\left[1\pm\sqrt{\frac{1-\varsigma_{mk}}{1-(1-2\beta_{mk})\,\varsigma_{mk}}}\right], \tag{S124}$$

$$\mathcal{P}_{mk}^\pm = \frac{\left(\kappa_{mk}^+\pm\kappa_{mk}^-\right)\mu_k^{\odot 2}}{2\left(1-\varkappa_{mk}^2\mu_k^{\odot 2}\right)}. \tag{S125}$$

To determine all vector elements $\left(x_{m(2k-1)},x_{m(2k)}\right)$; $k \in \{1,2,\ldots,N_T,N_T+1\}$ we need three independent systems of $2N_T+2$ equations (one system of equations for each spectral band). For $k \in \{1,2,\ldots,N_T\}$, the solution must meet the boundary conditions for all middle interfaces (Fig. 4), with one additional boundary condition for upward radiation coming out of the ground

(Line 1), and another for incoming downward radiation from above the canopy (Line $2N_T + 2$):

$$
\begin{array}{lll}
\text{Line 1:} & \dot{Q}^{\Uparrow}_{m1} - \varsigma_{m0}\left(\dot{Q}^{\Downarrow}_{mk} + \dot{Q}^{\odot}_{mk}\right) - (1 - \varsigma_{m0})\dot{Q}^{\blacklozenge}_{m0} = 0 & \\
\text{Line } 2k: & \dot{Q}^{\Downarrow}_{0_{mk}} - \dot{Q}^{\Downarrow}_{m(k+1)} = 0 & , k \in \{1, 2, \dots, K = N_T\} \\
\text{Line } 2k+1: & \dot{Q}^{\Uparrow}_{0_{mk}} - \dot{Q}^{\Uparrow}_{m(k+1)} = 0 & , k \in \{1, 2, \dots, K = N_T\} \\
\text{Line } 2N_T + 2: & \dot{Q}^{\Downarrow}_{0_{m(N_T+1)}} - \dot{Q}^{\Downarrow}_{m(\infty,a)} = 0 &
\end{array}
$$

$$(S126)$$

where ς_{i0} is the ground (soil and temporary surface water) scattering coefficient (Section S11), $\dot{Q}^{\blacklozenge}_{m0}$ is the ground black body emission, and $\dot{Q}^{\Downarrow}_{m(\infty,a)}$ is the above-canopy, downward diffuse radiation for the band. For the top boundary condition, it is also assumed that $\tilde{\Phi}_{N_T+1} = 0$; $\overline{\mu}_{N_T+1} = 1$; $\dot{Q}^{\blacklozenge}_{m(N_T+1)} = 0$; $\varsigma_{m(N_T+1)} = 1$ (no absorption or emission); and $\beta_{m(N_T+1)} = \beta^{\odot}_{m(N_T+1)} = 0$ (all irradiance is transmitted). Because $\varsigma_{m(N_T+1)} = 1$ creates singularities for $Đ^{\pm}_{m(N_T+1)}$, we use the limit $\varsigma_{m(N_T+1)} \to 0$, so that $Đ^{+}_{m(N_T+1)} = 1$ and $Đ^{-}_{m(N_T+1)} = 0$. Substituting Eq. (S110)-(S112) and Eq.(S122)-(S123) into Eq. (S126) yields

$$
\mathbf{S}_m \cdot \mathbf{x}_m = \mathbf{y}_m, \tag{S127}
$$

where $\mathbf{x}_m = \left(x_{m1}, x_{m2}, \dots, x_{m(2N_T+1)}, x_{m(2N_T+2)}\right)$ are the constants from Eq. (S122) and Eq. (S123); $\mathbf{S}_m$ is a $(2N_T + 2) \times (2N_T + 2)$ sparse matrix with following non-zero elements:

$$
\begin{array}{ll}
S_{m(1,1)} = \left(Đ^{-}_{m1} - \varsigma_{m0}Đ^{+}_{m1}\right)\exp\left(-\varkappa_{m1}\tilde{\Phi}_1\right) & \\
S_{m(1,2)} = \left(Đ^{+}_{m1} - \varsigma_{m0}Đ^{-}_{m1}\right)\exp\left(+\varkappa_{m1}\tilde{\Phi}_1\right) & \\
S_{m(2k,2k-1)} = Đ^{+}_{mk} & , k \in (1, 2, \dots, N_T + 1) \\
S_{m(2k,2k)} = Đ^{-}_{mk} & , k \in (1, 2, \dots, N_T + 1) \\
S_{m(2k,2k+1)} = -Đ^{+}_{m(k+1)}\exp\left(-\varkappa_{m(k+1)}\tilde{\Phi}_{m(k+1)}\right) & , k \in (1, 2, \dots, N_T) \\
S_{m(2k,2k+2)} = -Đ^{-}_{m(k+1)}\exp\left(+\varkappa_{m(k+1)}\tilde{\Phi}_{m(k+1)}\right) & , k \in (1, 2, \dots, N_T) \\
S_{m(2k+1,2k-1)} = Đ^{-}_{mk} & , k \in (1, 2, \dots, N_T + 1) \\
S_{m(2k+1,2k)} = Đ^{+}_{mk} & , k \in (1, 2, \dots, N_T + 1) \\
S_{m(2k+1,2k+1)} = -Đ^{-}_{m(k+1)}\exp\left(-\varkappa_{m(k+1)}\tilde{\Phi}_{m(k+1)}\right) & , k \in (1, 2, \dots, N_T) \\
S_{m(2k+2,2k+2)} = -Đ^{+}_{m(k+1)}\exp\left(+\varkappa_{m(k+1)}\tilde{\Phi}_{m(k+1)}\right) & , k \in (1, 2, \dots, N_T)
\end{array}
\tag{S128}
$$

and $\mathbf{y}_m = \left(y_{m1}, y_{m2}, \dots, y_{m(2N_T+1)}, y_{m(2N_T+2)}\right)$, where

$$
\begin{aligned}
y_{m1} &= \varsigma_{m0}\,\dot{Q}^{\odot}_{m1} + (1 - \varsigma_{m0})\left(\dot{Q}^{\blacklozenge}_{m0} - \dot{Q}^{\blacklozenge}_{m1}\right) - \left(P^{-}_{m1} - \varsigma_{m0}\,P^{+}_{m1}\right)\exp\left(-\frac{\tilde{\Phi}}{\mu^{\odot}_1}\right) \\
y_{m(2k)} &= P^{+}_{m(k+1)}\exp\left(-\frac{\tilde{\Phi}_{k+1}}{\mu^{\odot}_{k+1}}\right) - P^{+}_{mk} + \dot{Q}^{\blacklozenge}_{m(k+1)} - \dot{Q}^{\blacklozenge}_{mk} & ,k \in (1,2,\ldots,N_T) \\
y_{m(2k+1)} &= P^{-}_{m(k+1)}\exp\left(-\frac{\tilde{\Phi}_{k+1}}{\mu^{\odot}_{k+1}}\right) - P^{-}_{mk} + \dot{Q}^{\blacklozenge}_{m(k+1)} - \dot{Q}^{\blacklozenge}_{mk} & ,k \in (1,2,\ldots,N_T) \\
y_{m(2N_T+2)} &= \dot{Q}^{\Downarrow}_{m(\infty,a)} - P^{+}_{m(N_T+1)} - \dot{Q}^{\blacklozenge}_{m(N_T+1)}
\end{aligned}
$$

$$
\tag{S129}
$$

S13 Overview of the momentum transfer model

The momentum transfer model must first quantify two characteristic scales associated with the vertical structure of the vegetation, namely the displacement height (z_d) and the roughness length (z_0). The displacement height is defined according to Shaw and Pereira (1982) and represents the effective height of the mean drag from all cohorts and soil surface. The roughness length is defined after Raupach (1994, 1995) and represents the limit above the displacement height below which the typical logarithmic-based, surface layer wind profile is no longer valid. When the patch contains cohorts, we determine z_d and z_0 by adapting the model proposed by Massman (1997). This model is convenient because it does not assume fixed vegetation structures, therefore it can be determined and updated based on the demography of each patch. In ED-2.2, we use the discrete form of the original formulation, assuming that cohorts are dispersed uniformly in their patch space, such that the leaf and branch area indices are homogeneous in the horizontal plane for any given patch. The canopy environment is split in a fixed vertical grid with N_C layers spanning from the ground to the maximum vegetation height.

In the original formulation by Massman (1997), the displacement height is normalized by the canopy height; in ED-2.2 we apply a correction to scale the height with the effective canopy depth ($\bar{z}_c$) while accounting for the contribution from all cohorts including the tallest cohort (z_{t_1}):

$$
z_d = \bar{z}_c\left\{1 - \frac{1}{z_{t_1}}\sum_{j=1}^{N_C}\left[\exp\left(-2\,\frac{\Xi_{N_C} - \Xi_j}{\xi_{\mathrm{sfc}}}\right)\Delta z_{c_j}\right]\right\},
\tag{S130}
$$

$$
z_0 = (\bar{z}_c - z_d)\exp\left(-\kappa\sqrt{\frac{2}{\xi_{\mathrm{sfc}}}} + \tilde{\psi}_0\right),
\tag{S131}
$$

where κ is the von Kármán constant (Table S3); $\Delta z_{c_j} = z_{c_j} - z_{c_{j-1}}$ is the layer thickness ($z_{c_0} = 0$); ξ_{sfc} is the vegetated surface drag coefficient, which is related to the ratio of the wind speed at

the top cohort and the surface (Albini, 1981); Ξ_j is the cumulative cohort drag area per unit of ground area at layer j; and $\tilde{\psi}_0$ is the flux profile function of momentum at the roughness height (see Supplement S14.1), here approximated to 0.190 as in Raupach (1995).

Following Massman (1997), ξ_{sfc}, ξ_{c_j} and Ξ_{c_j} are defined as:

$$\xi_{\text{sfc}} = 2 \left[y_1 + y_2 \exp\left(y_3 \Xi_{c_{N_C}} \right) \right]^2, \tag{S132}$$

$$\Xi_{c_j} = \sum_{j'=1}^{j} \frac{\xi_{c_{j'}} \phi_{c_{j'}}}{\mathcal{P}_{c_{j'}}} \Delta z_{c_{j'}} \left(\frac{\xi_{c_{j'}}}{\mathcal{P}_{c_{j'}}} \phi_{c_{j'}} \Delta z_{c_{j'}} \right), \tag{S133}$$

$$\phi_{c_j} = \sum_{k=1}^{N_T} \left(\begin{cases} 0 & \text{, if } z_{t_k} < z_{c_{j-1}} \text{ or } z_{t_k}^- > z_{c_j} \\ \dfrac{\Phi_{t_k}}{\min\left(z_{c_j}, z_{t_k} \right) - \max\left(z_{t_k}^-, z_{c_{j-1}} \right)} & \text{, otherwise} \end{cases} \right), \tag{S134}$$

where ξ_{c_j} is the leaf-level drag coefficient due to cohorts at layer j; and $(y_1; y_2; y_3) = (0.320; 0.264; 15.1)$ are empirical constants (Massman, 1997). The sheltering factor for momentum ($\mathcal{P}_j$) accounts for the effects of adjacent leaves interfering in the viscous flow of air. The plant (leaves and wood) area density function at layer j (ϕ_j) is calculated assuming that the leaf and branch-wood area indices of individual cohorts are evenly distributed between the height of the crown bottom $z_{t_k}^-$ and the cohort height z_{t_k}, as determined by the allometric equations (see Supplement S18).

Wohlfahrt and Cernusca (2002) pointed out that the drag coefficient ξ and the shelter factor $\mathcal{P}$ are not completely separable, and provided a functional form of the combined ratio instead of describing ξ and $\mathcal{P}$ independently. The function used in ED-2.2 is an adaptation of the original fit as a function of plant area density function (Wohlfahrt and Cernusca, 2002), using a logistic function to reduce the number of parameters (Fig. S7):

$$\frac{\xi_{c_j}}{\mathcal{P}_{c_j}} = y_4 + \frac{y_5}{1 + \exp\left(y_6 \, \phi_{c_j} \right)}, \tag{S135}$$

where $(y_4; y_5; y_6) = (0.086; 1.192; 0.480)$.

In case no above-ground vegetation exists (i.e. a patch with no cohorts), we assume that the roughness height $z_{0\varnothing}$ is the bare soil roughness z_{0g} plus any snow or water standing on top of the ground z_{0s}:

$$z_{0\varnothing} = z_{0g} \left(1 - f_{\text{TSW}} \right) + z_{0s} f_{\text{TSW}}; \tag{S136}$$

the default values of z_{0g} and z_{0s} are available in Table S4.

S14 Derivation of conductances

S14.1 Canopy air space conductance

To obtain the conductance at the top of the canopy air space, we solve the surface layer model that is based on the Monin-Obukhov similarity theory (Monin and Obukhov, 1954; Foken, 2006). First, we define the momentum ($\dot{U}_{a,c}$) and buoyancy ($\dot{\Theta}_{a,c}$) fluxes between the free atmosphere and the canopy air space at the top of the canopy air space. Following (Monteith and Unsworth, 2008), these fluxes can be represented either by the gradient or the eddy flux form:

$$\dot{U}_{a,c} = \rho_c K_U \frac{\partial u}{\partial z} = \rho_c \overline{u'_z u'_{\mathbf{x}}}, \tag{S137}$$

$$\dot{\Theta}_{a,c} = -\rho_c K_\Theta q_{p_c} \frac{\partial \theta_\mathcal{V}}{\partial z} = -\rho_c q_{p_c} \overline{u'_z \theta'_\mathcal{V}}, \tag{S138}$$

where K_U and K_Θ are the eddy diffusivities of momentum and buoyancy, respectively; $u_{\mathbf{x}}$ is the horizontal wind speed, u_z is the vertical velocity; $\theta_\mathcal{V}$ is the virtual potential temperature; and q_{p_c} is the specific heat of the canopy air space (Supplement S6.3). The eddy diffusivities of enthalpy, moisture and CO_2 are assumed to be the same as the buoyancy, a common assumption based on observations (Stull, 1988).

The Monin-Obukhov similarity theory is based on the Buckingham's Π-theory (Stull, 1988), which requires as many fundamental scales as fundamental dimensions. The fundamental dimensions are the canopy air density (ρ_c) and three characteristic scales, namely the friction velocity ($u^\star$), characteristic virtual temperature gradient ($\theta_\mathcal{V}^\star$), and the diffusivity-corrected Obukhov length $\mathcal{L}$ (Panofsky, 1963):

$$u^\star = \sqrt{\frac{\dot{U}_{a,c}}{\rho}} = \sqrt{\left|\overline{u'_{\mathbf{x}} u'_z}\right|}, \tag{S139}$$

$$\theta_\mathcal{V}^\star = -\frac{1}{\kappa u^\star} \frac{\dot{\Theta}_{a,c}}{\rho\, q_{p_c}} = -\frac{\overline{u'_z \theta'_\mathcal{V}}}{u^\star}, \tag{S140}$$

$$\mathcal{L} = \frac{1}{\mathrm{Pr}} \frac{\dot{U}_{a,c}}{\dot{\Theta}_{a,c}} \frac{\theta_{\mathcal{V}_0}}{g} \frac{u^\star}{\kappa} \approx \frac{(\theta_{\mathcal{V}_a} + \theta_{\mathcal{V}_c})\, u^{\star 2}}{2\,\kappa\, g\, \theta_\mathcal{V}^\star}, \tag{S141}$$

where κ is the von Kármán constant, g is the gravity acceleration, and $\mathrm{Pr} \equiv K_U/K_\Theta$ is the turbulent Prandtl number (Table S3-S4). Another important dimensionless quantity is the bulk Richardson number Ri_B, defined as:

$$\mathrm{Ri}_B = \frac{2\,g\,(z^{\star} - z_0)\,(\theta_{\mathcal{V}_a} - \theta_{\mathcal{V}_c})}{(\theta_{\mathcal{V}_a} + \theta_{\mathcal{V}_c})\,u_a^2}, \tag{S142}$$

where $z^{\star} \equiv z_a - z_d$, z_a is the reference height, z_d is the displacement height, and z_0 is the roughness scale; both z_d and z_0 are determined by the momentum transfer model based on Massman (1997) (Supplement S13). The bulk Richardson number is informative on whether the layer between the canopy air space and the reference height z_a is unstable, neutral, or stable.

To determine the three remaining unknowns ($u^{\star}; \theta_{\mathcal{V}}^{\star}; \mathcal{L}$), we start from the general definition of dimensionless length scale ζ and two particular cases:

$$\zeta(z) = \frac{z - z_d}{\mathcal{L}}, \tag{S143}$$

$$\zeta^{\star} = \frac{z^{\star}}{\mathcal{L}} = \zeta_0 + \kappa \mathrm{Ri}_B \left(\frac{u_a}{u^{\star}}\right)^2 \frac{\theta_{\mathcal{V}}^{\star}}{\theta_{\mathcal{V}_a} - \theta_{\mathcal{V}_c}}, \tag{S144}$$

$$\zeta_0 = \frac{z_0}{\mathcal{L}} = \frac{z_0}{z^{\star}} \zeta^{\star}, \tag{S145}$$

where $z^{\star} = z_a - z_d$, where z_a (m) is the reference height above canopy, typically the height where the meteorological forcing measurements would be located in an eddy covariance tower; z_d is the displacement height (Eq. S130); z_0 (m) is the roughness length (Eq. S131); κ is the von Kármán constant (Table S3), Ri_B is the bulk Richardson number (Eq. S142); u_a is the wind speed at the reference height z_a; and $\theta_{\mathcal{V}_a}$ and $\theta_{\mathcal{V}_c}$ are the virtual temperature at the reference height and the canopy air space, respectively.

By choosing an appropriate combination of factors, Monin and Obukhov (1954) have shown that the dimensionless gradients of wind and temperature (here based on virtual potential temperature and the accounting for the Prandtl number) can be written as a function of the characteristic scales and dimensionless stability functions for momentum (φ_U) and heat (φ_Θ), which can be thought as correction factors for the logarithmic wind profile under non-neutral conditions (Monteith and Unsworth, 2008):

$$\frac{\partial}{\partial \zeta} \left(\frac{u_{\mathbf{x}}}{u^{\star}}\right) = \frac{1}{\kappa \zeta} \varphi_U(\zeta), \tag{S146}$$

$$\frac{\partial}{\partial \zeta} \left(\frac{\theta_{\mathcal{V}}}{\theta_{\mathcal{V}}^{\star}}\right) = \frac{\mathrm{Pr}}{\kappa \zeta} \varphi_\Theta(\zeta). \tag{S147}$$

Following Panofsky (1963), if we define the flux profile functions for momentum (ψ_U) and heat (ψ_Θ):

$$\psi_U(\zeta) = \int_0^\zeta \frac{1 - \varphi_U(\zeta')}{\zeta'} \, d\zeta', \tag{S148}$$

$$\psi_\Theta(\zeta) = \int_0^\zeta \frac{1 - \varphi_\Theta(\zeta')}{\zeta'} \, d\zeta', \tag{S149}$$

and integrate Eq. (S146)-(S147) between ζ_0, where wind is assumed to be zero, and any reference level ζ using the Leibniz integration rule, we obtain the horizontal wind and virtual potential temperature profile functions:

$$u_\mathbf{x}(\zeta) = \frac{u^\star}{\kappa} \left[\ln\left(\frac{\zeta}{\zeta_0}\right) - \psi_U(\zeta) + \psi_U(\zeta_0) \right], \tag{S150}$$

$$\theta_\mathcal{V}(\zeta) = \theta_{\mathcal{V}_c} + \frac{\mathrm{Pr}\,\theta_\mathcal{V}^\star}{\kappa} \left[\ln\left(\frac{\zeta}{\zeta_0}\right) - \psi_\Theta(\zeta) + \psi_\Theta(\zeta_0) \right]. \tag{S151}$$

If we substitute Eq. (S150)-(S151) for the specific case when $\zeta = \zeta^\star$ into Eq. (S144), we obtain an equation where the only unknown is $\zeta^\star$:

$$\zeta^\star = \frac{\mathrm{Ri}_B}{\mathrm{Pr}} \left(\frac{z^\star}{z^\star - z_0}\right) \frac{\left[\ln\left(\frac{\zeta^\star}{\zeta_0}\right) - \psi_U(\zeta^\star) + \psi_U(\zeta_0) \right]^2}{\ln\left(\frac{\zeta^\star}{\zeta_0}\right) - \psi_\Theta(\zeta^\star) + /\!\!/ \, \psi_\Theta(\zeta_0)}. \tag{S152}$$

The ED-2.2 model uses the empirical parameterization of the originally developed by Beljaars and Holtslag (1991). For the unstable cases, Beljaars and Holtslag (1991) used the Businger-Dyer flux profile equations (Businger et al., 1971). For the stable cases, Beljaars and Holtslag (1991) implemented an empirical formulation that improved the vertical mixing between the canopy air space and the air above under stable conditions:

$$\psi_U(\zeta) = \begin{cases} 2\ln\left[\frac{1+Y(\zeta)}{2}\right] + \ln\left[\frac{1+Y^2(\zeta)}{2}\right] - 2\arctan\left[Y(\zeta)\right] + \frac{\pi}{2} & \text{, if } \mathrm{Ri}_B < 0 \\ y_1\zeta + y_2\left(\zeta - \frac{y_3}{y_4}\right)\exp(-y_4\zeta) + \frac{y_2 y_3}{y_4} & \text{, if } \mathrm{Ri}_B \geq 0 \end{cases}, \tag{S153}$$

$$\psi_\Theta(\zeta) = \begin{cases} 2\ln\left[\frac{1+Y^2(\zeta)}{2}\right] & \text{, if } \mathrm{Ri}_B < 0 \\ 1 - \left(1 - \frac{y_1}{y_5}\zeta\right)^{y_5} + x_2\left(\zeta - \frac{y_3}{y_4}\right)\exp(-y_4\zeta) + \frac{y_2 y_3}{y_4} & \text{, if } \mathrm{Ri}_B \geq 0 \end{cases}, \tag{S154}$$

$$Y(\zeta) = \sqrt[4]{1 - y_6\zeta}, \tag{S155}$$

where $\mathbf{y} = \left(-1; -\frac{2}{3}; 5; 0.35; \frac{3}{2}; 13\right)$ are empirical and adjustable parameters. Equation (S152)

cannot be solved analytically, therefore $\zeta^\star$ is calculated using a root-finding technique. Once $\zeta^\star$ is determined, we can find $u^\star$ using Eq. (S150), and define the canopy conductance G_c (m s^{-1}) using Eq. (S151) as the starting point, similarly to Oleson et al. (2013):

$$G_c = \frac{u^\star \theta_{\mathcal{V}}^\star}{\theta_{\mathcal{V}_a} - \theta_{\mathcal{V}_c}} = \frac{\kappa u^\star}{\Pr\left[\ln\left(\frac{\zeta^\star}{\zeta_0}\right) - \psi_\Theta(\zeta^\star) + \psi_\Theta(\zeta_0)\right]}. \tag{S156}$$

S14.2   Derivation leaf and wood boundary layer conductances

Following Monteith and Unsworth (2008), convection can be of two types: forced convection, which depends on mechanic mixing associated with the fluid velocity; and free convection, which is due to buoyancy of the boundary layer fluid. Although convection is often dominated by either forced or free convection, in ED-2.2 we always assume that the total conductance is a simple combination of forced and free convection conductances as if they were parallel:

$$G_{Qx_k} = G_{Qx_k}^{\text{Free}} + G_{Qx_k}^{\text{Forced}}, \tag{S157}$$

where x_k can be either the leaf (λ_k) or the branch wood (β_k) boundary layer. For each convective regime, we define the conductance in terms of the Nusselt number Nu, a dimensionless number that corresponds to the ratio between heat exchange through convection and conduction:

$$G_{Qx_k} = \frac{\eta_c \, \text{Nu}}{x^\star}. \tag{S158}$$

where η_c is the thermal diffusivity of canopy air space and $x^\star$ is the characteristic size of the obstacle. For leaves, the characteristic size $x_{\lambda_k}^\star$ is a PFT-dependent constant corresponding to the typical leaf width , whereas for branch wood the typical size $x_{\beta_k}^\star$ is assumed to be the typical diameter of twigs (Tables S5-S6).

Free convection is a result of the thermal gradient between the obstacle surface and the fluid, and this is normally expressed in terms of the Grashof number Gr, a dimensionless index that relates buoyancy and viscous forces. In ED-2.2 we use the same empirical functions as Monteith and Unsworth (2008), using flat plate geometry for leaves and horizontal cylinder geometry for branch wood:

$$\text{Nu}_{\lambda_k}^{(\text{Free})} = \max\left[\underbrace{0.50\,\text{Gr}_{\lambda_k}^{\frac{1}{2}}}_{\text{Laminar}}, \underbrace{0.13\,\text{Gr}_{\lambda_k}^{\frac{1}{3}}}_{\text{Turbulent}}\right], \tag{S159}$$

$$\text{Nu}_{\beta_k}^{(\text{Free})} = \max\left[\underbrace{0.48\,\text{Gr}_{\beta_k}^{\frac{1}{2}}}_{\text{Laminar}}, \underbrace{0.09\,\text{Gr}_{\beta_k}^{\frac{1}{3}}}_{\text{Turbulent}}\right], \tag{S160}$$

$$\text{Gr}_{x_k} = \frac{\varepsilon_c\,g\,\left(x_{x_k}^{\star}\right)^3}{v_c^2}\,\left|T_{x_k} - T_c\right|, \tag{S161}$$

where ε_c is the thermal dilatation coefficient for the canopy air space and v_c is the kinematic viscosity of the canopy air space; x_k represents either the leaf (λ_k) or wood (β_k) surface; and g is the gravity acceleration. Like in Monteith and Unsworth (2008), thermal diffusivity and dynamic viscosity (both in $\text{m}^2\,\text{s}^{-1}$) are assumed to be linear functions of the canopy air space temperature:

$$\eta_c = 1.89 \cdot 10^{-5}\left[1 + 0.007\left(T_c - T_0\right)\right], \tag{S162}$$

$$v_c = 1.33 \cdot 10^{-5}\left[1 + 0.007\left(T_c - T_0\right)\right], \tag{S163}$$

where the first term on the right hand side are the reference values at temperature $T_0 = 273.15\,\text{K}$. Under the assumption that canopy air space is a perfect gas, thermal dilatation is $\varepsilon_c = T_c^{-1}$ (Dufour and van Mieghem, 1975).

For forced convection the flow of air through the object at different temperature causes the heat exchange, therefore Nusselt number is written as a function of the Reynolds number Re, a dimensionless index that relates inertial and viscous forces. Like in the free convection case, we use the same empirical functions as Monteith and Unsworth (2008) and the same shapes as the free convection case:

$$\text{Nu}_{\lambda_k}^{(\text{Forced})} = \max\left[\underbrace{0.60\,\text{Re}_{\lambda_k}^{0.5}}_{\text{Laminar}}, \underbrace{0.032\,\text{Re}_{\lambda_k}^{0.8}}_{\text{Turbulent}}\right], \tag{S164}$$

$$\text{Nu}_{\beta_k}^{(\text{Forced})} = \max\left[\underbrace{0.32 + 0.51\,\text{Re}_{\beta_k}^{0.52}}_{\text{Laminar}}, \underbrace{0.24\,\text{Re}_{\beta_k}^{0.60}}_{\text{Turbulent}}\right], \tag{S165}$$

$$\text{Re}_{x_k} = \frac{u_{t_k}\,x_{x_k}^{\star}}{\eta_c}, \tag{S166}$$

where u_{t_k} is the wind speed experienced by the cohort k, and x_k represents either the leaf (λ_k) or wood (β_k) surface.

The wind profile within the canopy air space is determined in two steps. Above the tallest cohort, we assume that the wind can be determined from the similarity theory; from Eq. (S143) we define $\zeta_{c_j} = \zeta\left(z_{c_j}\right)$, and use wind profile function from the similarity theory (Eq. S150) to determine the wind speed at the top of the vegetated layer $u_{c_{N_C}} = u\left(\zeta_{c_{N_C}}\right)$. Within the canopy, we estimate the wind speed reduction using the wind profile as a function of cumulative drag (Ξ_j; Albini, 1981; Massman, 1997); the wind speed experienced by the cohort is the average wind between the layers where the bottom ($\hat{z}_{t_k}$) and top (z_{t_k}) of the crown are located:

$$u_{c_j} = u_{c_{N_C}} \exp\left(-\frac{\Xi_{c_{N_C}} - \Xi_{c_j}}{\xi_{\text{sfc}}}\right) \tag{S167}$$

$$u_{t_k} = \max\left[0.25\,\text{m}\,\text{s}^{-1}, \frac{u_{c_{N_C}}}{z_{c_j(k)} - z_{c_{\hat{j}}(k)}} \sum_{j'=\hat{j}(k)}^{j(k)} \left(u_{c_{j'}} \Delta z_{c_{j'}}\right)\right], \tag{S168}$$

where $c_{\hat{j}(k)}$ and $c_j(k)$ are the canopy air space layers corresponding to the bottom and top of the cohort's crown. The minimum wind speed of $0.25\,\text{m}\,\text{s}^{-1}$ is imposed to avoid conductance to become unrealistically low and to account for some mixing due to gusts when the mean wind is very weak. Once the heat conductance is determined, we use the same vapor to heat ratio as Leuning et al. (1995) to calculate the water vapor conductance:

$$G_{Wx_k} = 1.075\,G_{Qx_k}, \tag{S169}$$

where x_k represents either the leaf (λ_k) or wood (β_k) surface. Similarly, we define the CO_2 boundary layer conductance for leaves using the ratio of diffusivities and convection between water and CO_2 ($f_{G\lambda}$, Table S4), following Cowan and Troughton (1971):

$$\hat{G}_{W\lambda_k} = f_{G\lambda}\,\hat{G}_{C\lambda_k}. \tag{S170}$$

S14.3   Derivation of surface conductance

The total resistance between the surface and the canopy air space is a combination of the air resistance if the surface were bare, and the resistance due to the presence of the vegetated canopy, assuming that these resistances are serial and thus additive (as mentioned by Walko et al., 2000); using that conductance is the inverse of resistance:

$$\frac{1}{G_{\text{Sfc}}} = \frac{1}{G_{\text{Bare}}} + \frac{1}{G_{\text{Veg}}}, \tag{S171}$$

where G_{Sfc} is the total surface conductance, G_{Bare} is the bare-ground equivalent conductance, and G_{Veg} is the conductance associated with vegetation presence. The bare ground conductance G_{Bare} can be approximated to be G_c (Eq. S156; see also Sellers et al., 1996). Two methods have been implemented conductance due to vegetation presence, one based on the Simple Biosphere Model (SiB-2, Sellers et al., 1996) ($G_{\text{Veg}}^{\text{SiB}}$), and one based on Massman and Weil (1999) ($G_{\text{Veg}}^{\text{MW99}}$), which incorporates the second-order closure method that accounts for the amount of shear in the sub-layer above the canopy and the geometric attributes that define the drag of air. Results in the main text used the SiB-2 based vegetation conductance.

S14.3.1 SiB-2 based vegetation conductance

In the SiB-2 based approach, we assume that the total resistance due to vegetation presence (inverse of conductance G_{Veg}) is equivalent to the total contribution of diffusivity from ground to the top of vegetated layer:

$$\frac{1}{G_{\text{Veg}}^{\text{SiB}}} = \int_{z_{0\varnothing}}^{z_{t_k}} \frac{1}{K_\Theta(z)} \mathrm{d}z \approx \sum_{j=1}^{N_C} \frac{\text{Pr}}{K_{U_{c_j}}} \Delta z_{c_j}, \tag{S172}$$

$$z_{0\varnothing} = z_{0s} f_{\text{TSW}} + z_{0g}(1 - f_{\text{TSW}}), \tag{S173}$$

where $j = 1, 2, \ldots, N_C$ are the discrete vertical layers used to describe the canopy air space, Δz_{c_j} is the thickness of canopy air space layer j, the index $z_{0\varnothing}$ is combined contribution to roughness from the temporary surface water (z_{0s}) and bare-ground (z_{0g}), f_{TSW} is the fraction of ground covered by temporary surface water, K_Θ is the eddy diffusivity for heat, $K_{U_{c_j}}$ is the eddy diffusivity for momentum of canopy air space layer j, $\text{Pr} = K_U K_\Theta^{-1}$ is the Prandtl number (Table S4; Businger et al., 1971). We further assume that $K_{U_{c_j}}$ is proportional to u_{c_j}, the horizontal wind speed at canopy air space layer j, and that Y_U is the scaling factor, i.e. $K_{U_{c_j}} \equiv Y_U u_{\mathbf{x}}$ (Sellers et al., 1986), and that within the vegetated layer the winds are determined through Eq. (S167). Therefore, Eq. (S172) becomes

$$\frac{1}{G_{\text{Veg}}^{\text{SiB}}} = \sum_{j=1}^{N_C} \left[\frac{\text{Pr}}{Y_U u_{c_j}} \exp\left(\frac{\Xi_{c_{N_C}} - \Xi_{c_j}}{\xi_{\text{Sfc}}} \right) \right], \tag{S174}$$

where ξ_{Sfc} is the drag coefficient of vegetated surfaces (Eq. S132) and Ξ_{c_j} is the cumulative cohort

drag area per unit of ground area at layer j (Eq. S133). If we assume that Y_U is constant and the wind profile is continuous, and combine Eq. (S137), Eq. (S139), Eq. (S146), and Eq. (S148) at the dimensionless length scale $\zeta(z_{c_{N_C}}) = \zeta_{c_{N_C}}$ (Eq. S143), Y_U can be estimated as:

$$Y_U = \frac{\kappa u^\star (z_{t_1} - z_d)}{u_{c_{N_C}}} \frac{1}{1 - \zeta_{c_{N_C}} \frac{\partial \psi_U}{\partial \zeta}(\zeta_{c_{N_C}})}. \tag{S175}$$

S14.3.2 Second Order Closure of Turbulent Transport from the Surface to Canopy

The method of Massman and Weil (1999) is a second-order closure method that derives $G_{\text{Veg}}^{\text{MW99}}$ from the shear in the sub-layer above the canopy and the geometric attributes of the canopy that define the drag of fluid. Massman and Weil (1999) base their method on some key simplifications to the the turbulent kinetic energy (TKE) budget equation: (1) no horizontal variability exists within any given patch (horizontal homogeneity); (2) the turbulent flow has proportional isotropy, i.e., the variance in each of the three wind directions is proportional to TKE.

$$\text{TKE} = \frac{1}{2}\left[\underbrace{\sigma_{u_x}^2 + \sigma_{u_y}^2}_{\sigma_{u_\mathbf{x}}^2} + \sigma_{u_z}^2 \right], \tag{S176}$$

$$\sigma_{u_\mathbf{x}}^2 = \overline{u'_\mathbf{x} u'_\mathbf{x}}, \tag{S177}$$

$$\sigma_{u_z}^2 = \overline{u'_z u'_z}, \tag{S178}$$

where $u_\mathbf{x} = \sqrt{u_x^2 + u_y^2}$ is the horizontal wind along the direction of the mean wind, and $u'_?$ is the departure from the mean wind in any of the wind directions. With the horizontal homogeneity and proportional isotropy assumptions, it is possible to derive an analytical solution to the TKE budget, and ultimately obtain an analytical solution for the vertical profile of standard deviation of wind speed (Eq. 10 of Massman and Weil, 1999):

$$\sigma_{u_k}(z_{c_j}) = \mathcal{S}_{u_k} y u^\star \left\{ Y_1 \exp\left[-\frac{3\left(\Xi_{c_{N_C}} - \Xi_{c_j}\right)}{\xi_{\text{Sfc}}} \right] + Y_2 \exp\left[-\frac{\sqrt{3} y \left(\Xi_{c_{N_C}} - \Xi_{c_j}\right)}{\beta} \right] \right\}^{\frac{1}{3}}, \tag{S179}$$

$$y = \left(\mathcal{S}_x^2 + \mathcal{S}_y^2 + \mathcal{S}_z^2\right)^{-\frac{1}{2}}, \tag{S180}$$

$$Y_1 = -\frac{3\beta \left(2\xi_{\text{Sfc}}\right)^{\frac{1}{2}}}{3\beta^2 y - y^3 \xi_{\text{Sfc}}^2}, \tag{S181}$$

$$Y_2 = \frac{1}{y^3} - Y_1, \tag{S182}$$

where Ξ_c is the cumulative drag profile (Eq. S133); ξ_{Sfc} is the vegetated surface drag coefficient (Eq. S132); and $\left(\mathcal{S}_{u_x}; \mathcal{S}_{u_y}; \mathcal{S}_{u_z}\right) = (2.40; 1.90; 1.25)$ are adjustable parameters that represent the ratio between above-canopy velocity variance and the momentum flux, taken from Raupach et al. (1991) as in Massman and Weil (1999); and the u_k subscript represents one of the wind directions (u_x, u_y, or u_z). In addition, the empirical β represents a joint eddy mixing length scale for both shear- and wake-driven turbulence. A sensitivity study of β using the ED-2.2 model implementation found that this parameter should be between 0.01 and 0.03 (Knox, 2012) to ensure that the turbulence intensity ($\iota_U = \sigma_{u_z}/u_{\mathbf{x}}$) is stable over the canopy depth as it approaches the soil surface. These values of β are also similar to the value of 0.05 found by Massman and Weil (1999). Depending on the the magnitude of ξ_{Sfc} and the choice of β, it is possible that Eq. (S179) yields negative (non-physical) values of σ_{u_k}; to avoid unrealistic solutions, β is dynamically set in ED-2.2. The model assigns an initial guess of $\beta = 0.03$ and, in case the solution is non-physical, it iteratively reduces the parameter until $\sigma_{\overline{u_z}}\sigma_{u_k}$ becomes positive.

Similar to the heat conductance between leaves, branches and the canopy air space (Section S14.2), the conductance between ground and canopy air space is related to the Nusselt number (Nu), following Eq. (S158). To account for the effects of both free (buoyant) convection and forced (mechanic) convection, the Nusselt number is parameterized as a function of the Reynolds (Re) and the Prandtl (Pr) numbers, with an additional modification to account for turbulence intensity (ι_U) (Sauer and Norman, 1995; Massman and Weil, 1999). To ensure that the conductance encompasses the entire canopy air space, we use the average turbulence intensity ($\overline{\iota_U}$) between the soil surface and the canopy air space depth (z_c):

$$\overline{\iota_U} = \frac{1}{z_c} \sum_{j=1}^{N_C} \frac{\sigma_{u_z}\left(z_{c_j}\right)}{u_{\mathbf{x}}\left(z_{c_j}\right)} \Delta z_{c_j}, \tag{S183}$$

$$G_{\mathrm{Veg}}^{\mathrm{MW99}} = z_0^{1/2}\left(1 + 2\,\overline{\iota_U}\right) \frac{\eta_c}{x_{\mathrm{Veg}}^{\star}} \mathrm{Re}^{b_1} \mathrm{Pr}^{b_2}\, u_{\mathbf{x}}(z_{t_1}) \sqrt{\frac{u_{\mathbf{x}}\left(z_0\right)}{u_{\mathbf{x}}\left(z_{t_1}\right)}}. \tag{S184}$$

where $(b_1; b_2) = (-1/2; -2/3)$ (Sauer and Norman, 1995); and $x_{\mathrm{Veg}}^{\star}$ is the mixing length scale for vegetated surface, and z_0 is the roughness length scale (Eq. S131).

S15   Phase equilibrium (saturation) of water vapor

The partial pressure of water vapor at phase equilibrium (p_{Sat}) is solely a function of temperature, following the Clapeyron equation (Dufour and van Mieghem, 1975; Murphy and Koop,

[2005]). Whether the phase equilibrium of water vapor refers to ice-vapor ($p_{vi}^{\equiv}$) or liquid-vapor ($p_{v\ell}^{\equiv}$) transitions also depends on the temperature, and in ED-2.2, we use the law of minimum:

$$p_{\text{Sat}}(T) = \min\left[p_{vi}(T), p_{v\ell}(T)\right]. \tag{S185}$$

Both p_{vi} and $p_{v\ell}$ are defined after the parameterization by (Murphy and Koop, 2005), which have high degree of accuracy ($< 0.05\%$) between 123 K and 332 K, and thus includes all the range of near-surface temperatures solved by ED-2.2:

$$p_{vi}(T) = \exp\left[9.550426 - \frac{5723.265}{T} + 3.53068\ln(T) - 0.00728332\,T\right], \tag{S186}$$

$$p_{v\ell}(T) = \exp\left\{Y_1(T) + Y_2(T)\tanh\left[0.0415\,(T - 218.8)\right]\right\}, \tag{S187}$$

$$Y_1(T) = 54.842763 - \frac{6763.22}{T} - 4.210\ln(T) + 0.000367\,T, \tag{S188}$$

$$Y_2(T) = 53.878 - \frac{1331.22}{T} - 9.44523\ln(T) + 0.014025\,T. \tag{S189}$$

Importantly, Eq. (S186) and Eq. (S187) yield the same value (within $4.1 \cdot 10^{-6}\%$ accuracy) at the water's triple point, which guarantees continuity of Eq. (S185).

The saturation specific humidity $w^{\equiv}$ is obtained using Eq. (S185) and the definition of specific humidity:

$$w_{\text{Sat}}(T, p) = \frac{\mathcal{M}_w\, p_{\text{Sat}}(T)}{\mathcal{M}_d\left[p - p_{\text{Sat}}(T)\right] + \mathcal{M}_w\, p_{\text{Sat}}(T)}, \tag{S190}$$

where $\mathcal{M}_d$ and $\mathcal{M}_w$ are the molar masses of dry air and water, respectively (Tab S3).

S16   Solver for the CO_2 assimilation rates and transpiration

Variables w_{l_k}, $\dot{V}_{C_k}^{\max}$, $\dot{R}_k$, ϖ_k, $\mathcal{K}_{O_k}$, $\mathcal{K}_{C_k}$, Γ_k, and $\mathcal{K}_{\text{ME}_k}$ are functions of leaf temperature and canopy air space pressure, and thus can be determined directly. In constrast, nine variables are unknown for each limitation case as well as for the case when the stomata are closed: $\dot{E}_k$, $\dot{A}_k$, $\dot{V}_{C_k}$, $\dot{V}_{O_k}$, c_{l_k}, c_{λ_k}, w_{λ_k}, $\hat{G}_{Wl_k}$, and $\hat{G}_{Cl_k}$. To solve the remaining unknowns, we first substitute Eq. (82) and either Eq. (85), Eq. (87) or Eq. (89) into Eq. (81) and write a general functional form for $\dot{A}_k$, similarly to Medvigy (2006), that is a function of only one unknown, c_{l_k}:

$$\dot{A}_k\left(c_{l_k}\right) = \frac{F_k^{\text{A}}\,c_{l_k} + F_k^{\text{B}}}{F_k^{\text{C}}\,c_{l_k} + F_k^{\text{D}}} - \dot{R}_k, \tag{S191}$$

where parameters F depend on the limitation and the photosynthetic pathway, as shown in Table S9.

We then combine Eq. (76) and Eq. (S170) to eliminate $\hat{G}_{Cl_k}$ and c_{λ_k}, and write an alternative equation for $\hat{G}_{Wl_k}$:

$$\hat{G}_{Wl_k} = \frac{f_{Gl}\,\hat{G}_{W\lambda_k}\,\dot{A}_k}{\hat{G}_{W\lambda_k}\left(c_c - c_{l_k}\right) - f_{G\lambda}\,\dot{A}_k}. \tag{S192}$$

To eliminate c_{λ_k} and w_{λ_k} from Eq. (91), we use Eq. (76) and Eq. (77). Then, we eliminate $\hat{G}_{Wl_k}$ by replacing the left hand side of Eq. (91) by the alternative Eq. (S192), yielding to the following function $\mathcal{F}(c_{l_k})$ for which we seek the solution $\mathcal{F}(c_{l_k}) = 0$:

$$\mathcal{F}(c_{l_k}) = \mathcal{F}_1(c_{l_k})\,\mathcal{F}_2(c_{l_k})\,\mathcal{F}_3(c_{l_k}) - 1, \tag{S193}$$

$$\mathcal{F}_1(c_{l_k}) = \frac{\left(f_{Gl} - f_{G\lambda}\,\dfrac{\hat{G}_{Wl_k}^{\varnothing}}{\hat{G}_{W\lambda_k}}\right)\dot{A}_k - \hat{G}_{Wl_k}^{\varnothing}\left(c_c - c_{l_k}\right)}{m_k\,\dot{A}_k}, \tag{S194}$$

$$\mathcal{F}_2(c_{l_k}) = \frac{\hat{G}_{W\lambda_k}\left(c_c - \Gamma_k\right) - f_{G\lambda}\,\dot{A}_k}{\hat{G}_{W\lambda_k}\left(c_c - c_{l_k}\right) + \left(f_{Gl} - f_{G\lambda}\right)\dot{A}_k}, \tag{S195}$$

$$\mathcal{F}_3(c_{l_k}) = 1 + \frac{w_c - w_{l_k}}{\Delta w_k}\,\frac{\hat{G}_{W\lambda_k}\left(c_c - c_{l_k}\right) - f_{G\lambda}\,\dot{A}_k}{\hat{G}_{W\lambda_k}\left(c_c - c_{l_k}\right) + \left(f_{Gl} - f_{G\lambda}\right)\dot{A}_k}. \tag{S196}$$

For the limitation cases in which Eq. (S191) does not depend on c_{l_k}, Eq. (S193) is reduced to a quadratic equation. For the other cases, Eq. (S193) becomes a fifth-order polynomial, which cannot be solved algebraically. Nevertheless, Eq. (S193) is still convenient because it highlights the range of plausible solutions, corresponding to the singularities associated with $\mathcal{F}_1$ and $\mathcal{F}_2$ — the singularities associated with $\mathcal{F}_3$ requires c_{l_k} to exceed c_c, which could be only achieved with negative $\hat{G}_{l_k w}$ or $\dot{A}_k < -\dot{M}_k$, and none of them are meaningful. Function $\mathcal{F}_1$ is singular when $\dot{A}_k = 0$; from Eq. (S192), this would require $\hat{G}_{Wl_k}$ to be 0, unless $c_{l_k} = c_c$. Function $\mathcal{F}_2$ is singular when $\dot{A}_k = \hat{G}_{C\lambda_k}\left(c_c - c_{l_k}\right)$; from Eq. (S192), this happens only when $c_{l_k} = c_c$ or at $\lim_{\hat{G}_{Wl_k}\to\infty}$. The singularities for when $c_c \neq c_{l_k}$ are obtained by substituting Eq. (S191) into Eq. (76), and by taking the $\lim_{\hat{G}_{Wl_k}\to 0}\left(\dot{A}_k\right)$ and $\lim_{\hat{G}_{Wl_k}\to\infty}\left(\dot{A}_k\right)$:

$$c_{l_k}^{\min} + \frac{F_k^{\mathrm{D}} \dot{M}_k - F_k^{\mathrm{B}}}{F_k^{\mathrm{C}} \dot{M}_k - F_k^{\mathrm{A}}} = 0, \tag{S197}$$

$$\left(c_{l_k}^{\max}\right)^2 + \frac{\hat{G}_{C\lambda_k} F_k^{\mathrm{D}} + F_k^{\mathrm{B}} - F_k^{\mathrm{C}}\left(\hat{G}_{C\lambda_k} c_c + \dot{M}_k\right)}{\hat{G}_{C\lambda_k} F_k^{\mathrm{C}}} c_{l_k}^{\max} + \frac{F_k^{\mathrm{B}} - F_k^{\mathrm{D}}\left(\hat{G}_{C\lambda_k} c_c + \dot{M}_k\right)}{\hat{G}_{C\lambda_k} F_k^{\mathrm{C}}} = 0. \tag{S198}$$

From Eq. (S198) up to two roots are possible, but normally only one is plausible. In case both values are greater than c_c, we use c_c as the upper boundary, because c_c is also a singularity; otherwise the root between $c_{l_k}^{\min}$ and c_c is selected. If none of them are in this range, then there is no viable solution for this limitation, and we assume that the stomata must be closed. Once the boundaries are defined, we seek the solution in the $\left]c_{l_k}^{\min}; c_{l_k}^{\max}\right[$ interval, where there is only one possible solution, as illustrated in Fig. S8.

Once all cases are determined, the solution is determined by a law of minimum (Collatz et al., 1991, 1992; Moorcroft et al., 2001):

$$\dot{A}_k = \min\left(\dot{A}_k^{\mathrm{RuBP}}, \dot{A}_k^{\mathrm{InSL}}, \dot{A}_k^{\mathrm{PAR}}\right), \tag{S199}$$

$$\dot{E}_k = \dot{E}_k^{L\star}, \tag{S200}$$

where $L\star$ is the limiting case chosen in Eq. (S199). When available light or c_{l_k} is near or below their compensation point, it is possible that none of the limiting cases yields a viable solution. In this case, we assume that photosynthesis cannot occur and that stomata are closed.

S17   Soil moisture limitation on photosynthesis

The stomatal conductance equation by Leuning (1995) was developed using well-watered seedlings, therefore it does not consider soil moisture limitation, which can be important in seasonally dry ecosystems. To account for soil water stress, we define a phenomenological scaling function $f_{W l_k}$ (wilting factor). The functional form of $f_{W l_k}$ follows the previous versions of ED (Moorcroft et al., 2001; Medvigy et al., 2009). However, in ED-2.2 we define water availability ($W_{g_j}^\star$) in terms of soil matric potential, similarly to CLM (Oleson et al., 2013), which produces a more gradual transition from no-stress conditions to completely closed stomata as soil moisture approaches the wilting point (Fig. S9).

In ED-2.2, the wilting factor $f_{W l_k}$ is defined as:

$$f_{Wl_k} = \cfrac{1}{1 + \cfrac{\text{Demand}}{\text{Supply}}} = \cfrac{1}{1 + \cfrac{\mathcal{M}_w \Lambda_k \dot{E}_k}{\hat{G}_{r_k} C_{r_k} W^\star_{g_{j0}}}}, \tag{S201}$$

$$W^\star_{g_j} = \sum_{j'=j}^{N_G} \left[\rho_\ell \left(\vartheta_{\text{Fc}} - \vartheta_{\text{Wp}} \right) \Psi^\star_{g_{j'}} \Delta z_{g_{j'}} \right], \tag{S202}$$

$$\Psi^\star_{g_j} = \ell_{g_j} \cfrac{\max \left[\min \left(\Psi_{g_j} + \frac{z_{g_j} + z_{g_{j+1}}}{2}, \Psi_{\text{Fc}} \right), \Psi_{\text{Wp}} \right] - \Psi_{\text{Wp}}}{\Psi_{\text{Fc}} - \Psi_{\text{Wp}}}, \tag{S203}$$

where $\hat{G}_{r_k}$ ($\text{m}^2 \text{kg}_{\text{C}}^{-1} \text{s}^{-1}$) is a PFT-dependent scaling parameter related to fine root conductance (Tables S5-S6); $\mathcal{M}_w$ is the molar mass of water (Table S3); $\dot{E}_k$ ($\text{mol}_{\text{W}} \text{m}_{\text{Leaf}}^{-2} \text{s}^{-1}$) is the leaf-level transpiration rate if soil moisture is not limiting; C_{r_k} ($\text{kg}_{\text{C}} \text{m}^{-2}$) is the fine root biomass per individual; Λ_k ($\text{m}^2 \text{m}^{-2}$) is the leaf area index of cohort k; $W^\star_{g_j}$ ($\text{kg}_{\text{W}} \text{m}^{-2}$) is the available water for photosynthesis integrated from soil layer j to surface; $j0$ is the deepest soil layer that the cohort k can access water; z_{g_j} and Δz_{g_j} are the depth and thickness of soil layer j (z_{g_j} is always negative, and Δz_{g_j} is always positive); ρ_ℓ ($\text{kg}_{\text{w}} \text{m}^{-3}$) is the density of liquid water; ϑ_{Fc} and ϑ_{Wp} ($\text{m}^3 \text{m}^{-3}$) are the volumetric soil moistures at field capacity and at permanent wilting point, Ψ_{g_j} (m) is the matric potential of layer j, Ψ_{Fc} and Ψ_{Wp} (m) are the matric potentials at field capacity and wilting point, $\Psi^\star_{g_j}$ (unitless) is a factor that represents the reduction of available water due to force needed to extract the water.

S18 Allometric equations

In ED-2.2, size is defined by a suite of dimensions, including tree height z_{t_k} and rooting depth z_{r_k} which directly affect the cohort access to light and water, and the carbon stocks in different tissues. Most allometric equations use the diameter at the breast height (DBH, cm) as the size-dependent explanatory variable. The only time DBH becomes the dependent variable is when the code calculates the growth of structural tissues (Δt_{CD}): structural carbon stocks are updated based on the cohort's net carbon balance, and DBH is calculated to be consistent with the updated structural carbon stocks. In this supplement, we present the allometric equations of ED-2.2 for tropical PFTs; the temperate counterparts have been previously described in Albani et al. (2006) and Medvigy et al. (2009).

The tree height of any cohort k (z_{t_k}) is determined through a modified Weibull function:

$$z_{t_k} = \min \left\{ z_{t_{\max}}, \mathcal{Z}_0 + \mathcal{Z}_\infty \left[1 - \exp \left(-\mathcal{Z}_1 \cdot \text{DBH}_k^{\mathcal{Z}_2} \right) \right] \right\}, \tag{S204}$$

where $\mathcal{Z}_0$, $\mathcal{Z}_1$, $\mathcal{Z}_2$, and $\mathcal{Z}_\infty$ are PFT-dependent coefficients; and $z_{t_{\max}}$ is the maximum tree height, imposed to avoid excessive extrapolation of the allometric equations for carbon stocks. The coefficients are shown in Tables S5-S6; coefficients for tropical trees are provided by Poorter et al. (2006) allometric equation for moist forests in Bolivia; coefficients for temperate trees are from Albani et al. (2006).

The tree height at the bottom of the crown ($z_{t_k}^-$) is based on Poorter et al. (2006), and it is currently applied to tropical, subtropical, and temperate trees. For grasses, we fix the height to 1% of the total height, to avoid numeric singularities while assuming that most of the grass vertical profile has leaves:

$$z_{t_k}^- = \begin{cases} \max\left(0.05, 0.01\, z_{t_k}\right) & \text{, if cohort } k \text{ is grass} \\ \max\left(0.05,\, z_{t_k} - 0.31\, z_{t_k}^{1.098}\right) & \text{, if cohort } k \text{ is tree} \end{cases}. \tag{S205}$$

Maximum leaf biomass ($C_{l_k}^\bullet$, $\mathrm{kg\,m^{-2}}$), corresponding to the state when leaves are fully flushed, is derived from the allometric equations presented by Cole and Ewel (2006) and Calvo-Alvarado et al. (2008) for several commercial species in Costa Rica:

$$C_{l_k}^\bullet = n_{t_k} \mathcal{C}_{0l_k} \mathrm{DBH}_k^{\mathcal{C}_{1l_k}}, \tag{S206}$$

where n_{t_k} ($\mathrm{plant\,m^{-2}}$) is the plant demographic density, and $\mathcal{C}_{0l}$ and $\mathcal{C}_{1l}$ are the PFT-dependent coefficients (Tables S5-S6). For tropical PFTs, the default parameters are derived from the allometric equations presented by Cole and Ewel (2006) and Calvo-Alvarado et al. (2008) for several commercial species in Costa Rica; for temperate PFTs, the default parameters are the same as in Albani et al. (2006) and Medvigy et al. (2009).

Maximum root biomass ($C_{r_k}^\bullet$, $\mathrm{kg\,m^{-2}}$) and maximum sapwood biomass ($C_{\sigma_k}^\bullet$, $\mathrm{kg\,m^{-2}}$) are determined from $C_{l_k}^\bullet$ using the same functional form as Moorcroft et al. (2001), whose formulation of sapwood biomass was was based on the pipe model by Shinozaki et al. (1964a,b):

$$C_{r_k}^\bullet = f_{r_k} C_{l_k}^\bullet, \tag{S207}$$

$$C_{\sigma_k}^\bullet = \frac{\mathrm{SLA}_k}{f_{\sigma_k}} z_{t_k} C_{l_k}^\bullet, \tag{S208}$$

where f_{r_k} and f_{σ_k} are PFT-dependent parameters, currently assumed to be the same as in the original ED-1 (Moorcroft et al., 2001, Tables S5-S6); SLA (Tables S5-S6) is the specific leaf area, determined from Kim et al. (2012) fit of specific leaf area as a function of leaf turnover rate, using the GLOPNET leaf economics dataset (Wright et al., 2004).

Total structural (heartwood) biomass (C_{h_k}, $\mathrm{kg_C\,m^{-2}}$) ~~is based on~~ functional form is the same functional form for all PFTs. For temperate PFTs, the parameters are the same as in Albani et al. (2006) and Medvigy et al. (2009). For tropical PFTs, the parameters are based on Baker et al. (2004) equation of above-ground biomass, which is in turn based on the allometric equation by Chave et al. (2001) for French Guiana. This allometric equation was used instead of the allometric equation based on Chambers et al. (2001) because in ED-2.2 the function relating C_{h_k} and DBH_k must be bijective (i.e. given n_{t_k}, each DBH_k is associated with a single value of C_{h_k} and vice versa), which cannot be attained with the polynomial fits of higher order. Structural biomass was assumed to be the difference between above-ground biomass and the biomass of leaves and 70% of the total sapwood, corresponding to the above-ground fraction. The estimate was fitted against DBH, yielding to:

$$
C_{h_k} = \begin{cases} n_{t_k}\, \mathcal{C}_{0h_k}\, \mathrm{DBH}^{\mathcal{C}_{1h_k}} & , \text{if } \mathrm{DBH}_k \leq \mathrm{DBH}_{\mathrm{Crit}} \\ n_{t_k}\, \mathcal{C}_{2h_k}\, \mathrm{DBH}^{\mathcal{C}_{3h_k}} & , \text{if } \mathrm{DBH}_k > \mathrm{DBH}_{\mathrm{Crit}} \end{cases},
\tag{S209}
$$

where $\mathrm{DBH}_{\mathrm{Crit}}$ is the minimum DBH that results in $z_{t_k} = 35.0$ m, and the coefficients $\mathcal{C}_{0h}$, $\mathcal{C}_{1h}$, $\mathcal{C}_{2h}$, $\mathcal{C}_{3h}$ are defined for each PFT (Tables S5-S6).

The size-dependent rooting depth (z_{r_k}) is defined from an exponential function that allows tree depths to reach 5 m once trees reach canopy size ($z_{t_k} = 35$ m):

$$
z_{r_k} = -1.114\, \mathrm{DBH}_k^{0.422}.
\tag{S210}
$$

The maximum rooting depth is shallow compared to Nepstad et al. (1994) results, however it produces a rooting profile similar to other dynamic global vegetation models, and reflects that little variation in soil moisture exists at very deep layers (Christoffersen, 2013).

Leaf area index (Λ_k, $\mathrm{m^2_{Leaf}\,m^{-2}}$) is determined from leaf biomass and specific leaf area:

$$
\Lambda_k = \mathrm{SLA}_k\, C_{l_k},
\tag{S211}
$$

where n_k ($\mathrm{plant\,m^{-2}}$) is the demographic density of cohort k.

No allometric equation was found for wood area index (Ω_k, $\mathrm{m^2_{Wood}\,m^{-2}}$) for evergreen forests. We assumed the same allometric equation for temperate zone by Hörmann et al. (2003) for trees, and imposed maximum area at $\mathrm{DBH}_{\mathrm{Crit}}$, similarly to C_{l_k}:

$$\Omega_k = \begin{cases} 0 & \text{if cohort } k \text{ is grass} \\ n_k\, 0.0096 \min\left(\mathrm{DBH}, \mathrm{DBH}_{\mathrm{Crit}}\right)^{2.0947} & \text{if cohort } k \text{ is broadleaf tree} \\ n_k\, 0.02765 \min\left(\mathrm{DBH}, \mathrm{DBH}_{\mathrm{Crit}}\right)^{1.9769} & \text{if cohort } k \text{ is conifer} \end{cases} . \tag{S212}$$

Crown area index (X_k, $\mathrm{m}^2_{\mathrm{Crown}}\,\mathrm{m}^{-2}$) is also based on Poorter et al. (2006), but re-written so it is a function of DBH_k. Like in the previous cases, crown area was capped at $\mathrm{DBH}_{\mathrm{Crit}}$, and local crown area was not allowed to exceed 1.0 or to be less than the leaf area index:

$$X_k = \begin{cases} \min\left[1.0, \max\left(\Lambda_k, n_k\, 1.126\, \mathrm{DBH}^{1.052}\right)\right] & \text{if cohort is tropical/subtropical} \\ \min\left[1.0, \max\left(\Lambda_k, n_k\, 2.490\, \mathrm{DBH}^{0.807}\right)\right] & \text{if cohort is temperate} \end{cases} . \tag{S213}$$

References

Albani, M., Medvigy, D., Hurtt, G. C., and Moorcroft, P. R.: The contributions of land-use change, CO$_2$ fertilization, and climate variability to the eastern US carbon sink, Glob. Change Biol., 12, 2370–2390, doi:10.1111/j.1365-2486.2006.01254.x, 2006.

Albini, F. A.: A phenomenological model for wind speed and shear stress profiles in vegetation cover layers, J. Appl. Meteor., 20, 1325–1335, doi:10.1175/1520-0450(1981)020<1325:APMFWS>2.0.CO;2, 1981.

Baccini, A., Goetz, S. J., Walker, W. S., Laporte, N. T., Sun, M., Sulla-Menashe, D., Hackler, J., Beck, P. S. A., Dubayah, R., Friedl, M. A., Samanta, S., and Houghton, R. A.: Estimated carbon dioxide emissions from tropical deforestation improved by carbon-density maps, Nature Clim. Change, 2, 182–185, doi:10.1038/nclimate1354, 2012.

Baker, T. R., Phillips, O. L., Malhi, Y., Almeida, S., Arroyo, L., Di Fiore, A., Erwin, T., Killeen, T. J., Laurance, S. G., Laurance, W. F., Lewis, S. L., Lloyd, J., Monteagudo, A., Neill, D. A., Patiño, S., Pitman, N. C. A., M. Silva, J. N., and Vásquez Martínez, R.: Variation in wood density determines spatial patterns in Amazonian forest biomass, Glob. Change Biol., 10, 545–562, doi:10.1111/j.1365-2486.2004.00751.x, 2004.

Beljaars, A. C. M. and Holtslag, A. A. M.: Flux parameterization over land surfaces for atmospheric models, J. Appl. Meteor., 30, 327–341, doi:10.1175/1520-0450(1991)030<0327:FPOLSF>2.0.CO;2, 1991.

Botta, A., Viovy, N., Ciais, P., Friedlingstein, P., and Monfray, P.: A global prognostic scheme of leaf onset using satellite data, Glob. Change Biol., 6, 709–725, doi:10.1046/j.1365-2486.2000.00362.x, 2000.

Brooks, R. H. and Corey, A. T.: Hydraulic properties of porous media, Hydrology Papers 3, Colorado State University, Fort Collins, U.S.A., 1964.

Businger, J. A., Wyngaard, J. C., Izumi, Y., and Bradley, E. F.: Flux-profile relationships in the atmospheric surface layer, J. Atmos. Sci., 28, 181–189, doi:10.1175/1520-0469(1971)028<0181:FPRITA>2.0.CO;2, 1971.

Calvo-Alvarado, J. C., McDowell, N. G., and Waring, R. H.: Allometric relationships predicting foliar biomass and leaf area:sapwood area ratio from tree height in five Costa Rican rain forest species, Tree Physiol., 28, 1601–1608, doi:10.1093/treephys/28.11.1601, 2008.

Camillo, P. and Schmugge, T. J.: A computer program for the simulation of heat and moisture flow in soils, Technical Memorandum TM-82121, NASA, Greenbelt, United States, 1981.

Chambers, J. Q., dos Santos, J., Ribeiro, R. J., and Higuchi, N.: Tree damage, allometric relationships, and above-ground net primary production in central Amazon forest, Forest Ecol. Manag., 152, 73–84, doi:10.1016/S0378-1127(00)00591-0, 2001.

Chave, J., Riéra, B., and Dubois, M.-A.: Estimation of biomass in a neotropical forest of French Guiana: spatial and temporal variability, J. Trop. Ecol., 17, 79–96, doi:10.1017/S0266467401001055, 2001.

Christoffersen, B. O.: The ecohydrological mechanisms of resilience and vulnerability of Amazonian tropical forests to water stress, Ph.d. dissertation, University of Arizona, Tucson, AZ, USA, URL http://hdl.handle.net/10150/293566, 2013.

Clapp, R. B. and Hornberger, G. M.: Empirical equations for some soil hydraulic properties, Water Resour. Res., 14, 601–604, doi:10.1029/WR014i004p00601, 1978.

Cole, T. G. and Ewel, J. J.: Allometric equations for four valuable tropical tree species, Forest Ecol. Manag., 229, 351–360, doi:10.1016/j.foreco.2006.04.017, 2006.

Collatz, G., Ribas-Carbo, M., and Berry, J.: Coupled photosynthesis-stomatal conductance model for leaves of C_4 plants, Aust. J. Plant Physiol., 19, 519–538, doi:10.1071/PP9920519, 1992.

Collatz, G. J., Ball, J., Grivet, C., and Berry, J. A.: Physiological and environmental regulation of stomatal conductance, photosynthesis and transpiration: a model that includes a laminar boundary layer, Agric. For. Meteorol., 54, 107–136, doi:10.1016/0168-1923(91)90002-8, 1991.

Cosby, B. J., Hornberger, G. M., Clapp, R. B., and Ginn, T. R.: A statistical exploration of the relationships of soil moisture characteristics to the physical properties of soils, Water Resour. Res., 20, 682–690, doi:10.1029/WR020i006p00682, 1984.

Cowan, I. and Troughton, J.: The relative role of stomata in transpiration and assimilation, Planta, 97, 325–336, doi:10.1007/BF00390212, 1971.

Dufour, L. and van Mieghem, J.: Thermodynamique de l'atmosphère, Institut Royal Météorologique de Belgique, Gembloux, Belgium, 2 edn., in French, 1975.

Foken, T.: 50 years of the Monin–Obukhov similarity theory, Boundary-Layer Meteorol., 119, 431–447, doi:10.1007/s10546-006-9048-6, 2006.

Forest Products Laboratory: Wood handbook – wood as an engineering material, General Technical Report FPL-GTR-190, U.S. Department of Agriculture, Madison, WI, doi:10.2737/FPL-GTR-190, 2010.

Goudriaan, J.: Crop meteorology: a simulation study, Ph.D. thesis, Wageningen University and Research Centre, Wageningen, Netherlands, URL http://library.wur.nl/WebQuery/clc/104086, 1977.

Gu, L., Meyers, T., Pallardy, S. G., Hanson, P. J., Yang, B., Heuer, M., Hosman, K. P., Liu, Q., Riggs, J. S., Sluss, D., and Wullschleger, S. D.: Influences of biomass heat and biochemical energy storages on the land surface fluxes and radiative temperature, J. Geophys. Res., 112, D02 107, doi:10.1029/2006JD007425, 2007.

Hodnett, M. and Tomasella, J.: Marked differences between van Genuchten soil water-retention parameters for temperate and tropical soils: a new water-retention pedo-transfer functions developed for tropical soils, Geoderma, 108, 155–180, doi:10.1016/S0016-7061(02)00105-2, 2002.

Hörmann, G., Irrgan, S., Jochheim, H., Lukes, M., Meesenburg, H., Müller, J., Scheler, B., Scherzer, J., Schüler, G., Schultze, B., Strohbach, B., Suckow, F., Wegehenkel, M., and Wessolek, G.: Wasserhaushalt von Waldökosystemen: methodenleitfaden zur bestimmung der wasserhaushaltskomponenten auf level II-Flächen, Technical note, Bundesministerium für

Verbraucherschutz, Ernährung und Landwirtschaft (BMVEL), Bonn, Germany, URL http://www.wasklim.de/download/Methodenband.pdf, in German, 2003.

Jin, J., Gao, X., Sorooshian, S., Yang, Z.-L., Bales, R., Dickinson, R. E., Sun, S.-F., and Wu, G.-X.: One-dimensional snow water and energy balance model for vegetated surfaces, Hydrol. Process., 13, 2467–2482, doi:10.1002/(SICI)1099-1085(199910)13:14/15<2467::AID-HYP861>3.0.CO;2-J, 1999.

Jones, H. G.: Plants and Microclimate: A quantitative approach to environmental plant physiology, Cambridge Univ. Press, Cambridge, UK, 3rd edn., doi:10.1017/CBO9780511845727, 2014.

Kim, Y., Knox, R. G., Longo, M., Medvigy, D., Hutyra, L. R., Pyle, E. H., Wofsy, S. C., Bras, R. L., and Moorcroft, P. R.: Seasonal carbon dynamics and water fluxes in an Amazon rainforest, Glob. Change Biol., 18, 1322–1334, doi:10.1111/j.1365-2486.2011.02629.x, 2012.

Knox, R. G.: Land conversion in Amazonia and Northern South America; influences on regional hydrology and ecosystem response, Ph.D. dissertation, Massachusetts Institute of Technology, Cambridge, MA, URL https://dspace.mit.edu/handle/1721.1/79489, 2012.

Kursar, T. A., Engelbrecht, B. M. J., Burke, A., Tyree, M. T., EI Omari, B., and Giraldo, J. P.: Tolerance to low leaf water status of tropical tree seedlings is related to drought performance and distribution, Funct. Ecol., 23, 93–102, doi:10.1111/j.1365-2435.2008.01483.x, 2009.

Leuning, R.: A critical appraisal of a combined stomatal-photosynthesis model for C$_3$ plants, Plant Cell Environ., 18, 339–355, doi:10.1111/j.1365-3040.1995.tb00370.x, 1995.

Leuning, R., Kelliher, F. M., de Pury, D. G. G., and Schulze, E.-D.: Leaf nitrogen, photosynthesis, conductance and transpiration: scaling from leaves to canopies, Plant Cell Environ., 18, 1183–1200, doi:10.1111/j.1365-3040.1995.tb00628.x, 1995.

Louis, J.-F.: A parametric model of vertical eddy fluxes in the atmosphere, Boundary-Layer Meteorology, 17, 187–202, doi:10.1007/BF00117978, 1979.

Massman, W. J.: An analytical one-dimensional model of momentum transfer by vegetation of arbitrary structure, Boundary-Layer Meteorol., 83, 407–421, doi:10.1023/A:1000234813011, 1997.

Massman, W. J. and Weil, J. C.: An analytical one-dimensional second-order closure model of turbulence statistics and the Lagrangian time scale within and above plant canopies of arbitrary structure, Boundary-Layer Meteorol., 91, 81–107, doi:10.1023/A:1001810204560, 1999.

Medvigy, D. M.: The state of the regional carbon cycle: results from a constrained coupled ecosystem-atmosphere model, Ph.D. dissertation, Harvard University, Cambridge, MA, 2006.

Medvigy, D. M., Wofsy, S. C., Munger, J. W., Hollinger, D. Y., and Moorcroft, P. R.: Mechanistic scaling of ecosystem function and dynamics in space and time: Ecosystem Demography model version 2, J. Geophys. Res.-Biogeosci., 114, G01 002, doi:10.1029/2008JG000812, 2009.

Monin, A. S. and Obukhov, A. M.: Osnovnye zakonomernosti turbulentnogo pere- meshivanija v prizemnom sloe atmosfery (Basic laws of turbulent mixing in the atmosphere near the ground), Trudy Geofiz. Inst. AN SSSR, 24, 163–187, URL http://mcnaughty.com/keith/papers/Monin_and_Obukhov_1954.pdf, original in Russian. Translation available at the URL, 1954.

Monteith, J. L. and Unsworth, M. H.: Principles of environmental physics, Academic Press, London, 3rd edition edn., 418 pp., 2008.

Moorcroft, P. R., Hurtt, G. C., and Pacala, S. W.: A method for scaling vegetation dynamics: The Ecosystem Demography model (ED), Ecol. Monogr., 71, 557–586, doi:10.1890/0012-9615(2001)071[0557:AMFSVD]2.0.CO;2, 2001.

Murphy, D. M. and Koop, T.: Review of the vapour pressures of ice and supercooled water for atmospheric applications, Quart. J. Royal Meteorol. Soc., 131, 1539–1565, doi:10.1256/qj.04.94, 2005.

Nepstad, D. C., de Carvalho, C. R., Davidson, E. A., Jipp, P. H., Lefebvre, P. A., Negreiros, G. H., da Silva, E. D., Stone, T. A., Trumbore, S. E., and Vieira, S.: The role of deep roots in the hydrological and carbon cycles of Amazonian forests and pastures, Nature, 372, 666–669, doi:10.1038/372666a0, 1994.

Niu, G.-Y. and Yang, Z.-L.: An observation-based formulation of snow cover fraction and its evaluation over large North American river basins, J. Geophys. Res.-Atmos., 112, D21 101, doi:10.1029/2007JD008674, 2007.

Oleson, K. W., Lawrence, D. M., Bonan, G. B., Drewniak, B., Huang, M., Koven, C. D., Levis, S., Li, F., Riley, W. J., Subin, Z. M., Swenson, S. C., Thornton, P. E., Bozbiyik, A., Fisher, R., Heald, C. L., Kluzek, E., Lamarque, J.-F., Lawrence, P. J., Leung, L. R., Lipscomb, W., Muszala, S., Ricciuto, D. M., Sacks, W., Sun, Y., Tang, J., and Yang, Z.-L.: Technical description of version 4.5 of the Community Land Model (CLM), Technical Report NCAR/TN-503+STR, NCAR, Boulder, CO, doi:10.5065/D6RR1W7M, 420pp., 2013.

Panofsky, H. A.: Determination of stress from wind and temperature measurements, Quart. J. Royal Meteorol. Soc., 89, 85–94, doi:10.1002/qj.49708937906, 1963.

Parlange, M., Cahill, A., Nielsen, D., Hopmans, J., and Wendroth, O.: Review of heat and water movement in field soils, Soil Till. Res., 47, 5–10, doi:10.1016/S0167-1987(98)00066-X, 1998.

Poorter, L., Bongers, L., and Bongers, F.: Architecture of 54 moist-forest tree species: traits, trade-offs, and functional groups, Ecology, 87, 1289–1301, doi:10.1890/0012-9658(2006)87[1289:AOMTST]2.0.CO;2, 2006.

Raupach, M. R.: Simplified expressions for vegetation roughness length and zero-plane displacement as functions of canopy height and area index, Boundary-Layer Meteorol., 71, 211–216, doi:10.1007/BF00709229, 1994.

Raupach, M. R.: Corrigenda, Boundary-Layer Meteorol., 76, 303–304, doi:10.1007/BF00709356, 1995.

Raupach, M. R., Antonia, R. A., and Rajagopalan, S.: Rough-wall turbulent boundary layers, Appl. Mech. Rev., 44, 1–25, doi:10.1115/1.3119492, 1991.

Rogers, A., Medlyn, B. E., Dukes, J. S., Bonan, G., von Caemmerer, S., Dietze, M. C., Kattge, J., Leakey, A. D. B., Mercado, L. M., Niinemets, U., Prentice, I. C., Serbin, S. P., Sitch, S., Way, D. A., and Zaehle, S.: A roadmap for improving the representation of photosynthesis in Earth system models, New Phytol., 213, 22–42, doi:10.1111/nph.14283, 2017.

Romano, N. and Santini, A.: Field, in: Methods of soil analysis: Part 4 physical methods, edited by Dane, J. H. and Topp, G. C., SSSA Book Series 5.4, chap. 3.3.3, pp. 721–738, Soil Science Society of America, Madison, WI, 2002.

Sauer, T. and Norman, J.: Simulated canopy microclimate using estimated below-canopy soil surface transfer coefficients, Agric. For. Meteorol., 75, 135–160, doi:10.1016/0168-1923(94)02208-2, 1995.

Saxton, K. E. and Rawls, W. J.: Soil water characteristic estimates by texture and organic matter for hydrologic solutions, Soil Sci. Soc. Am. J., 70, 1569–1578, doi:10.2136/sssaj2005.0117, 2006.

Sellers, P. J.: Canopy reflectance, photosynthesis and transpiration, Int. J. Remote Sens., 6, 1335–1372, doi:10.1080/01431168508948283, 1985.

Sellers, P. J., Mintz, Y., Sud, Y. C., and Dalcher, A.: A Simple Biosphere model (SIB) for use within general circulation models, J. Atmos. Sci., 43, 505–531, doi:10.1175/1520-0469(1986)043<0505:ASBMFU>2.0.CO;2, 1986.

Sellers, P. J., Randall, D. A., Collatz, G. J., Berry, J. A., Field, C. B., Dazlich, D. A., Zhang, C., Collelo, G. D., and Bounoua, L.: A revised land surface parameterization (SiB2) for atmospheric GCMs. Part I: model formulation, J. Climate, 9, 676–705, doi:10.1175/1520-0442(1996)009<0676:ARLSPF>2.0.CO;2, 1996.

Shaw, R. H. and Pereira, A.: Aerodynamic roughness of a plant canopy: A numerical experiment, Agric. For. Meteorol., 26, 51–65, doi:10.1016/0002-1571(82)90057-7, 1982.

Shinozaki, K., Yoda, K., Hozumi, K., and Kira, T.: A quantitative analysis of plant form – the pipe model theory. I. Basic analyses, Jpn. J. Ecol., 14, 97–105, doi:10.18960/seitai.14.3_97, 1964a.

Shinozaki, K., Yoda, K., Hozumi, K., and Kira, T.: A quantitative analysis of plant form – the pipe model theory. II. Further evidence of the theory and its application in forest ecology, Jpn. J. Ecol., 14, 133–139, doi:10.18960/seitai.14.4_133, 1964b.

Stull, R. B.: An introduction to boundary layer meteorology, vol. 13 of *Atmospheric and Oceanographic Sciences Library*, Springer Netherlands, Dordrecht, Netherlands, doi:10.1007/978-94-009-3027-8, 1988.

The HDF Group: Hierarchical data format, version 5, URL http://www.hdfgroup.org/HDF5/, 2016.

Verseghy, D. L.: Class—A Canadian land surface scheme for GCMS. I. Soil model, Intl. J. Climatol., 11, 111–133, doi:10.1002/joc.3370110202, 1991.

Viskari, T., Hardiman, B., Desai, A. R., and Dietze, M. C.: Model-data assimilation of multiple phenological observations to constrain and predict leaf area index, Ecol. Appl., 25, 546–558, doi:10.1890/14-0497.1, 2015.

Walko, R. L., Band, L. E., Baron, J., Kittel, T. G. F., Lammers, R., Lee, T. J., Ojima, D., Pielke, R. A., Taylor, C., Tague, C., Tremback, C. J., and Vidale, P. L.: Coupled atmosphere–biophysics–hydrology models for environmental modeling, J. Appl. Meteor., 39, 931–944, doi:10.1175/1520-0450(2000)039<0931:CABHMF>2.0.CO;2, 2000.

Wohlfahrt, G. and Cernusca, A.: Momentum transfer by a mountain meadow canopy: a simulation analysis based on Massman's (1997) model, Boundary-Layer Meteorol., 103, 391–407, doi:10.1023/A:1014960912763, 2002.

Wright, I. J., Reich, P. B., Westoby, M., Ackerly, D. D., Baruch, Z., Bongers, F., Cavender-Bares, J., Chapin, T., Cornelissen, J. H. C., Diemer, M., Flexas, J., Garnier, E., Groom, P. K., Gulias, J., Hikosaka, K., Lamont, B. B., Lee, T., Lee, W., Lusk, C., Midgley, J. J., Navas, M.-L., Niinemets, U., Oleksyn, J., Osada, N., Poorter, H., Poot, P., Prior, L., Pyankov, V. I., Roumet, C., Thomas, S. C., Tjoelker, M. G., Veneklaas, E. J., and Villar, R.: The worldwide leaf economics spectrum, Nature, 428, 821–827, doi:10.1038/nature02403, 2004.

Wright, S. J., Jaramillo, M. A., Pavon, J., Condit, R., Hubbell, S. P., and Foster, R. B.: Reproductive size thresholds in tropical trees: variation among individuals, species and forests, J. Trop. Ecol., 21, 307–315, doi:10.1017/S0266467405002294, 2005.

Zhang, X., Friedl, M. A., Schaaf, C. B., Strahler, A. H., Hodges, J. C. F., Gao, F., Reed, B. C., and Huete, A.: Monitoring vegetation phenology using MODIS, Remote Sens. Environ., 84, 471–475, doi:10.1016/S0034-4257(02)00135-9, 2003.